



HAL
open science

Luminescent lanthanide nanoparticles for ultrasensitive enzyme-linked immunosorbent assay "ELISA"

Ali Kassir

► **To cite this version:**

Ali Kassir. Luminescent lanthanide nanoparticles for ultrasensitive enzyme-linked immunosorbent assay "ELISA". Other. Université de Strasbourg, 2022. English. NNT: 2022STRAF027. tel-04398163

HAL Id: tel-04398163

<https://theses.hal.science/tel-04398163>

Submitted on 16 Jan 2024

HAL is a multi-disciplinary open access archive for the deposit and dissemination of scientific research documents, whether they are published or not. The documents may come from teaching and research institutions in France or abroad, or from public or private research centers.

L'archive ouverte pluridisciplinaire **HAL**, est destinée au dépôt et à la diffusion de documents scientifiques de niveau recherche, publiés ou non, émanant des établissements d'enseignement et de recherche français ou étrangers, des laboratoires publics ou privés.

ÉCOLE DOCTORALE DES SCIENCES CHIMIQUES
Institut Pluridisciplinaire Hubert Curien

THÈSE présentée par :

Ali KASSIR

soutenue le : 13 décembre 2022

pour obtenir le grade de : **Docteur de l'université de Strasbourg**

Discipline/ Spécialité : Chimie

**Luminescent lanthanide nanoparticles for
ultrasensitive Enzyme-Linked
Immunosorbent Assay "ELISA"**

THÈSE dirigée par :

Dr. CHARBONNIERE Loïc

Directeur de thèse, CNRS Strasbourg

RAPPORTEURS :

Dr. COUDRET Christophe

Rapporteur externe, CNRS Toulouse

Dr. HAGEGE Agnès

Rapportrice externe, CNRS Lyon

AUTRES MEMBRES DU JURY :

Dr. CHEIGNON Clémence

Co-encadrante de thèse, Université de Strasbourg

To my family,

Acknowledgments

Tout d'abord, je tiens à remercier mon directeur de thèse, Dr Loïc Charbonnière de m'avoir fait confiance pour cette thèse. Je vous remercie pour votre accompagnement durant ces 3 ans. Vous êtes le meilleur modèle d'un directeur, leader et encadrant qu'un jeune peut souhaiter. Merci d'avoir été toujours accessible et à l'écoute. Au niveau scientifique, j'avais la chance de profiter de vos connaissances très riches et diverses, votre rigueur et votre créativité. Votre passion pour les nouvelles idées et votre ambition illimitée ont été ma motivation et ma garantie pour avancer, surtout dans les moments difficiles. Je vous remercie d'avoir respecté et soutenu mes idées, de m'avoir laissé une autonomie, de m'avoir orienté et conseillé sans imposer. Travailler dans votre équipe a été pour moi un vrai privilège.

Je voudrais remercier autant Dr. Clémence Cheignon pour son encadrement durant ces 3 ans. Merci de m'avoir accompagné au labo au début de ma thèse et m'avoir formé aux différentes techniques avec ta rigueur et ta pédagogie. Tu as toujours été disponible pour mes questions et mes demandes et tu m'as toujours facilité la vie au labo ! Ta gentillesse, ton humour et ton énergie sont de valeur à l'équipe. Merci de m'avoir ramené aux urgences et désolé de t'avoir inquiété. Merci de m'avoir toujours encouragé et forcé à sourire ! Les quatre jours à Göteborg étaient courts, mais c'était un plaisir de partager cette expérience avec toi.

Je tiens également à remercier les membres de jury, Dr. Agnès Hagège et Dr. Christophe Coudret de m'avoir fait l'honneur d'accepter d'examiner mon travail de thèse.

Je remercie l'Agence Nationale de la Recherche d'avoir financé cette thèse dans le cadre du programme d'investissement d'avenir.

Je remercie toutes les personnes et les plateformes d'analyses qui ont contribué de près ou de loin à l'avancement de ce travail. Merci à Dris Ihiawakrim (IPCMS) pour les analyses TEM, Mireille Del Nero et Olivier Courson (IPHC-Radiochimie) pour les analyses zeta et DLS (avant d'acheter notre propre appareil), Lai Truong-Phuoc (ICPEES) pour les analyses XRD, Anne Boos et Pascal Ronot (IPHC-RePSeM) pour les analyses ICP-AES.

Je voudrais remercier Loïc une autre fois, mais cette fois pour la merveilleuse équipe qu'il a pu constituer. Vous devez être aussi le meilleur recruteur pour pouvoir assembler ces personnes combinant l'excellence scientifique et humaine.

Merci Dr. Zouhair pour votre bonne humeur, votre encouragement, vos conseils, et toutes les discussions de valeur qu'on a pu avoir. Merci Aline pour ta gentillesse et ton sourire, merci de m'avoir formé sur l'Edinburg et le Fluorolog. Alex, merci pour ta rigueur sur les règles du laboratoire tout en gardant le trait d'humour. Merci de m'avoir aidé en synthèse et d'être toujours à l'écoute pour mes questions et mes demandes. Merci Câline pour ton professionnalisme et ta bonne humeur, merci pour le bonjour et le bonsoir de la journée.

Au cours de ces 3 ans, j'avais le plaisir de rencontrer de nombreuses personnes pour des périodes plus ou moins courtes, mais je suis reconnaissant pour tous les moments passés avec eux. Elsa et Kevin, on a commencé en thèse ensemble et on finit ensemble, merci pour les échanges d'info et des petites expériences, et pour toutes les discussions qu'on a pu avoir. Léna, Gemma, Anli, Lucas, Waygen et Manon, vous avez vraiment apporté une bonne ambiance au labo, avec votre gentillesse, bonne humeur et dynamisme. Merci Charlotte pour les repas de midi et toutes les discussions diverses qu'on a pu avoir. Cyrille, Mainak, Mohamadou et Joan merci pour votre humour, les rigolades, mais aussi tous les échanges scientifiques très intéressantes. Merci à vous tous pour faire du labo un endroit agréable à y être.

Je voudrais remercier toutes les personnes qui ont passé au labo pendant ma thèse. Rich, Lucie et Chen, merci pour toutes les conversations scientifiques (ou pas) qu'on a pu avoir. Votre contribution au labo a été remarquable. Merci également à tous les stagiaires qui ont pu rejoindre l'équipe pour des périodes différentes, surtout ceux que j'ai partiellement encadré, Margaux, Imane et Mohammed. Merci pour votre gentillesse et votre sérieux, j'espère que j'ai pu vous apprendre un minimum qui vous était utile.

Mes 3 ans de thèse étaient pleins d'ups and downs, et toutes les journées n'auraient pas pu être faciles sans la présence de nombreuses personnes avec qui j'ai partagé une importante étape de ma vie et qui m'ont permis de me défouler pendant ma thèse. Awada, Ghorayeb, et tous les amis de Strasbourg, je suis reconnaissant pour le temps qu'on a pu partager. Chacun de vous avait un impact sur moi d'une façon ou d'une autre. Malgré qu'on n'eût jamais les mêmes points de vue, mais c'était cette différence qui a renforcé notre relation. Merci pour toutes les discussions intéressantes (ou pas), les sorties, les repas, les soirées de folie, les nombreuses aventures et tous les autres plans qui n'ont jamais été réalisés !

Rachiny, Haidar, et tous les amis d'Al Ouloum, cette période qui m'a fait l'homme que je suis maintenant. Merci pour toutes les mémoires, les longues discussions et les échanges sur nos petites expériences quotidiennes malgré la distance.

En arrivant vers la fin de mes études, je ne peux pas oublier de remercier les personnes qui m'ont donné l'opportunité de re-exister, qui m'ont soutenu dans une certaine période de ma vie, et qui ont contribué à mon avancement. Merci Dr Miguel, Dr Samar, Dr Raya, Dr Rawad, Mr Al Daouk, et un très grand merci à Randa, Rehab et Lina. Merci à Maya, Moustafa, Rim, Nour et Mr Ghassani pour votre présence, ça comptait beaucoup pour moi. Fneich, mon pote d'enfance, un grand merci à toi frère.

Le grand merci va bien surtout à ma famille. Ils étaient pour moi, une vraie source d'inspiration et ont été toujours à mes côtés. Sans leur soutien je n'aurais pas été là. Aucun amour n'est plus beau, plus grand, plus sincère que celui d'une sœur. Heureusement j'ai trois ! Merci à ma sœur Batoul, mon plus grand support dans la vie et la personne que j'admire le plus. Ma sœur Aya, mon « confiance booster », merci pour les conseils et les encouragements. Merci à vous deux aussi de m'avoir fait « khalo » pour 5 magnifiques enfants, Rawad, Mabelle, Amar, Melissa et Habib. Ma sœur Nour, ma meilleure amie, merci pour ta douceur et ta tendresse. Je t'aimerai toujours plus que tout et je serai toujours là pour toi. Ali et Ibrahim, avec votre gentillesse, dynamisme et morales, vous avez vite fait partie de notre belle famille. Merci d'avoir été les frères que je n'ai jamais eus. Merci pour votre soutien continu et d'avoir pris soin de mes parents en mon absence.

Et enfin, c'est avec le cœur ému que je remercie mes chers parents. Je ne les remercierai jamais assez pour tout ce qu'ils ont fait depuis ma naissance et pendant toute période de ma vie. Je sais que j'étais un lourd fardeau, mais j'espère que je vous ai apporté plus de bonheur et de fierté que de tristesse et d'épuisement.

Maman, mon ange gardien, merci de m'avoir donné et « redonné » la vie ! Merci pour toutes tes sacrifices qui ont toujours éclairé mon chemin. Merci de m'avoir élevé et donné tes valeurs pour être l'homme que je suis maintenant, dans ce monde où le respect, l'honnêteté, la noblesse et l'amour n'ont plus le même sens. Ils seront gravés à jamais dans mon esprit et j'en resterai toujours fier. Papa, mon idole, tu n'es plus le seul docteur dans la famille ! Merci pour ton soutien inconditionnel dans tous mes choix personnels et professionnels. La phrase « tu ressembles à ton père » reste ma plus grande fierté dans la vie. Merci de me donner tes traits, ta force, ta persévérance, ta patience et ta sagesse. J'espère que tu seras toujours fier de moi.

Merci

*“The idea is not to live forever, it is to create
something that will”*

— Andy Warhol

List of abbreviations

A

Ab : Antibody

ACN : Acetonitrile

Ag : Antigen

AP : Alkaline phosphatase

B

BSA : Bovine serum albumin

C

CAGR : Compound annual growth rate

CAT : Catalase

CLIA : Chemiluminescence immunoassay

COVID-19 : Coronavirus disease 2019

CRT : Cathode ray tube

D

DAD : Diode array detector

DELFLIA : Dissociation-enhanced lanthanide fluorescence immunoassay

DLS : Dynamic light scattering

DNA : Deoxyribonucleic acid

E

EALL : Enzyme-amplified lanthanide luminescence

ECL : Electrochemiluminescence

ED : Electric dipoles

EDTA : Ethylenediaminetetraacetic acid

EDX : Energy dispersive X-ray spectroscopy

EIA : Enzyme immunoassay

ELISA : Enzyme linked immunosorbent assay

ESI : Electrospray ionization

EQ : Electric quadrupoles

F

FIA : Fluoroimmunoassay

FP : Fluorescence polarization

FRET : Fluorescence resonance energy transfer

H

HBA : *p*-hydroxybenzoic

HEPES : 4-(2-Hydroxyethyl)-1-piperazine ethane sulfonic acid

HIV : Human immunodeficiency virus

HLA : Human leukocyte antigen

HOMO : Highest occupied molecular orbital

HPAA : *p*-hydroxyphenylacetic acid

HPLC : High performance liquid chromatography

HPPA : *p*-hydroxyphenylpropionic acid

HRP : Horseradish peroxidase

2-HIP : 2-hydroxyisophthalete

I

IA : Immunoassay

ICP-AES : Inductively coupled plasma atomic emission spectroscopy

IG : Immunoglobulin

IP : Isophthalate

L

LDE : Laser doppler electrophoresis

LED : Light emitting diode

LIA : Liposome immunoassay

Ln : Lanthanide

LOD : Limit of detection

LOQ : Limit of quantification

LUMO : Lowest unoccupied molecular orbital

M

M : mol.L⁻¹

MALDI : Matrix assisted laser desorption/ionization

MD : Magnetic dipoles

MES : 2-(N-morpholino)ethane sulfonic acid

MHPA : Methyl 4-hydroxyphenyl acetate

MLCT : Metal to ligand charge transfer

MOPS : 3-(N-Morpholino)-Propane sulfonic acid

MS : Mass spectrometry

MW : Molecular weight

N

N_{eq} : Equivalent ligand number

NADH : Nicotinamide adenine dinucleotide

NIR : Near infra-red

NMR : Nuclear Magnetic Resonance

NP : Nanoparticle

P

PAP : Pulmonary alveolar proteinosis

PC : Polycarbonate

PCR : Polymerase chain reaction

pH : Potential of Hydrogen

pI : Isoelectric point

pK_a : Negative logarithm of the acid dissociation constant

PMMA : polymethyl methacrylate

PS : Polystyrene

PSA : Prostate-specific antigen

PV : Photovoltaic

Q

Q_{int} : Intrinsic quantum Yield

Q_{ext} : External quantum Yield

QDs : Quantum dots

R

RIA : Radioimmunoassay

RNA : Ribonucleic acid

RT : Retention time

S

SA : Streptavidin

SARS-CoV-2 : Severe acute respiratory syndrome coronavirus 2

SD : Standard deviation

S/N : Signal to noise ratio

STD : Sexually transmitted disease

T

TDM : Therapeutic drug monitoring

TEM : Transmission electron microscopy

TMB : 3,3',5,5'-Tetramethylbenzidine

TR : Time-resolved

Tris : Tris(hydroxymethyl)aminomethane

U

UV : Ultraviolet

V

Vis : Visible

X

XRD : X-ray diffraction

Greek letters

β : High energy and speed electrons (β^-) or positrons (β^+)

γ : Gamma ray

ε : Molar attenuation coefficient

ζ : Zeta potential

η : Efficiency of sensitization

θ : Angle between the incident beam and the crystallographic reflecting plane.

λ : Wavelength

π : pi-bond

τ : Lifetime

Table of contents

List of abbreviations	1
Table of contents	5
Chapter I : Introduction.....	11
1. IMMUNOASSAYS.....	13
1.1. Prominence of immunoassays	13
1.2. Principle.....	15
1.3. Formats	17
1.4. Detection methods	19
2. ENZYME LINKED IMMUNOSORBENT ASSAY “ELISA”.....	24
2.1. The rise of ELISA.....	24
2.2. Applications of ELISA	26
2.3. Operational mechanism	28
2.4. Standardized ELISA format	29
2.5. ELISA protocols	30
2.6. Enzymes and Substrates	33
2.6.1. Enzymes.....	33
2.6.2. Substrates	34
2.7. Sensitivity of ELISA	36
3. ENZYME AMPLIFIED LANTHANIDE LUMINESCENCE.....	38
3.1. Definition of lanthanides	38
3.2. Properties of lanthanides	39
3.2.1. Chemical properties	40
3.2.2. Magnetic properties	40
3.2.3. Optical properties:.....	41
3.3. Coordination chemistry of lanthanides.....	48
3.4. Luminescence applications of lanthanides	49

3.5.	Lanthanides application in bioassays	50
3.5.1.	Time resolved luminescence detection	50
3.5.2.	Enzyme amplified lanthanide luminescence.....	51
4.	LANTHANIDE DOPED NANOPARTICLES	53
5.	SCOPE OF THE THESIS	56
6.	REFERENCES	58
Chapter II : Ultrabright lanthanide nanoparticles.....		73
1.	INTRODUCTION	75
2.	SYNTHESIS OF LN-DOPED LaF_3 NPs	76
3.	CHARACTERIZATION OF THE NANOPARTICLES	78
3.1.	Morphology and size	78
3.2.	Structure.....	79
3.3.	Colloidal properties	80
3.4.	Composition.....	82
3.5.	Concentration.....	82
4.	PHOTOSENSITIZING LIGAND	85
4.1.	Synthesis of 2-hydroxyisophtalic acid.....	86
4.2.	Spectroscopic properties of 2-hydroxyisophtalic acid.....	88
4.3.	Photosensitization of $\text{La}_{0.9}\text{Tb}_{0.1}\text{F}_3$ NPs	89
4.3.1.	Bare nanoparticles.....	89
4.3.2.	Brightness of dye-sensitized NPs.....	91
4.3.3.	Excited state lifetime.....	92
4.3.4.	Effect of pH on the sensitization.....	94
4.4.	Photosensitization of $\text{Tb}_{0.85}\text{La}_{0.14}\text{Eu}_{0.01}\text{F}_3$ NPs	95
4.4.1.	Bare nanoparticles.....	96
4.4.2.	Brightness of dye-sensitized NPs.....	99
4.4.3.	Excited state lifetime.....	100
4.4.4.	Titration of $\text{Tb}_{0.85}\text{La}_{0.14}\text{Eu}_{0.01}\text{F}_3$ NPs with nalidixic acid	101

5. CONCLUSION.....	104
6. EXPERIMENTAL PART.....	105
6.1. Reagents.....	105
6.2. Synthesis of 2-hydroxyisophthalic acid.....	107
6.3. Spectroscopic measurements.....	108
6.4. Titration of the nanoparticles.....	108
7. REFERENCES.....	110

Chapter III : Hydroxylation of isophthalates by HRP..... 115

1. INTRODUCTION.....	117
2. PRELIMINARY APPROACH.....	117
3. HYDROXYLATION OF ISOPHTHALATE BY HRP.....	120
3.1. Antenna vs pre-antenna.....	122
3.2. Enzymatic reaction.....	123
3.3. Tb sensitization following the reaction.....	126
3.3.1. Effect of citrate on Tb sensitization.....	126
3.3.2. Effect of H ₂ O ₂ on Tb sensitization.....	128
3.3.3. Final enzymatic assay.....	131
4. EFFECT OF THE PRE-ANTENNA.....	132
4.1. Study of the sensitization.....	132
4.2. Enzymatic assay.....	134
5. REACTION KINETICS STUDY.....	136
5.1. Effect of pH.....	136
5.2. Effect of the temperature.....	137
6. CONCLUSION.....	139

7. EXPERIMENTAL PART	140
7.1. Reagents.....	140
7.2. Spectroscopic measurements	140
7.3. Enzymatic assays	141
8. REFERENCES	142

Chapter IV : Dimerization of phenols by HRP..... 145

1. INTRODUCTION	147
2. OXIDATION OF PHENOLS BY HRP.....	149
2.1. Sensitization of Tb-NPs by the oxidation product.....	149
2.2. Effect of the substrate	152
3. OXIDATION OF THE MHPA BY HRP	155
3.1. Spectral properties of the dimer.....	155
3.2. Reaction kinetics.....	156
3.3. Optimization of reaction conditions	157
3.3.1. Effect of pH.....	157
3.3.2. Effect of H ₂ O ₂ concentration	158
3.3.3. Effect of substrate concentration	160
3.3.4. Effect of the temperature	161
3.4. Monitoring of the reaction by HPLC-UV.....	162
3.4.1. Synthesis of the MHPA-dimer.....	162
3.4.2. Identification of the reaction products	164
3.5. Calibration of the assay	165
4. REACTION WITH HRP CONJUGATE.....	167
4.1. Oxidation of MHPA by Streptavidin-HRP.....	167
4.2. Effect of the pH	168
4.3. Effect of the buffer	169

5.	APPLICATION TO ELISA	170
5.1.	Proof of concept.....	170
5.2.	Effect of the NPs type.....	171
5.3.	Calibration of the final assay	173
6.	CONCLUSION.....	175
7.	EXPERIMENTAL PART	176
7.1.	Reagents.....	176
7.2.	Spectroscopic measurements	176
7.3.	Enzymatic assays	176
7.4.	Synthesis of the MHPA-dimer	177
7.5.	Monitoring of the reaction by HPLC-UV.....	178
7.6.	ELISA procedure	178
8.	REFERENCES	180
Chapter V : Conclusion and perspectives.....		185
Résumé en Français		193
Conferences and publications		203

Chapter I

Introduction: Detection in Enzyme Linked Immunosorbent Assay

1. Immunoassays

1.1. Prominence of immunoassays

An immunoassay is a bioanalytical method that aims at detecting the presence or measuring the concentration of a specific analyte in complex biological matrices. In 1959, the first ever immunoassay was described by Berson and Yalow for insulin detection.¹ This pioneering work got honored later by awarding the Nobel Prize in Medicine to Rosalyn Yalow "for the development of radioimmunoassays of peptide hormones" in 1977.² Their decision to not patent this technology helped to accelerate the progress of immunoassay development, which has witnessed striking advances in the last few decades. Since then, many immunoassays have been developed to provide qualitative, quantitative, or semi quantitative detection of a wide variety of analytes.



Figure 1: Rosalyn S. Yalow at the Nobel Banquet in Stockholm, Dec. 14, 1977.²

An accurate early-stage detection of analytes is a critical requirement in all bioanalytical settings for effective monitoring, and evaluating the quality of health, environment, or foods. Immunoassays (IAs) emerged to efficiently play this role and became key player in various applications, such as clinical diagnostics, biopharmaceutical analysis, environmental monitoring, security, and food testing.

a) Clinical

Many diseases can be exclusively diagnosed based on the determination of their biomarkers via IAs. The management of the disease and the effectiveness of the therapeutic regimen can also be monitored by IAs. Therefore, IAs play a critical role in the clinical decision-making. To date, a lot of IAs have been developed for biomarkers in several clinical areas such as hepatology, endocrinology, oncology, inflammation, allergy, drug monitoring...³⁻⁶ and several diseases like cardiac, renal, autoimmune and infectious diseases.⁷⁻¹⁰ Nevertheless, there are always continuous efforts to cover less prevalent or novel biomarkers. A recent example was developing IAs for SARS-CoV-2 detection. These fast and less expensive methods helped enormously in containing COVID-19 pandemic.¹¹

b) Industrial

Since their emergence, IAs have been notably used in biopharmaceutical industries. The most widely used IAs are those for Chinese hamster ovary protein, powerful tool used in the biopharmaceutical industry for the mass-production of therapeutic proteins, and frequently monitored by IAs.¹² Other biopharmaceuticals are also analyzed by IAs in industries, whether it was the manufactured product, or a compound related to the manufacturing or analysis process. IAs are routinely used in pharmaceutical industries for the analysis of antibodies used or produced for drug discovery.¹³ Therefore, there is a growing need for IAs in industry.

c) Environment and security

Environmental monitoring is of great importance to improve life quality and to keep it safe and secure. In this context, IAs appeared as efficient screening tools for the analysis of polluting substances such as harmful chemicals (pesticides, arsenic, mercury...) and toxins.¹⁴⁻¹⁷ The outbreak of these substances could be extremely toxic to the environment and human health and could lead to epidemics. Another important advance was the development of IAs for the analysis of biowarfare agents in environmental samples.¹⁸

d) Food safety

Many allergens, adulterants, harmful or unauthorized substances may exist in food, posing a threat to consumers health. IAs have been widely applied to analyze different hazards in food samples to ensure food safety.¹⁹ The most common are those for testing food allergens, which are one of the main concerns in the Western society.²⁰ On another hand, IAs were the frontline tools for monitoring and containing many outbreaks of food contaminations by foodborne pathogens, such as *Salmonella enterica*, *Escherichia coli O157:H7* and others.²¹

1.2. Principle

In IAs, the detection and the quantification of a specific analyte in biological samples are based on the interaction between the analyte and its specific antibody. When these immunoanalytical reagents are mixed and incubated, the antibody is bound to the analyte, forming an immune complex. By a prior appropriate labeling, one can trace the formation of the complex by monitoring the resulting analytical signal. This signal is then correlated to the concentration of the targeted analyte.²²

In the immune complex, antibodies (Abs) constitute the key component. They are proteins produced in animals and human bodies by immunological responses to the presence of antigens (Ags).²³ Each Ab has a unique structure recognized by a corresponding Ag in a lock-and-key mechanism. Basically, Abs are generated by injecting a host animal with the Ag of interest in an immunization process and subsequent harvest of serum.²⁴ Based on their structures and biological functions, we distinguish five classes of Abs (immunoglobulin IgG, IgA, IgE, IgM, and IgD). IgG is the most common type found in blood circulation and the most frequently used for IAs because it is readily available and exists at the highest level.²⁵

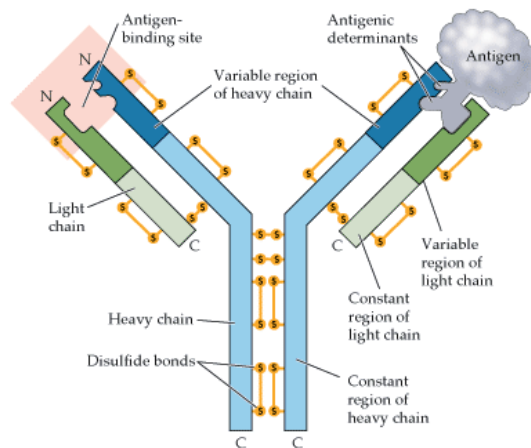


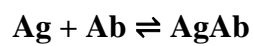
Figure 2: Schematic representation of an immunoglobulin G (IgG).²⁶

IgG structure is represented by a Y-shaped form consisting of four polypeptide units as shown in Figure 2. Two of them are known as heavy chains (blue) with a molecular weight of 55–60 kDa. The other two sequences are light chains (green) with a molecular weight of 20–24 kDa. The two double-ended segments of the Y contain variable and hypervariable regions (dark color) which create an active portion that recognizes a specific area of the Ag. The segment at the other end cannot bind to Ag but is able to affix to different surfaces.²⁷

On another hand, the analyte detected by IA may be natural Ags including macromolecules such as proteins and nucleic acids, or haptens such as toxins, drugs, and hormones. Haptens are substances with low molecular weight, typically < 1kDa which can combine with a specific Ab but lack antigenicity of their own. They are not capable of invoking an immune response when injected into animals. However, they can be detected as long as proper Abs that have the adequate properties for the assay can be produced.²⁸

IAs are characterized by unique specificity and important sensitivity of detection with great flexibility of application, thanks to these properties:

- The exceptional specificity for the substance to which each Ab binds. Abs recognize analytes based on their structure as well as their content and can be very specific. They can bind to only a small part of an Ag (known as the epitope) and are able to discriminate between highly similar epitopes of different Ags in a complex biological medium.²⁹
- The strength of binding affinity between an Ab and its target resulting in a very stable complex. Binding between Ab and Ag is best described as an equilibrium process:



The Ag-Ab interaction consists of fundamental forces including hydrogen bonding, ionic attraction (electrostatic), hydrophobic interaction, and Van der Waals forces. Abs have affinity constants in the range of 10^9 M^{-1} and up to 10^{12} M^{-1} for their corresponding Ags, indicating high affinity, and consequently high sensitivity of the IAs.²⁹

- The ability of the Abs to bind to an extremely wide range of natural and man-made biomolecules. Originally, IAs required purification of polyclonal Abs from human and animal sources so there was a very limited supply. Kohler and Milstein then reported the hybridoma method for unlimited production of monoclonal Abs.³⁰ Monoclonal Abs can only bind one epitope of the Ag, which provide higher degree of affinity and specificity in comparison with polyclonal Abs, that can bind several epitopes. This innovative work contributed enormously to the growth of IAs and the development of different formats.
- The efficient labeling for optimal signal detection and convenient assay interpretation. Diverse labeling systems can be applied for tracing the formation of the immune complex. Particular labeling could even provide an amplification of the signal, which open additional prospect for improved sensitivity of the IAs.

- Increased specificity and sensitivity can be gained in an IA by coupling a biotin-avidin interaction (one of the strongest non-covalent interactions in the nature) by using biotin-conjugated Ab and then introducing labeled avidin (or analogue like streptavidin SA).³¹ In some applications, multiple labels can be used by taking advantage of the multiplicity of SA-biotin binding. One SA molecule can bind four biotin molecules, so this complex scheme would involve a biotin conjugate followed by addition of SA, which could then bind three more labeled biotin conjugates as illustrated in Figure 3.

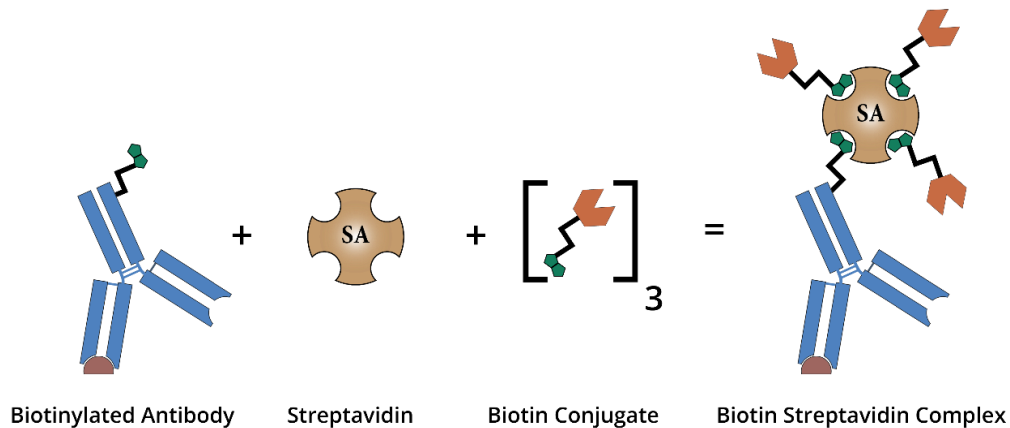


Figure 3: Biotin-Streptavidin conjugation system applied to IA.³²

1.3. Formats

IAs can be performed in many different formats and can be characterized regarding the assay homogeneity, or the competitive aspect of the assay procedure.

a) Homogeneous IAs:

This is procedurally the simplest assay format, in which detection reagents (labeled Ab) are directly added to the analyte-containing sample in solution. However, specific binding reactions do not easily permit to distinguish between bound and unbound detection Ab without a separation step. In this case, they can be discriminated based on physical, or chemical changes arising once the binding event occurs.³³ This format usually requires advanced instruments and particular labeling to acquire readout signals.

The advantage here is that the assay is very simple, doesn't involve any immobilization or washing step. However, analyzed matrices can contain interferences that may alter the assay performance. These assays are more effective for analytes at higher concentrations, otherwise, extensive purification or preconcentration steps are usually required.

b) Heterogeneous IAs:

This is a much more common IA format. The targeted analyte is immobilized on a solid support by a specific binding process such as adsorption or chemical reaction. Then, labeled Abs which bind specifically to the analyte can be added. After that, excess unbound Abs and untargeted Ags are washed away. Both sensitivity and reliability are improved compared with a homogeneous format due to the removal of possible interferents.³⁴

When coupled with sandwich format assay, the analyte is specifically immobilized using the corresponding Ab, already coated onto the solid support. Then, a different Ab (secondary), specific for another part of the analyte molecule, is added for signal generation as shown in Figure 4. After an incubation step, the "sandwich" immunocomplex is formed, followed by the washing step. The advantage of this technique is the increased specificity obtained due to two separate recognition steps provided by the two Abs types that are generally selected to recognize two different epitopes on the analyte.

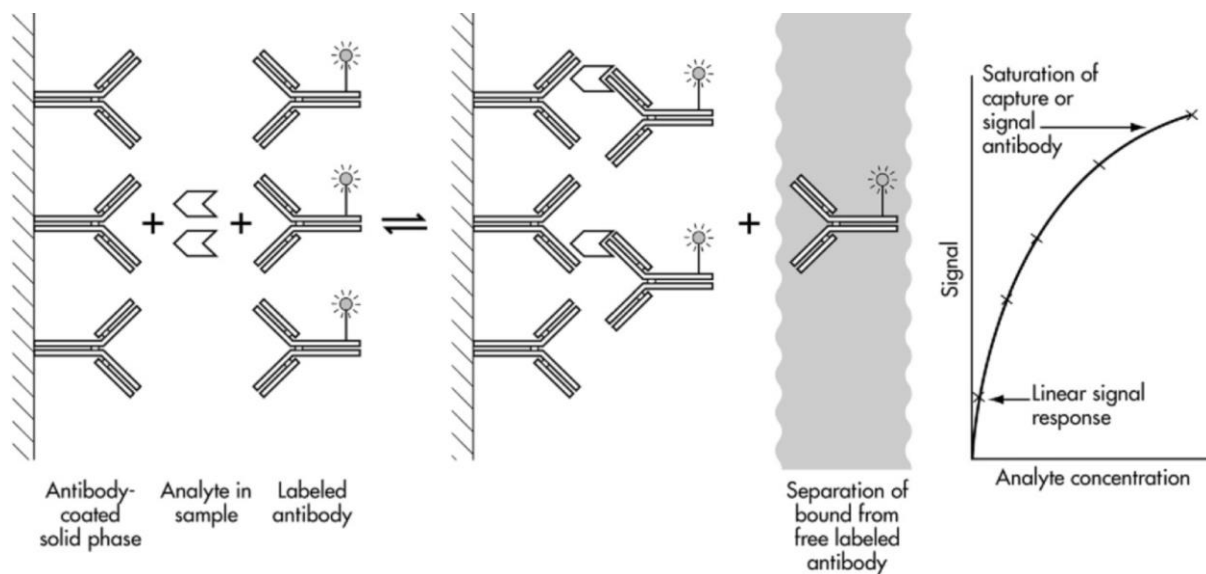


Figure 4: Illustration of heterogeneous "sandwich" immunoassay.³⁵

This is usually the preferred assay format (heterogeneous sandwich assay) when the application demands the highest degree of sensitivity and selectivity.²⁹ However, this format has some limitations. The assay format depends heavily on the surface area/volume ratio and thus the test is limited by the number of binding sites. Also, this test requires the addition of an immobilization step into the fabrication procedure. This step should be carefully designed to avoid nonspecific bindings into the solid phase.

c) Competitive IAs

Sandwich assays are only possible with large enough analytes (> 1 kDa) having at least two binding regions (epitopes) and are defined as “noncompetitive” assays. However, for small molecules, a “competitive” format can be applied, and performed similarly in either homogeneous or heterogeneous formats.

In competitive assays, a known concentration of labeled analyte is added to the sample, which competes with the analyte of the sample for the binding to a specific antibody, as shown in Figure 5. As the amount of analyte in the sample increases, the amount of labeled Ags bound to the Abs decreases, resulting in a decrease in the detection signal. Therefore, the generated signal is inversely dependent on the Ag concentration. This mode is less sensitive, but particularly important for small antigens (< 1 kDa) with limited number of epitopes.³⁶

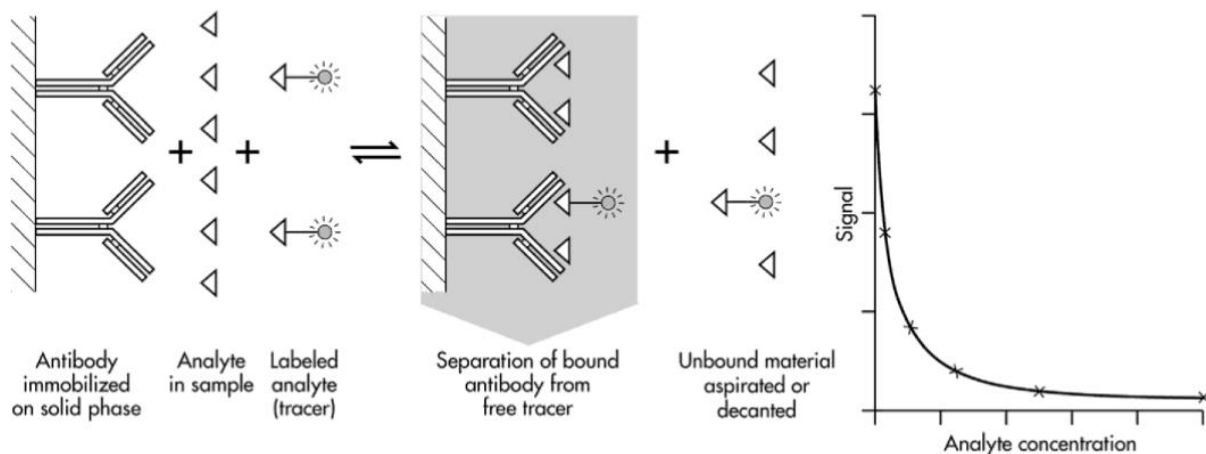


Figure 5: Illustration of heterogeneous “competitive” immunoassay.³⁵

1.4. Detection methods

IAs come in many different variations, including labeling and labeling-free assays. The detection in the labeling-free format is based on the immunoreaction itself like immunoprecipitation and immunodiffusion, or the measurement of the small physicochemical changes accompanying the immunological binding event. This includes optical, electrochemical, or mass-sensitive transduction.³⁷ In contrast, the labeling format consists in coupling some detectable labels or tracers to either the Ab or Ag to produce detectable analytical signal. And that provides higher sensitivity compared to labeling-free assays.

There are many different types of labels that can be used in IAs. The choice of label depends on the analytical sensitivity desired for the measurement, as well as the IA format.

a) Radioimmunoassay

The earliest IAs used isotopic labels, typically β and γ particle emitters, such as ^{125}I , ^{131}I , ^3H , ^{57}Co , and ^{32}P . These were appropriately named radioimmunoassays (RIA).³⁸ The appeal of radioactive labels is based on the extreme sensitivity of detection achieved due to very low background interference. RIA methods have been successfully used for the determination of many pharmaceutically important compounds in biological fluids.³⁹ However, RIAs are now rarely used in clinical laboratories due to concerns regarding safe handling and disposal of radioactive materials. Given the inherent instability of radiolabels, RIAs are considered as environmentally unfriendly. On another hand, a radiolabel can generate only one detectable signal event (decay) within its lifetime. To achieve the best detection limits, the measurement times must be prolonged to minutes and even hours or days in some cases.

As early as the 1970s, a wide variety of alternative nonisotopic labels have been established and widely used in IAs. These types of labels include fluorescent molecules, chemiluminescent labels, and enzymes, as well as many other newly developed unique labels. Some of these labels are even able to achieve detection limits well below those possible with radiolabels, without the problems that occur when working with radioactive materials.

b) Fluoroimmunoassay

Fluoroimmunoassay (FIA) is analogous to RIA except that the label is a fluorophore rather than a radioisotope. In fluorescence, a single photon of light is absorbed by a molecule (excitation) and re-emitted at a slightly lower energy, or longer wavelength (emission). In theory, this should be a more sensitive detection method, compared to radioisotopic decay. A single label can be measured many times during a relatively short measurement interval, thus increasing its detectability. The sufficient sensitivity of fluorescence emission permits even single molecule detection.⁴⁰

However, a major challenge with fluorescence detection in IAs is that many substances present in the complex samples are fluorescent and can cause a high background interfering with the specific signal. One way to avoid this interference was the use of time-resolved fluoroimmunoassay (TRFIA) with chelates of lanthanides or metalloporphyrins as labels.⁴¹

The advantage in these assays is the possibility to resolve the background fluorescence from the specific assay fluorescence.⁴² Disadvantages include potentially unstable metal-chelator binding and low fluorescence yields compared to fluorophore labels. But this opened up for more variations involving time-resolved techniques such as the fluorescence resonance energy transfer immunoassay (FRET).⁴³ Other types of FIA include the fluorescence polarization immunoassay (FPIA) based on a fluorescent label which can be excited by plane-polarized light. The rotation rate may be assessed by measuring fluorescence intensity in the vertical and horizontal planes. Generally, the time it takes a molecule to rotate through a given angle is an indication of its size. When the labeled molecule that rotates rapidly is bound to the analyte, the rotation rate decreases, and this decrease is measured. FPIA is widely applied in drug discovery and therapeutic monitoring.⁴⁴

c) Chemiluminescence and electrochemiluminescence Immunoassays

A chemiluminescent label consists of an organic molecule, which, when triggered by a chemical reaction, decomposes into an excited fluorescent molecule. It gives a single detectable event per label as the original chemical state cannot be regenerated.⁴⁵ Chemiluminescence Immunoassays (CLIA) are very useful, because they provide very low limits of detection with little to no background interference. Chemiluminescent labels exist as both biologically derived and chemically manufactured compounds. For instance, electrochemiluminescence (ECL) utilizes a molecule such as ruthenium (II) complex that undergoes chemiluminescence at a given redox potential, in one of the most sensitive nonenzymatic detection methods. The mechanism is shown in Figure 6.

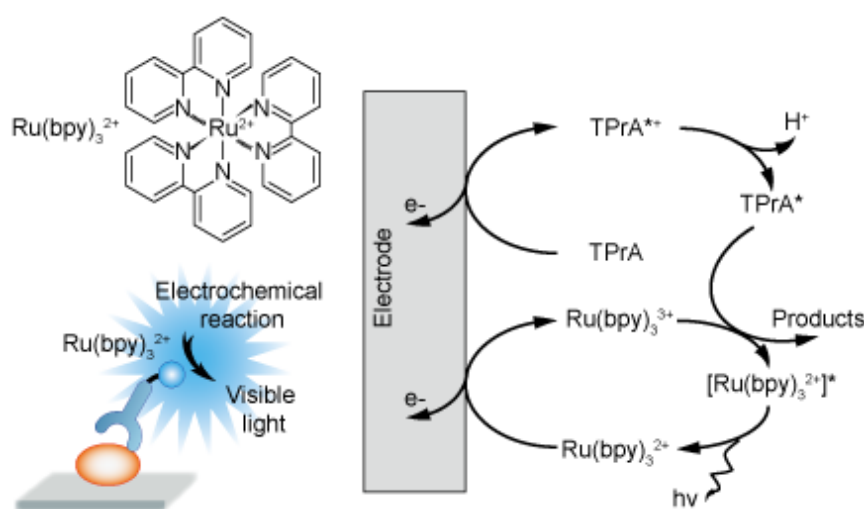


Figure 6: Mechanism of $\text{Ru}(\text{bpy})_3$ electrochemiluminescence system. TPrA: Tripropylamine.⁴⁶

d) Enzyme Immunoassay

The enzyme immunoassay (EIA) simply consists in the use of an enzyme as an immunoassay label. By appropriate chemical technique, the enzyme molecule can be coupled onto the immunoanalytical reagents (Ab), while maintaining the immunoanalytical reaction in the normal way. The enzyme catalytic activity is then measured by adding a substrate, and subsequent monitoring the turnover of the substrate to product.⁴⁷ The product must possess measurable physical or chemical differences from the substrate. The substrates for enzyme detection systems can be chosen to produce a colored product for photometric monitoring, a fluorescent product, a chemiluminescent product or even to form an intermediate substrate for a second enzymatic reaction to produce further amplification. The measured signal is finally correlated to the analyte concentration.

One significant advantage for enzyme labels is the amplification of detection signal. One enzyme label can produce many reporter molecules, providing drastic enhancement in the detection sensitivity. Enzyme immunoassays will be detailed in part 2 of Chapter I.

e) Liposome Immunoassay

Liposome immunoassays (LIA) involve liposome-encapsulating signal-generating labels, such as fluorescent probes, metals, and chelates. In LIA, liposomes are prepared and then coupled to either analyte or Ab by a suitable procedure, carrying out the assay in normal way. Detection in LIA relies on the lysis of the bounded liposomes by addition of a detergent and releasing the encapsulated signal-generating marker, as shown in Figure 7, which is then measured and related to the analyte concentration. This technique allows significant amplification of the detection signal and can be applied for the analysis of various pharmaceutical compounds.⁴⁸

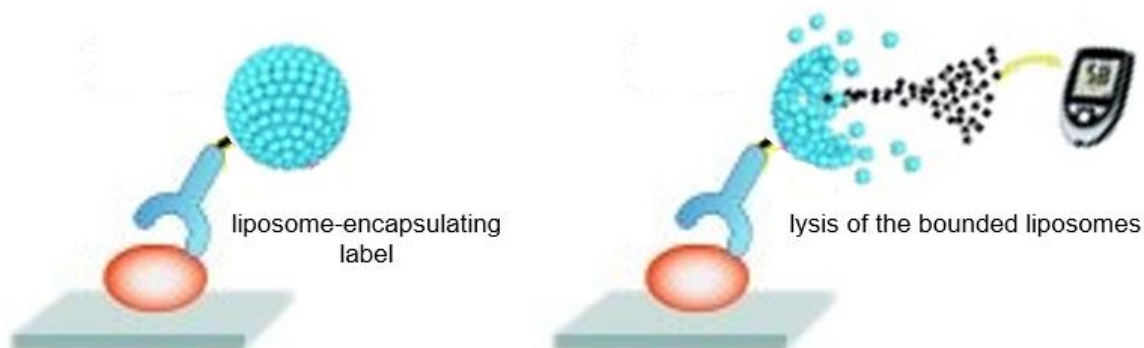



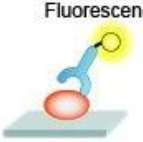
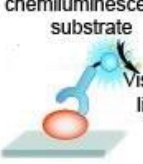
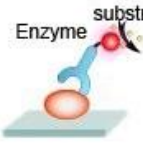
Figure 7: Mechanism of a liposome immunoassay.

f) Alternative labels and technologies

Alternative detection techniques have been developed in response to the demands for lower detection limits, an increase in label specificity, or more flexibility in applications. It is worthy to mention methods based on particles such as the particle enhanced turbidimetric and nephelometric IAs.⁴⁹ In addition, noble-metal (Au, Ag, Pt, and Pd) nanoparticles, have been widely used as important labels due to their excellent biocompatibility and stability, and their optical/electrochemical properties for signal tracing.⁵⁰

Another technique that has proven its efficiency in this regard is the use of DNA or RNA as labels in non-competitive IAs, as amplification of the signal can be accomplished through polymerase chain reaction (PCR), resulting in very high sensitivity.⁵¹ A summary of the most used label types along with their intrinsic sensitivity is represented in Table 1.

Table 1: List of the most used IA labels with their relative sensitivity.⁵²

IA type	Illustration	Label sensitivity (M)
Radioimmunoassay		RIA: 1×10^{-15}
Fluoroimmunoassay		FIA: 1×10^{-10}
		FPIA: 1×10^{-14}
		TRFIA: 1×10^{-17}
Chemiluminescence		CLIA: 1×10^{-13}
		ECLIA: 2×10^{-20}
Enzyme immunoassay		Photometric: 1×10^{-16}
		Fluorescence: 1×10^{-19}
		Chemiluminescence: 1×10^{-21}

2. Enzyme linked immunosorbent assay “ELISA”

2.1. The rise of ELISA

Throughout the evolving process of immunoassays, the idea of using enzyme labels faced serious doubts and hesitation. Theoretically, the concept seemed to be a revolutionary advance toward a safe, environmentally friendly IA, with new records in detection sensitivity. But practically, it was believed that enzymes are too large for biomolecules to be used as labels, and their presence would most likely cause steric troubles (Figure 8). Such concerns were addressed by careful planning and execution of the assays. The first advance in this regard was back to 1966, when Avrameas and Uriel reported a successful Ab and Ag coupling to enzymes such as alkaline phosphatase, and glucose oxidase among others.⁵³

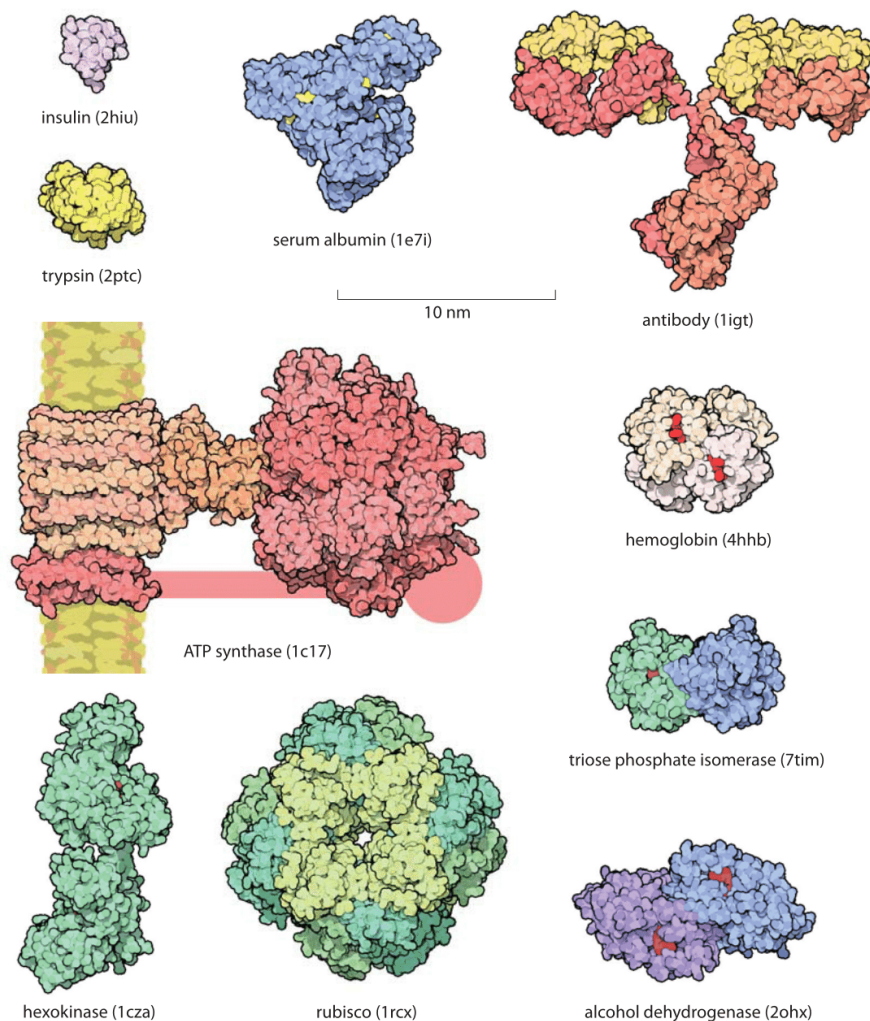


Figure 8: Representative examples of different enzymes size in comparison with Ab and different biomolecules.⁵⁴

In 1971, two independent studies (Engvall and Perlmann⁵⁵; Van Weemen and Schuurs⁵⁶) proved the feasibility of enzymes as immunoassay labels and reported the step-by-step process of performing an enzyme immunoassay.

Engvall and Perlmann were first to conceptualize an Enzyme Linked Immunosorbent assay, currently termed “ELISA”.

At the time, RIAs were in full bloom, but they were too sophisticated for many areas of research and diagnosis because they required expensive equipment and used antigens and antibodies labeled with radioactive isotopes with short half-lives. We wanted something simpler with the same sensitivity. - Eva Engvall, 2010.⁵⁷

They also employed ELISA method for the determination of IgG levels in rabbit serum using the alkaline phosphatase as the enzyme label.⁵⁵ At first, this work got rejected by several journals, stating that measuring rabbit IgG is nothing new.⁵⁷ This was before they received the German scientific award of the “Biochemische Analytik” in 1976 for this invention.



Figure 9: From left to right, Dr. Eva Engvall, Dr. Anton Schuurs, Dr. Peter Perlmann, Dr. Bauke van Weemen Biochemische Analytik award, Munich, April 1976.⁵⁸

Since then, the ELISA method paved the path for further advances becoming a routine laboratory research worldwide. ELISA proved its applicability in various fields including food industry, immunology, diagnosis, drug monitoring, pharmaceutical industry, vaccine development, and transplantation. The global ELSIA market is growing fast at a compound annual growth rate CAGR > 5%, as shown in Figure 10.⁵⁹

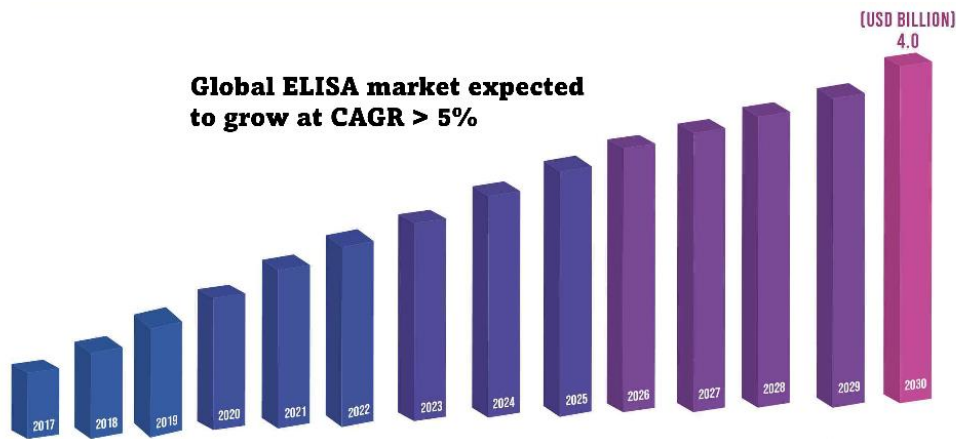


Figure 10: ELISA projected market size.⁵⁹

2.2. Applications of ELISA

a) Food industry

ELISA is the main platform for identifying food allergens such as those present in milk, eggs, peanuts, walnuts and almonds.^{60,61} ELISA can be employed to corroborate the authenticity of food products.⁶² It is also an essential technique for quality control of fish, milk (and sub products), irradiated food, genetically modified food, or other harmful food components that can be transferred to human.

b) Diagnosis

ELISA has proven to be a capable platform applied worldwide for detecting variety of disease types in human and animals. It has offered a high throughput detection of infectious diseases like Influenza, Ebola, covid19,⁶³⁻⁶⁵ sexually transmitted diseases (STDs) including HIV, hepatitis, syphilis, chlamydia,^{66,67} and regional or endemic diseases like Dengue fever, Chagas disease, West Nile virus, etc...⁶⁸⁻⁷⁰

Advances of ELISA technique have also promised its application in detecting tumor markers like prostate-specific antigen (PSA), carcinoembryonic antigen, and other biomarkers of breast cancer and ovarian cancer.⁷¹⁻⁷⁴

On another hand, ELISA widely served for pregnancy tests, as it can detect multiple markers from the maternal blood, saliva, or urine at the early stages of the pregnancy.⁷⁵ It is also used as a reliable method for measuring congenital infections such as HIV or toxoplasmosis during the pregnancy.^{76,77}

c) Immunology

Various studies have demonstrated ELISA as the gold standard method that is rapid and cost-effective for measuring and monitoring the immune system responses to understand various immune diseases. ELISA was applied for the diagnosis and monitoring of several autoimmune diseases such as Pulmonary alveolar proteinosis (PAP) and Bullous pemphigoid, and for studying the risks and relevance of developing other autoimmune diseases.⁷⁸⁻⁸⁰ ELISA has also shown great potentials in studying the humoral response of the immune system towards different classes of infections such as leprosy infection, and the human endogenous retrovirus.^{81,82}

d) Drug Monitoring and Pharmaceutical Industry

ELISA techniques have found a variety of applications in pharmaceutical industry. ELISA-based therapeutic drug monitoring (TDM) has been introduced as a facile and cost-effective method for measuring the concentrations of the drugs in plasma samples.⁸³

ELISA is also widely used for drug abuse detection including amphetamine, methamphetamine, 3,4-methylenedioxymethamphetamine, cocaine, benzoylecgonine, etc. Not to forget the role of ELISA in the detection of hormones such as testosterone, prolactin, follicular stimulating hormone, and others.^{84,85}

e) Vaccine Development

ELISA serves as a great candidate for vaccine development. The serum from immunized animal or human model can be tested to detect the presence of antibodies against certain types of antigens, which were intentionally injected to the host.⁸⁶ ELISA technique has proven to have a unique position in profiling of elicited immune responses, which are widely performed for vaccine trials around the world.⁸⁷

f) Transplantation

When transplantation is required, the pre-transplant cross-matching test represents one of the most important steps for a successful relocation of the organ. ELISA-based cross-matching test can be performed between the recipient's anti-HLA antibody and the donor's identified HLA types to monitor any incompatibility between the examined samples.⁸⁸ ELISA is also particularly applied for pre-transplant evaluation and prediction of success rate in cases of renal and liver transplant.^{89,90}

2.3. Operational mechanism

The main general steps to completing an ELISA are:

a) Immobilization

In fact, the term “immunosorbent” in ELISA is related to the immobilization of the targeted analyte (Ag) on a solid support in a heterogeneous assay. This can be done either through direct non-specific adsorption, or through specific capturing by another Ab (sandwich assay).

b) Blocking

After the immobilization of the Ag, the surface is normally coated with a blocking agent. It will permanently bind to the surface and reduce the chance of non-specific binding in the next steps of the assay. Common protein blockers include bovine serum albumin (BSA), newborn calf serum, normal whole serum, casein, non-fat dry milk, and fish gelatin.⁹¹

c) Immunoreaction

Then, the enzyme labeled Ab is added and the mixture is incubated. The Ab is subsequently bound to the immobilized Ag forming the immune complex.

d) Washing

Between each step, the system is thoroughly washed with a buffer solution to remove unbound proteins without affecting the bound ones. Typical washing buffers consist of low concentration of non-ionic detergents such as Tween-20 in phosphate buffered saline solutions. In heterogeneous assays, the washing step basically serves to eliminate unbound labeled Abs to isolate the signal arising from bound ones. Herein, it also helps to get rid of every unbound constituent of the biological sample that can affect the enzyme activity. Whence the advantage of ELISA heterogeneity over other developed homogeneous EIA.⁹²

e) Detection

Finally, the substrate is added to develop the enzymatic reaction, forming the product which possess measurable physical or chemical property. Therefore, this signal is a direct function of the concentration of the analyte that is present on the surface.

2.4. Standardized ELISA format

One of the significant challenges in manufacturing of ELISA platforms is the suitable choice of solid material. The appropriate physics and chemistry of the solid phase play a critical role in protein immobilization. Immobilized proteins on the surface should preserve their integrity, native conformation, as well as their biological function and activity.

Several developments in this regard were crucial in making the ELISA into what it is today. The first was the use of plastic coating technique to immobilize the Ag or the Ab. Polystyrene (PS) is a cost-effective, highly transparent, and relatively hydrophilic material suitable for protein adsorption. PS (or other similar materials such as polymethyl methacrylate (PMMA) and polycarbonate (PC)) is known in its nature to be inert, so it does not possess active functional groups that can involve substantial interaction of biomolecules with its surface. One of the most commonly used methods is to modify and functionalize this surface with hydroxyl ($-OH$), amine ($-NH_2$), or carboxyl ($-COOH$) groups.⁹³

The presence of such functionalities allows the adsorption of the protein (Ab or Ag) to the activated surface by their free polarizable groups (Figure 11). This process provides reproducible, and relatively durable adsorption of protein onto the PS surface. In addition, it makes washing steps extremely simple and centrifugation steps are no longer needed. Since then, different techniques have been developed for optimized immobilization of Ab, Ag and other proteins on the supporting surfaces.⁹⁴

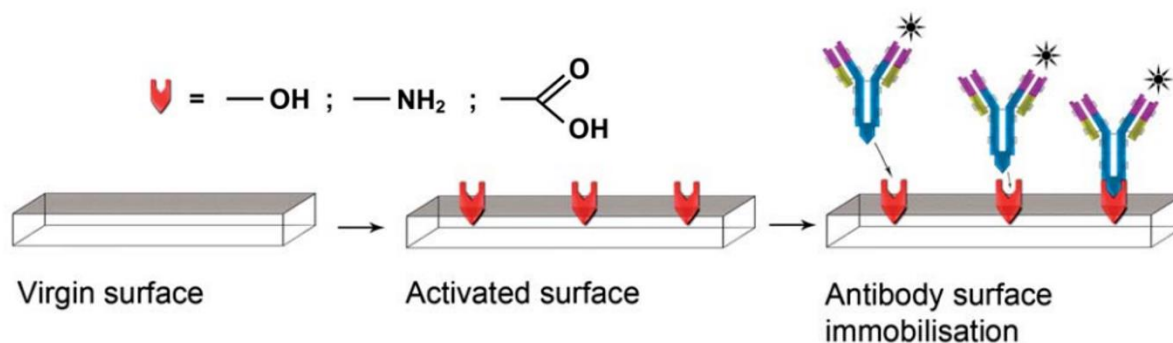


Figure 11: Surface functionalization and subsequent antibody surface immobilization.⁹³

The next development was the introduction of microtiter plates as an assay format. The most common configuration is 96-well plate composed of 8 rows and 12 columns (Figure 12). Typical wells can be charged with a volume of approximately 350 μ L.

Later, microplates with 384 and 1536 wells were also developed, having their main applications in high throughput screening. This standardized format allowed the subsequent development of all sorts of gadgets and tools for practical execution of assays, including multichannel pipettes, washing devices, and plate readers.



Figure 12: Assay manipulation in 96-well microtiter plate using a multichannel pipette.

Microplate readers are instruments that provide the final detection outcomes through recording the signal depending on the applied detection method. It provides high throughput performance, compatibility, cost-effectiveness as well as multi-mode operation. Incorporated software, varied types of plate formats, plate incubators and shakers, injectors, could be additional assets to the ELISA microplate readers.

2.5. ELISA protocols

Different ELISA protocols are typically used depending on the purpose of the assay, the type of the analyzed samples, and the purity of the reagents. Regarding the Ag immobilizing strategy and the type of Ab-Ag interaction (direct recognition or competition), ELISA can be presented in different formats described below.⁹⁵

a) Direct ELISA

This is the simplest form of ELISA (Figure 13). It is a two-step assay (without counting washing and blocking steps). In a first step, the analyte of interest is attached to the solid surface of the well. In the following step, the enzyme-labeled primary antibody is introduced to the assay. This type of assay requires isolated and purified samples as other proteins in the sample might interact with the solid phase, thus introducing errors in the assay.

It should be noted that the immunoreactivity of the primary Ab might be adversely affected by labeling with enzymes. The labeled primary antibody is not commonly used, thus this type of assay is limited. Another issue can also be faced in case the analyte is adsorbed in a way that makes its epitope inaccessible for Ab recognition.

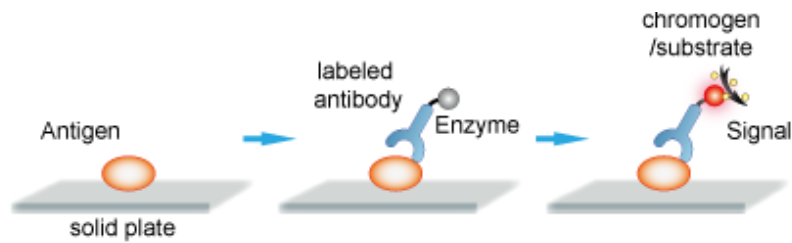


Figure 13: The flowchart of direct ELISA.⁹⁶

b) Indirect ELISA

Indirect ELISA follows the same steps as direct ELISA except that the primary Ab is not labeled. So in an additional third step, labeled secondary Ab is added to specifically bind to the primary Ab (Figure 14). While this assay offers better accessibility to a wide variety of secondary labeled antibodies, it always lacks the optimal specificity of the assay.

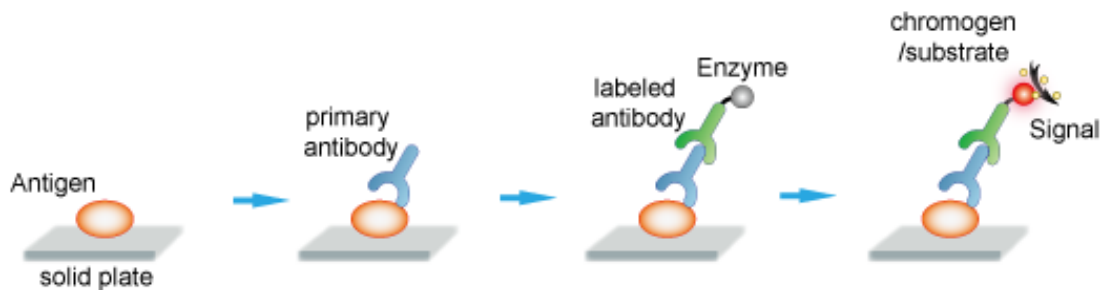


Figure 14: The flowchart of indirect ELISA.⁹⁶

c) Sandwich ELISA

The sandwich ELISA is one of the most efficient formats. In a sandwich assay, as suggested by its name, the analyte of interest is wrapped in between the primary and the secondary antibodies from both sides. Here, the immobilization of the Ag is done through specific capturing by specific Ab fixed to the solid phase. The next step can be similar to either direct or indirect ELISA (Figure 15). This strategy offers better control over the specificity of the assay as the capture Ab can be highly purified.

Nonetheless, in the absence of the analyte of interest, there is a small chance for the secondary Ab to bind to the primary Ab and to produce a false positive signal.

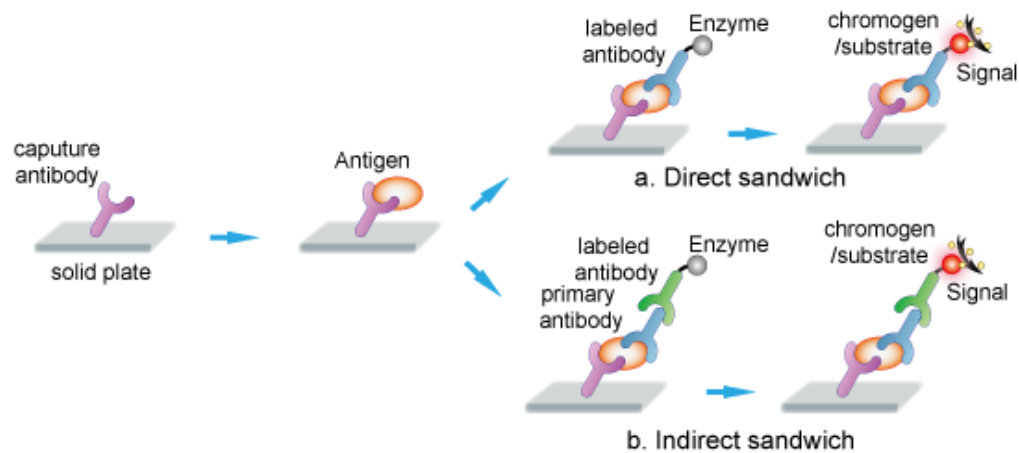


Figure 15: The flowchart of sandwich ELISA.⁹⁶

d) Competitive ELISA

Competitive ELISA adopt a slightly different strategy. In this protocol, the key event is the process of competitive reaction between the sample Ag and competitive Ag bound to the wells of a microtiter plate (Figure 16).

First, the labeled Ab is incubated with the sample and the resulting Ab-Ag complexes are added to wells that have been coated with the same Ag as competitor. After the incubation, any unbound Ab is washed off. The more Ag in the sample, the more Ab will be bound to the sample Ag, and there will be a smaller amount of Ab available to bind to the competitive Ag. Therefore, the signal is inversely correlated with the presence of the analyte of interest.

Competitive assays can be executed in direct, indirect, or sandwich mode. This assay is lengthy, tedious, and consumes large sample volumes, but it provides a high degree of specificity for measurements of antigen concentration in complex mixtures.

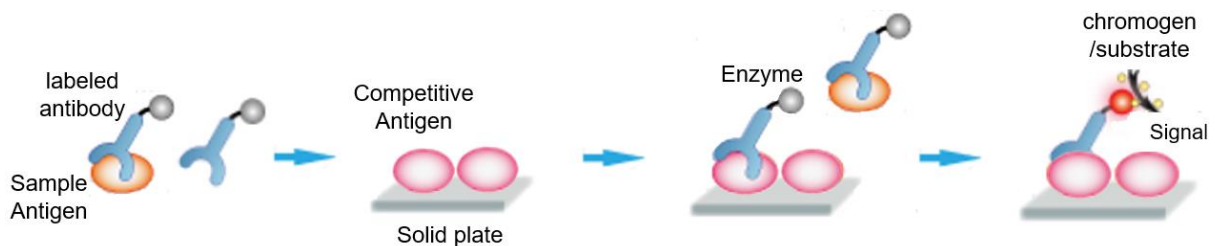


Figure 16: The flowchart of direct competitive ELISA.⁹⁶

2.6. Enzymes and Substrates

Enzymes are macro-biomolecular catalysts that can accelerate chemical reactions of molecules known as substrates. Upon reaction, the enzyme chemically modifies the substrate into a measurable product, while the signal readout is related to the activity of the enzyme.

Enzymes applied in ELISA should meet basic requirements including high purity, high conversion rate, desirable specificity, high stability as well as the ability to be covalently linked to Ab while preserving the activity and catalytic capacity after conjugation. Every class of enzymes requires a specific type of substrate. Substrates have to offer ease of preparation and storability, as well as high reactivity at relatively low enzyme concentrations to promote the efficiency of the assay.⁹⁷

2.6.1. Enzymes

Among different enzymes, horseradish peroxidase (HRP) and alkaline phosphatase (AP) are two of the most popular enzymes used for labeling the Abs. These enzymes are relatively inexpensive, and commercially available, while offering high substrate turnover. Conjugation of enzymes to Abs involves the formation of a stable, covalent linkage between the enzyme and the antigen-specific monoclonal or polyclonal antibody in which neither the Ag-combining site of the Ab nor the active site of the enzyme is functionally altered.⁹⁸

a) Horseradish peroxidase (HRP)

Horseradish peroxidase (MW : 44 kD) is one of the most suitable candidates for conjugation to Abs.⁹⁹ HRP is a combination of a porphyrin protein comprised of a colorless glycoprotein known as apoenzyme (enzyme, with the maximum absorption peak at 275 nm) and a dark brown iron porphyrin ring compound known as prosthetic group (haem, with the maximum absorption peak at 403 nm). HRP readily combines with hydrogen peroxide (H₂O₂), and the resultant [HRP-H₂O₂] complex can oxidize a variety of organic hydrogen donor substrates.

The small size of this enzyme helps to avoid steric hindrance with neighboring proteins. It is inexpensive while varied types of corresponding substrates are commercially available for this enzyme.¹⁰⁰ However, HRP shows incompatibility with various preservatives including sodium azide presenting a major drawback.

Such preservatives are often used to reduce the chance of microbial contamination in typical biological buffers. Even at low concentrations, sodium azide can alter the activity of HRP. Other interfering compounds are mainly metals found in water as well as the endogenous peroxidases present in biological samples. To reduce such undesirable effects, sterilized buffers are prepared with ultrapure water, and a pretreatment is necessary to the samples that are suspected of having high peroxidase levels.

b) Alkaline phosphatase “AP”

Extracted from *Escherichia coli*, AP is approximately double in size (MW : 80 kD), when compared to HRP. AP catalyzes the removal of phosphate group from various compounds that are phosphorylated.¹⁰¹ Due to its size, fewer number of enzymes can be conjugated to the antibody of interest. This also means that the large AP molecule can potentially cause steric hindrance in proximity of the Ag-Ab complexes. This phenomenon can reduce the efficiency of the enzyme. AP shows better stability and produces lower background noise in comparison to HRP, but it is more expensive. AP can be inactivated when exposed to chelating agents, inorganic phosphates, or acidic environment (pH < 4.5). This enzyme can only be used in alkaline environment, thus any acidic buffer must be avoided once the enzyme labeled Abs are immobilized in the wells.

Other than the HRP and AP, different enzymes have been also applied in ELISA, such as β -galactosidase, acetylcholinesterase, catalase, urease, etc...⁹⁷ These did not get the same success as HRP and AP due to lower performances.

2.6.2. Substrates

As a result of a specific enzymatic reaction, various substrates provide different means for quantification of the analyte of interest in the assay. The substrate can result in a colored or luminescent measurable product with a signal proportional to the amount of enzyme conjugated antibody.

a) Colorimetric Assay

Colorimetric assays result in colored reaction products capable of absorbing light in the visible range. The optical density measured for the reaction product is typically proportional to the amount of analyte of interest in a defined concentration range.

The specific wavelength is generally provided by the manufacturers of the assay. The readout signals are judged in contrast to the recorded background signals (signal to noise). Colorimetric detection strategy took the conventional clinical practice to the next level by making the visual judgment of the detection results possible. The presence of the analyte of interest can be confirmed by the naked eye, which permitted the foundation of paper-based diagnostic devices including paper strips.¹⁰² Many paper or fiber-based bioanalytical platforms such as pregnancy test paper strips are now commercially available that work based on the principles of colorimetric assay.

b) Fluorescent Assay

In fluorescent assays, the conjugate enzyme converts the substrate to a fluorophore product (generally polyaromatic hydrocarbons or heterocycles).

Fluorophores can be photoexcited at a specific wavelength and return to the ground energy state by emitting light at slightly lower energy. Recorded fluorescence is proportional to the concentration of the analyte of interest. A fluorescent assay can be more sensitive in comparison to the colorimetric assay. However, it typically produces higher background signal due to the sensitive nature of the fluorescent assay in regard to a biological medium.

c) Bio and chemiluminescent Assay

In these cases, the enzyme converts the substrate into a reaction product in his excited state that emits light as it returns to the ground state. Bioluminescence and chemiluminescence vary in the way the electron excitement takes place. In bioluminescence, application of bioluminescent compounds such as luciferin and firefly luciferase provide the emission.¹⁰³ When triggered by a chemical reaction (mainly excitation through oxidation), it results in chemiluminescence. Both bioluminescence and chemiluminescence are broadly used for various types of ELISA. Due to the highly sensitive nature of these luminescent compounds, such assays result in greatly enhanced signals, while having a wide dynamic range. The luminescence detection benefits from intense and prolonged light emission, low background signal, as well as signal amplification. Measured luminescence in relative light units (RLU) is typically proportional to the concentration of the analyte of interest.

A recap list of the main enzymes used in ELISA with their corresponding substrates and detection methods is presented in Table 2.

Table 2: List of the main enzymes used in ELISA with their corresponding substrates and detection method.

Enzyme	Substrate	Detection	
Alkaline phosphatase (AP)	<i>p</i> -nitrophenyl phosphate (p-NPP)	Colorimetric	
	4-methylumbelliferyl phosphate (4-MUP)		
Horseradish peroxidase (HRP)	3,3',5,5' tetramethylbenzidine (TMB)		
	2,2'-azino-di[3-ethyl-benzothiazoline] sulfonate (ABTS)		
	<i>o</i> -phenylenediamine (OPD)		
	<i>p</i> -hydroxyphenyl acetic acid (HPA)		Fluorescence
	3-(<i>p</i> -hydroxyphenyl) propionic acid (HPPA)		
	Luminal/luminol	Chemiluminescence	
Polyphenols and acridine esters			

2.7. Sensitivity of ELISA

Among various old and new immunoassay formats, ELISA are probably the most widely used techniques, due to their specificity, simplicity, flexibility, low cost, and most importantly the enzymatic signal amplification enabling high sensitivity.

Actually, detecting low abundance analytes in complex samples is one of the most pressing issues in analytical chemistry. Tests for low abundance biomarkers such as PSA and human pancreatic and gastrointestinal cancer marker are routinely used for tumor monitoring.

Still, the ultimate detection sensitivity of ELISA is not good enough to tackle this challenge, especially in the early stages of the disease progression. Therefore, there is significant clinical relevance to increase the sensitivity of ELISA without modifying the basic workflow (applicable to any existing ELISA setup).

Basically, the sensitivity of an ELISA depends on two factors:

a) The immunoreaction: where the sensitivity relies on the affinity of the Ab to the Ag. In this regard, many advances were reported, such as the big accomplishment in producing monoclonal Abs. Also, introducing biotin–avidin systems provided further improvement.¹⁰⁴

b) The enzymatic signal amplification: Herein, the sensitivity depends on the efficiency of the enzymatic reaction (specificity and kinetics), and the detectable signal of the product.

Continuous efforts have been made in developing substrates for more sensitive response. However, these usually end up with organic chromophores or fluorophores. These organic compounds, either being simple or sophisticated molecules, still suffer from few drawbacks:

- Under light exposure, they may go through undesired photochemical reactions, leading to the destruction of the dye, and instability of the signal.
- For fluorescent compounds, the energy difference between the absorption and the emission (Stokes' shift) is very low, so that the absorption and emission spectra notably overlap. This results in the need for efficient filtering to avoid spectral crosstalk between the excitation and emission channels, causing a partial loss of signal intensity.
- Most importantly, in complex biological fluids (such those analyzed by ELISA), the enzymatically amplified signal of organic fluorophores can be interfered by the residual autofluorescence arising from endogenous sample components. Fluorophores have broad emission bands in UV-Vis region, where various biological compounds can emit.

Very few are the strategies that succeeded to improve the sensitivity of ELISA without modifying the basic workflow.¹⁰⁵ However, enzyme amplified lanthanide luminescence is a strategy that have achieved transcendent success in this regard.

3. Enzyme amplified lanthanide luminescence

3.1. Definition of lanthanides

Lanthanides (lanthanoids) are the series of 15 chemical elements having atomic numbers from 57 “Lanthanum” to 71 “Lutetium” (Figure 17). These elements, along with the chemically similar “Scandium” and “Yttrium”, are commonly called “rare earth” elements.¹⁰⁶

Period	Group	1	2	3	4	5	6	7	8	9	10	11	12	13	14	15	16	17	18	
1		H 1.008																	He 4.003	
2		Li 6.941	Be 9.012											B 10.81	C 12.01	N 14.01	O 16	F 19	Ne 20.18	
3		Na 22.99	Mg 24.31											Al 26.98	Si 28.09	P 30.97	S 32.07	Cl 35.45	Ar 39.95	
4		K 39.10	Ca 40.08	Sc 44.96	Ti 47.88	V 50.94	Cr 52	Mn 54.94	Fe 55.85	Co 58.47	Ni 58.69	Cu 63.55	Zn 65.39	Ga 69.72	Ge 72.59	As 74.92	Se 78.96	Br 79.9	Kr 83.8	
5		Rb 85.47	Sr 87.62	Y 88.91	Zr 91.22	Nb 92.91	Mo 95.94	Tc (98)	Ru 101.1	Rh 102.9	Pd 106.4	Ag 107.9	Cd 112.4	In 114.8	Sn 118.7	Sb 121.8	Te 127.6	I 126.9	Xe 131.3	
6		Cs 132.9	Ba 137.3	La 138.9	Hf 178.5	Ta 180.9	W 183.9	Re 186.2	Os 190.2	Ir 192.2	Pt 195.1	Au 197	Hg 200.5	Tl 204.4	Pb 207.2	Bi 209	Po (210)	At (210)	Rn (222)	
7		Fr (223)	Ra (226)	Ac (227)	Rf (257)	Db (260)	Sg (263)	Bh (262)	Hs (265)	Mt (266)	Ds (271)	Rg (272)	Uub (285)	Uut (284)	Uuq (289)	Uup (288)	Uuh (292)	Uus 0	Uuo 0	
	6				58 Ce 140.1	59 Pr 140.9	60 Nd 144.2	61 Pm (147)	62 Sm 150.4	63 Eu 152	64 Gd 157.3	65 Tb 158.9	66 Dy 162.5	67 Ho 164.9	68 Er 167.3	69 Tm 168.9	70 Yb 173	71 Lu 175		
	7				90 Th 232	91 Pa (231)	92 U (238)	93 Np (237)	94 Pu (242)	95 Am (243)	96 Cm (247)	97 Bk (247)	98 Cf (249)	99 Es (254)	100 Fm (253)	101 Md (256)	102 No (254)	103 Lr (257)		

Figure 17: Periodic table of the chemical elements.¹⁰⁷

In 1787, a Swedish artillery officer and amateur geologist, Lieutenant Carl Axel Arrhenius visited the Ytterby Mine and noticed an unusual black stone which occurred in narrow layers through the mineral quartz beds.¹⁰⁸ For a complete chemical analysis of his black stone, Arrhenius turned to Johan Gadolin, a Finnish mineralogist-chemist. It was in 1794 that Gadolin succeeded to isolate a novel oxide from the mineral and concluded it was a new earth. He named that oxide “yttria”, and the mineral was named “gadolinite” for him.

Later in 1842, Mosander further separated other oxides from Yttria and named the fractions “erbia”, “terbia” and “ytterbia”, which in turn led to the separation of more of the rare earths.

Due to their very similar chemical properties, the isolation of these elements faced serious difficulties. Most famously in the case of thulium, where 15 000 operations of fractional crystallization were necessary to remove the last traces of erbium.¹⁰⁹ Later, new separation methods were developed, notably cation-exchange chromatography, that are based on the small difference in the stability of lanthanide chelates.¹¹⁰ Such separations work very well on the small scale but on the industrial scale, solvent extraction is the preferred technique.¹¹¹

3.2. Properties of lanthanides

The lanthanides belong to the same period and the same group of the periodic table. They are classified as f block elements due to the filling up of their 4f orbitals.

The general electronic configuration of a lanthanide (Ln) is:



Even though the 4f orbitals have higher energy levels, they are closer to the nucleus than 5s, 5p and 6s orbitals which are already filled (Figure 18). Interestingly, this configuration is the source of all the physical, chemical, magnetic and optical properties of lanthanides.¹¹²

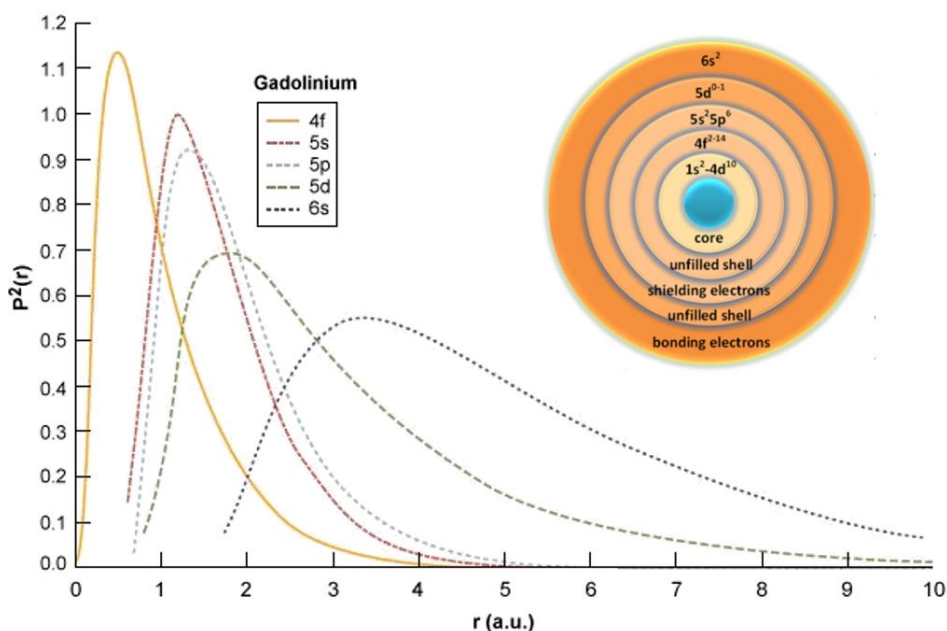


Figure 18: Electron probabilities $P_2(r)$ for the 4f, 5s, 5p, 5d and 6s subshells in Gadolinium (Gd).¹¹³

3.2.1. Chemical properties

Each lanthanide differs from the one immediately before in having one or more electrons in the 4f (with some exceptions) and an extra proton in the nucleus of the atom. However, increasing their atomic number is accompanied by a decrease in the atomic radius which is called lanthanide contraction. In fact, inner 4f orbitals are very diffused ones, and are rather ineffective in screening the nucleus. As the atomic number increases, the nuclear charge increases without significant increase in screening effect. This leads to a gradual increase in the attraction of the nucleus to the electrons in the outer shell, and a consequent contraction in the ionic radius.¹¹⁴

Thanks to their electronic structure, Ln are highly electropositive elements that are very prone to lose 3 electrons. Therefore, their most stable oxidation state is +III with electronic configuration $[\text{Xe}]4f^n$. 4f electrons are shielded from external interactions by the outer $5s^2$ and $5p^6$ filled orbitals in the Xenon core. Thus, these orbitals are not usually involved in bonding and are even very little influenced by the external environment. Consequently, Ln^{3+} ions display similar chemical properties regardless of the number of electrons in these orbitals. They are also able to preserve these properties without being affected by changes in their environment such as solvents or other conditions.¹¹²

The stability of the trivalent state results from the very large fourth ionization potential. Exceptionally, Ce can form +IV compounds, whereas Eu and Yb, which have large third ionization energy, can form +II compounds instead. The properties of these cations are very different from those of the trivalent Ln.¹¹⁵

3.2.2. Magnetic properties

In an incomplete 4f orbital, electrons are either single or partially paired. The magnetic effects of the different electrons cannot be canceled out. Consequently, all Ln, except Lutetium and Lanthanum, are highly paramagnetic.¹¹⁶ Interestingly, the magnetic properties are weakly dependent on the environment.

Hence, Ln find application as materials for the manufacture of superconductors, high coercivity magnets... but also at the molecular level in magnetic resonance imaging (Gd complexes as contrast agents), or magnetic probes for other biological applications.¹¹⁷

3.2.3. Optical properties:

Electronic transitions involving lanthanide ions are of different kinds:

- Interconfigurational 4f-5d transitions when a 4f electron is moved into an empty 5d orbital. These transitions are energetic and usually occur at $\lambda < 250$ nm.¹¹⁸
- Intraconfigurational 4f-4f transitions featuring rearrangement of the electrons within the 4fⁿ orbital. From these transitions, arise exceptional optical properties of Ln.

a) Energy levels of 4fⁿ

To study the 4f-4f transitions, it is important to understand the split for 4fⁿ electronic configuration that generates the different energy levels for electron filling of the 4f orbitals.¹¹⁹ This phenomenon is a result of several interactions within the ion, as clarified in Figure 19, where Eu³⁺ ion is taken as an example.

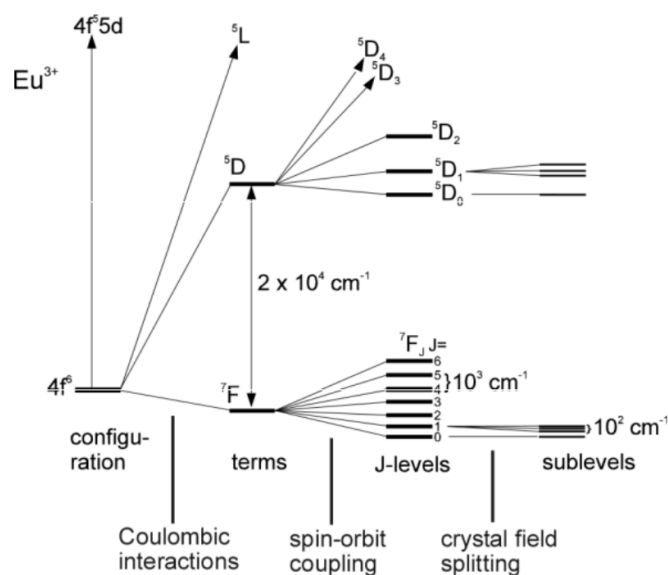


Figure 19: The interactions leading to the electronic energy levels for the $[Xe]4f^6$ configuration of Eu^{3+} .¹²⁰

The Coulombic interaction is the largest and represents the electron-electron repulsions within the 4f orbitals. It yields terms “L” with a separation in the order of 10^4 cm^{-1} . These terms are in turn split into several J-levels by spin-orbit coupling, which is relatively large (10^3 cm^{-1}) because of the heavy Ln nucleus. These interactions define the free ion levels that are described by the term symbols $(2S+1)L_J$. $2S+1$ represents the total spin multiplicity, L the total orbital angular momentum and J the total angular momentum of the f electrons.

When present in a coordinating environment, such as a crystal or an organic ligand, the individual J-levels are further split up by the electric field of the matrix, which is usually referred to as the crystal field. Due to the shielding effect by the outer orbitals, the crystal field weakly affect the free-ions states (10^3 cm^{-1}) and is only treated as a perturbation (Stark effect).¹²¹ The resulted energy diagram for emissive Ln^{3+} is represented in Figure 20.

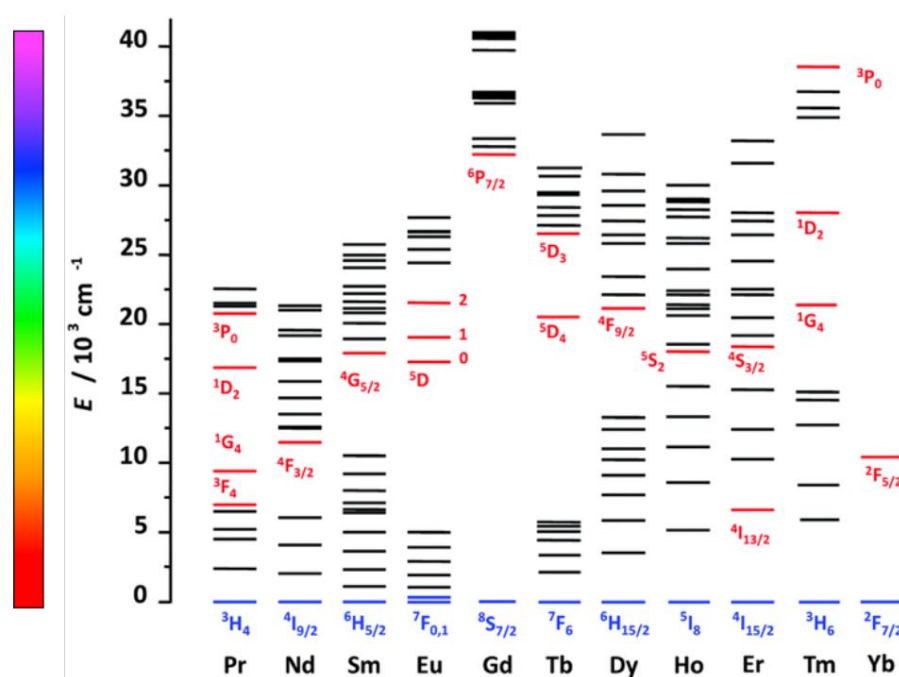


Figure 20: Partial energy diagrams for the Ln^{3+} ions. The red and blue lines indicate the main luminescent and the fundamental levels, respectively.¹²²

b) Radiative 4f-4f transition

The 4f energy levels are well defined, shielded and have little interaction with the chemical environment of the ion. Therefore, an intraconfigurational 4f-4f transition induces sharp absorption and emission spectra, resulting in specific spectroscopic signature for each lanthanide. Their emission lines cover the entire spectrum, from UV (Gd^{3+}) to Vis (Sm^{3+} , Eu^{3+} , Tb^{3+} and Dy^{3+}) and NIR (Tm^{3+} , Nd^{3+} , Ho^{3+} , Er^{3+} and Yb^{3+}) spectral ranges, while some ions are simultaneous visible and NIR emitters (Figure 21). Judged by energy gap criterion, Eu^{3+} , Tb^{3+} and Gd^{3+} ions have the strongest luminescence.

However, La^{3+} and Lu^{3+} do not possess luminescent properties because their 4f orbitals are empty or full. On another hand, Pm^{3+} has a potential for luminescence properties, but this element is radioactive and does not have a stable isotope.

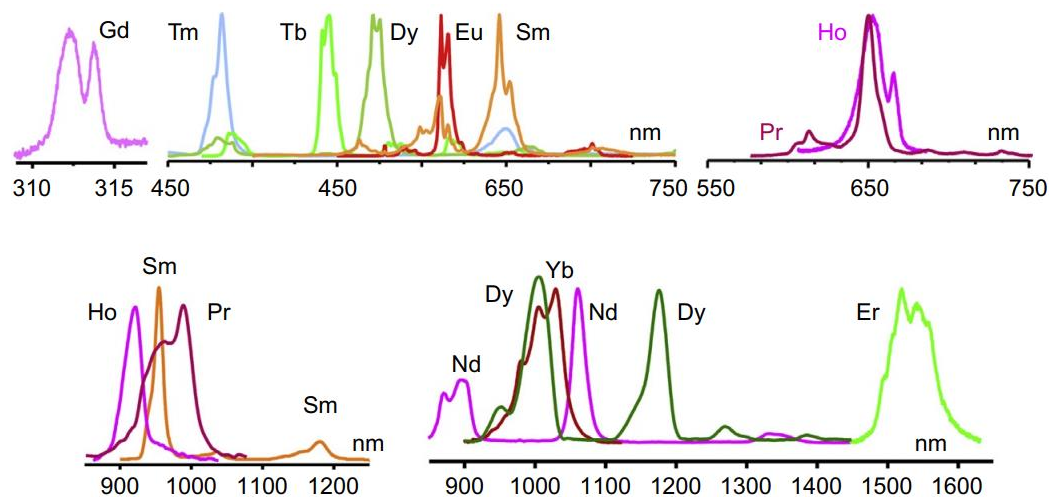


Figure 21: Normalized emission spectra of luminescent Ln^{3+} ions.¹²³

A transition between two electronic states is achieved either between electric dipoles (EDs), magnetic dipoles (MDs), or electric quadrupoles (EQs). Laporte parity selection rule implies that states with the same parity cannot be achieved by ED transitions, so as a free Ln^{3+} f-f transitions are forbidden by the ED mechanism.

However, in a coordinating environment, the ligand field allows the mixing of electronic states of opposite parity into the $[\text{Xe}]4f^n$ configuration, which relaxes the selection rules and the transitions become partially allowed.¹²⁴ They are called induced EDs. MDs are allowed, but their intensity is weak. EQs are also allowed, but they are even weaker than MDs so that they are usually not observed or identified.¹²⁵ Figure 22 shows a comparison between purely MD transition of Eu^{3+} , and induced ED one.

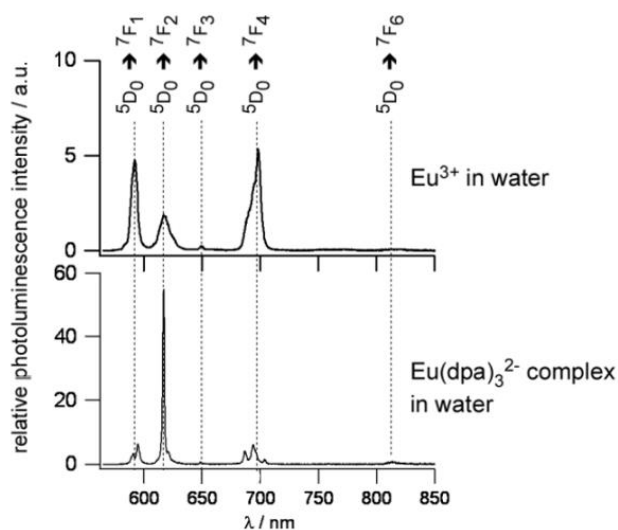


Figure 22: Emission spectra of the Eu^{3+} ion in different environments.¹²⁶

Overall, the probability of the 4f–4f transitions to happen remains relatively weak, in both directions. With molar absorption coefficients typically less than $10 \text{ M}^{-1}\text{cm}^{-1}$, it is very difficult to directly excite a Ln^{3+} ion unless a powerful source of energy is used (laser). Under light exposure, Ln^{3+} ions show high resistance to photobleaching and photochemical degradation because 4f electrons do not play a role in chemical bonding, so no chemical bond can be broken in the photocycle. Once excited, the return to the ground state is a disadvantaged pathway and this results in a very long lifetime of the excited state of a Ln^{3+} ion, and so very long luminescence lifetime.

c) Photosensitization of Ln luminescence

In 1942, Weissman discovered that the luminescence of Eu^{3+} ions could be strongly enhanced in the presence of some specific organic aromatic ligand.¹²⁷ Interestingly, the excitation spectrum showed a maximum at wavelengths where the ion does not absorb. However, it perfectly matched the excitation spectrum of the introduced ligand. That confirmed that the excitation was a multistep process with absorption of the ligand, energy transfer to Eu^{3+} followed by its emission (Figure 23). That process is known as “antenna effect”.¹²⁸

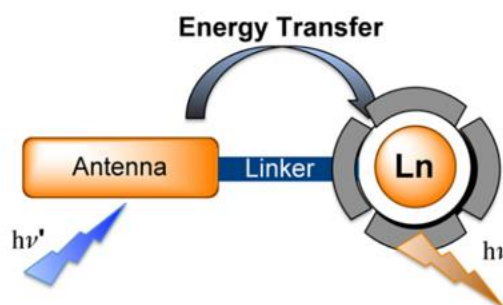


Figure 23: Descriptive of antenna effect.¹²⁹

The antenna is a heteroaromatic compound designed to coordinate to the Ln^{3+} ion providing very high absorption through the aromatic moieties. The standard mechanism of antenna effect is described in the Jablonski diagram shown in Figure 24. The process starts with the absorption of photons by the ligand, passing to its excited state S_1 . Normally, the most favorable pathway of de-excitation is going back to S_0 through fluorescence of the ligand. But the presence of a Ln^{3+} ion favors an intersystem crossing, initially spin forbidden, to the triplet state T_1 (heavy atom effect).¹³⁰ In case where the T_1 of the ligand and the excited state of the Ln^{3+} ion are appropriately placed, an energy transfer occurs. The excited Ln^{3+} ion returns to its ground state by exhibiting its characteristic luminescence.

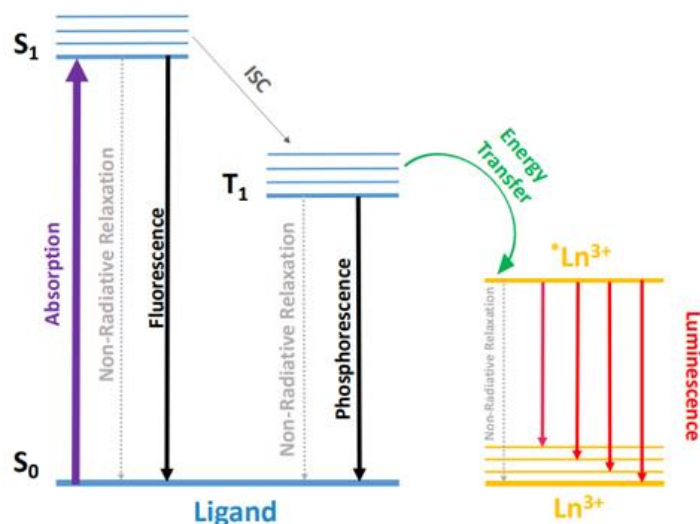


Figure 24: Jablonski diagram detailing the mechanism of energy transfer from the ligand to the Ln^{3+} ion.

Interestingly, while the excitation of the ligand is generally performed in the UV to blue spectral region, emission is observed in the visible or NIR domain. This difference called “pseudo-Stokes’ shift” is large, so there is no need for efficient filtering between the excitation and emission channels.

The luminescent quantum yield is the number of emitted photons per number of absorbed photons and is often determined by a comparison method with a known quantum yield.¹³¹

$$Q = \frac{\text{Number of emitted photons}}{\text{Number of absorbed photons}} \quad \text{Equation 1}$$

The efficiency of the photosensitization “ η_{sens} ” is determined by the ratio of the external quantum yield “ Q_{ext} ” of a Ln^{3+} complex obtained upon ligand excitation, to the intrinsic quantum yield Q_{int} of the Ln^{3+} ion obtained by direct excitation of the Ln f-f transition.

$$\eta_{\text{sens}} = \frac{Q_{\text{ext}}}{Q_{\text{int}}} \quad \text{Equation 2}$$

Energy transfer typically occurs by Förster or Dexter mechanisms.^{132,133} The first is based on the electrostatic interaction between dipole moments of the donor and the acceptor, whereas the second relies on double electron transfer.¹³⁴ It is not that important to distinguish between these mechanisms as long as an efficient transfer is achieved.

This efficiency strongly depends on the donor-acceptor distance to the inversed sixth power, thus a close contact between the ligand and the Ln^{3+} ion is mandatory for an efficient sensitization.

Assuming a good coordination of the ligand to the Ln^{3+} ion, the other key to an efficient sensitization is the energy gap between the T_1 of the ligand and the emissive state of Ln^{3+} ion. It must be close enough to allow the transfer ($<5000 \text{ cm}^{-1}$) but far enough to avoid back energy transfer to the ligand ($>1700 \text{ cm}^{-1}$).¹³⁵

d) Lanthanide spectral conversion

The photosensitization of Ln allows the excitation of the ligand with high-energy photon in the UV to blue region, while the emission is observed at lower energy in the visible or NIR. This conversion following Stokes' spectral shift is known as a downshifting mechanism. Thanks to their ladder-like energy levels and their long excited state lifetime, lanthanides are able to perform other spectral conversion types illustrated in Figure 25.

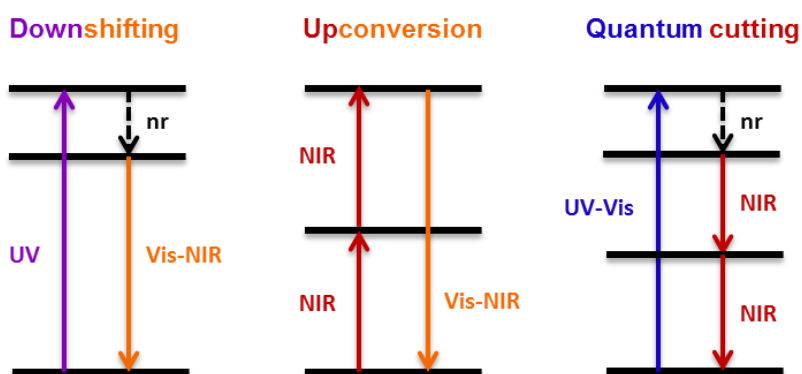


Figure 25: Schematic representation of different Ln spectral conversion mechanisms.

The upconversion is an optical phenomenon following anti-Stokes' spectral shift. It is based on the sequential absorption of two or more low-energy photons (NIR), reaching higher excitation energy level and leading to the emission at shorter wavelength in the visible range.¹³⁶ This phenomenon is an interesting tool for biological imaging thanks to the deep penetration of NIR light in tissues with minimal absorption of the biological medium components, thus reducing the background noise.¹³⁷

In quantum cutting (or downconversion), one incident high-energy photon generates multiple low-energy photons following Stokes' spectral shift. This mechanism found one of its first applications in the lighting industry, then appeared to notably contribute to the next generation of photovoltaic (PV) technologies by converting visible photons into several near-infrared (NIR) photons in order to minimize the energy losses in the PV modules.¹³⁸

e) Non radiative relaxation of Ln

The excited states of lanthanide ions do not decay solely by radiative processes. Nonradiative relaxation is a generally occurring process, and therefore Q_{int} is always less than 1. If k_r represents the rate of the radiative processes and k_{nr} that of nonradiative processes, the intrinsic quantum yield is given by equation 3.

$$Q_{int} = \frac{k_r}{k_r + \sum k_{nr}} \quad \text{Equation 3}$$

States that lie only slightly higher than the luminescent state of Ln^{3+} ion can, with the aid of thermal activation, provide an alternative deactivation path in a back energy transfer and contribute to k_{nr} . Other nonradiative relaxations are mediated by matrices containing high-energy vibrations such as organic media and aqueous solutions. In these conditions, H_2O molecules can exist in the first or second coordination spheres of the Ln^{3+} complex. Through vibrational energy transfer, O-H oscillators can deactivate Ln^{3+} luminescence because of the matching gap between their vibrational energy levels and the Ln^{3+} emissive state. This results in a decrease in both the intensity and the lifetime of the Ln emission, a phenomenon called “quenching” of the lanthanide luminescence.

O-H, N-H and C-H oscillators are the most effective quenchers in solution.¹³⁹ The latter become an issue when they exist in the Ln^{3+} complexing ligand. So for a Ln^{3+} complex to be more luminescent in aqueous solution, it needs a ligand with minimal quenching oscillators, well designed for an optimal protection of Ln^{3+} ion and efficient exclusion of H_2O molecules and other organic chelates from the first coordination spheres. This will decrease nonradiative relaxations and improve the quantum yield of the emission.

The brightness of the emissive complex is related to the product of its molar absorption coefficient “ ϵ ” by the overall (external) quantum yield “ Q_{ext} ” as described in equation 4.

$$B = \epsilon(\lambda_{exc}) \times Q_{ext} \quad \text{Equation 4}$$

By significantly improving its absorption, an appropriate antenna allows to boost the low brightness of Ln^{3+} ions.

Exchanging O-H for O-D usually leads to a dramatic increase in observed lifetime and quantum yield of the luminescence. O-D is a lower energy vibration, and a less efficient quencher. Selective deuteration of the surrounding matrix (D_2O) provides a way to study the contributions of different vibrations to k_{nr} .¹⁴⁰

3.3. Coordination chemistry of lanthanides

Ln^{3+} ions are classified as "hard" Lewis acids, so they have binding affinity to ligands with rich electron donor atoms (O, N, halogens). It is generally agreed that this Ln^{3+} -ligand coordination occurs predominantly by ionic interactions because the 4f valence electrons are not readily available for bonding.¹⁴¹ Therefore, Ln^{3+} ions have strong preference for negatively charged donor groups such as carboxylate, phosphonate, and neutral donors that possess large ground-state dipole moments such as amide carbonyl oxygens.

Due to the electrostatic character of the interaction, there is little or no stereochemical directionality in the Ln^{3+} -ligand coordination. Therefore, the geometry of coordination as well as the primary coordination numbers depend almost entirely on the ligand characteristics (steric properties and donor groups). With a suitable design of the ligand, lanthanide complexes can exhibit coordination numbers ranging from 3 to 12, with 8 (37%) and 9 (26%) being the most common. Complexes with coordination numbers of 6 (9%), 7 (8%), and 10 (11%) are also represented. Coordination numbers 3 to 5 occur with bulky ligands, but there are few examples. While complexes with polydentate macrocyclic ligands, coronands, cryptands, calixarenes, and acyclic and cyclic Schiff bases have coordination numbers that often extend to 11 and 12.¹⁴²

The only Ln^{3+} property of importance in this regard is the ionic radius. Due to the lanthanide contraction, the coordination number decreases when the atomic number increases.

Figure 26 presents examples of Ln^{3+} complexes with classic triazacyclononane chelate exhibiting weak brightness (A) or photosensitized by terpyridine polyacid chelate (B).

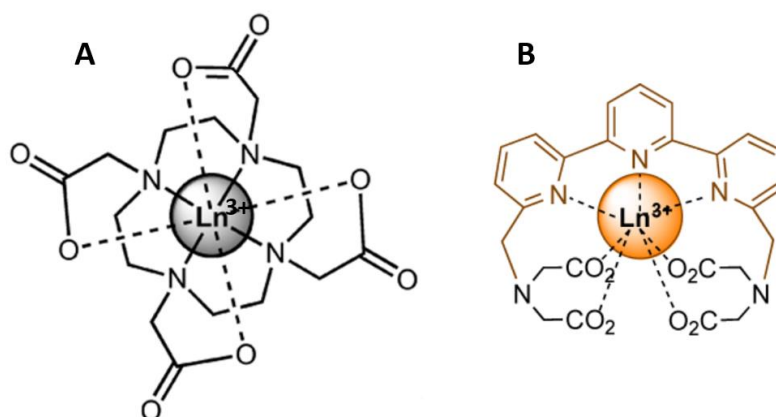


Figure 26: Examples of Ln^{3+} complexes with classic chelating ligand (A) and antenna ligand (B).¹²⁹

3.4. Luminescence applications of lanthanides

a) Lighting and display

The tunable excitation and enhanced absorption of lanthanide complexes showed great potential in applications as phosphors such as in lighting (fluorescent lamp, color televisions, optical amplifiers, LED and organic light emitting diode OLED), display (cathode ray tube, CRT) and many other optical applications.¹⁴³

b) Light conversion applications

Solar cells can harvest sunlight and convert it to electricity, in a promising green technology. Though great advances in this field, the efficiency of solar cells are not satisfying compared to their cost. One of the main reasons is the poor match of the cells band gap with the entire solar spectrum. The energy beyond the band gap is not efficiently harvested. Luminescent lanthanide complexes can be applied to improve this efficiency by converting short/long wavelength to visible/NIR light as great downshifting/upconversion agents.¹⁴⁴

c) Sensing and bio-imaging

The long luminescence lifetime and large Stokes shift of lanthanide complexes, together with enhanced absorption and tunable luminescence, make them quite unique and beneficial for application in sensing and bio-imaging. Much work has been done using lanthanide complexes for sensing anions, cations, small molecules,¹⁴⁵ temperature,¹⁴⁶ viscosity¹⁴⁷ and UV light.¹⁴⁸ They are also utilized in luminescence imaging,¹⁴⁹ photodynamic therapy,¹⁵⁰ and many other bioanalytical applications.¹⁵¹

Some of the main luminescence applications of lanthanides are presented in figure 27.

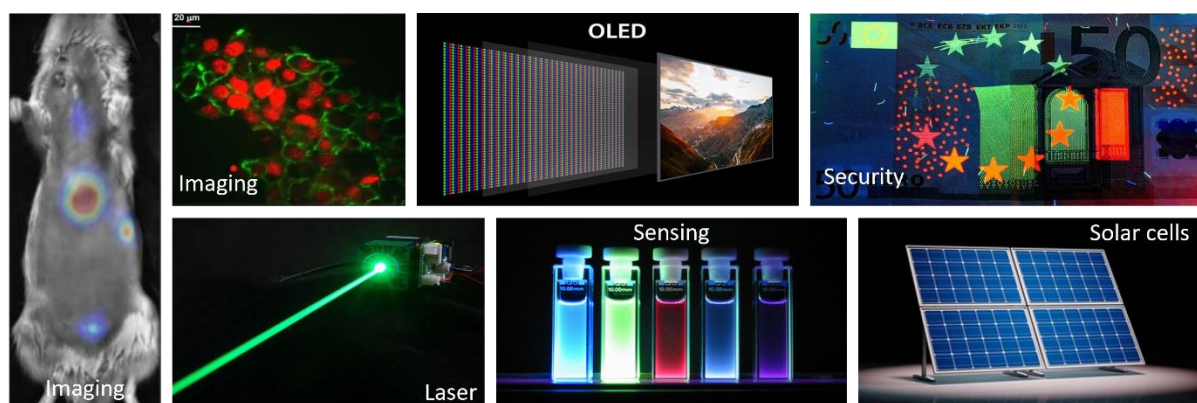


Figure 27: Different luminescence applications of lanthanides.

3.5. Lanthanides application in bioassays

3.5.1. Time resolved luminescence detection

Luminescence processes do not occur on the same timescale. The emission of different species can have different decay rates depending on the excited state lifetime of each species.

The luminescence of a long-lived species can be selectively detected by applying a delay between the pulsed excitation and the acquisition of the emission. This delay allows a complete decay of the fluorescence of unwanted short-lived species, before recording the targeted long-lived emission. This so called “time resolved (or gated) detection” allows then a background free detection of molecules with long luminescence lifetime. The principle of time-resolved detection is described in Figure 28.

This technique is particularly exploited for detection in biological samples, where typical background is due to short-lived residual autofluorescence of organic molecules. A sufficiently long-lived luminescent entity can serve as a label in bioassays for high sensitivity, such as in time-resolved fluoroimmunoassay. An appropriate long-lived label has an emission lifetime in the microsecond to millisecond range, while a theoretical delay in the order of 10–100 ns after the excitation is sufficient to reduce all organic background intensities and significantly improve the signal to noise ratio.¹⁵²

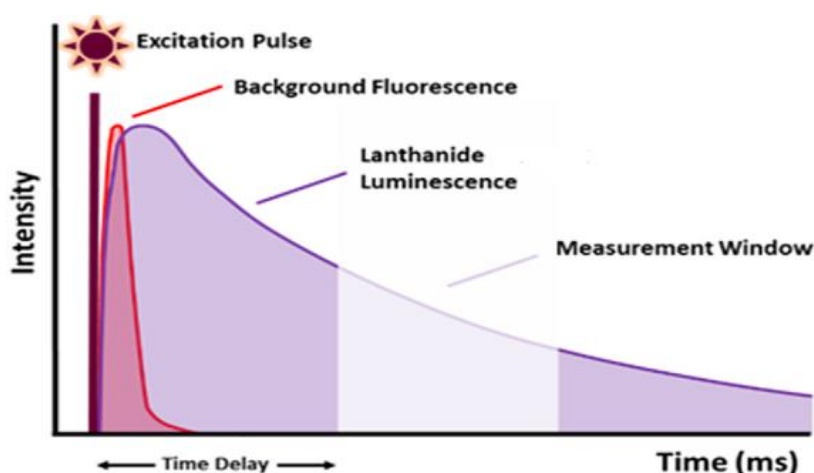


Figure 28: Principle of time-resolved detection.¹⁵³

As mentioned, lanthanides have an extremely long luminescence lifetime up to the millisecond for some of them. Therefore, lanthanide complexes were the most used in time resolved fluoroimmunoassay and many other time-resolved applications.^{154,155}

3.5.2. Enzyme amplified lanthanide luminescence

Time resolved luminescence detection of lanthanides and the enzymatic amplification are two independent strategies used to improve the sensitivity of immunoassays, as described in part 1.4 of this chapter. The first relies on the unique luminescence properties of lanthanides with the suppression of background noise while the second aims to amplify the specific signal. Therefore, the combination of these two strategies seemed a highly promising approach. It consists in the enzyme-catalyzed formation of a ligand, which is, in contrast to the substrate, able to chelate and photosensitize Ln^{3+} ions. The luminescence of the formed complex is selectively measured by time-resolved detection. This strategy is called enzyme-amplified lanthanide luminescence (EALL). It can be used to simply detect enzymatic conversions where the enzyme is the analyte to detect, but it is also capable of detecting affinity reactions (Ab-Ag) in assays where the enzyme is used as a label as in ELISA.¹⁵⁶

One disadvantage is the requirement for an additional signal development step compared with conventional ELISA assays. It consists of the addition of lanthanide ions, usually with Ln chelates to form the luminescent complexes. However, this extra step should not be an obstacle in an automated analyzer system.

The first EALL was reported in 1991 by Evangelista *et al.*¹⁵⁷ They developed a method for the determination of alkaline phosphatase enzyme (AP) using 5-fluorosalicylic phosphate as a substrate. The product of the enzymatic reaction, 5-fluorosalicylic acid, is detected as a luminescent complex with Tb and EDTA at basic pH, as described in Figure 29.

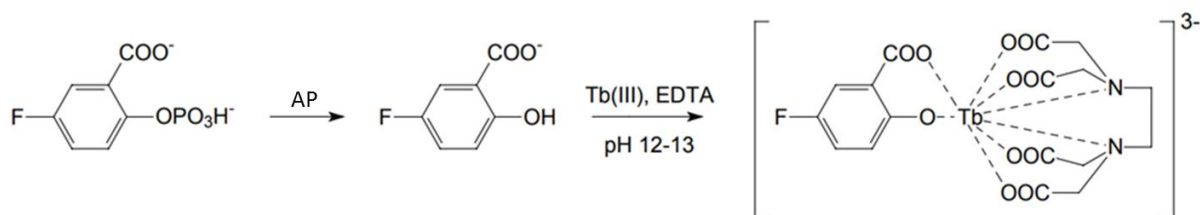


Figure 29: Example of EALL. Enzymatic formation of salicylic acid followed by Tb^{3+} photosensitization.¹⁵⁷

The method was then applied in a model immunoassay for Rat IgG with alkaline phosphatase as marker. The reaction can be normally followed by monitoring the blue fluorescence of the dephosphorylated organic product, but the sensitivity is much inferior compared with time-resolved detection of the formed Ln complex.

Salicylic acid derivatives were continuously used for different enzymes such as xanthine oxidase and β -galactosidase. Both forming salicylic acid which showed to be an efficient chelating antenna for Tb.¹⁵⁷ For glucose oxidase enzyme detection, 1,10-phenanthroline-2,9-dicarboxylic acid dihydrazide substrate was used. When enzymatically oxidized, it liberates the carboxylic acid groups and becomes able to form a luminescent complex with Eu.¹⁵⁷

Later, other attempts were made by using different enzymes and substrates. Zheng et al described an EALL method using p-hydroxybenzoic acid as substrate for Hemin catalysis.¹⁵⁸ A dimer was formed and detected by means of Tb luminescence at basic pH (Figure 30). This method has been applied for the determination of tuberculosis Abs.

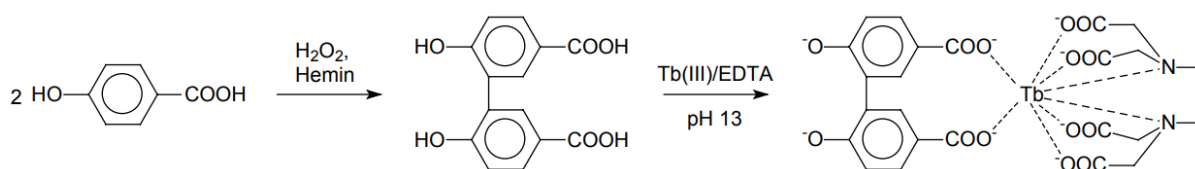


Figure 30: Example of EALL. Enzymatic dimerization followed by Tb³⁺ photosensitization.¹⁵⁸

Tb and Eu demonstrated to be the best fit for EALL application due to their compatibility with the products of the enzymatic reactions and their particularly strong long-lived luminescence in the visible region.

EALL then highlighted important flexibility, as substrates can be designed for a variety of enzymes.¹⁵⁹ Some enzymes were not familiar with protein conjugation to be used as bioassay labels, which limited their application.¹⁶⁰⁻¹⁶²

Thanks to the very high amplification factors possible using enzyme labels, EALL has demonstrated the best single label sensitivity compared with other reported time-resolved fluorometric detection methods. Moreover, some EALL detection methods reported a higher sensitivity in comparison to the very sensitive radioisotopic detection.¹⁵⁶

Most developed EALL methods have been performed at alkaline pH, to allow the coordination of the ligand to the lanthanide. However, at high pH, it is required to add EDTA chelate to avoid the formation of insoluble lanthanide hydroxide. This is very unfavorable in terms of sensitivity because the EDTA itself sensitizes Ln to a small extent contributing to the background signal, while excess of EDTA also reduces the efficiency of the sensitization by the antenna. These drawbacks limited their development and commercialization.

4. Lanthanide doped nanoparticles

Lanthanide complexes display highly useful and specific optical properties and are widely used in several applications providing decent performances. Even though, continuous efforts were spent in order to improve the photophysical properties of lanthanides and overcome the few drawbacks to release their full potential.

In the last decade, Ln^{3+} doped nanomaterials have emerged as excellent alternatives to Ln complexes.¹⁶³ It consists in incorporating the Ln^{3+} ions into a stable host material. Since their shielded energy levels are hardly affected by the surrounding environment, they can be incorporated into a wide variety of matrices without reducing their characteristic optical properties. On the contrary, the surrounding crystal field could even lift the parity selection rule, promoting the 4f-4f transitions and giving rise to enhanced optical properties.¹⁶⁴

Particularly, inorganic matrices have been widely studied and applied as host materials and showed high stability and compatibility for Ln^{3+} doping as shown in Figure 31.

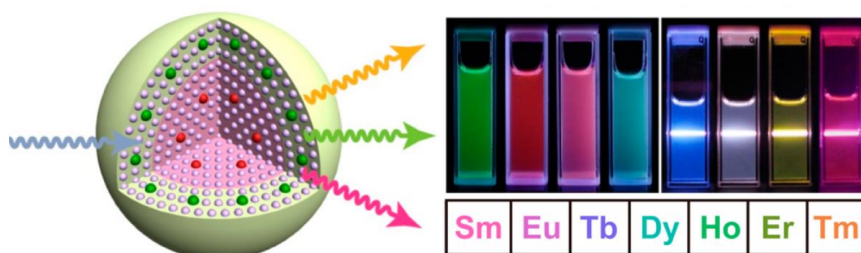


Figure 31: Doping lanthanide ions in an inorganic host material.¹⁶⁵

The most important feature provided by lanthanide nanoparticles (Ln-NPs) is the protection of Ln^{3+} ions from nonradiative deactivations by the vibrations of solvents or chelating molecules. This protection improves the luminescence quantum yield of Ln^{3+} emission.¹⁶⁶

In Ln-NPs, we can distinguish two Ln environments. Ln^{3+} ions in the very external layers can always be influenced by OH, NH and CH oscillators of the surrounding medium and their luminescence can be quenched as for Ln complexes. In contrast, Ln^{3+} ions embedded in the core of the NPs are strongly protected from the surrounding medium. They can still be prone to nonradiative deactivations through impurities of the matrix or energy transfer processes assisted by phonons having the energy of vibration of the host lattice.¹⁶⁷ However, phonons of the lattice are generally of much lower energy than OH, NH or CH oscillators.¹⁶⁸

In some cases, the nonradiative decays can be so small that the observed luminescence lifetimes of the Ln^{3+} ions are close to the radiative lifetimes, affording an almost quantitative lanthanide luminescence quantum yield, as it is observed for some Eu doped NPs.¹⁶⁹

In addition, NPs have a large advantage over Ln complexes in the possibility of mixing different Ln^{3+} ions in the same matrix, especially for upconversion NPs, or for NPs with multiplexing capabilities. The structural design of such NPs can be adapted to optimize the average donor-acceptor distance for improving energy transfer efficiency.¹⁷⁰

Inspired by the properties of lanthanide complexes, several works aimed to connect organic ligands to Ln-NPs for an improved brightness. Significant progress has been made for the engineering and synthesis of ultrabright dye-sensitized Ln-NPs. A basic approach involves a simple coordination of the organic antennas at the NP surface. In this model, the distance between the capping ligand and the doped Ln^{3+} ions can be chemically modulated to improve the energy transfer and the protection of Ln^{3+} ions.¹⁷¹ In other approaches, the entire Ln(III) chelate can be either encapsulated into the host material or grafted on the surface.¹⁷² The three strategies for the design of dye-sensitized Ln-NPs are described in Figure 32.

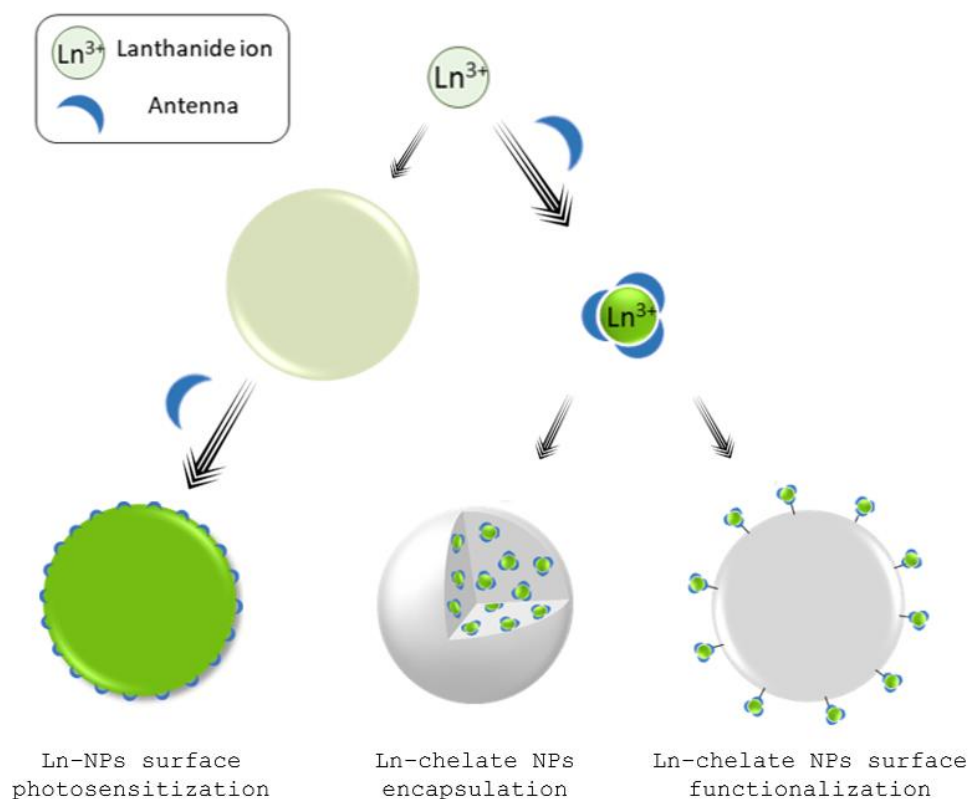


Figure 32: Representation of the three strategies for the design of dye-sensitized Ln-NPs.¹⁷³

These approaches allow cumulating the spectroscopic performances of lanthanide complexes. Each type of dye-sensitized Ln-NPs has its advantages and limitations that make it the most suitable depending on the application. For example, the luminescence of Tb³⁺ ions in doped NPs with surface capping antennas can reach higher lifetimes (up to 8.3 ms – quite close to the radiative lifetime¹⁷⁴) in comparison with Ln-chelate encapsulated NPs (2.06 ms) and Ln-chelate surface functionalized NPs (1.66 ms).¹⁷³ Embedding Ln³⁺ ions in the core of the NPs while capped with well-designed ligands clearly affords the better protection from nonradiative deactivations.

The study of Ln-NPs became a highly interdisciplinary field that has been rapidly expanding at the frontiers of material sciences, photochemistry, and biophysics. The characteristics of these NPs, such as size, shape, doping rate, optical emission, and surface properties, are fundamental factors that ultimately influence their application.

For biological applications, these NPs must be bright, small sized (*in vivo* application), water dispersible, practical for surface functionalization and stable in water and biological medium for long duration. Many studies reported luminescent Ln-NPs sensitized by capping organic antennas showing evidence for the energy transfer from the ligands at the surface to the doped Ln³⁺ ions.¹⁷⁵ However, most of these studies were performed in organic solvents.

Charbonnière *et al.* were first to report in water sensitization of 5% Eu-doped LaF₃-AEP (AEP for aminoethyl-phosphate) NPs by partial AEP exchange with 6-carboxy-5'-methyl-2,2'-bipyridine.¹⁷⁶ Later in the same group, Goetz *et al.* reported the sensitization of 10% Tb-doped LaF₃ using eleven different ligands derived from dipicolinic acid and 2-hydroxyisophthalic acid with varying coordination and photosensitizing abilities.¹⁷⁷ Since then, the SynPA team of Charbonnière reinforced their interest in dye-sensitized Ln-NPs by highlighting several advances in this field. In this regard, great efforts were done by employing different Ln³⁺ ions, many doping strategies and terrific number of designed ligands in order to reach highly bright NPs able to be used in multiple applications.^{178,179}

Globally, dye-sensitized Ln-NPs have found a growing interest in their study and their development, and found multiple applications especially in bioanalytical fields such as in bio-imaging, bioassays, drug delivery and photodynamic therapy.¹⁸⁰

5. Scope of the thesis

The objective of this PhD project was to develop a new ultrasensitive ELISA detection method based on luminescent lanthanide nanoparticles. In the first part above, the project is introduced by describing and connecting the different concepts that constitute the context of this research. A brief literature review also summarized the evolution in this field and allowed to define the limitations that actually inspired and led to this work.

The main idea was to exploit the exceptional properties of Ln^{3+} doped NPs to overcome the limitations of commercial detection methods typically based on organic chromophores or fluorophores. Several studies have already tried to employ the lanthanides in immunoassays for sensitive time resolved detection. It started with using Ln complexes as a direct label such as the successful dissociation-enhanced lanthanide fluorescence immunoassay (DELFI), and then developed by the enzymatic amplification strategy.¹⁸¹ Interestingly, in a comparative study, these approaches were shown to give less variability than ELISA.¹⁸² Some works did use Ln-NPs in immunoassays, but they were limited to the use as single labels.¹⁸³

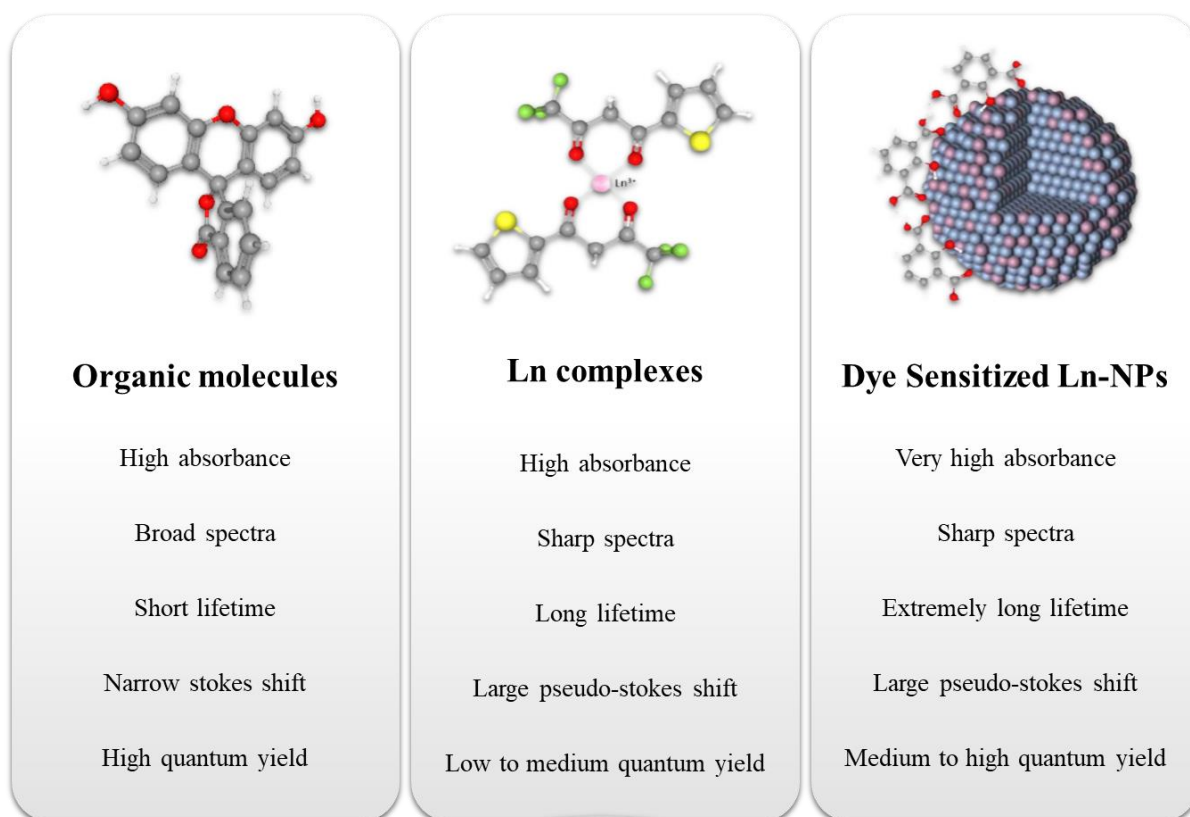


Figure 33: Comparison of luminescence properties between organic molecules, Ln complexes and dye-sensitized Ln-NPs.

Dye-sensitized Ln-NPs can overcome the limitations of organic molecules and Ln-complexes as well. They provide sharp specific emission band with large pseudo Stokes shift and extremely long lifetime (in the ms), enabling very selective and sensitive detection. In comparison with Ln complexes, dye-sensitized Ln-NPs add improvement in brightness and lifetime as well as better stability at larger range of pH enabling better applicability.

Herein, the aim was to use the basic workflow of ELISA, taking advantage of the enzymatic amplification, and combine it with the enhanced spectroscopic properties of lanthanides when doped in inorganic NPs. The principle of the detection method is to employ an enzymatic reaction that converts an inactive substrate into a ligand able to photosensitize Ln-NPs.

Chapter II focuses on the synthesis and the study of Ln-NPs. The targeted NPs were fully characterized for their morphology, size, composition, charge and especially their luminescence properties. Chapters III and IV consist in testing different enzymatic reactions in regard of our purpose. Different enzyme mechanisms are used, and different substrates are evaluated. By a judicious choice of the substrate and the enzymatic reaction, the goal is to transform a substrate which cannot photosensitize the NPs into an active form that can be properly coordinated to the surface of NPs and efficiently sensitize Ln³⁺ ions. For each reaction, the best conditions of buffer, pH, temperature, and concentrations are investigated to optimize both the enzymatic reaction and the NPs sensitization. When showing interesting performance, the system was implemented into an ELISA type immunoassay following the protocol described in Figure 34. The developed detection method was then evaluated for its sensitivity and compared to that of commercial detection method.

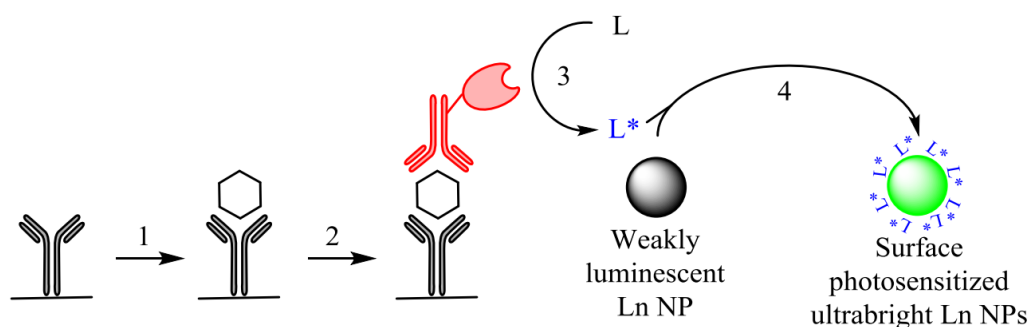


Figure 34: Principle of ELISA with the developed detection method. 1) Fixation of the analyte 2) Recognition by an enzyme-labeled antibody. 3) Enzymatic reaction and formation of the antenna 4) Sensitization of NPs.

Finally, Chapter V presents the general conclusion of this study. The work that has been done is evaluated in regards of the main objectives, highlighting the different contributions, challenges, and future perspectives in this research field.

6. References

- (1) Yalow, R. S.; Berson, S. A. Assay of Plasma Insulin in Human Subjects by Immunological Methods. *Nature* **1959**, *184* (4699), 1648–1649. <https://doi.org/10.1038/1841648b0>.
- (2) *The Nobel Prize in Physiology or Medicine 1977*. NobelPrize.org. <https://www.nobelprize.org/prizes/medicine/1977/summary/> (accessed 2022-09-20).
- (3) Suzuki, F.; Hosaka, T.; Imaizumi, M.; Kobayashi, M.; Ohue, C.; Suzuki, Y.; Fujiyama, S.; Kawamura, Y.; Sezaki, H.; Akuta, N.; Kobayashi, M.; Saitoh, S.; Arase, Y.; Ikeda, K.; Kumada, H. Potential of Ultra-Highly Sensitive Immunoassays for Hepatitis B Surface and Core-Related Antigens in Patients with or without Development of Hepatocellular Carcinoma after Hepatitis B Surface Antigen Seroclearance. *Hepatol. Res.* **2021**, *51* (4), 426–435. <https://doi.org/10.1111/hepr.13602>.
- (4) Yang, X.; Liu, X.; Gu, B.; Liu, H.; Xiao, R.; Wang, C.; Wang, S. Quantitative and Simultaneous Detection of Two Inflammation Biomarkers via a Fluorescent Lateral Flow Immunoassay Using Dual-Color SiO₂@QD Nanotags. *Microchim. Acta* **2020**, *187* (10), 570. <https://doi.org/10.1007/s00604-020-04555-6>.
- (5) Popescu, F.-D.; Vieru, M. Precision Medicine Allergy Immunoassay Methods for Assessing Immunoglobulin E Sensitization to Aeroallergen Molecules. *World J. Methodol.* **2018**, *8* (3), 17–36. <https://doi.org/10.5662/wjm.v8.i3.17>.
- (6) Ates, H. C.; Roberts, J. A.; Lipman, J.; Cass, A. E. G.; Urban, G. A.; Dincer, C. On-Site Therapeutic Drug Monitoring. *Trends Biotechnol.* **2020**, *38* (11), 1262–1277. <https://doi.org/10.1016/j.tibtech.2020.03.001>.
- (7) Squire, K. J.; Zhao, Y.; Tan, A.; Sivashanmugan, K.; Kraai, J. A.; Rorrer, G. L.; Wang, A. X. Photonic Crystal-Enhanced Fluorescence Imaging Immunoassay for Cardiovascular Disease Biomarker Screening with Machine Learning Analysis. *Sens. Actuators B Chem.* **2019**, *290*, 118–124. <https://doi.org/10.1016/j.snb.2019.03.102>.
- (8) Oliveira, J. J.; Karrar, S.; Rainbow, D. B.; Pinder, C. L.; Clarke, P.; Rubio García, A.; Al-Assar, O.; Burling, K.; Morris, S.; Stratton, R.; Vyse, T. J.; Wicker, L. S.; Todd, J. A.; Ferreira, R. C. The Plasma Biomarker Soluble SIGLEC-1 Is Associated with the Type I Interferon Transcriptional Signature, Ethnic Background and Renal Disease in Systemic Lupus Erythematosus. *Arthritis Res. Ther.* **2018**, *20* (1), 152. <https://doi.org/10.1186/s13075-018-1649-1>.
- (9) Nalli, C.; Somma, V.; Andreoli, L.; Büttner, T.; Schierack, P.; Mahler, M.; Roggenbuck, D.; Tincani, A. Anti-Phospholipid IgG Antibodies Detected by Line Immunoassay Differentiate Patients with Anti-Phospholipid Syndrome and Other Autoimmune Diseases. *Autoimmun. Highlights* **2018**, *9* (1), 1–11. <https://doi.org/10.1007/s13317-018-0106-0>.
- (10) Kim, H.; Chung, D.-R.; Kang, M. A New Point-of-Care Test for the Diagnosis of Infectious Diseases Based on Multiplex Lateral Flow Immunoassays. *Analyst* **2019**, *144* (8), 2460–2466. <https://doi.org/10.1039/C8AN02295J>.
- (11) Mohit, E.; Rostami, Z.; Vahidi, H. A Comparative Review of Immunoassays for COVID-19 Detection. *Expert Rev. Clin. Immunol.* **2021**, *17* (6), 573–599. <https://doi.org/10.1080/1744666X.2021.1908886>.
- (12) Van Manen-Brush, K.; Zeitler, J.; White, J. R.; Younge, P.; Willis, S.; Jones, M. Improving Chinese Hamster Ovary Host Cell Protein ELISA Using Ella®: An Automated Microfluidic Platform. *BioTechniques* **2020**, *69* (3), 186–192. <https://doi.org/10.2144/btn-2020-0074>.

- (13) Platchek, M.; Lu, Q.; Tran, H.; Xie, W. Comparative Analysis of Multiple Immunoassays for Cytokine Profiling in Drug Discovery. *SLAS Discov. Adv. Sci. Drug Discov.* **2020**, *25* (10), 1197–1213. <https://doi.org/10.1177/2472555220954389>.
- (14) Jara, M. D. L.; Alvarez, L. A. C.; Guimarães, M. C. C.; Antunes, P. W. P.; de Oliveira, J. P. Lateral Flow Assay Applied to Pesticides Detection: Recent Trends and Progress. *Environ. Sci. Pollut. Res.* **2022**, *29* (31), 46487–46508. <https://doi.org/10.1007/s11356-022-20426-4>.
- (15) Xu, X.; Xu, X.; Wu, A.; Song, S.; Kuang, H.; Xu, C.; Liu, L. Ultrasensitive Detection of Four Organic Arsenic Compounds at the Same Time Using a Five-Link Cardboard-Based Assay. *Food Chem.* **2022**, *390*, 133214. <https://doi.org/10.1016/j.foodchem.2022.133214>.
- (16) Jin, X.; He, R.; Ju, X.; Zhang, J.; Wang, M.; Xing, C.; Yuan, J. Development and Optimization of an Immunoassay for the Detection of Hg(II) in Lake Water. *Food Sci. Nutr.* **2019**, *7* (5), 1615–1622. <https://doi.org/10.1002/fsn3.991>.
- (17) Pöhlmann, C.; Elßner, T. Multiplex Immunoassay Techniques for On-Site Detection of Security Sensitive Toxins. *Toxins* **2020**, *12* (11), 727. <https://doi.org/10.3390/toxins12110727>.
- (18) Ziegler, I.; Vollmar, P.; Knüpfer, M.; Braun, P.; Stoecker, K. Reevaluating Limits of Detection of 12 Lateral Flow Immunoassays for the Detection of *Yersinia Pestis*, *Francisella Tularensis*, and *Bacillus Anthracis* Spores Using Viable Risk Group-3 Strains. *J. Appl. Microbiol.* **2021**, *130* (4), 1173–1180. <https://doi.org/10.1111/jam.14863>.
- (19) Xiao, X.; Hu, S.; Lai, X.; Peng, J.; Lai, W. Developmental Trend of Immunoassays for Monitoring Hazards in Food Samples: A Review. *Trends Food Sci. Technol.* **2021**, *111*, 68–88. <https://doi.org/10.1016/j.tifs.2021.02.045>.
- (20) Fu, L.; Qian, Y.; Zhou, J.; Zheng, L.; Wang, Y. Fluorescence-Based Quantitative Platform for Ultrasensitive Food Allergen Detection: From Immunoassays to DNA Sensors. *Compr. Rev. Food Sci. Food Saf.* **2020**, *19* (6), 3343–3364. <https://doi.org/10.1111/1541-4337.12641>.
- (21) Xu, C.; Kuang, H.; Xu, L. Pathogen Immunoassay in Food. In *Food Immunoassay*; Xu, C., Kuang, H., Xu, L., Eds.; Springer: Singapore, 2019; pp 255–319. https://doi.org/10.1007/978-981-13-9034-0_8.
- (22) Schwickart, M.; Vainshtein, I. Immunoassays. In *Nijkamp and Parnham's Principles of Immunopharmacology*; Parnham, M. J., Nijkamp, F. P., Rossi, A. G., Eds.; Springer: Cham, 2019; pp 243–253. https://doi.org/10.1007/978-3-030-10811-3_15.
- (23) Storey, M.; Jordan, S. An Overview of the Immune System. *Nurs. Stand. R. Coll. Nurs. G. B. 1987* **2008**, *23* (15–17), 47–56; quiz 58, 60. <https://doi.org/10.7748/ns2008.12.23.15.47.c6738>.
- (24) Laustsen, A. H.; Greiff, V.; Karatt-Vellatt, A.; Muyltermans, S.; Jenkins, T. P. Animal Immunization, in Vitro Display Technologies, and Machine Learning for Antibody Discovery. *Trends Biotechnol.* **2021**, *39* (12), 1263–1273. <https://doi.org/10.1016/j.tibtech.2021.03.003>.
- (25) Sadeghalvad, M.; Rezaei, N. *Introduction on Monoclonal Antibodies*; IntechOpen, 2021. <https://doi.org/10.5772/intechopen.98378>.
- (26) Gahan, P. B. Life: The Science of Biology (7th Edn) W. K. Purves, D. Sadava, G. H. Orians and H. C. Heller, W. H. Freeman & Co, 1121 Pp., ISBN 0-7167-9856-5 (2004). *Cell Biochem. Funct.* **2005**, *23* (3), 221–221. <https://doi.org/10.1002/cbf.1179>.
- (27) Chiu, M. L.; Goulet, D. R.; Teplyakov, A.; Gilliland, G. L. Antibody Structure and Function: The Basis for Engineering Therapeutics. *Antibodies* **2019**, *8* (4), 55. <https://doi.org/10.3390/antib8040055>.

- (28) Tsumuraya, T.; Hirama, M. Rationally Designed Synthetic Haptens to Generate Anti-Ciguatoxin Monoclonal Antibodies, and Development of a Practical Sandwich ELISA to Detect Ciguatoxins. *Toxins* **2019**, *11* (9), 533. <https://doi.org/10.3390/toxins11090533>.
- (29) Wild, D.; Kodak, E. *The Immunoassay Handbook*; Elsevier, 2013. <https://doi.org/10.1016/C2010-0-66244-4>.
- (30) Leavy, O. The Birth of Monoclonal Antibodies. *Nat. Immunol.* **2016**, *17* (1), S13–S13. <https://doi.org/10.1038/ni.3608>.
- (31) Serebrennikova, K. V.; Samsonova, J. V.; Osipov, A. P. Enhancement of the Sensitivity of a Lateral Flow Immunoassay by Using the Biotin–Streptavidin System. *Mosc. Univ. Chem. Bull.* **2018**, *73* (3), 131–134. <https://doi.org/10.3103/S0027131418030070>.
- (32) *Biotin and Streptavidin | AAT Bioquest*. <https://www.aatbio.com/catalog/biotin-and-streptavidin> (accessed 2022-08-28).
- (33) Liu, H.; Rong, P.; Jia, H.; Yang, J.; Dong, B.; Dong, Q.; Yang, C.; Hu, P.; Wang, W.; Liu, H.; Liu, D. A Wash-Free Homogeneous Colorimetric Immunoassay Method. *Theranostics* **2016**, *6* (1), 54–64. <https://doi.org/10.7150/thno.13159>.
- (34) Dinis-Oliveira, R. J. Heterogeneous and Homogeneous Immunoassays for Drug Analysis. *Bioanalysis* **2014**, *6* (21), 2877–2896. <https://doi.org/10.4155/bio.14.208>.
- (35) Wild, D. Chapter 1.2 - Immunoassay for Beginners. In *The Immunoassay Handbook (Fourth Edition)*; Wild, D., Ed.; Elsevier: Oxford, 2013; pp 7–10. <https://doi.org/10.1016/B978-0-08-097037-0.00002-6>.
- (36) Wang, X.; Cohen, L.; Wang, J.; Walt, D. R. Competitive Immunoassays for the Detection of Small Molecules Using Single Molecule Arrays. *J. Am. Chem. Soc.* **2018**, *140* (51), 18132–18139. <https://doi.org/10.1021/jacs.8b11185>.
- (37) Hassanpour, S.; Hasanzadeh, M. Label-Free Electrochemical-Immunoassay of Cancer Biomarkers: Recent Progress and Challenges in the Efficient Diagnosis of Cancer Employing Electroanalysis and Based on Point of Care (POC). *Microchem. J.* **2021**, *168*, 106424. <https://doi.org/10.1016/j.microc.2021.106424>.
- (38) Pablo, F. de; Scanes, C. G.; Weintraub, B. D. *Handbook of Endocrine Research Techniques*; Academic Press, 1993.
- (39) Alhabbab, R. Y. Radioimmunoassay (RIA). In *Basic Serological Testing*; Alhabbab, R. Y., Ed.; Techniques in Life Science and Biomedicine for the Non-Expert; Springer: Cham, 2018; pp 77–81. https://doi.org/10.1007/978-3-319-77694-1_11.
- (40) Lakowicz, J. R. Introduction to Fluorescence. In *Principles of Fluorescence Spectroscopy*; Lakowicz, J. R., Ed.; Springer US: Boston, MA, 1999; pp 1–23. https://doi.org/10.1007/978-1-4757-3061-6_1.
- (41) Hemmilá, I.; Mikkala, V.-M. Time-Resolution in Fluorometry Technologies, Labels, and Applications in Bioanalytical Assays. *Crit. Rev. Clin. Lab. Sci.* **2001**, *38* (6), 441–519. <https://doi.org/10.1080/20014091084254>.
- (42) Lei, L.; Peng, L.; Yang, Y.; Han, B. Development of Time-Resolved Fluoroimmunoassay for Detection of Cylindrospermopsin Using Its Novel Monoclonal Antibodies. *Toxins* **2018**, *10* (7), 255. <https://doi.org/10.3390/toxins10070255>.
- (43) Rusanen, J. New Applications for TR-FRET-Based Homogeneous Immunoassays in Diagnosis of Infectious and Autoimmune Diseases, University of Helsinki, 2022.
- (44) Bojescu, E.-D.; Prim, D.; Pfeifer, M. E.; Segura, J.-M. Fluorescence-Polarization Immunoassays within Glass Fiber Micro-Chambers Enable Tobramycin Quantification in Whole Blood for Therapeutic Drug Monitoring at the Point of Care. *Anal. Chim. Acta* **2022**, 340240. <https://doi.org/10.1016/j.aca.2022.340240>.
- (45) Zhao, L.; Sun, L.; Chu, X. Chemiluminescence Immunoassay. *TrAC Trends Anal. Chem.* **2009**, *28* (4), 404–415. <https://doi.org/10.1016/j.trac.2008.12.006>.

- (46) Vo-Dinh, T. Chemiluminescence. In *digital Encyclopedia of Applied Physics*; Wiley-VCH Verlag GmbH & Co. KGaA, Ed.; Wiley: Weinheim, Germany, 2003; p eap063. <https://doi.org/10.1002/3527600434.eap063>.
- (47) Maggio, E. T. *Enzyme Immunoassay*; CRC Press, 2018.
- (48) Sforzi, J.; Palagi, L.; Aime, S. Liposome-Based Bioassays. *Biology* **2020**, *9* (8), 202. <https://doi.org/10.3390/biology9080202>.
- (49) Nakano, K.; Iwami, D.; Yamada, T.; Morita, K.; Yasuda, K.; Shibuya, H.; Kahata, K.; Shinohara, N.; Shimizu, C. Development of a Formula to Correct Particle-Enhanced Turbidimetric Inhibition Immunoassay Values So That It More Precisely Reflects High-Performance Liquid Chromatography Values for Mycophenolic Acid. *Transplant. Direct* **2017**, *4* (1), e337. <https://doi.org/10.1097/TXD.0000000000000754>.
- (50) Chen, X.; Ding, L.; Huang, X.; Xiong, Y. Tailoring Noble Metal Nanoparticle Designs to Enable Sensitive Lateral Flow Immunoassay. *Theranostics* **2022**, *12* (2), 574–602. <https://doi.org/10.7150/thno.67184>.
- (51) Tabatabaei, M. S.; Islam, R.; Ahmed, M. Applications of Gold Nanoparticles in ELISA, PCR, and Immuno-PCR Assays: A Review. *Anal. Chim. Acta* **2021**, *1143*, 250–266. <https://doi.org/10.1016/j.aca.2020.08.030>.
- (52) Clarke, W.; Sokoll, L. J.; Rai, A. J. Chapter 12 - Immunoassays. In *Contemporary Practice in Clinical Chemistry (Fourth Edition)*; Clarke, W., Marzinke, M. A., Eds.; Academic Press, 2020; pp 201–214. <https://doi.org/10.1016/B978-0-12-815499-1.00012-0>.
- (53) Avrameas, S.; Uriel, J. Method of antigen and antibody labelling with enzymes and its immunodiffusion application. *Comptes Rendus Hebd. Seances Acad. Sci. Ser. Sci. Nat.* **1966**, *262* (24), 2543–2545.
- (54) Philips, R. M. & R. *How big is the average protein?* <http://book.bionumbers.org/how-big-is-the-average-protein/> (accessed 2022-08-28).
- (55) Engvall, E.; Perlmann, P. Enzyme-Linked Immunosorbent Assay (ELISA). Quantitative Assay of Immunoglobulin G. *Immunochemistry* **1971**, *8* (9), 871–874. [https://doi.org/10.1016/0019-2791\(71\)90454-x](https://doi.org/10.1016/0019-2791(71)90454-x).
- (56) Van Weemen, B. K.; Schuurs, A. H. W. M. Immunoassay Using Antigen-Enzyme Conjugates. *FEBS Lett.* **1971**, *15* (3), 232–236. [https://doi.org/10.1016/0014-5793\(71\)80319-8](https://doi.org/10.1016/0014-5793(71)80319-8).
- (57) Engvall, E. The ELISA, Enzyme-Linked Immunosorbent Assay. *Clin. Chem.* **2010**, *56* (2), 319–320. <https://doi.org/10.1373/clinchem.2009.127803>.
- (58) Lequin, R. M. Enzyme Immunoassay (EIA)/Enzyme-Linked Immunosorbent Assay (ELISA). *Clin. Chem.* **2005**, *51* (12), 2415–2418. <https://doi.org/10.1373/clinchem.2005.051532>.
- (59) *Enzyme-Linked Immunosorbent Assay (ELISA) Testing Market Size, Report 2021-2030*. <https://www.precedenceresearch.com/enzyme-linked-immunosorbent-assay-testing-market> (accessed 2022-08-28).
- (60) Peng, J.; Song, S.; Xu, L.; Ma, W.; Liu, L.; Kuang, H.; Xu, C. Development of a Monoclonal Antibody-Based Sandwich ELISA for Peanut Allergen Ara h 1 in Food. *Int. J. Environ. Res. Public Health* **2013**, *10* (7), 2897–2905. <https://doi.org/10.3390/ijerph10072897>.
- (61) Peng, J.; Meng, X.; Deng, X.; Zhu, J.; Kuang, H.; Xu, C. Development of a Monoclonal Antibody-Based Sandwich ELISA for the Detection of Ovalbumin in Foods. *Food Agric. Immunol.* **2014**, *25* (1), 1–8. <https://doi.org/10.1080/09540105.2012.716398>.
- (62) Asensio, L.; González, I.; García, T.; Martín, R. Determination of Food Authenticity by Enzyme-Linked Immunosorbent Assay (ELISA). *Food Control* **2008**, *19* (1), 1–8. <https://doi.org/10.1016/j.foodcont.2007.02.010>.

- (63) Schieffelin, J.; Moses, L. M.; Shaffer, J.; Goba, A.; Grant, D. S. Clinical Validation Trial of a Diagnostic for Ebola Zaire Antigen Detection: Design Rationale and Challenges to Implementation. *Clin. Trials* **2016**, *13* (1), 66–72. <https://doi.org/10.1177/1740774515621013>.
- (64) Tarigan, S.; Indriani, R.; Durr, P. A.; Ignjatovic, J. Characterization of the M2e Antibody Response Following Highly Pathogenic H5N1 Avian Influenza Virus Infection and Reliability of M2e ELISA for Identifying Infected among Vaccinated Chickens. *Avian Pathol.* **2015**, *44* (4), 259–268. <https://doi.org/10.1080/03079457.2015.1042428>.
- (65) Luo, J.; Brakel, A.; Krizsan, A.; Ludwig, T.; Mötzing, M.; Volke, D.; Lakowa, N.; Grünewald, T.; Lehmann, C.; Wolf, J.; Borte, S.; Milkovska-Stamenova, S.; Gabert, J.; Fingas, F.; Scholz, M.; Hoffmann, R. Sensitive and Specific Serological ELISA for the Detection of SARS-CoV-2 Infections. *Viol. J.* **2022**, *19* (1), 50. <https://doi.org/10.1186/s12985-022-01768-4>.
- (66) Maters, A. W.; Wright, C. V.; Lee, M. T.; Schwichtenberg, G.; Detrick, B. Detection of Type-Specific Antibodies to HSV-1 and HSV-2: Comparative Analysis of a Chemiluminescence Immunoassay with a Conventional ELISA. *Diagn. Microbiol. Infect. Dis.* **2012**, *73* (3), 273–274. <https://doi.org/10.1016/j.diagmicrobio.2012.03.023>.
- (67) Nandi, S.; Maity, S.; Bhunia, S. C.; Saha, M. K. Comparative Assessment of Commercial ELISA Kits for Detection of HIV in India. *BMC Res. Notes* **2014**, *7* (1), 436. <https://doi.org/10.1186/1756-0500-7-436>.
- (68) Prince, H. E.; Lapé-Nixon, M.; Givens, T. S.; Bradshaw, T.; Nowicki, M. J. Elimination of Falsely Reactive Results in a Commercially-Available West Nile Virus IgM Capture Enzyme-Linked Immunosorbent Assay by Heterophilic Antibody Blocking Reagents. *J. Immunol. Methods* **2017**, *444*, 24–28. <https://doi.org/10.1016/j.jim.2017.02.007>.
- (69) Aria, L.; Acosta, M. E.; Guillen, Y.; Rojas, A.; Meza, T.; Infanzón, B.; Aria, L.; Acosta, M. E.; Guillen, Y.; Rojas, A.; Meza, T.; Infanzón, B. ELISA Chagas Test IICS V.1 Evaluation for the Diagnosis of Chagas Disease. *Mem. Inst. Investig. En Cienc. Salud* **2016**, *14* (3), 7–13. [https://doi.org/10.18004/mem.iics/1812-9528/2016.014\(03\)07-013](https://doi.org/10.18004/mem.iics/1812-9528/2016.014(03)07-013).
- (70) Hunsperger, E. A.; Yoksan, S.; Buchy, P.; Nguyen, V. C.; Sekaran, S. D.; Enria, D. A.; Vazquez, S.; Cartozian, E.; Pelegrino, J. L.; Artsob, H.; Guzman, M. G.; Olliaro, P.; Zwang, J.; Guillerm, M.; Kliks, S.; Halstead, S.; Peeling, R. W.; Margolis, H. S. Evaluation of Commercially Available Diagnostic Tests for the Detection of Dengue Virus NS1 Antigen and Anti-Dengue Virus IgM Antibody. *PLoS Negl. Trop. Dis.* **2014**, *8* (10), e3171. <https://doi.org/10.1371/journal.pntd.0003171>.
- (71) Chin, A. R.; Fong, M. Y.; Somlo, G.; Wu, J.; Swiderski, P.; Wu, X.; Wang, S. E. Cross-Kingdom Inhibition of Breast Cancer Growth by Plant MiR159. *Cell Res.* **2016**, *26* (2), 217–228. <https://doi.org/10.1038/cr.2016.13>.
- (72) Scholler, N.; Crawford, M.; Sato, A.; Drescher, C. W.; O'Briant, K. C.; Kiviat, N.; Anderson, G. L.; Urban, N. Bead-Based ELISA for Validation of Ovarian Cancer Early Detection Markers. *Clin. Cancer Res.* **2006**, *12* (7), 2117–2124. <https://doi.org/10.1158/1078-0432.CCR-05-2007>.
- (73) Aldhaferi, H. N.; AlSaimary, I. E.; AlMusaffer, M. M. The Estimation of Prostate Specific Antigen (PSA) Concentrations in Patients with Prostatitis by Fully Automated ELISA Technique. *J. Med. Res. Health Sci.* **2020**, *3* (11), 1100–1104. <https://doi.org/10.15520/jmrhs.v3i11.279>.
- (74) Wang, Y.; Zhao, G.; Zhang, Y.; Pang, X.; Cao, W.; Du, B.; Wei, Q. Sandwich-Type Electrochemical Immunosensor for CEA Detection Based on Ag/MoS₂@Fe₃O₄ and an Analogous ELISA Method with Total Internal Reflection Microscopy. *Sens. Actuators B Chem.* **2018**, *266*, 561–569. <https://doi.org/10.1016/j.snb.2018.03.178>.

- (75) Senapati, S.; Sammel, M. D.; Butts, S. F.; Takacs, P.; Chung, K.; Barnhart, K. T. Predicting First Trimester Pregnancy Outcome: Derivation of a Multiple Marker Test. *Fertil. Steril.* **2016**, *106* (7), 1725-1732.e3. <https://doi.org/10.1016/j.fertnstert.2016.08.044>.
- (76) El-Bali, M.; Zagloul, D. a. M.; Khodari, Y. a. W.; Al-Harhi, S. A. Appraisal of Prenatal Anti-Toxoplasma Gondii (IgG+IgM)- IHA/IgM-ELISA Screening in Single Samples via IgG Avidity Test. *J. Egypt. Soc. Parasitol.* **2016**, *46* (1), 201–208. <https://doi.org/10.21608/jesp.2016.88972>.
- (77) Makunyane, L. L.; Moodley, J.; Titus, M. J. HIV Transmission in Twin Pregnancy : Maternal and Perinatal Outcomes. *South. Afr. J. Infect. Dis.* **2017**, *32* (2), 54–56. <https://doi.org/10.1080/23120053.2016.1257262>.
- (78) Uchida, K.; Nakata, K.; Carey, B.; Chalk, C.; Suzuki, T.; Sakagami, T.; Koch, D. E.; Stevens, C.; Inoue, Y.; Yamada, Y.; Trapnell, B. C. Standardized Serum GM-CSF Autoantibody Testing for the Routine Clinical Diagnosis of Autoimmune Pulmonary Alveolar Proteinosis. *J. Immunol. Methods* **2014**, *402* (1), 57–70. <https://doi.org/10.1016/j.jim.2013.11.011>.
- (79) Hsu, C.-K.; Huang, H.-Y.; Chen, W.-R.; Nishie, W.; Ujiie, H.; Natsuga, K.; Fan, S.-T.; Wang, H.-K.; Lee, J. Y.-Y.; Tsai, W.-L.; Shimizu, H.; Cheng, C.-M. Paper-Based ELISA for the Detection of Autoimmune Antibodies in Body Fluid—The Case of Bullous Pemphigoid. *Anal. Chem.* **2014**, *86* (9), 4605–4610. <https://doi.org/10.1021/ac500835k>.
- (80) Yen, Y.-F.; Lan, Y.-C.; Huang, C.-T.; Jen, I.-A.; Chen, M.; Lee, C.-Y.; Chuang, P.-H.; Lee, Y.; Morisky, D. E.; Chen, Y.-M. A. Human Immunodeficiency Virus Infection Increases the Risk of Incident Autoimmune Hemolytic Anemia: A Population-Based Cohort Study in Taiwan. *J. Infect. Dis.* **2017**, *216* (8), 1000–1007. <https://doi.org/10.1093/infdis/jix384>.
- (81) Bobosha, K.; Fat, E. M. T. K.; Eeden, S. J. F. van den; Bekele, Y.; Schip, J. J. van der P.; Dood, C. J. de; Dijkman, K.; Franken, K. L. M. C.; Wilson, L.; Aseffa, A.; Spencer, J. S.; Ottenhoff, T. H. M.; Corstjens, P. L. A. M.; Geluk, A. Field-Evaluation of a New Lateral Flow Assay for Detection of Cellular and Humoral Immunity against Mycobacterium Leprae. *PLoS Negl. Trop. Dis.* **2014**, *8* (5), e2845. <https://doi.org/10.1371/journal.pntd.0002845>.
- (82) Marni, G.; Cossu, D.; Cocco, E.; Frau, J.; Marrosu, M. G.; Niegowska, M.; Sechi, L. A. Epitopes of HERV-Wenv Induce Antigen-Specific Humoral Immunity in Multiple Sclerosis Patients. *J. Neuroimmunol.* **2015**, *280*, 66–68. <https://doi.org/10.1016/j.jneuroim.2015.03.003>.
- (83) Schmitz, E. M. H.; Kerkhof, D. van de; Hamann, D.; Dongen, J. L. J. van; Kuijper, P. H. M.; Brunsveld, L.; Scharnhorst, V.; Broeren, M. A. C. Therapeutic Drug Monitoring of Infliximab: Performance Evaluation of Three Commercial ELISA Kits. *Clin. Chem. Lab. Med.* **2016**, *54* (7), 1211–1219. <https://doi.org/10.1515/cclm-2015-0987>.
- (84) Agius, R.; Nadulski, T. Utility of ELISA Screening for the Monitoring of Abstinence from Illegal and Legal Drugs in Hair and Urine. *Drug Test. Anal.* **2014**, *6* (S1), 101–109. <https://doi.org/10.1002/dta.1644>.
- (85) Moura, J. F.; DeLacerda, L.; Sandrini, R.; Borba, F. M.; Castelo, D. N.; Sade, E. R.; Sella, S.; Minozzo, J. C.; Calfe, L. G.; Figueiredo, B. C. ELISA for Determination of Human Growth Hormone: Recognition of Helix 4 Epitopes. *J. Biomed. Biotechnol.* **2004**, *2004* (3), 143–149. <https://doi.org/10.1155/S1110724304308090>.
- (86) Jung, M.; Won, H.; Shin, M.-K.; Oh, M. W.; Shim, S.; Yoon, I.; Yoo, H. S. Development of Actinobacillus Pleuropneumoniae ApxI, ApxII, and ApxIII-Specific ELISA Methods for Evaluation of Vaccine Efficiency. *J. Vet. Sci.* **2019**, *20* (2). <https://doi.org/10.4142/jvs.2019.20.e2>.

- (87) Matsuyama, T.; Sano, N.; Takano, T.; Sakai, T.; Yasuike, M.; Fujiwara, A.; Kawato, Y.; Kurita, J.; Yoshida, K.; Shimada, Y.; Nakayasu, C. Antibody Profiling Using a Recombinant Protein–Based Multiplex ELISA Array Accelerates Recombinant Vaccine Development: Case Study on Red Sea Bream Iridovirus as a Reverse Vaccinology Model. *Vaccine* **2018**, *36* (19), 2643–2649. <https://doi.org/10.1016/j.vaccine.2018.03.059>.
- (88) Schlaf, G.; Stöhr, K.; Rothhoff, A.; Altermann, W. ELISA-Based Crossmatching Allowing the Detection of Emerging Donor-Specific Anti-HLA Antibodies through the Use of Stored Donors' Cell Lysates. *Case Rep. Transplant.* **2015**, *2015*, e763157. <https://doi.org/10.1155/2015/763157>.
- (89) Satoh, A.; Kawagishi, N.; Minegishi, M.; Takahashi, H.; Akamatsu, Y.; Doi, H.; Satomi, S. Development of a Novel ELISA for Detection of Anti-A and Anti-B Antibodies in Recipients of ABO-Incompatible Living Donor Liver Grafts. *Tohoku J. Exp. Med.* **2007**, *211* (4), 359–367. <https://doi.org/10.1620/tjem.211.359>.
- (90) Chacko, M. P.; Mathan, A.; Daniel, D.; Basu, G.; Varughese, S. Significance of Pre-Transplant Anti-HLA Antibodies Detected on an ELISA Mixed Antigen Tray Platform. *Indian J. Nephrol.* **2013**, *23* (5), 351–353. <https://doi.org/10.4103/0971-4065.116303>.
- (91) Sentandreu, M. Á.; Aubry, L.; Toldrá, F.; Ouali, A. Blocking Agents for ELISA Quantification of Compounds Coming from Bovine Muscle Crude Extracts. *Eur. Food Res. Technol.* **2007**, *224* (5), 623–628. <https://doi.org/10.1007/s00217-006-0348-3>.
- (92) Engvall, E. Enzyme Immunoassay ELISA and EMIT. In *Methods in Enzymology; Immunochemical Techniques, Part A*; Academic Press, 1980; Vol. 70, pp 419–439. [https://doi.org/10.1016/S0076-6879\(80\)70067-8](https://doi.org/10.1016/S0076-6879(80)70067-8).
- (93) Hosseini, S.; Ibrahim, F.; Djordjevic, I.; Koole, L. H. Recent Advances in Surface Functionalization Techniques on Polymethacrylate Materials for Optical Biosensor Applications. *Analyst* **2014**, *139* (12), 2933–2943. <https://doi.org/10.1039/C3AN01789C>.
- (94) Ju, H.; Lai, G.; Yan, F. 1 - Introduction. In *Immunosensing for Detection of Protein Biomarkers*; Ju, H., Lai, G., Yan, F., Eds.; Elsevier, 2017; pp 1–30. <https://doi.org/10.1016/B978-0-08-101999-3.00001-3>.
- (95) Alhajj, M.; Farhana, A. Enzyme Linked Immunosorbent Assay. In *StatPearls*; StatPearls Publishing: Treasure Island (FL), 2022.
- (96) *ELISA Guide - Creative Diagnostics*. <https://www.creative-diagnostics.com/ELISA-guide.htm> (accessed 2022-08-28).
- (97) Blake, C.; Gould, B. J. Use of Enzymes in Immunoassay Techniques. A Review. *Analyst* **1984**, *109* (5), 533–547. <https://doi.org/10.1039/AN9840900533>.
- (98) Winston, S. E.; Fuller, S. A.; Eveleigh, M. J.; Hurrell, J. G. R. Conjugation of Enzymes to Antibodies. *Curr. Protoc. Mol. Biol.* **2000**, *50* (1), 11.1.1–11.1.7. <https://doi.org/10.1002/0471142727.mb1101s50>.
- (99) Hermanson, G. T. Chapter 22 - Enzyme Modification and Conjugation. In *Bioconjugate Techniques (Third Edition)*; Hermanson, G. T., Ed.; Academic Press: Boston, 2013; pp 951–957. <https://doi.org/10.1016/B978-0-12-382239-0.00022-4>.
- (100) Krainer, F. W.; Glieder, A. An Updated View on Horseradish Peroxidases: Recombinant Production and Biotechnological Applications. *Appl. Microbiol. Biotechnol.* **2015**, *99* (4), 1611–1625. <https://doi.org/10.1007/s00253-014-6346-7>.
- (101) Sharma, U.; Pal, D.; Prasad, R. Alkaline Phosphatase: An Overview. *Indian J. Clin. Biochem.* **2014**, *29* (3), 269–278. <https://doi.org/10.1007/s12291-013-0408-y>.
- (102) Verma, M. S.; Tsaloglou, M.-N.; Sisley, T.; Christodouleas, D.; Chen, A.; Milette, J.; Whitesides, G. M. Sliding-Strip Microfluidic Device Enables ELISA on Paper. *Biosens. Bioelectron.* **2018**, *99*, 77–84. <https://doi.org/10.1016/j.bios.2017.07.034>.

- (103) Ren, W.; Li, Z.; Xu, Y.; Wan, D.; Barnych, B.; Li, Y.; Tu, Z.; He, Q.; Fu, J.; Hammock, B. D. One-Step Ultrasensitive Bioluminescent Enzyme Immunoassay Based on Nanobody/Nanoluciferase Fusion for Detection of Aflatoxin B1 in Cereal. *J. Agric. Food Chem.* **2019**, *67* (18), 5221–5229. <https://doi.org/10.1021/acs.jafc.9b00688>.
- (104) Kendall, C.; Ionescu-Matiu, I.; Dreesman, G. R. Utilization of the Biotin/Avidin System to Amplify the Sensitivity of the Enzyme-Linked Immunosorbent Assay (ELISA). *J. Immunol. Methods* **1983**, *56* (3), 329–339. [https://doi.org/10.1016/S0022-1759\(83\)80022-2](https://doi.org/10.1016/S0022-1759(83)80022-2).
- (105) Tsurusawa, N.; Chang, J.; Namba, M.; Makioka, D.; Yamura, S.; Iha, K.; Kyosei, Y.; Watabe, S.; Yoshimura, T.; Ito, E. Modified ELISA for Ultrasensitive Diagnosis. *J. Clin. Med.* **2021**, *10* (21), 5197. <https://doi.org/10.3390/jcm10215197>.
- (106) Cotton, S. Introduction to the Lanthanides. In *Lanthanide and Actinide Chemistry*; John Wiley & Sons, Ltd, 2006; pp 1–7. <https://doi.org/10.1002/0470010088.ch1>.
- (107) *Rare Earth Elements*. <https://www.rareelementresources.com/rare-earth-elements#.YyjkxXZByUk> (accessed 2022-09-19).
- (108) Evans, C. H. *Episodes from the History of the Rare Earth Elements*; Springer: Dordrecht.
- (109) James, C. THULIUM I.1. *J. Am. Chem. Soc.* **1911**, *33* (8), 1332–1344. <https://doi.org/10.1021/ja02221a007>.
- (110) Cheisson, T.; Schelter, E. J. Rare Earth Elements: Mendeleev’s Bane, Modern Marvels. *Science* **2019**, *363* (6426), 489–493. <https://doi.org/10.1126/science.aau7628>.
- (111) Zhu, Z.; Pranolo, Y.; Cheng, C. Y. Separation of Uranium and Thorium from Rare Earths for Rare Earth Production – A Review. *Miner. Eng.* **2015**, *77*, 185–196. <https://doi.org/10.1016/j.mineng.2015.03.012>.
- (112) Cotton, S. The Lanthanides - Principles and Energetics. In *Lanthanide and Actinide Chemistry*; John Wiley & Sons, Ltd, 2006; pp 9–22. <https://doi.org/10.1002/0470010088.ch2>.
- (113) Freeman, A. J.; Watson, R. E. Theoretical Investigation of Some Magnetic and Spectroscopic Properties of Rare-Earth Ions. *Phys. Rev.* **1962**, *127* (6), 2058–2075. <https://doi.org/10.1103/PhysRev.127.2058>.
- (114) Ferru, G.; Reinhart, B.; Bera, M. K.; Olvera de la Cruz, M.; Qiao, B.; Ellis, R. J. The Lanthanide Contraction beyond Coordination Chemistry. *Eur. J. Chem.* **2016**, *22* (20), 6899–6904. <https://doi.org/10.1002/chem.201601032>.
- (115) Johnson, D. A. Recent Advances in the Chemistry of the Less-Common Oxidation States of the Lanthanide Elements. In *Advances in Inorganic Chemistry and Radiochemistry*; Emeléus, H. J., Sharpe, A. G., Eds.; Academic Press, 1977; Vol. 20, pp 1–132. [https://doi.org/10.1016/S0065-2792\(08\)60038-2](https://doi.org/10.1016/S0065-2792(08)60038-2).
- (116) Cotton, S. Electronic and Magnetic Properties of the Lanthanides. In *Lanthanide and Actinide Chemistry*; John Wiley & Sons, Ltd, 2006; pp 61–87. <https://doi.org/10.1002/0470010088.ch5>.
- (117) Bottrill, M.; Kwok, L.; Long, N. J. Lanthanides in Magnetic Resonance Imaging. *Chem. Soc. Rev.* **2006**, *35* (6), 557–571. <https://doi.org/10.1039/B516376P>.
- (118) Van Pieterse, L.; Reid, M. F.; Wegh, R. T.; Soverna, S.; Meijerink, A. $4f_n \rightarrow 4f_{n-1} 5d$ Transitions of the Light Lanthanides: Experiment and Theory. *Phys. Rev. B* **2002**, *65* (4), 045113. <https://doi.org/10.1103/PhysRevB.65.045113>.
- (119) Bünzli, J.-C. G.; Eliseeva, S. V. Basics of Lanthanide Photophysics. In *Lanthanide Luminescence: Photophysical, Analytical and Biological Aspects*; Hänninen, P., Härmä, H., Eds.; Springer Series on Fluorescence; Springer: Berlin, Heidelberg, 2011; pp 1–45. https://doi.org/10.1007/4243_2010_3.
- (120) Werts, M. H. V. Making Sense of Lanthanide Luminescence. *Sci. Prog.* **1933-2005**, *88* (2), 101–131.

- (121) Bünzli, J.-C. G.; Pecharsky, V. K. *Handbook on the Physics and Chemistry of Rare Earths, Volume 52 - 1st Edition*. <https://www.elsevier.com/books/handbook-on-the-physics-and-chemistry-of-rare-earths/bunzli/978-0-444-63877-9> (accessed 2022-08-23).
- (122) Bünzli, J.-C. G.; Piguet, C. Taking Advantage of Luminescent Lanthanide Ions. *Chem. Soc. Rev.* **2005**, *34* (12), 1048–1077. <https://doi.org/10.1039/B406082M>.
- (123) Bünzli, J.-C. G. Chapter 287 - Lanthanide Luminescence: From a Mystery to Rationalization, Understanding, and Applications. In *Handbook on the Physics and Chemistry of Rare Earths*; Bünzli, J.-C. G., Pecharsky, V. K., Eds.; Including Actinides; Elsevier, 2016; Vol. 50, pp 141–176. <https://doi.org/10.1016/bs.hpcpre.2016.08.003>.
- (124) Vleck, J. H. Van. The Puzzle of Rare-Earth Spectra in Solids. *J. Phys. Chem.* **1937**, *41* (1), 67–80. <https://doi.org/10.1021/j150379a006>.
- (125) Becker, H. G. O. Turro, N. J.: Modern Molecular Photochemistry. XI, 628 S. Mit Zahlr. Abb., 23 × 16 Cm. Menlo Park, California, Reading, Massachusetts, Don Mills, Ontario-Sydney: The Benjamin/Cummings Publ. Co., Inc. 1968. Kunststoff. *J. Für Prakt. Chem.* **1980**, *322* (4), 704–704. <https://doi.org/10.1002/prac.19803220426>.
- (126) Werts, M. H. V.; Jukes, R. T. F.; Verhoeven, J. W. The Emission Spectrum and the Radiative Lifetime of Eu³⁺ in Luminescent Lanthanide Complexes. *Phys. Chem. Chem. Phys.* **2002**, *4* (9), 1542–1548. <https://doi.org/10.1039/B107770H>.
- (127) Weissman, S. I. Intramolecular Energy Transfer The Fluorescence of Complexes of Europium. *J. Chem. Phys.* **1942**, *10* (4), 214–217. <https://doi.org/10.1063/1.1723709>.
- (128) Alpha, B.; Ballardini, R.; Balzani, V.; Lehn, J.-M.; Perathoner, S.; Sabbatini, N. Antenna Effect in Luminescent Lanthanide Cryptates: A Photophysical Study. *Photochem. Photobiol.* **1990**, *52* (2), 299–306. <https://doi.org/10.1111/j.1751-1097.1990.tb04185.x>.
- (129) Heffern, M. C.; Matosziuk, L. M.; Meade, T. J. Lanthanide Probes for Bioresponsive Imaging. *Chem. Rev.* **2014**, *114* (8), 4496–4539. <https://doi.org/10.1021/cr400477t>.
- (130) Cui, G.; Fang, W. State-Specific Heavy-Atom Effect on Intersystem Crossing Processes in 2-Thiothymine: A Potential Photodynamic Therapy Photosensitizer. *J. Chem. Phys.* **2013**, *138* (4), 044315. <https://doi.org/10.1063/1.4776261>.
- (131) J. Charbonniere, L. Luminescent Lanthanide Labels. *Curr. Inorg. Chem.* **2011**, *1* (1), 2–16.
- (132) Tanner, P. A.; Zhou, L.; Duan, C.; Wong, K.-L. Misconceptions in Electronic Energy Transfer: Bridging the Gap between Chemistry and Physics. *Chem. Soc. Rev.* **2018**, *47* (14), 5234–5265. <https://doi.org/10.1039/C8CS00002F>.
- (133) Mara, M. W.; Tatum, D. S.; March, A.-M.; Doumy, G.; Moore, E. G.; Raymond, K. N. Energy Transfer from Antenna Ligand to Europium(III) Followed Using Ultrafast Optical and X-Ray Spectroscopy. *J. Am. Chem. Soc.* **2019**, *141* (28), 11071–11081. <https://doi.org/10.1021/jacs.9b02792>.
- (134) Cravencoco, A.; Ye, C.; Gräfenstein, J.; Börjesson, K. Interplay between Förster and Dexter Energy Transfer Rates in Isomeric Donor–Bridge–Acceptor Systems. *J. Phys. Chem. A* **2020**, *124* (36), 7219–7227. <https://doi.org/10.1021/acs.jpca.0c05035>.
- (135) Omagari, S.; Nakanishi, T.; Kitagawa, Y.; Seki, T.; Fushimi, K.; Ito, H.; Meijerink, A.; Hasegawa, Y. Critical Role of Energy Transfer Between Terbium Ions for Suppression of Back Energy Transfer in Nonanuclear Terbium Clusters. *Sci. Rep.* **2016**, *6* (1), 37008. <https://doi.org/10.1038/srep37008>.
- (136) Zhou, B.; Shi, B.; Jin, D.; Liu, X. Controlling Upconversion Nanocrystals for Emerging Applications. *Nat. Nanotechnol.* **2015**, *10* (11), 924–936. <https://doi.org/10.1038/nnano.2015.251>.
- (137) Liang, G.; Wang, H.; Shi, H.; Wang, H.; Zhu, M.; Jing, A.; Li, J.; Li, G. Recent Progress in the Development of Upconversion Nanomaterials in Bioimaging and Disease

- Treatment. *J. Nanobiotechnology* **2020**, *18* (1), 154. <https://doi.org/10.1186/s12951-020-00713-3>.
- (138) Ferro, S. M.; Wobben, M.; Ehrler, B. Rare-Earth Quantum Cutting in Metal Halide Perovskites – a Review. *Mater. Horiz.* **2021**, *8* (4), 1072–1083. <https://doi.org/10.1039/D0MH01470B>.
- (139) Beeby, A.; Clarkson, I. M.; Dickins, R. S.; Faulkner, S.; Parker, D.; Royle, L.; Sousa, A. S. de; Williams, J. A. G.; Woods, M. Non-Radiative Deactivation of the Excited States of Europium, Terbium and Ytterbium Complexes by Proximate Energy-Matched OH, NH and CH Oscillators: An Improved Luminescence Method for Establishing Solution Hydration States. *J. Chem. Soc. Perkin Trans. 2* **1999**, *0* (3), 493–504. <https://doi.org/10.1039/A808692C>.
- (140) Horrocks, W. DeW.; Sudnick, D. R. Lanthanide Ion Probes of Structure in Biology. Laser-Induced Luminescence Decay Constants Provide a Direct Measure of the Number of Metal-Coordinated Water Molecules. *J. Am. Chem. Soc.* **1979**, *101* (2), 334–340. <https://doi.org/10.1021/ja00496a010>.
- (141) Bünzli, J.-C. G. Review: Lanthanide Coordination Chemistry: From Old Concepts to Coordination Polymers. *J. Coord. Chem.* **2014**, *67* (23–24), 3706–3733. <https://doi.org/10.1080/00958972.2014.957201>.
- (142) Dennis, K. P. N.; Jianzhuang, J.; Kuninobu, K.; Kenichi, M. Chapter 210 Half-Sandwich Tetrapyrrole Complexes of Rare Earths and Actinides. In *Handbook on the Physics and Chemistry of Rare Earths*; Elsevier, 2001; Vol. 32, pp 611–653. [https://doi.org/10.1016/S0168-1273\(01\)32009-3](https://doi.org/10.1016/S0168-1273(01)32009-3).
- (143) Utochnikova, V. V. Chapter 318 - Lanthanide Complexes as OLED Emitters. In *Handbook on the Physics and Chemistry of Rare Earths*; Bünzli, J.-C. G., Pecharsky, V. K., Eds.; Including Actinides; Elsevier, 2021; Vol. 59, pp 1–91. <https://doi.org/10.1016/bs.hpcr.2021.05.001>.
- (144) Fix, T.; Nonat, A.; Imbert, D.; Di Pietro, S.; Mazzanti, M.; Slaoui, A.; Charbonnière, L. J. Enhancement of Silicon Solar Cells by Downshifting with Eu and Tb Coordination Complexes. *Prog. Photovolt. Res. Appl.* **2016**, *24* (9), 1251–1260. <https://doi.org/10.1002/pip.2785>.
- (145) Shuvaev, S.; Starck, M.; Parker, D. Responsive, Water-Soluble Europium(III) Luminescent Probes. *Chem. – Eur. J.* **2017**, *23* (42), 9974–9989. <https://doi.org/10.1002/chem.201700567>.
- (146) Rodrigues, M.; Piñol, R.; Antorrena, G.; Brites, C. D. S.; Silva, N. J. O.; Murillo, J. L.; Cases, R.; Díez, I.; Palacio, F.; Torras, N.; Plaza, J. A.; Pérez-García, L.; Carlos, L. D.; Millán, A. Implementing Thermometry on Silicon Surfaces Functionalized by Lanthanide-Doped Self-Assembled Polymer Monolayers. *Adv. Funct. Mater.* **2016**, *26* (2), 200–209. <https://doi.org/10.1002/adfm.201503889>.
- (147) Bui, A. T.; Grichine, A.; Duperray, A.; Lidon, P.; Riobé, F.; Andraud, C.; Maury, O. Terbium(III) Luminescent Complexes as Millisecond-Scale Viscosity Probes for Lifetime Imaging. *J. Am. Chem. Soc.* **2017**, *139* (23), 7693–7696. <https://doi.org/10.1021/jacs.7b02951>.
- (148) Shahi, P. K.; Singh, A. K.; Rai, S. B.; Ullrich, B. Lanthanide Complexes for Temperature Sensing, UV Light Detection, and Laser Applications. *Sens. Actuators Phys.* **2015**, *222*, 255–261. <https://doi.org/10.1016/j.sna.2014.12.021>.
- (149) Amoroso, A. J.; Pope, S. J. A. Using Lanthanide Ions in Molecular Bioimaging. *Chem. Soc. Rev.* **2015**, *44* (14), 4723–4742. <https://doi.org/10.1039/C4CS00293H>.
- (150) Ung, P.; Clerc, M.; Huang, H.; Qiu, K.; Chao, H.; Seitz, M.; Boyd, B.; Graham, B.; Gasser, G. Extending the Excitation Wavelength of Potential Photosensitizers via Appendage of a Kinetically Stable Terbium(III) Macrocyclic Complex for Applications

- in Photodynamic Therapy. *Inorg. Chem.* **2017**, *56* (14), 7960–7974. <https://doi.org/10.1021/acs.inorgchem.7b00677>.
- (151) Sy, M.; Nonat, A.; Hildebrandt, N.; Charbonnière, L. J. Lanthanide-Based Luminescence Biolabelling. *Chem. Commun.* **2016**, *52* (29), 5080–5095. <https://doi.org/10.1039/C6CC00922K>.
- (152) Time-Resolved Protein Fluorescence. In *Principles of Fluorescence Spectroscopy*; Lakowicz, J. R., Ed.; Springer US: Boston, MA, 2006; pp 577–606. https://doi.org/10.1007/978-0-387-46312-4_17.
- (153) Aulsebrook, M. L.; Graham, B.; Grace, M. R.; Tuck, K. L. Lanthanide Complexes for Luminescence-Based Sensing of Low Molecular Weight Analytes. *Coord. Chem. Rev.* **2018**, *375*, 191–220. <https://doi.org/10.1016/j.ccr.2017.11.018>.
- (154) Gudgin Dickson, E. F.; Pollak, A.; Diamandis, E. P. Time-Resolved Detection of Lanthanide Luminescence for Ultrasensitive Bioanalytical Assays. *J. Photochem. Photobiol. B* **1995**, *27* (1), 3–19. [https://doi.org/10.1016/1011-1344\(94\)07086-4](https://doi.org/10.1016/1011-1344(94)07086-4).
- (155) Matsuya, T.; Hoshino, N.; Okuyama, T. Design of Lanthanide Complex Probes for Highly Sensitive Time-Resolved Fluorometric Detection Methods and Its Application to Biochemical, Environmental and Clinical Analyses. *Curr. Anal. Chem.* *2* (4), 397–410.
- (156) Steinkamp, T.; Karst, U. Detection Strategies for Bioassays Based on Luminescent Lanthanide Complexes and Signal Amplification. *Anal. Bioanal. Chem.* **2004**, *380* (1), 24–30. <https://doi.org/10.1007/s00216-004-2682-2>.
- (157) Evangelista, R. A.; Pollak, A.; Gudgin Templeton, E. F. Enzyme-Amplified Lanthanide Luminescence for Enzyme Detection in Bioanalytical Assays. *Anal. Biochem.* **1991**, *197* (1), 213–224. [https://doi.org/10.1016/0003-2697\(91\)90381-3](https://doi.org/10.1016/0003-2697(91)90381-3).
- (158) Zheng, X.-Y.; Lu, J.-Z.; Zhu, Q.-Z.; Xu, J.-G.; Li, Q.-G. Study of a Lanthanide Fluorescence System With a Coupled Reaction Based on Hemin Catalysis. *Analyst* **1997**, *122* (5), 455–458. <https://doi.org/10.1039/A606560K>.
- (159) Hewitt, S. H.; Butler, S. J. Application of Lanthanide Luminescence in Probing Enzyme Activity. *Chem. Commun.* **2018**, *54* (50), 6635–6647. <https://doi.org/10.1039/C8CC02824A>.
- (160) Barrios, A. M.; Craik, C. S. Scanning the Prime-Site Substrate Specificity of Proteolytic Enzymes: A Novel Assay Based on Ligand-Enhanced Lanthanide Ion Fluorescence. *Bioorg. Med. Chem. Lett.* **2002**, *12* (24), 3619–3623. [https://doi.org/10.1016/S0960-894X\(02\)00786-2](https://doi.org/10.1016/S0960-894X(02)00786-2).
- (161) Steinkamp, T.; Schweppe, F.; Krebs, B.; Karst, U. A Tripod Ligand as New Sensitizer for the Enzyme Amplified Lanthanide Luminescence Determination of Esterase. *Analyst* **2003**, *128* (1), 29–31. <https://doi.org/10.1039/B210411N>.
- (162) Bhowmik, S.; Maitra, U. A Novel “pro-Sensitizer” Based Sensing of Enzymes Using Tb(III) Luminescence in a Hydrogel Matrix. *Chem. Commun.* **2012**, *48* (38), 4624–4626. <https://doi.org/10.1039/C2CC30904A>.
- (163) Liu, Y.; Tu, D.; Zhu, H.; Chen, X. Lanthanide-Doped Luminescent Nanoprobes: Controlled Synthesis, Optical Spectroscopy, and Bioapplications. *Chem. Soc. Rev.* **2013**, *42* (16), 6924–6958. <https://doi.org/10.1039/C3CS60060B>.
- (164) Zheng, W.; Huang, P.; Tu, D.; Ma, E.; Zhu, H.; Chen, X. Lanthanide-Doped Upconversion Nano-Bioprobes: Electronic Structures, Optical Properties, and Biodetection. *Chem. Soc. Rev.* **2015**, *44* (6), 1379–1415. <https://doi.org/10.1039/C4CS00178H>.
- (165) Wang, F.; Liu, X. Multicolor Tuning of Lanthanide-Doped Nanoparticles by Single Wavelength Excitation. *Acc. Chem. Res.* **2014**, *47* (4), 1378–1385. <https://doi.org/10.1021/ar5000067>.

- (166) Bao, G.; Wen, S.; Lin, G.; Yuan, J.; Lin, J.; Wong, K.-L.; Bünzli, J.-C. G.; Jin, D. Learning from Lanthanide Complexes: The Development of Dye-Lanthanide Nanoparticles and Their Biomedical Applications. *Coord. Chem. Rev.* **2021**, *429*, 213642. <https://doi.org/10.1016/j.ccr.2020.213642>.
- (167) Homann, C.; Krukewitt, L.; Frenzel, F.; Grauel, B.; Würth, C.; Resch-Genger, U.; Haase, M. NaYF₄:Yb,Er/NaYF₄ Core/Shell Nanocrystals with High Upconversion Luminescence Quantum Yield. *Angew. Chem. Int. Ed.* **2018**, *57* (28), 8765–8769. <https://doi.org/10.1002/anie.201803083>.
- (168) Haase, M.; Schäfer, H. Upconverting Nanoparticles. *Angew. Chem. Int. Ed.* **2011**, *50* (26), 5808–5829. <https://doi.org/10.1002/anie.201005159>.
- (169) Ju, Q.; Liu, Y.; Tu, D.; Zhu, H.; Li, R.; Chen, X. Lanthanide-Doped Multicolor GdF₃ Nanocrystals for Time-Resolved Photoluminescent Biodetection. *Chem. Eur. J.* **2011**, *17*, 8549–8554. <https://doi.org/10.1002/chem.201101170>.
- (170) Gorris, H. H.; Wolfbeis, O. S. Photon-Upconverting Nanoparticles for Optical Encoding and Multiplexing of Cells, Biomolecules, and Microspheres. *Angew. Chem. Int. Ed.* **2013**, *52* (13), 3584–3600. <https://doi.org/10.1002/anie.201208196>.
- (171) Bhuckory, S.; Hemmer, E.; Wu, Y.-T.; Yahia-Ammar, A.; Vetrone, F.; Hildebrandt, N. Core or Shell? Er³⁺ FRET Donors in Upconversion Nanoparticles. *Eur. J. Inorg. Chem.* **2017**, *2017* (44), 5186–5195. <https://doi.org/10.1002/ejic.201700904>.
- (172) Cardoso Dos Santos, M.; Runser, A.; Bartenlian, H.; Nonat, A. M.; Charbonnière, L. J.; Klymchenko, A. S.; Hildebrandt, N.; Reisch, A. Lanthanide-Complex-Loaded Polymer Nanoparticles for Background-Free Single-Particle and Live-Cell Imaging. *Chem. Mater.* **2019**, *31* (11), 4034–4041. <https://doi.org/10.1021/acs.chemmater.9b00576>.
- (173) Cheignon, C.; Kassir, A. A.; Soro, L. K.; Charbonniere, L. J. Dye-Sensitized Lanthanide Containing Nanoparticles for Luminescence Based Applications. *Nanoscale* **2022**. <https://doi.org/10.1039/D1NR06464A>.
- (174) Carnall, W. T. Chapter 24 The Absorption and Fluorescence Spectra of Rare Earth Ions in Solution. In *Handbook on the Physics and Chemistry of Rare Earths*; Non-metallic Compounds - I; Elsevier, 1979; Vol. 3, pp 171–208. [https://doi.org/10.1016/S0168-1273\(79\)03007-5](https://doi.org/10.1016/S0168-1273(79)03007-5).
- (175) Zhang, J.; Shade, C. M.; Chengelis, D. A.; Petoud, S. A Strategy to Protect and Sensitize Near-Infrared Luminescent Nd³⁺ and Yb³⁺: Organic Tropolonate Ligands for the Sensitization of Ln(3+)-Doped NaYF₄ Nanocrystals. *J. Am. Chem. Soc.* **2007**, *129* (48), 14834–14835. <https://doi.org/10.1021/ja074564f>.
- (176) Charbonnière, L. J.; Rehspringer, J.-L.; Ziessel, R.; Zimmermann, Y. Highly Luminescent Water-Soluble Lanthanide Nanoparticles through Surface Coating Sensitization. *New J. Chem.* **2008**, *32* (6), 1055–1059. <https://doi.org/10.1039/b719700d>.
- (177) Goetz, J.; Nonat, A.; Diallo, A.; Sy, M.; Sera, I.; Lecointre, A.; Lefevre, C.; Chan, C. F.; Wong, K.-L.; Charbonnière, L. J. Ultrabright Lanthanide Nanoparticles. *ChemPlusChem* **2016**, *81* (6), 526–534. <https://doi.org/10.1002/cplu.201600007>.
- (178) Charpentier, C.; Cifliku, V.; Goetz, J.; Nonat, A.; Cheignon, C.; Cardoso Dos Santos, M.; Francés-Soriano, L.; Wong, K.-L.; Charbonnière, L. J.; Hildebrandt, N. Ultrabright Terbium Nanoparticles for FRET Biosensing and in Situ Imaging of Epidermal Growth Factor Receptors. *Chem. Eur. J.* **2020**, *26* (64), 14602–14611. <https://doi.org/10.1002/chem.202002007>.
- (179) Cheignon, C.; Heurté, M.; Knighton, R. C.; Kassir, A. A.; Lecointre, A.; Nonat, A.; Boos, A.; Christine, C.; Asfari, Z.; Charbonnière, L. J. Investigation of the Supramolecular Assembly of Luminescent Lanthanide Nanoparticles Surface Functionalized by *P*- Sulfonato-Calix[4]Arenes with Charged Aromatic Compounds.

- Eur. J. Inorg. Chem.* **2021**, 2021 (36), 3761–3770. <https://doi.org/10.1002/ejic.202100546>.
- (180) Zhu, X.; Zhang, H.; Zhang, F. Ligand-Based Surface Engineering of Lanthanide Nanoparticles for Bioapplications. *ACS Mater. Lett.* **2022**, 4 (9), 1815–1830. <https://doi.org/10.1021/acsmaterialslett.2c00528>.
- (181) Hagan, A. K.; Zuchner, T. Lanthanide-Based Time-Resolved Luminescence Immunoassays. *Anal. Bioanal. Chem.* **2011**, 400 (9), 2847–2864. <https://doi.org/10.1007/s00216-011-5047-7>.
- (182) Kadkhodayan, S.; Elliott, L. O.; Mausisa, G.; Wallweber, H. A.; Deshayes, K.; Feng, B.; Fairbrother, W. J. Evaluation of Assay Technologies for the Identification of Protein–Peptide Interaction Antagonists. *Assay Drug Dev. Technol.* **2007**, 5 (4), 501–514. <https://doi.org/10.1089/adt.2007.070>.
- (183) Härmä, H.; Soukka, T.; Lövgren, T. Europium Nanoparticles and Time-Resolved Fluorescence for Ultrasensitive Detection of Prostate-Specific Antigen. *Clin. Chem.* **2001**, 47 (3), 561–568. <https://doi.org/10.1093/clinchem/47.3.561>.

Chapter II

Ultrabright lanthanide nanoparticles

1. Introduction

The interest in lanthanide doped nanoparticles appeared in the late 1990s. First attempts for the preparation of such NPs were made at very high temperatures, resulting in poor dispersibility with dimensions in the submicrometer range.¹ High-quality luminescent NPs require controlled crystalline phases, narrow size distribution and uniform morphology for tuning their physicochemical properties and exploring their potential applications in diverse fields. For bioapplications, these NPs should have a small size and good dispersity for integration with biological molecules and macromolecules.²

Later, extensive attention has been paid to liquid phase synthesis and some efforts have also been made to prepare NPs directly in aqueous solutions. A variety of synthetic strategies have been proposed to synthesize high-quality Ln-doped luminescent NPs. These included thermal decomposition, high-temperature coprecipitation, hydrothermal synthesis, microwave-assisted synthesis, cation exchange and ionic liquid-based synthesis.³

The quality of the synthesized NPs is not only affected by a specific synthetic method but also strongly depends on the nature of the crystal host. The luminescence properties of Ln³⁺ are typically dependent on the structure, local site symmetry, crystal field strength, and phonon energy of the host materials. Generally, the host materials are desired to be transparent within the wavelength range of interest, with low phonon energy, high optical damage threshold, and close lattice matches with Ln³⁺ dopants.⁴ To date, a large number of matrices suitable for Ln³⁺ ions doping have been reported, such as oxides, fluorides, phosphates, vanadates and silicates among others.⁵

The ability to manipulate the color output of Ln-NPs is particularly important for their applications. The strategies for tuning the color output typically involve regulating dopant/host combinations and dopant concentrations. Each Ln³⁺ ion has a unique set of energy levels and therefore could offer a set of distinct emission peaks with distinguishable spectroscopic fingerprints. Importantly, different emission peaks of a given Ln ion could be selectively enhanced or suppressed through the control of its surrounding environment in the host lattice, thereby leading to tunable optical emissions.⁶

In this chapter, the synthesis and the characterization of ultrabright Ln-NPs are described. The study of their luminescence properties is also demonstrated, especially when photosensitized by efficient antennas.

2. Synthesis of Ln-doped LaF₃ NPs

Among the different host materials, fluorides have low phonon energy which allows low multiphonon relaxation rates and minimal nonradiative energy losses.⁷ LaF₃ crystals have low phonon energy (300 cm⁻¹), high chemical and thermal stability, and lattice matching with the majority of Ln³⁺ ions. They are transparent in the visible and NIR regions so they can be doped with all Ln³⁺ ions without deleterious effects.⁸ LaF₃ are then considered as ideal host materials for many applications.

Wang *et al.* were first to report a simple synthesis of Ln³⁺ doped LaF₃ NPs directly in aqueous solution without using any surfactant that can create inhomogeneous domains near the particle surface.⁹ In their study, various Ln³⁺ ions with emission in the Vis and NIR regions were doped into the nanocrystals including Tb³⁺, Eu³⁺, Ce³⁺, and Nd³⁺.

Tb³⁺ and Eu³⁺ ions have been then extensively studied on account of their ideal luminescent properties and they are frequently applied in Ln doped NPs.^{10,11} Both Ln present relatively strong luminescence in aqueous solution, exhibiting multiple emissions in the visible region. Eu³⁺ ions mainly emit red light, while Tb³⁺ ions are green light emitters. Therefore, their detection is achieved by simple and cheap equipment, in contrast to IR detection which requires more complex and costly equipment. Moreover, Tb³⁺ and Eu³⁺ ions have relatively large energy gaps and are moderately affected by nonradiative deactivations by the host material and high-energy oscillators. They consequently present better luminescence and longer lifetimes in comparison to other Ln.¹²

Thanks to their energy levels, Tb³⁺ and Eu³⁺ also find various families of simple organic ligands, capable of photosensitizing their emission. The sensitization of these two Ln is widely investigated, and some empirical rules have been developed to rationalize the matching of a ligand excited state levels with the emissive levels of the Tb³⁺ or Eu³⁺.¹³

After the selection of the host material and the dopant Ln, the synthesis of the NPs was achieved inspired by the method developed by Wang *et al.* The method was upgraded and continuously optimized at team SynPA, becoming one of the specialties of the laboratory, and a research focus for many studies and applications.

This synthesis consists in mixing LaCl_3 and LnCl_3 (TbCl_3 , EuCl_3 or both) together with amounts that will determine the doping level of Ln^{3+} in the NPs. Then, a solution of NH_4F is added dropwise to the mixture at room temperature, initiating the reaction of NPs formation as shown in Figure 35. The added quantity of NH_4F corresponds to three equivalents for each equivalent of Ln. The rate of NH_4F addition was found to strongly influence the morphology of NPs and their size dispersion. This addition rate being operator-dependent, the synthesis lacked the reproducibility. The synthesis has been improved by the automatization of this step using a syringe pump for a constant rate, eliminating the manipulative fluctuations.

In a next step, the mixture is heated at 150°C in a microwave oven for 12 minutes. The temperature and the reaction time are critical for controlling the thermodynamic and kinetic growth of the NPs.¹⁴ The synthesis in microwave oven provides a regular and homogeneous heating with a quick and constant temperature rise. A heat treatment at above 100°C is still required to prompt the reaction and to improve the crystallinity of the resulting NPs. The growth of NPs occurs by mechanisms such as Ostwald ripening or oriented attachment. Ostwald ripening involves the dissolution of the high-energy small NPs then ripening of the surface of bigger NPs.¹⁵ Oriented attachment occurs by the alignment of small particles following a preferential crystal orientation and growing together into a single crystal.¹⁶

Finally, the NPs are purified from any reagent left in solution. The obtained colloidal solution is centrifuged, and the supernatant is eliminated. This step is repeated 3 times and the final white solid was dispersed in ultrapure water using ultrasound bath for 1h at 60°C .

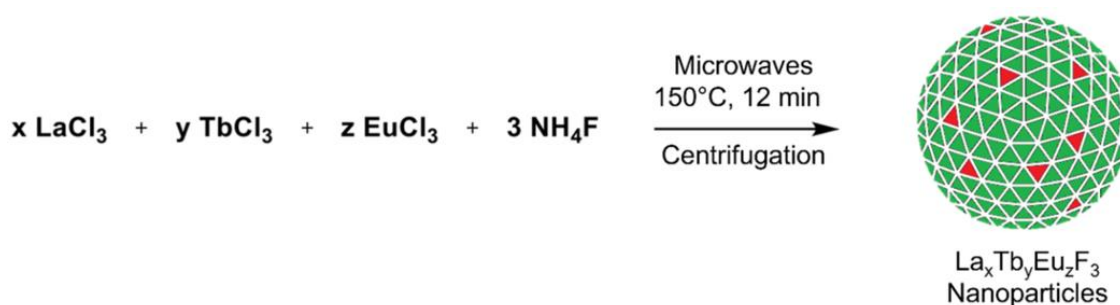


Figure 35: Microwave-assisted synthesis of $\text{La}_x\text{Tb}_y\text{Eu}_z\text{F}_3$ NPs (Tb in green and Eu in red).

Tb-doped NPs ($\text{La}_{0.9}\text{Tb}_{0.1}\text{F}_3$) and Tb/Eu co-doped NPs ($\text{Tb}_{0.85}\text{La}_{0.14}\text{Eu}_{0.01}\text{F}_3$) are selected in accordance with previous works for their stability, their structure, and their interesting spectroscopic properties.¹⁷ These NPs were synthesized following the described procedure with a yield ranging between 80 and 90%. The final NPs suspensions after purification are found acidic at a pH of around 4.6 and stored at 5°C as stock solutions.

3. Characterization of the nanoparticles

The synthesized $\text{La}_{0.9}\text{Tb}_{0.1}\text{F}_3$ and $\text{Tb}_{0.85}\text{La}_{0.14}\text{Eu}_{0.01}\text{F}_3$ NPs are fully characterized for their morphology and size by transmission electron microscopy (TEM) and their structure by X-ray diffraction (XRD). The colloidal stability of these NPs in aqueous solution is evaluated by measuring their zeta potential by laser doppler electrophoresis (LDE) and their hydrodynamic diameter by dynamic light scattering (DLS). The exact composition is also verified by inductively coupled plasma atomic emission spectroscopy (ICP-AES).

3.1. Morphology and size

The size of NPs is an important parameter that affects their properties and applicability. Transmission electron microscopy (TEM) is a microscopy technique that uses a beam of electrons to visualize specimens and generates a highly-magnified image.

TEM images of the synthesized NPs show rounded or slightly elongated shape for both types as shown in Figure 36. These images allowed to measure an average diameter of 20 ± 6 nm for $\text{La}_{0.9}\text{Tb}_{0.1}\text{F}_3$ NPs. They also show light spots within the particle core in a donut-like shape, which may indicate a lower atom density.¹⁸ $\text{Tb}_{0.85}\text{La}_{0.14}\text{Eu}_{0.01}\text{F}_3$ NPs are found to have bigger size with a diameter of 35 ± 7 nm while showing high atom density in the entire NP. This size increase contradicts the fact of replacing La^{3+} ions by smaller Tb^{3+} ions, unless there is a change in the crystal structure. The size distribution of both NPs is represented in Figure 37.

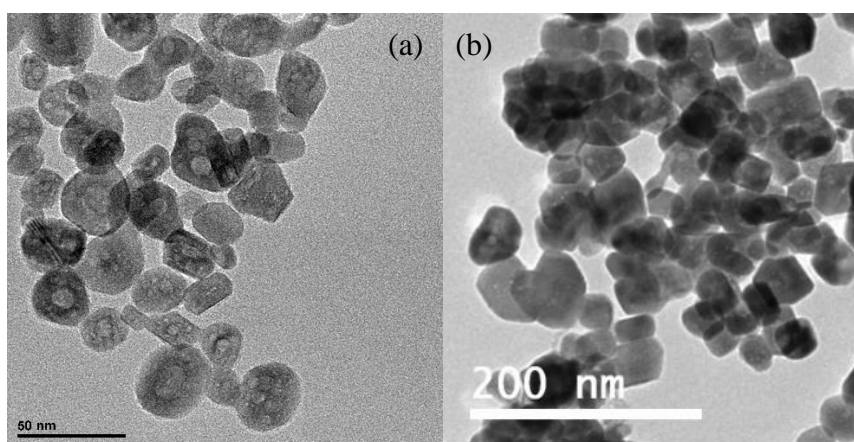


Figure 36: Transmission electron microscopy image of (a) $\text{La}_{0.9}\text{Tb}_{0.1}\text{F}_3$ and (b) $\text{Tb}_{0.85}\text{La}_{0.14}\text{Eu}_{0.01}\text{F}_3$ NPs.

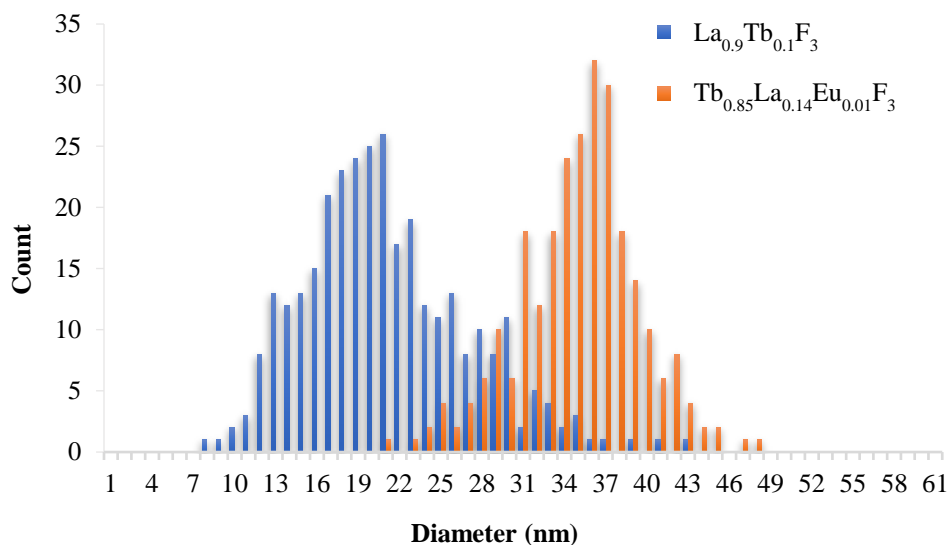


Figure 37: Particle size distribution of $\text{La}_{0.9}\text{Tb}_{0.1}\text{F}_3$ and $\text{Tb}_{0.85}\text{La}_{0.14}\text{Eu}_{0.01}\text{F}_3$ NPs determined by TEM.

3.2. Structure

The XRD pattern of $\text{La}_{0.9}\text{Tb}_{0.1}\text{F}_3$ NPs completely matches with the peak positions and the intensities of pure hexagonal LaF_3 crystals.¹⁹ In a side study, it has been demonstrated that this crystal structure depends on the Tb doping level. Figure 38 shows the evolution of the structure with increasing Tb doping level. When exceeding 70% in Tb, a modification in the crystal structure can be noticed, all the way to reach a pure orthorhombic crystal for TbF_3 .

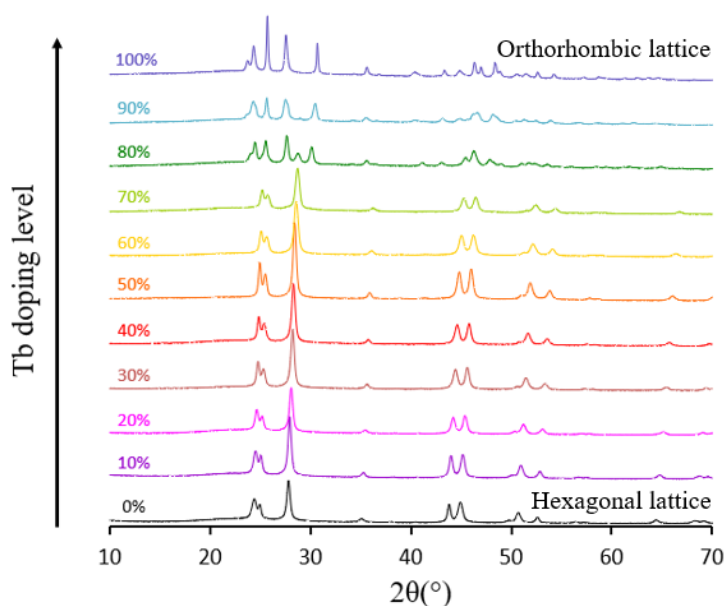


Figure 38: X ray diffraction pattern of $\text{La}_{1-x}\text{Tb}_x\text{F}_3$ NPs with increasing Tb doping level.

As expected, the XRD pattern of $Tb_{0.85}La_{0.14}Eu_{0.01}F_3$ NPs (Figure 39) shows peaks for both crystal structures, mainly orthorhombic, which can explain the bigger size of these NPs. More advanced data can be extracted from XRD patterns but are not fundamental for our study.

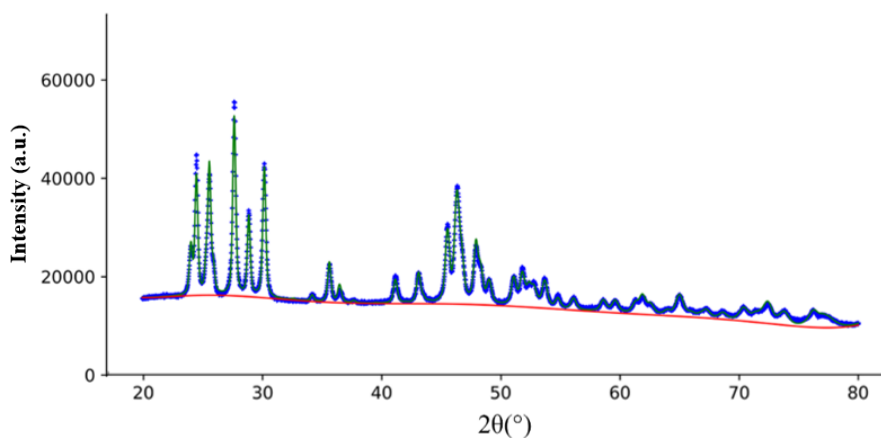


Figure 39: X ray diffraction pattern of $Tb_{0.85}La_{0.14}Eu_{0.01}F_3$ NPs.

3.3. Colloidal properties

a) Zeta potential

The stability of particles in solution is a crucial parameter to control. It depends on the balance of attractive and repulsive forces between the particles. Attractive forces are basically Van Der Waals interactions, while repulsive ones consist in electrostatic interactions due to the charge that develops at the interface between the particle surface and its liquid medium. This surface charge is called zeta (ζ) potential.²⁰

The magnitude of the ζ -potential gives an indication of the stability of the colloidal system. If the particles in suspension have a large negative or positive ζ -potential, they tend to repel each other, and attractive forces will be negligible. However, if the particles have low ζ -potential values, then attractive forces will be dominant, and particles will tend to aggregate. Aggregations cause a loss of the specific surface area and of the properties of the particles.

ζ -potential of the synthesized NPs is measured by Laser Doppler Electrophoresis (LDE). It consists in putting the NPs in movement by applying an electric field. By launching a laser to these NPs, their mobility can be measured (Figure 40), and then related to ζ -potential.

The measurements in aqueous solution at pH = 5.0 show $\zeta = (+)37 \pm 8$ mV for $La_{0.9}Tb_{0.1}F_3$ NPs and $(+)35 \pm 7$ mV for $Tb_{0.85}La_{0.14}Eu_{0.01}F_3$ NPs. Both NPs show good colloidal stability in such conditions, allowing to store the stock solutions at this pH without risk of aggregation.

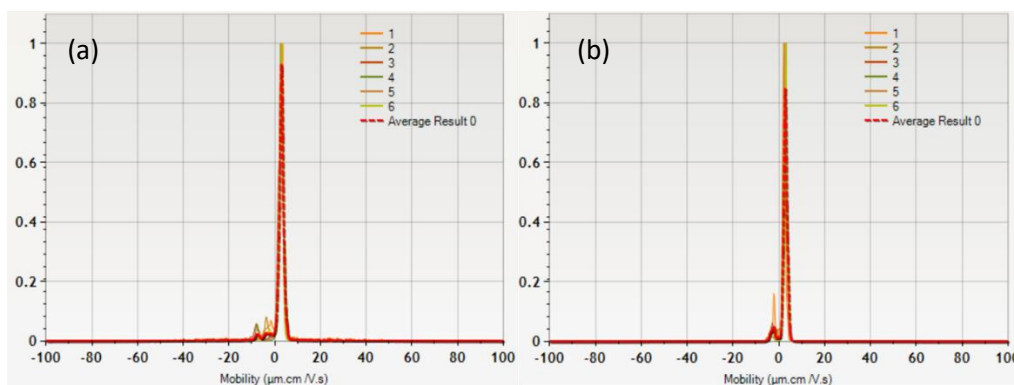


Figure 40: Mobility of (a) $\text{La}_{0.9}\text{Tb}_{0.1}\text{F}_3$ and (b) $\text{Tb}_{0.85}\text{La}_{0.14}\text{Eu}_{0.01}\text{F}_3$ NPs measured by LDE.

In addition, the positive zeta potential in both cases indicates that the NPs maintained the coordination affinity of Ln ions toward negatively charged ligands, which allows further exploitation of the NPs surface.

b) Hydrodynamic diameter

In aqueous medium, NPs develop an electric dipole layer and acquire a hydrodynamic diameter that can be measured by dynamic light scattering (DLS).²⁰ Launching a laser into the particles in Brownian motion and looking at the scattered light in a specific direction allows to analyze the NPs size distribution.

DLS measurements show an average hydrodynamic diameter of 49 ± 14 nm for $\text{La}_{0.9}\text{Tb}_{0.1}\text{F}_3$ NPs and 62 ± 18 nm for $\text{Tb}_{0.85}\text{La}_{0.14}\text{Eu}_{0.01}\text{F}_3$ NPs as shown in Figure 41. The difference in size between TEM diameter and the hydrodynamic one cannot be justified only by the presence of water molecules around the NPs. It seems that a slight aggregation occurred to find a stable state under these conditions, but no flagrant aggregation or polydispersity is noticed.

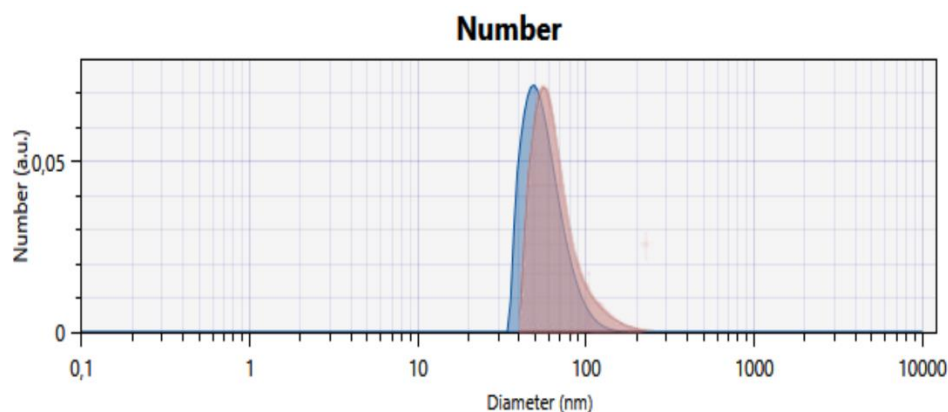


Figure 41: Hydrodynamic diameter of $\text{La}_{0.9}\text{Tb}_{0.1}\text{F}_3$ (blue) and $\text{Tb}_{0.85}\text{La}_{0.14}\text{Eu}_{0.01}\text{F}_3$ NPs (red) measured by DLS.

3.4. Composition

The doping levels in these NPs are basically determined by the added quantity of Ln during the synthesis. The exact doping levels can be verified using the elemental mass concentrations “ C_m ” (g.L^{-1}) measured by ICP-AES. Mass concentrations are converted to molar concentrations “ C ” (mol.L^{-1}) according to equation 1:

$$C = \frac{C_m}{M} \quad \text{Equation 1}$$

With M : Molar mass (g.mol^{-1})

Then the molar fraction X_{Ln} of each dopant is calculated according to equation 2:

$$X_{Ln} = \frac{C_{Ln}}{\sum C} \quad \text{Equation 2}$$

In all cases, the exact doping levels perfectly match with the added ratios in the synthesis as demonstrated in Table 3. These values have been also confirmed by energy dispersive X-ray spectroscopy (EDX) included in TEM analysis.

Table 3: Elemental mass concentrations of Ln measured by ICP-AES and the exact doping percentage calculated for $\text{La}_{0.9}\text{Tb}_{0.1}\text{F}_3$ and $\text{Tb}_{0.85}\text{La}_{0.14}\text{Eu}_{0.01}\text{F}_3$ NPs.

La_{0.9}Tb_{0.1}F₃	La	Tb	Eu
C_m (mg.kg⁻¹)	9240 ± 228	1187 ± 29	0
X_{Ln}	0.90 ± 0.02	0.10 ± 0.002	0
Tb_{0.85}La_{0.14}Eu_{0.01}F₃	La	Tb	Eu
C_m (mg.kg⁻¹)	1342 ± 27	9322 ± 200	127 ± 1
X_{Ln}	0.14 ± 0.002	0.85 ± 0.02	0.01

3.5. Concentration

The molar concentration of the NPs in aqueous suspension can be calculated assuming two hypotheses. The first one is to consider that the NPs are perfectly spherical, allowing to calculate the volume of the NPs “ V_{NPs} ” (m^3) using TEM observations using the equation 3:

$$V_{NPS} = \frac{4}{3} \times \pi \times R^3 \quad \text{Equation 3}$$

With R : Radius of the NPs (m)

The second assumption consists in estimating the density of the NPs as the weighted average of LaF₃, TbF₃ and EuF₃ densities according to their doping level. The density of the NPs “d_{NPS}” (g.m⁻³) is calculated following equation 4.

$$d_{NPS} = \sum(X_{Ln} \times d_{LnF_3}) \quad \text{Equation 4}$$

With d_{LnF₃} : density of LaF₃, TbF₃ and EuF₃ (g.m⁻³)

Thereby, the molecular weight of a NP “M_{NPS}” (g.mol⁻¹) can be estimated using equation 5.

$$M_{NP} = V_{NPS} \times d_{NPS} \times N_a \quad \text{Equation 5}$$

With N_a : Avogadro number

In addition, the molar mass of a single La_{x_{La}}Tb_{x_{Tb}}Eu_{x_{Eu}}F₃ pattern “M_{pattern}” (g.mol⁻¹) can be simply calculated using equation 6.

$$M_{pattern} = \sum(X_{Ln} \times M_{Ln}) + 3 \times M_F \quad \text{Equation 6}$$

Knowing the molecular weight of a NP and the molar mass of a single pattern, the number of patterns in a NP “N_{patterns}” can be deduced following equation 7.

$$N_{patterns} = \frac{M_{NP}}{M_{pattern}} \quad \text{Equation 7}$$

And finally, the concentration of the NPs “C_{NPS}” (mol.L⁻¹) is calculated by dividing the concentration of any Ln by the number of this Ln in a NP as in equation 8.

$$C_{NPS} = \frac{C_{Ln}}{X_{Ln} \times N_{patterns}} \quad \text{Equation 8}$$

During three years of thesis, several NP batches were synthesized and characterized with the same procedure, and the results indicate a remarkable reproducibility. Table 4 recapitulates the characteristics of the different synthesized batches.

Table 4: Summary of the characteristics of different $\text{La}_{0.9}\text{Tb}_{0.1}\text{F}_3$ and $\text{Tb}_{0.85}\text{La}_{0.14}\text{Eu}_{0.01}\text{F}_3$ synthesized batches

$\text{La}_{0.9}\text{Tb}_{0.1}\text{F}_3$	1	2	3	4
Volume (mL)	10	10	20	20
pH	4.5	4.4	4.6	4.6
Concentration (M)	4.72×10^{-7}	5.54×10^{-7}	2.56×10^{-7}	2.43×10^{-7}
Yield (%)	80	90	85	81
NP diameter (nm)	20 ± 6	-	-	-
Hydrodynamic diameter (nm)	54 ± 16	52 ± 15	54 ± 15	49 ± 14
ζ-potential (mV)	37 ± 8	39 ± 8	35 ± 6	37 ± 8

$\text{Tb}_{0.85}\text{La}_{0.14}\text{Eu}_{0.01}\text{F}_3$	1	2	3
Volume (mL)	10	10	10
pH	4.5	4.6	4.6
Concentration (M)	1.70×10^{-7}	1.69×10^{-7}	1.82×10^{-7}
Yield (%)	86	86	90
Core diameter (nm)	34 ± 7	-	-
Hydrodynamic diameter (nm)	58 ± 15	62 ± 17	62 ± 18
ζ-potential (mV)	42 ± 9	36 ± 7	35 ± 7

4. Photosensitizing ligand

The choice of the capping ligand is crucial to get optimal spectroscopic properties of Ln NPs. This ligand must provide a high molar extinction coefficient, good coordination, and efficient photosensitization, but also the ability to ensure the NPs dispersibility and stability.

The chromophore needs to be judiciously selected for intramolecular energy transfer to occur from its triplet state to the emissive Ln³⁺ ion. For the sensitization of Tb³⁺ ions, a singlet–triplet energy gap of less than 7000 cm⁻¹ is desirable, with the S₁ state preferably laying at less than 29 000 cm⁻¹ above the ground state.²¹

In the literature, many ligands based on the 2-hydroxyisophthalic acid have been used to sensitize Tb³⁺ ions.²² In contrast to traditional, highly preorganized ligands used for Ln³⁺ complexes, this NPs capping ligand ensure a required planar coordination on the surface of NPs in order to perfectly bind to the Ln³⁺ ions while preventing their leaching from the NP. The two carboxylic acid groups in this ligand have pK_a values at 3.46 and 4.46, which means that they can be easily deprotonated. The resulting double negatively charged carboxylate groups ensure a good affinity of this ligand toward the positively charged surface of the NPs.

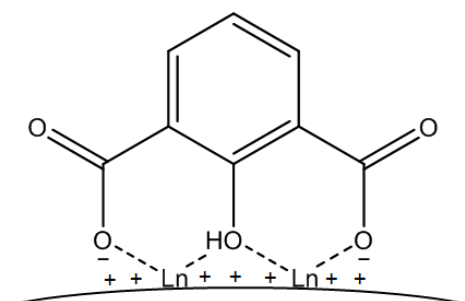


Figure 42: Coordination of 2-hydroxyisophthalic acid to the Ln ions at the surface of NPs.

2-hydroxy-isophthalic acid is a bis-dentate chelate because the hydroxyl group allows to form two 6-membered ring with two Ln³⁺ ions as shown in Figure 42.²³ Hydroxyl group has higher pK_a and is mainly protonated. However, neutral donor groups can bind when present in multidentate ligands that contain at least one or two other charged donor groups.

4.1. Synthesis of 2-hydroxyisophthalic acid

The first step of the synthesis of the 2-hydroxyisophthalic acid consists in the oxidation of the two methyl groups of the commercially available 2,6-dimethylanisole to form the carboxylic acid groups as described in Figure 43.

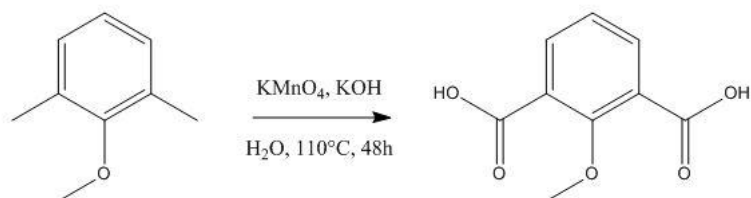
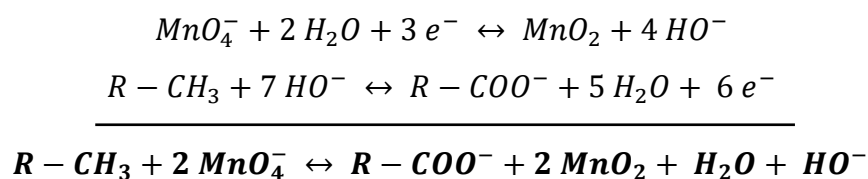


Figure 43: Oxidation of 2,6-dimethylanisole with $KMnO_4$ and KOH .

The oxidation was performed using $KMnO_4$ in alkaline conditions, and the solution changes from violet to brown color after heating at reflux for 48h. This change is due to the reduction of MnO_4^- to MnO_2 . This redox reaction follows the equation below :



The solution was then neutralized and the formed MnO_2 precipitate is eliminated by filtration. The filtrate was concentrated and acidified to pH 2 until a white precipitate appeared, which is collected by filtration. This intermediate 2-methoxyisophthalic acid was not further purified to prevent any loss of the compound and was directly used for the next step.

The second step consists in the O-demethylation of the intermediate compound in presence of HBr and $AcOH$ (Figure 44). The mixture is heated at $120^\circ C$ overnight.

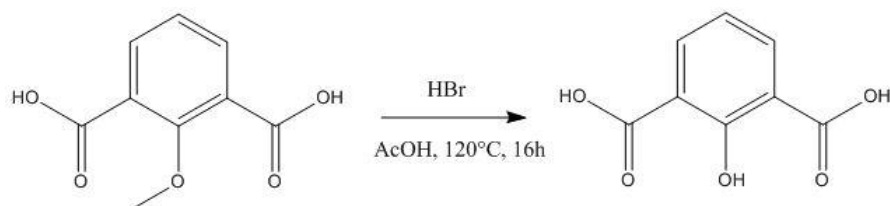


Figure 44: O-demethylation of phenol group with HBr and $AcOH$.

The volatiles were then removed under vacuum and the white solid was purified by recrystallisation from methanol/water mixture to obtain the 2-hydroxyisophthalic acid with a 68% yield over both steps. The elemental analysis indicates a purity of 99% of the final ligand, validated by the ^1H NMR shown in Figure 45.

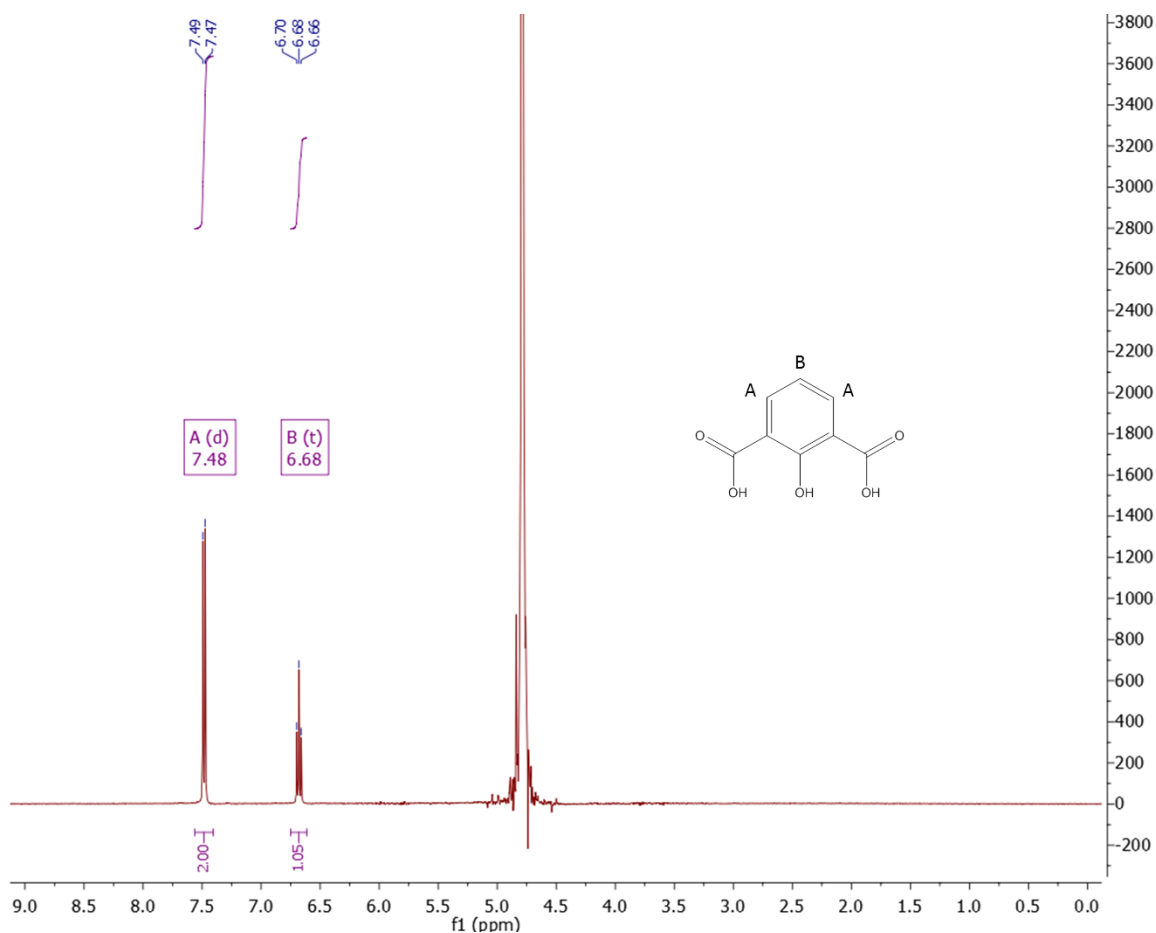


Figure 45: ^1H NMR spectrum of synthesized 2-hydroxyisophthalic acid in $\text{D}_2\text{O} + \text{NaOD}$ (300 MHz, 25 °C).

4.2. Spectroscopic properties of 2-hydroxyisophthalic acid

The triplet state of 2-hydroxyisophthalic acid is known to be approximately at 23 000 cm^{-1} ,²⁴ this energy level is close to the excited state of Tb^{3+} ion at 20 500 cm^{-1} .²⁵ This compatibility favors the energy transfer and allows an efficient photosensitization.

Once the ligand synthesized, its absorption and emission spectra are measured in 0.05 M HEPES buffer solution at pH 7.0. These spectra are shown in Figure 46.

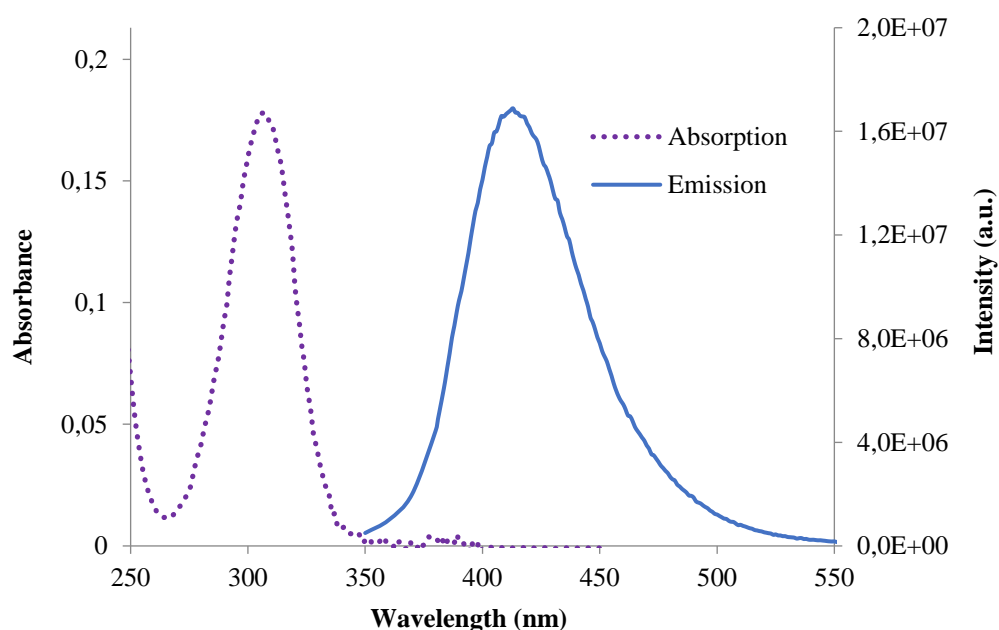


Figure 46: Absorption and emission ($\lambda_{exc} = 306 \text{ nm}$) spectra of 2-hydroxyisophthalate.

2-hydroxyisophthalate displayed a maximal absorption at $\lambda_{abs} = 306 \text{ nm}$ with a molar extinction coefficient $\epsilon_{306} = 4500 \text{ M}^{-1} \cdot \text{cm}^{-1}$. Upon excitation at 306 nm, this fluorophore has a maximal emission at $\lambda_{em} = 412 \text{ nm}$. The excitation spectrum for an emission at 412 nm perfectly matches with the absorption spectrum. It indicates that the emission at 412 nm involves the same species that absorb at 306 nm with no fluctuations of intermolecular interactions during the transition. The latter can lead to inhomogeneous broadening and deviation of the excitation spectrum.²⁶

Interestingly, the resultant Stokes shift is large enough that the respective excitation and emission bands do not overlap. This will prevent an energy loss by self-absorption and subsequently allows optimal transfer to Tb^{3+} ions when capping the NPs.

4.3. Photosensitization of $\text{La}_{0.9}\text{Tb}_{0.1}\text{F}_3$ NPs

4.3.1. Bare nanoparticles

The TR-excitation and emission spectra of bare $\text{La}_{0.9}\text{Tb}_{0.1}\text{F}_3$ NPs at 5×10^{-10} M in 0.05 M HEPES at pH 7.0 are shown in Figure 47. The emission spectrum shows very weak Tb characteristic bands at 490, 545, 584 and 622 nm attributed to the $^5\text{D}_4 \rightarrow ^7\text{F}_J$ transitions of Tb ($J = 6$ to 3, respectively). Such weak intensity is explained by the poor absorbance of Tb.

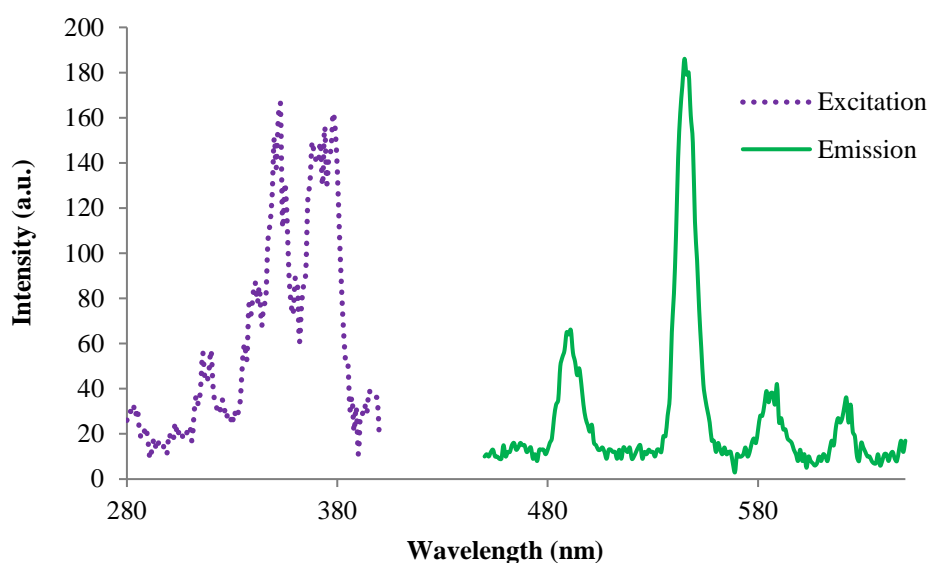


Figure 47: Excitation ($\lambda_{em} = 545$ nm) and emission ($\lambda_{exc} = 350$ nm) spectra of bare $\text{La}_{0.9}\text{Tb}_{0.1}\text{F}_3$ NPs.

1.1.1. Spectroscopic titration of $\text{La}_{0.9}\text{Tb}_{0.1}\text{F}_3$ NPs

The capacity of the 2-hydroxyisophthalate to photosensitize Tb-NPs was evaluated by a systematic spectroscopic titration (Figure 48). It consists in the addition of increasing concentrations of the ligand to a number of wells containing a constant concentration of NPs (5×10^{-10} M). This titration was performed in 50 mM HEPES at pH 7.0.

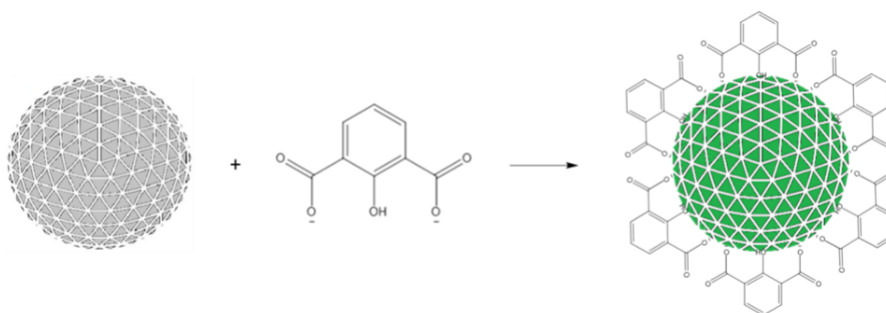


Figure 48: Titration of $\text{La}_{0.9}\text{Tb}_{0.1}\text{F}_3$ NPs by 2-hydroxyisophthalate ligand.

First, an excitation spectrum after ligand addition was measured for an emission at 545 nm. This spectrum shows an intense excitation band at 325 nm, a wavelength where Tb does not specifically absorb, but rather corresponds to the maximal excitation of the ligand (inset of Figure 49). The intensity of this band gradually increases at higher ligand concentrations. However, a red shift of the ligand excitation is noticed upon the coordination to the NPs (306 to 325 nm). When coordinated, this π -acceptor ligand displays metal to ligand charge transfer effect “MLCT”, which results in a decrease in HOMO-LUMO gap associated with a red shift in the excitation band.

The TR-emission spectra in each well were then measured after an excitation at 325 nm. The evolution of the emission spectra with increasing concentrations of ligand is shown in Figure 49. A gradual increase in the intensity of the same characteristic Tb emission bands is a clear evidence of an efficient energy transfer by the antenna effect.

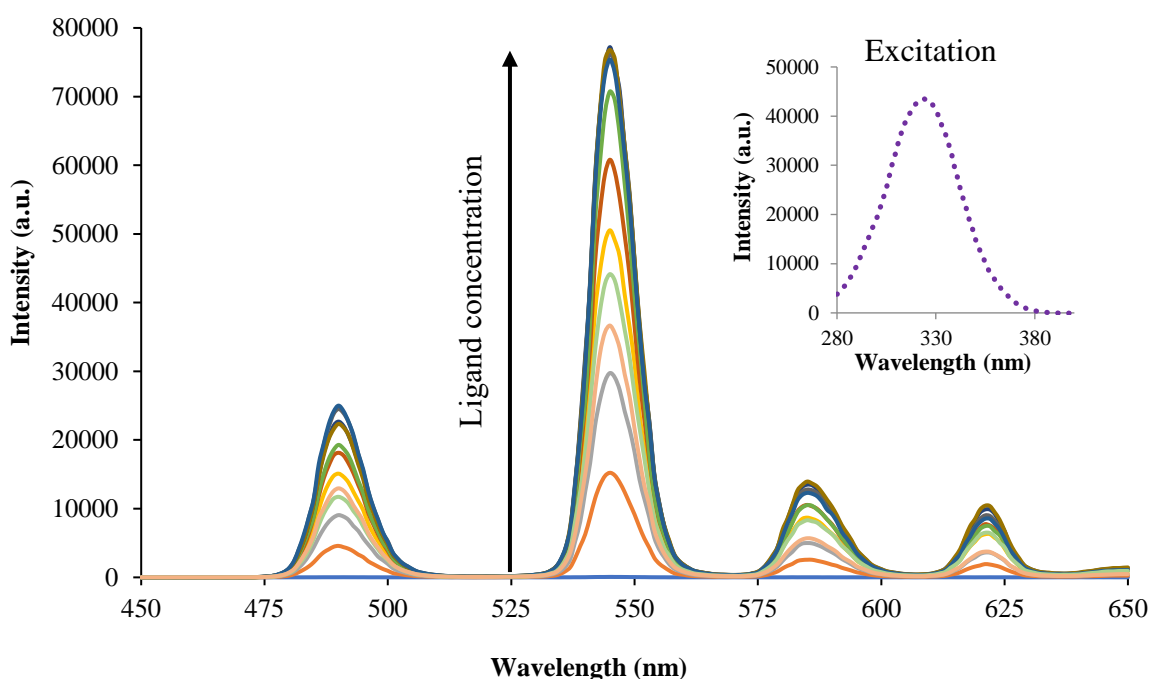


Figure 49: TR-emission spectra of $La_{0.9}Tb_{0.1}F_3$ NPs ($\lambda_{exc} = 325$ nm) upon addition of increasing ligand concentrations. Inset : TR-excitation spectra ($\lambda_{em} = 545$ nm).

After a strong amplification of Tb emission bands, the emission intensity reaches a maximum at a certain ligand concentration and remains constant.

Figure 50 presents the evolution of the integration of the $^5D_4 \rightarrow ^7F_5$ emission band of Tb peaking at 545 nm as a function of the added ligand equivalents per NP.

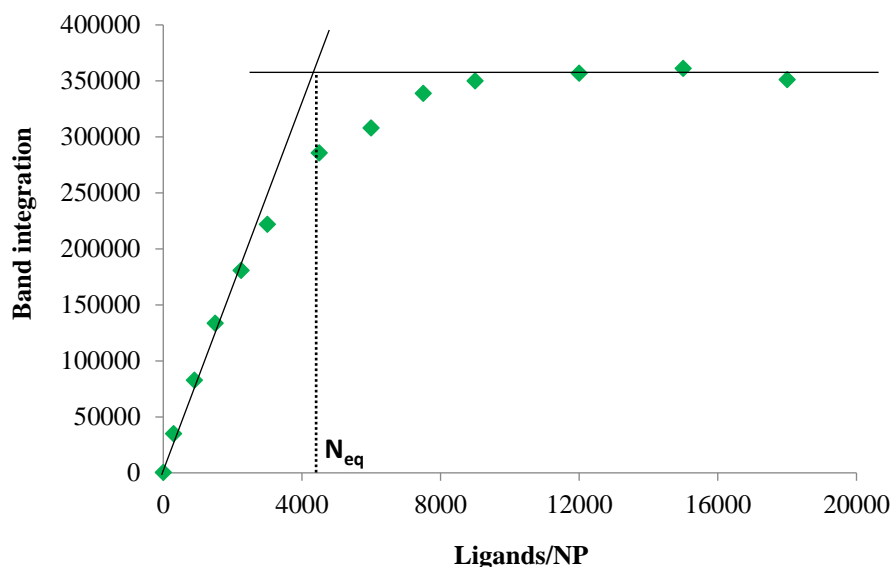


Figure 50: Evolution of the Tb emission band peaking at 545 nm as a function of the ligand equivalents per NP.

This graph allows to define an arbitrary equivalent ligand number (N_{eq}), estimated by the intercept between the two straight lines corresponding to the increasing region and to the constant region. This intercept indicates that at this ligands/NP ratio, the surface of the NPs is totally capped by the ligands, and any further added ligands are unable to coordinate to the NPs. At very high ligand concentrations, the emission intensity could slightly drop down due to inner filter effect. The high absorption of free ligands in solution attenuates the excitation beam for the NP-coordinated ligands, leading to lower emission.

This equivalent ligand number is empirical and operator-dependent which increases the margin of error. Nevertheless, this method was demonstrated to be effectively reproducible for a given type of NPs and ligand. It gives good indications when comparing different ligands or testing a new batch of NPs. Herein, N_{eq} is determined at approximately 4500 ligands per NP, which theoretically provides a 4500 times cumulation of the molar extinction coefficient of a single ligand.

4.3.2. Brightness of dye-sensitized NPs

Experimentally, an exact determination of the molar extinction coefficient requires the isolation and purification of fully capped NPs to ensure that the absorption arises solely from coordinated ligands. Many works in the lab demonstrated that the molar extinction coefficient of capped NPs approximatively corresponds to the theoretical cumulation effect.¹⁷

The resulting strong molar extinction coefficient with the good overall luminescence quantum yields of these NPs allow to get excellent brightness, $> 10^6 \text{ M}^{-1} \cdot \text{cm}^{-1}$,²⁷ exceeding that of QDs and semiconducting nanopolymers (10^5 - $10^6 \text{ M}^{-1} \cdot \text{cm}^{-1}$).^{28,29}

In this work, the focus is not only on the brightness of the sensitized NPs, but rather on the relative brightness brought by the sensitization in comparison to the brightness of bare NPs. So for an overall evaluation of the photosensitization effect, a luminescence amplification factor is defined. This factor is calculated by the ratio of the maximum 545 nm band integration to that of the NPs in the absence of any ligand. Here, the fully capped NPs are 500 times more luminescent than bare NPs.

4.3.3. Excited state lifetime

It is worth mentioning the importance of time-resolved detection of the photosensitized Tb emission. In fact, the coordination of the ligand and the energy transfer to the NPs is not quantitative, and the residual broad fluorescence band of the ligand could appear. At high concentrations, excess of free ligands does not exhibit energy transfer, increasing the ligand emission band which can overlap the first two Tb emission bands (Figure 51). This interference is eliminated by time-resolved detection thanks to the long lifetime of these NPs.

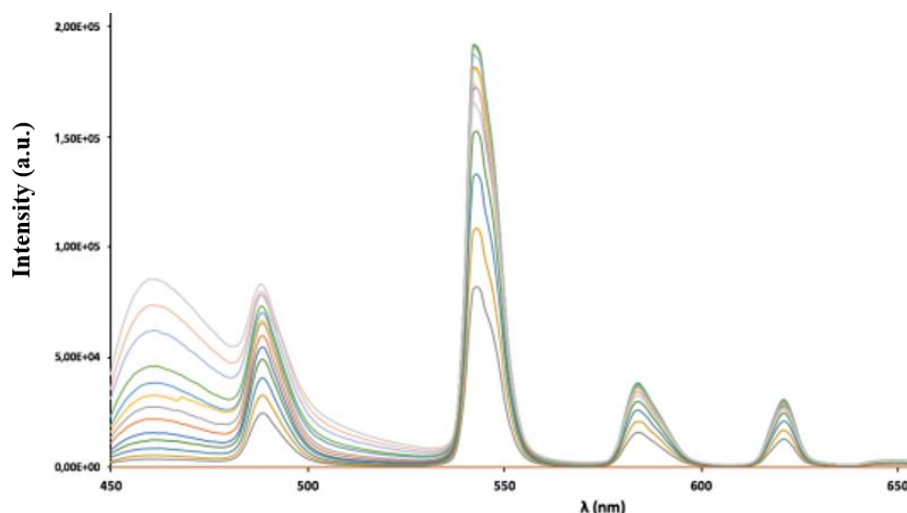


Figure 51: Example of steady-state emission ($\lambda_{exc} = 329 \text{ nm}$) of dye-sensitized $\text{La}_{0.9}\text{Tb}_{0.1}\text{F}_3$ NPs emission.¹⁷

When a fluorescent compound is excited, the excited state is populated and the return to the ground state (emission) decays exponentially with time, following equation 9.

$$I_{em}(t) = I_0 e^{-\frac{t}{\tau}} \quad \text{equation 9}$$

With I_0 : Intensity at 0 s after excitation

$I_{em}(t)$: Intensity at time t

t : Time (s)

τ : Excited state lifetime (s)

The excited state lifetime of capped NPs can be then determined by measuring the emission intensity of Tb as a function of time as shown in Figure 52.

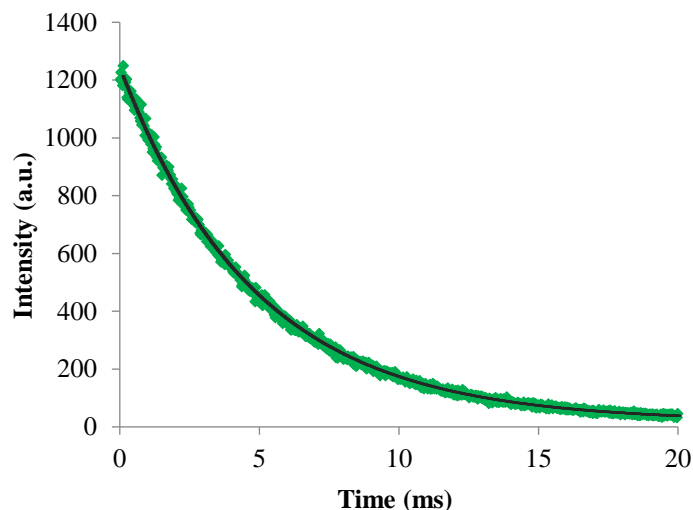


Figure 52: Photoluminescence decay ($\lambda_{exc} = 325$ nm, $\lambda_{em} = 545$ nm) and fit curve (black) of Tb in sensitized $La_{0.9}Tb_{0.1}F_3$ NPs.

Tb emission shows a slow biexponential decay, indicating two different lifetime values, corresponding to two different Tb environments. The first constitutes 46% of Tb ions with a lifetime of 3.41 ms, while the second exhibits a lifetime of 1.28 ms for the remaining 54%.

The longer lifetime can be attributed to Tb ions in the core of the NPs, whereas the shorter lifetime corresponds to Tb ions on the surface. Since being less protected from water, surface Tb ions are more susceptible to undergo non-radiative deactivations by vibration of O-H bonds with the surrounding solvent, which reduces the lifetime of the excited state of the concerned ions. The longer lifetime can also be related to Tb-to-Tb energy transfer within the particle or ligand mediated energy migration on the surface.^{30,31}

Interestingly, these lifetimes are higher than that reported for Tb-DO3A complex sensitized by the same 2-hydroxyisophthalate ligand, which is at 1.14 ms.³² In addition to the great brightness of these dye-sensitized NPs, these characteristics make them serious competitors against the best luminescent probes in market, such as Lumi-4-Tb[®] marker, with a brightness of 1.6×10^4 $M^{-1} \cdot cm^{-1}$ and luminescence lifetime of 2.6 ms.³³

4.3.4. Effect of pH on the sensitization

$\text{La}_{0.9}\text{Tb}_{0.1}\text{F}_3$ NPs are demonstrated to be efficiently sensitized by 2-hydroxyisophthalate at neural pH. The effect of pH on the sensitization is then studied by measuring the intensity of Tb emission at 545 nm at different pH. The results are plotted in Figure 53.

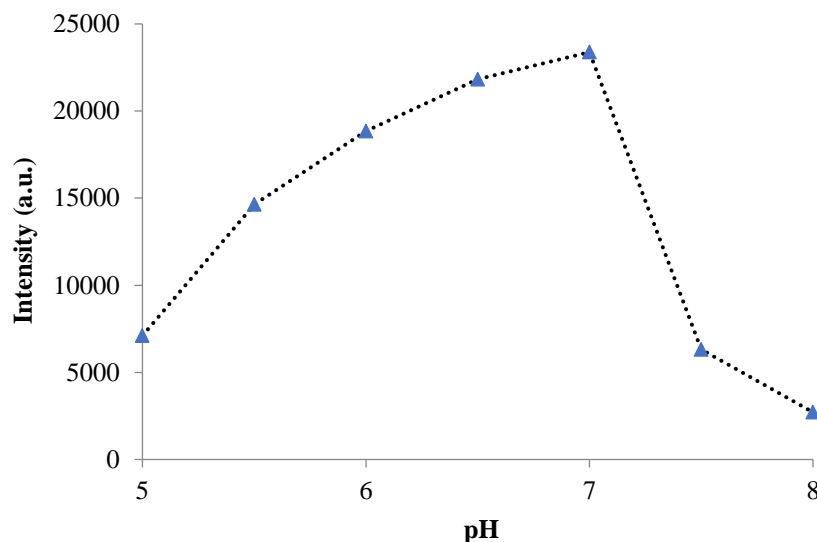


Figure 53: The intensity of Tb emission ($\lambda_{exc} = 325 \text{ nm}$) in dye-sensitized $\text{La}_{0.9}\text{Tb}_{0.1}\text{F}_3$ NPs at different pH.

In the range of pH between 5 and 7, the intensity of Tb emission gradually increases with pH augmentation. The carboxylic acid groups of the ligand have pKa values at 3.46 and 4.46. When increasing the pH from 5.0 to 7.0, these groups are deprotonated which favors the coordination at the positively charged surface of the NPs. Better coordination allows more efficient energy transfer, which explains the higher intensity of Tb emission. At pH > 7.0, a sharp drop of the intensity is observed. In this pH range, the ligand should not be affected by pH change, thus this drop is surely related to the NPs behavior.

To study this behavior, the ζ -potential and the hydrodynamic diameter of bare NPs are monitored at different pH. The results are shown in Table 5, while zeta potential is plotted as a function of pH in Figure 54.

Table 5: Zeta potential and hydrodynamic diameter of bare $\text{La}_{0.9}\text{Tb}_{0.1}\text{F}_3$ NPs at different pH.

pH	5.0	6.0	7.0	8.0	9.0	10.0
ζ -potential (mV)	+37	+32	+24	-11	-29	-35
Hydrodynamic diameter (nm)	49	51	56	224	62	64

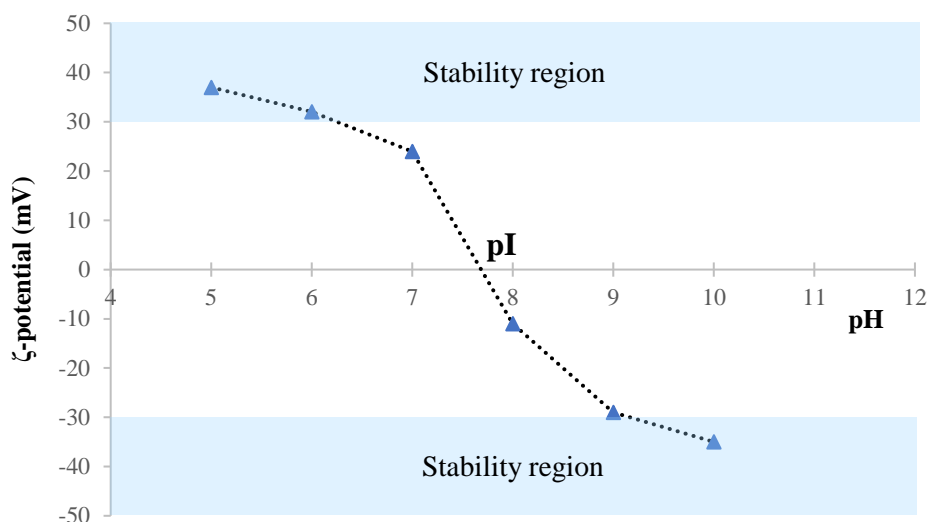


Figure 54: ζ -potential of bare $La_{0.9}Tb_{0.1}F_3$ NPs as a function of pH.

Up to a pH of 7.0, the NPs present high positively charged surface with good colloidal stability. At $pH > 7.0$, ζ -potential sharply turns negative, due to the presence of HO^- groups at the surface of NPs. At a certain pH between 7.0 and 8.0, the NPs can have a state with no net electrical charge, corresponding to their isoelectric point “pI”.

Around this pI, at low ζ -potential ($-30 < \zeta < +30$), the NPs tend to aggregate as demonstrated by the big size of hydrodynamic diameter. At higher pH, NPs regain a moderate stability with high negatively charged surface. However, at these pH, it is hard to coordinate negatively charged ligand to the NPs, unless they have high affinity to compete with HO^- on the surface of NPs.

4.4. Photosensitization of $Tb_{0.85}La_{0.14}Eu_{0.01}F_3$ NPs

$Tb_{0.85}La_{0.14}Eu_{0.01}F_3$ were chosen to present a different approach of Ln NPs. Several works have been described to photosensitize Eu NPs to obtain their red emission in water.^{34,35} These works show high potential, but Eu emission has always been more vulnerable to nonradiative deactivations by O-H oscillators.³⁶

The study of these Tb/Eu co-doped NPs consists of two objectives. The first is to investigate the spectroscopic properties of Tb ions at higher doping rate and in different environments. The second is to enhance the spectroscopic properties of Eu ions by promoting an energy transfer from Tb ions on the surface to Eu ions protected in the core of the NPs. The aim is to improve the lifetime and the quantum yield of Eu luminescence in aqueous solution.

4.4.1. Bare nanoparticles

The TR-excitation and emission spectra of bare $\text{Tb}_{0.85}\text{La}_{0.14}\text{Eu}_{0.01}\text{F}_3$ NPs at 5×10^{-10} M in 0.05 M HEPES at pH 7.0 are shown in Figure 55. The emission spectrum shows the weak Tb characteristic bands present in that of $\text{La}_{0.9}\text{Tb}_{0.1}\text{F}_3$ NPs. The bands peaking at 490 and 545 nm arise from pure Tb emission.

In addition, at 1%, Eu characteristic emission bands are observed with intensities comparable to that of Tb emission. These bands can be attributed to the $^5\text{D}_0 \rightarrow ^7\text{F}_J$ transitions of Eu ($J = 0$ to 4). The one at 690 nm is distinguished as pure Eu emission while the other bands overlap with those of Tb emission in the region between 570 and 640 nm.

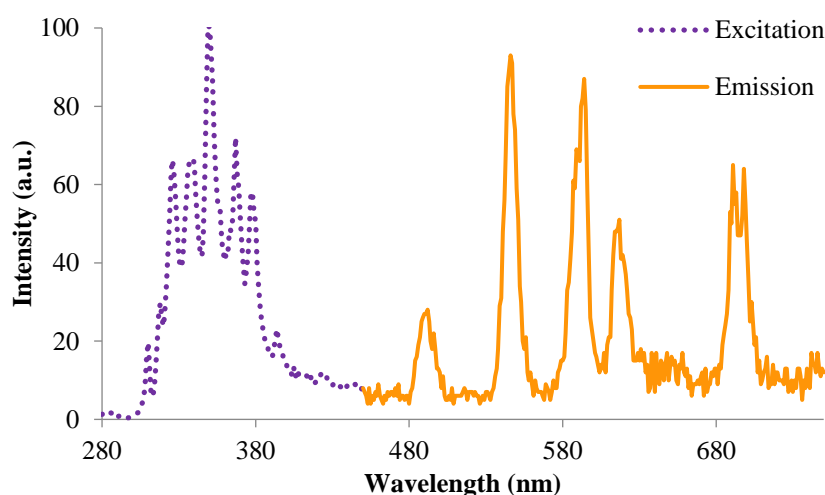


Figure 55: Excitation ($\lambda_{em} = 590$ nm) and emission ($\lambda_{exc} = 350$ nm) spectra of bare $\text{Tb}_{0.85}\text{La}_{0.14}\text{Eu}_{0.01}\text{F}_3$ NPs.

1.1.2. Spectroscopic titration of $\text{Tb}_{0.85}\text{La}_{0.14}\text{Eu}_{0.01}\text{F}_3$ NPs

The spectroscopic titration was performed similarly to that of $\text{La}_{0.9}\text{Tb}_{0.1}\text{F}_3$ NPs with 2-hydroxyisophthalate in 50 mM HEPES at pH 7.0 (Figure 56).

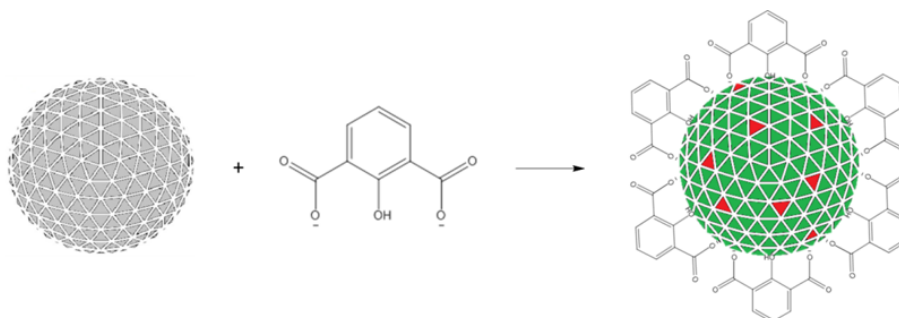


Figure 56: Titration of $\text{Tb}_{0.85}\text{La}_{0.14}\text{Eu}_{0.01}\text{F}_3$ NPs by 2-hydroxyisophthalate ligand.

The TR-excitation spectrum after ligand addition was measured for an emission at 545 nm as well as for an emission at 691 nm. Both spectra show the same intense excitation band at 325 nm, corresponding to the maximal excitation of the ligand (inset of Figure 57). The intensity of this band gradually increases at higher ligand concentrations.

The TR-emission spectra in each well were then measured by time-resolved detection after an excitation at 325 nm. The evolution of the emission spectra with increasing concentrations of ligand is shown in Figure 57. A gradual increase in intensity of both Tb and Eu emission bands is observed.

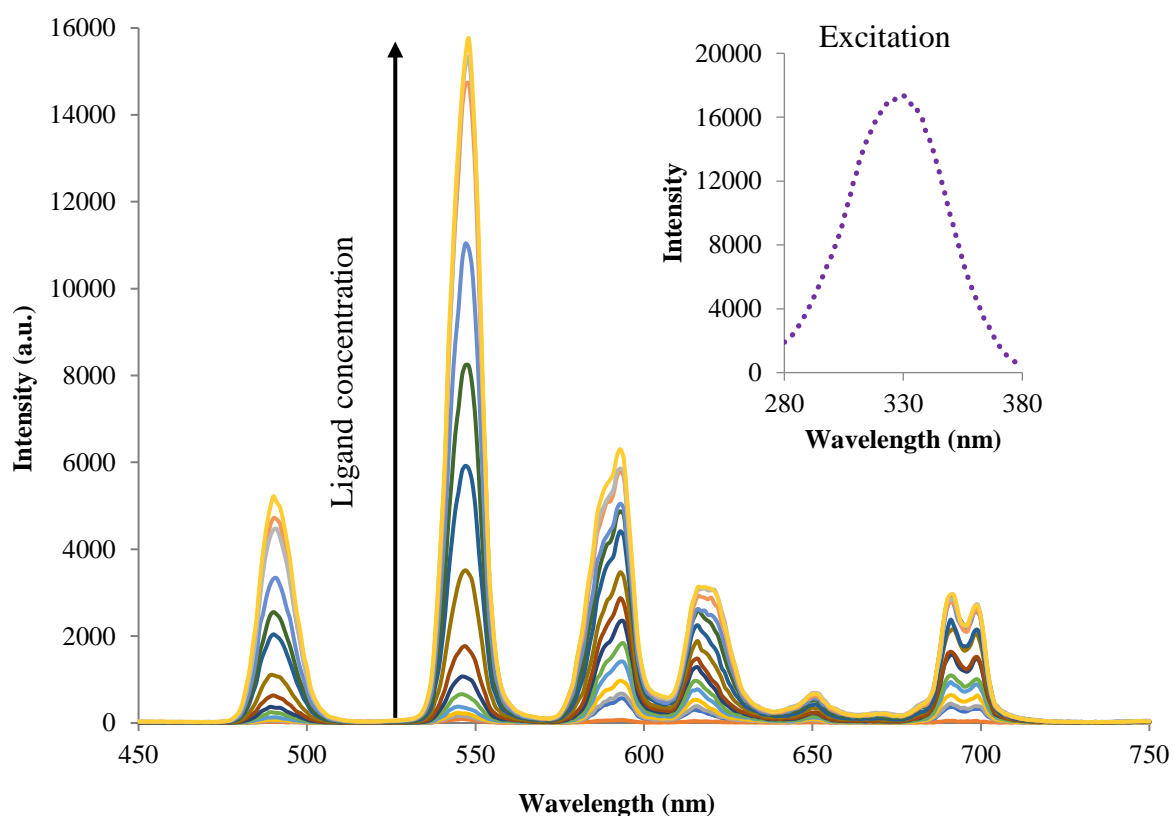


Figure 57: TR-emission spectra of $Tb_{0.85}La_{0.14}Eu_{0.01}F_3$ NPs ($\lambda_{exc} = 325$ nm) upon addition of increasing ligand concentrations. Inset : TR-excitation spectra ($\lambda_{em} = 590$ nm).

2-hydroxyisophthalate is already demonstrated to sensitize Tb ions, but is unable to sensitize Eu ions, as shown by the titration of Eu only doped NPs $La_{0.9}Eu_{0.1}F_3$. The ligand addition results in a very weak increase of the characteristic Eu emission bands indicating an inefficient sensitization as shown in Figure 58.

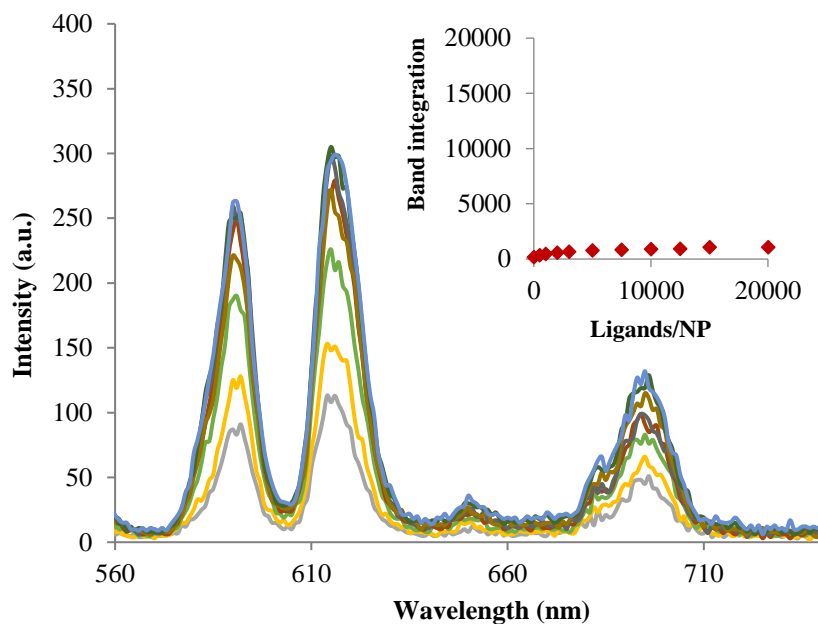


Figure 58: TR-emission spectra of $\text{La}_{0.9}\text{Eu}_{0.1}\text{F}_3\text{NPs}$ ($\lambda_{\text{exc}} = 325 \text{ nm}$) upon addition of increasing ligand concentrations. Inset : Evolution of Eu emission as a function of the ligand equivalents per NP.

This observation leads to questioning the significant increase of Eu emission bands in $\text{Tb}_{0.85}\text{La}_{0.14}\text{Eu}_{0.01}\text{F}_3$ NPs. To understand this phenomenon, the evolution of the Tb emission band peaking at 545 nm and Eu emission band peaking at 692 nm during the titration of $\text{Tb}_{0.85}\text{La}_{0.14}\text{Eu}_{0.01}\text{F}_3$ NPs are plotted as a function of ligand equivalents per NP (Figure 59).

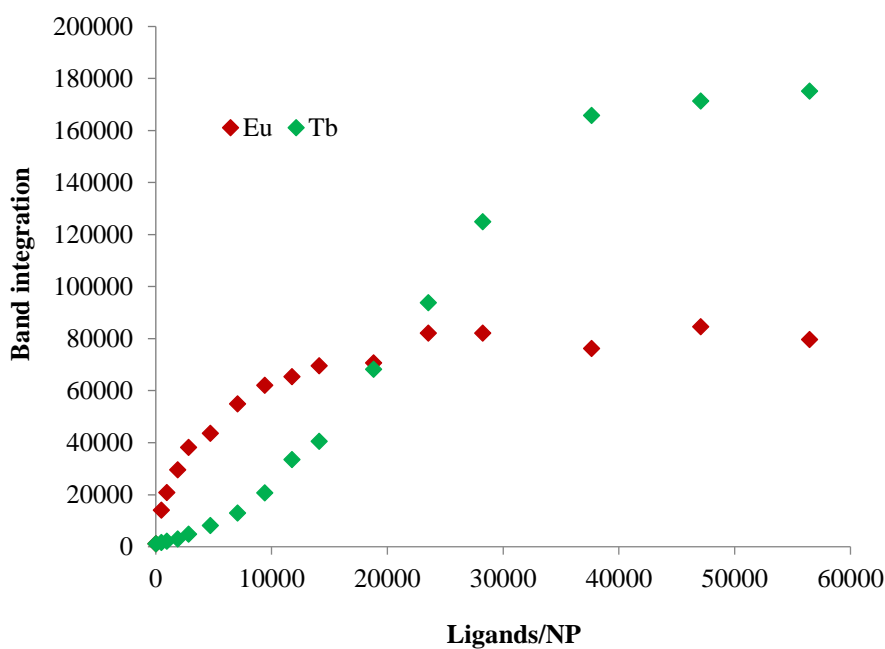


Figure 59: Evolution of the Tb emission band peaking at 545 nm and Eu emission band peaking at 692 nm as a function of ligand equivalents per NP.

The first ligand additions up to 5000 ligands/NP show a sharp increase of Eu emission band while only small increase is observed for that of Tb. Knowing that this ligand hardly sensitizes Eu ions, this strong emission is certainly due to the sensitization of Tb ions by the ligand followed by a quantitative energy transfer to Eu ions. When Eu emission approaches the constant region between 5000 and 10 000 ligands/NP, an increase of Tb emission is noticed. Once the 1% Eu are saturated, the sharp increase of Tb emission is then observed.

This process proves that $\text{Tb}_{0.85}\text{La}_{0.14}\text{Eu}_{0.01}\text{F}_3$ NPs allow to promote an energy transfer from Tb to Eu ions. This transfer is possible thanks to the proximity of the energy levels of Tb and Eu excited states. That of Tb being slightly higher than that of Eu, the transfer $\text{Tb} \rightarrow \text{Eu}$ is favored as represented in Figure 60.

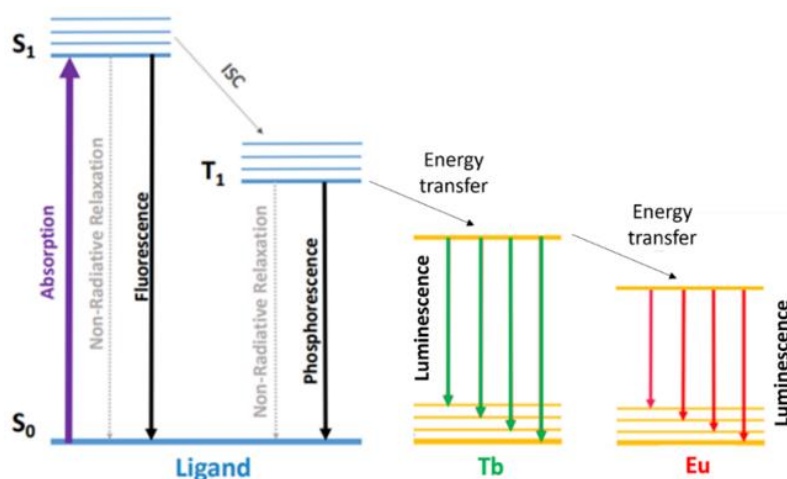


Figure 60: Jablonski diagram describing the energy transfer from the ligand to Tb ions and finally to Eu ions.

The intensity of Tb emission keeps increasing up to 30 000 ligands/NP. This N_{eq} is higher than that determined for $\text{La}_{0.9}\text{Tb}_{0.1}\text{F}_3$ NPs at 4500. This can be related to the bigger size of NPs and the change of the crystal structure, allowing to coordinate more ligands.

4.4.2. Brightness of dye-sensitized NPs

Due to the high N_{eq} providing strong molar extinction coefficient, and the enhanced quantum yield of Eu emission, these NPs present outstanding brightness ($> 10^7 \text{ M}^{-1} \cdot \text{cm}^{-1}$)²⁷ and became a center of several studies and further investigations in the laboratory. However, in terms of amplification factor, sensitized Tb emission is 200 times stronger than that of bare NPs, while sensitized Eu emission shows a factor of 100.

4.4.3. Excited state lifetime

The photoluminescence lifetime of Tb and Eu ion in the capped $Tb_{0.85}La_{0.14}Eu_{0.01}F_3$ NPs was determined by measuring the emission intensity of both Ln as a function of time as shown in Figure 61.

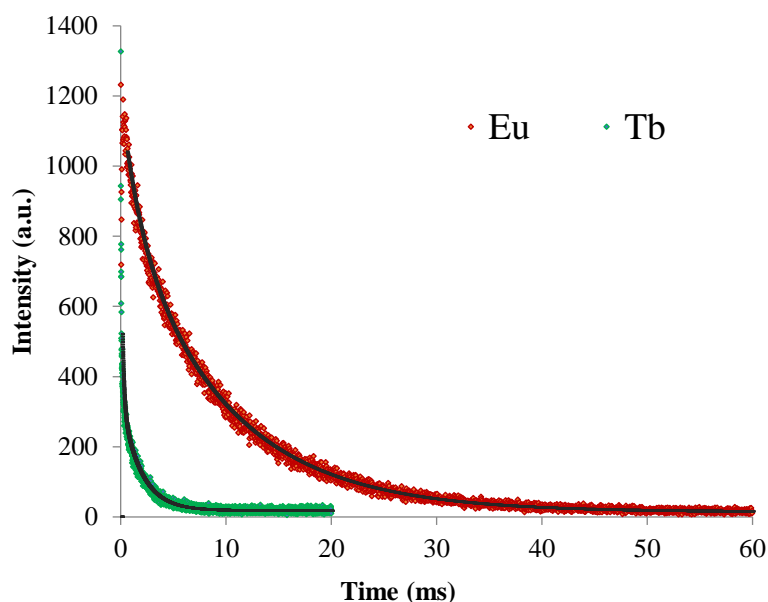


Figure 61: Photoluminescence decay ($\lambda_{exc} = 325$ nm) and fit curve (black) of Tb (green, $\lambda_{em} = 545$ nm) and Eu (red, $\lambda_{em} = 691$ nm) in dye-sensitized $Tb_{0.85}La_{0.14}Eu_{0.01}F_3$ NPs.

The emission of both Tb at 545 nm and Eu at 691 nm shows biexponential decays, indicating two different lifetime values, corresponding to two different Ln species. For Tb ions, the first constitutes 94% with a lifetime of 1.07 ms, while the second showing a lifetime of 124 μ s for the rest 6%. These lifetimes are much shorter compared to previous measurements with $La_{0.9}Tb_{0.1}F_3$ NPs (3.41 and 1.28 ms). These short values are due to the nonradiative energy transfer from Tb to Eu, and to a possible self-quenching due to the high Tb doping level.

For Eu ions, the biexponential decay is slower with a first component at 9.58 ms, representing 95% of the population, and the second shows a lifetime of 1.68 ms for the rest 5%. The resulting extremely long lifetime is close to the radiative lifetimes observed in the absence of non-radiative deactivation.³⁷

Indeed, that is due to an optimal protection of Eu ions with a doping level of 1% in the matrix against the vibrational quenching by the aqueous environment.

This luminescence lifetime as well as the exceptional brightness of these NPs make them prime candidates for biological imaging, capable of competing with commercial references.³³ In addition, simultaneous Tb and Eu emission detection at different wavelengths allows multiplexed detection techniques.

4.4.4. Titration of $Tb_{0.85}La_{0.14}Eu_{0.01}F_3$ NPs with nalidixic acid

In contrast to 2-hydroxyisophtalic acid, the nalidixic acid shown in Figure 62 is a quinolone ligand well known to form complexes with Ln cations. Interestingly, the triplet state of this ligand is suitable for a direct sensitization of both Tb and Eu.³⁸

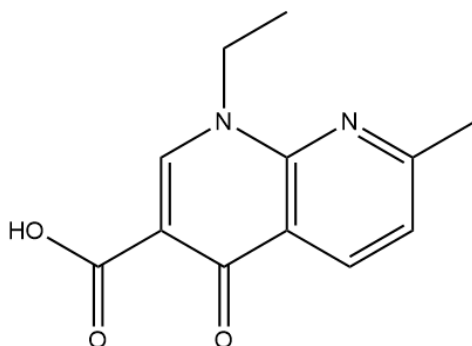


Figure 62: Nalidixic acid

A spectroscopic titration of 5×10^{-10} M $Tb_{0.85}La_{0.14}Eu_{0.01}F_3$ NPs was performed with the nalidixate ligand in 50 mM HEPES at pH 7.0 as described in Figure 63.

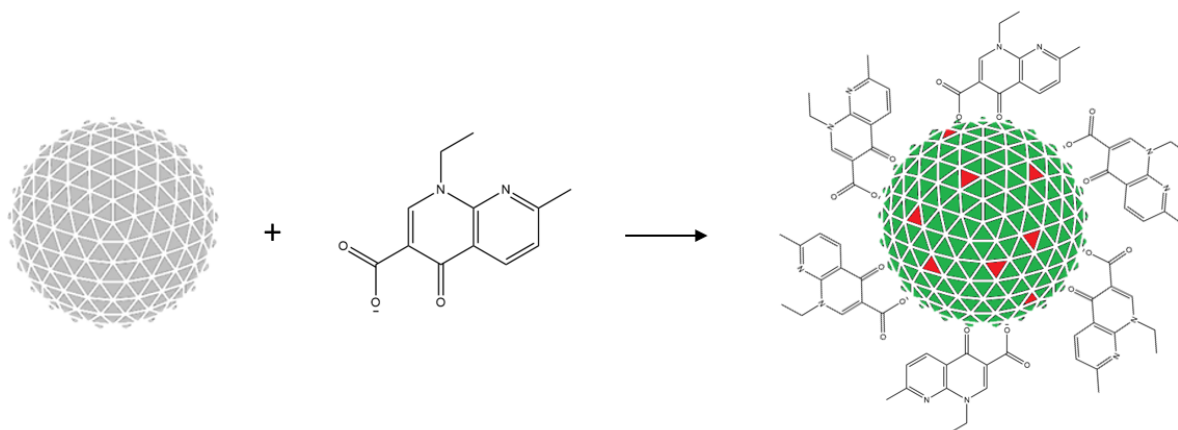


Figure 63: Titration of $Tb_{0.85}La_{0.14}Eu_{0.01}F_3$ NPs by nalidixate ligand.

The excitation spectrum after ligand addition was measured for an emission at 545 nm as well as for an emission at 691 nm. Both spectra show the same intense excitation band at 318 nm, corresponding to the maximal excitation of the ligand. The intensity of this band gradually increases at higher ligand concentrations.

The evolution of the Tb emission band peaking at 545 nm and that of Eu emission band peaking at 692 nm are plotted as a function of ligand equivalents per NP (Figure 64).

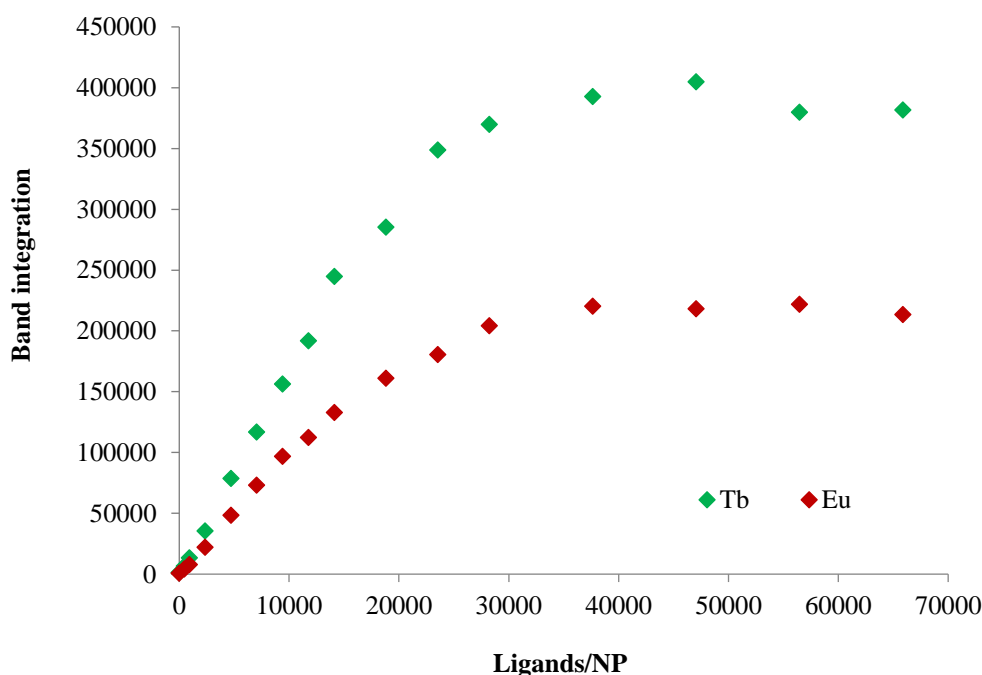


Figure 64: Evolution of the Tb emission band peaking at 545 nm and Eu emission band peaking at 692 as a function of ligand equivalents per NP ($\lambda_{exc} = 318$ nm).

As this ligand efficiently photosensitizes Eu and Tb ions, a gradual increase in the intensity of both Tb and Eu emission bands is observed, signaling simultaneous energy transfer by the antenna effect. After a strong amplification, Tb and Eu emission intensities simultaneously reached a maximum at approximately 30 000 ligand/NP and remains constant. The higher increasing slope and the higher maximum intensity of Tb emission is due to the difference in the doping rate between the two Ln. However, the luminescence ratio does not reflect at all the ratio of the doping rate. That proves one more time the enhancement of the spectroscopic properties of the 1% of Eu in $Tb_{0.85}La_{0.14}Eu_{0.01}F_3$ NPs, thanks to their optimal localization in a convenient environment of the NPs.

The nalidixate ligand provides the same amplification factor of 250 for both Tb and Eu sensitization. In addition, lifetime values of Eu luminescence are at 9.23 ms (93%) and 1.77 ms (7%), comparable to those obtained with 2-hydroxyisophthalate. However, Tb luminescence lifetimes are significantly shorter at 0.59 ms (79%) and 0.07 ms (3%).

The higher Tb luminescence lifetime with 2-hydroxyisophthalate sensitization can be explained by the better protection provided by the planar coordination on the surface of NPs. As for quinolone ligands, they are more suitable for coordination to Ln complexes. For Eu ions, the coordinated ligand does not affect their environment, because they are already confined in the core of NPs.

Table 6 summarizes the lifetime measurements of Tb and Eu emission in different NPs and with different sensitizing ligands.

Table 6: Summary of Tb and Eu photoluminescence lifetime measurements.

NPs	La _{0.9} Tb _{0.1} F ₃		Tb _{0.85} La _{0.14} Eu _{0.01} F ₃			
	2-hydroxyisophthalate		2-hydroxyisophthalate		nalidixate	
Tb (ms)	3.41 (54%)	1.28 (46%)	1.07 (94%)	0.124 (6%)	0.59 (97%)	0.07 (3%)
Eu (ms)	-		9.58 (95%)	1.68 (5%)	9.23 (93%)	1.77 (7%)

5. Conclusion

In this chapter, the aim was to prepare ultrabright dye-sensitized Ln-NPs and to investigate their physical, chemical, and spectroscopic properties. $\text{La}_{0.9}\text{Tb}_{0.1}\text{F}_3$ and $\text{Tb}_{0.85}\text{La}_{0.14}\text{Eu}_{0.01}\text{F}_3$ NPs were selected for their stability and their remarkable spectroscopic properties in the best interest of the supreme objective of the project.

The NPs have been synthesized *via* microwave-assisted technique and then characterized for their physicochemical properties by different techniques. These analyses show high quality NPs with small size, narrow distribution, uniform morphology, good colloidal stability, controlled composition, and crystalline phases.

To unleash their spectroscopic properties, the sensitization of these NPs was performed using 2-hydroxyisophthalate as an efficient antenna for Tb ions. This ligand is synthesized and used for NPs spectroscopic titrations, offering a strong photosensitization of Tb with important signal amplification and long luminescence lifetime.

On another hand, a Tb \rightarrow Eu energy transfer was demonstrated in the $\text{Tb}_{0.85}\text{La}_{0.14}\text{Eu}_{0.01}\text{F}_3$ NPs. Embedding 1% of Eu in the NPs provided cascade energy transfer from the ligand to the Tb ions on the surface and finally to the Eu ions protected in the core of the NPs. This process improved the quantum yield and the brightness of Eu luminescence in aqueous solution and provided an extremely long lifetime, close to the radiative lifetime of Eu ions.

Both $\text{La}_{0.9}\text{Tb}_{0.1}\text{F}_3$ and $\text{Tb}_{0.85}\text{La}_{0.14}\text{Eu}_{0.01}\text{F}_3$ ultrabright NPs demonstrated to be promising new tools in the development of luminescent probes, especially for use in bioanalysis. Particularly, $\text{La}_{0.9}\text{Tb}_{0.1}\text{F}_3$ NPs present higher stability, higher amplification factor and longer lifetime of Tb emission through the sensitization by 2-hydroxyisophthalate. Added to that the simpler approach compared to $\text{Tb}_{0.85}\text{La}_{0.14}\text{Eu}_{0.01}\text{F}_3$, these NPs were initially used to start the development of a sensitive ELISA detection method.

In the next step, the aim was to sensitize these NPs by a ligand resulting from an enzymatic reaction. Different ligands have been tested, and different enzymatic approaches came in mind in order to design this system. These approaches are discussed in detail in chapter III and chapter IV.

6. Experimental part

6.1. Reagents

High purity Ln salts, ammonium fluoride and nalidixic acid were purchased from Sigma. 2,6-dimethyl anisole was purchased from TCI. Potassium permanganate was purchased from VWR. Other solvents and products were purchased from Sigma, Acros, Alfa Aesar, fluorochem.

1.2. Synthesis of Ln-doped nanoparticles

A solution of NH_4F (0.72 M, 3.51 mL) in water was added using a syringe pump with a rate of 0.1 mL/min to a stirred aqueous mixture of LaCl_3 , TbCl_3 , and EuCl_3 (when needed) at room temperature, resulting in the formation of a slightly turbid solution. The proportions of added Ln salts are indicated in Table 7.

Table 7: The proportions of added Ln salts for the synthesis of the different NPs.

NPs	LaCl_3	TbCl_3	EuCl_3
$\text{La}_{0.9}\text{Tb}_{0.1}\text{F}_3$	0.05 M, 14.4 mL	0.05 M, 1.6 mL	-
$\text{Tb}_{0.85}\text{La}_{0.14}\text{Eu}_{0.01}\text{F}_3$	0.05 M, 2.24 mL	0.05 M, 13.6 mL	0.05 M, 160 μL

The mixture was heated in a microwave oven at 150°C for 12 min. After cooling, the precipitate was collected by centrifugation at 9000 rpm for 25 min. The isolated solid was dispersed in milliQ water (20 mL) with sonication at 60 °C for 30 min. The collection of the solid by centrifugation followed by dispersion in milliQ water is repeated three time for efficient purification from free La^{3+} , Tb^{3+} and Eu^{3+} in solution (Yield: 80-90%).

1.3. Characterization of nanoparticles

a) Transmission Electron Microscopy (TEM)

TEM measurements were performed with a JEOL 2100F electron microscope operating at 200kV equipped with a GATAN GIF 200 electron imaging filter, coupled with energy dispersive X-ray (EDX) spectroscopy, with a point-to-point resolution of 0.23 nm.

Powder samples were dispersed in water and a drop of this suspension deposited on TEM grids. The grid was prepared with a porous membrane covered by an amorphous carbon layer. These measurements were carried out at the IPCMS.

b) X-ray diffraction (XRD)

XRD patterns were recorded at room temperature using a Bruker D8 Advance diffractometer equipped with a monochromatic copper radiation source ($K\alpha = 1.54056 \text{ \AA}$) and a Sol-X detector in the $20\text{-}60^\circ$ (2θ) range with a scan step of 0.02° . These measurements were carried out at the ICPEES.

c) Colloidal properties

The zeta potential and the hydrodynamic diameter were measured using an AMERIGO system developed by Cordouan technologies, based on dynamic light scattering (DLS) and laser Doppler electrophoresis (LDE), respectively. All measurements were done in milliQ water at room temperature.

DLS measurements were performed directly with the stock solution by external probe with laser at 638 nm. The experimental correlograms are fitted by SBL mathematical algorithm and the results are treated by number of NPs. Particle refractive Index : 1.56 ; absorption at 638 nm : 0,01.

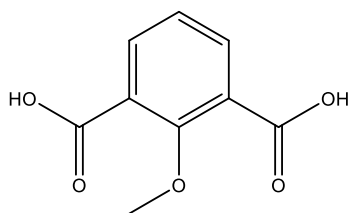
LDE measurements were performed in solutions diluted 50 times from stock solution at 20.27 V/cm applied electric field. Zeta potential is directly linked to the mobility of NPs according to the theory of Smoluchovski.

d) Inductively Coupled Plasma Atomic Emission Spectroscopy (ICP-AES)

NPs suspensions in milliQ water were dissolved by acidic attack. ICP-AES analyses were performed with a Varian 720-ES spectrometer equipped with a quartz Meinhard nebulizer and a cyclone spray chamber. The concentration was then determined by comparison with commercial standard samples. These measurements were carried out at “La plateforme d’Analyse des inorganiques” of the IPHC.

6.2. Synthesis of 2-hydroxyisophthalic acid

a) Intermediate compound



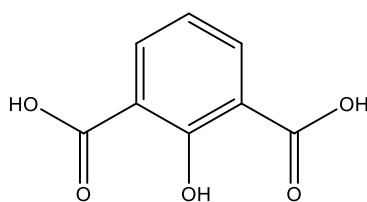
Chemical Formula: C₉H₈O₅

Molecular Weight: MW = 196.16 g.mol⁻¹

A suspension of 2,6-dimethylanisole (5 mL, 36 mmol), potassium permanganate (35.2 g, 220 mmol) and potassium hydroxide (6.2 g, 110 mmol) in water (200 mL) was stirred at reflux (110°C) for 48h. The reaction mixture was cooled to room temperature. The solution was acidified to pH 7 with concentrated HCl and the solid was filtered off. The mixture was adjusted to pH 2 with concentrated HCl and the resulting precipitate was collected by filtration and washed with cold concentrated HCl.

¹H-NMR (300 MHz, D₂O): δ 7.33 (d, $J = 7.5$ Hz, 2H), 7.17 (t, $J = 7.5$ Hz, 1H), 3.78 (s, 3H).

b) 2-hydroxyisophthalic acid



Chemical Formula: C₈H₆O₅

Molecular Weight: MW = 182.13 g.mol⁻¹

A suspension of 2-methoxyisophthalic acid (1 g) in 48% HBr/AcOH (20 mL) was heated at 120°C for 18h. The volatiles were removed under vacuum and the residue was purified by recrystallisation from methanol/water and dried to give a white powder with a 68% yield.³⁹

¹H-NMR (300 MHz, D₂O) : δ 7.48 (d, $J = 7.5$ Hz, 2H), 6.68 (t, $J = 7.5$ Hz, 1H).

c) NMR Spectroscopy

NMR spectra were recorded on a Bruker 300 MHz spectrometer. Chemical shifts are reported in ppm using non-deuterated residual solvents as reference.⁴⁰ The multiplicity of signals is given for the ¹H NMR spectra (s: singlet, d: doublet, t: triplet) and the coupling constants J are given in Hertz (Hz). The data were analyzed with MestReNova software.

d) Elemental analysis

Elemental analyses were recorded on a Flash 200 of ThermoFischer Scientific. These measurements were carried out by the “Service d’analyses, de mesures physiques et de spectroscopie optique” of the University of Strasbourg.

6.3. Spectroscopic measurements

UV/Vis absorption spectra were recorded on a Analytik Jena Specord spectrometer. Steady-state excitation and emission spectra were recorded on an Edinburgh Instrument FLP920 spectrometer working with a continuous 450W Xe Lamp and a red sensitive photomultiplier in Peltier housing. All spectra were corrected for the instrumental functions. Photoluminescence lifetimes were measured on the same instrument working in the Multi-Channel Spectroscopy (MCS) mode, using a Xenon flash lamp as the excitation source. Errors on lifetimes are estimated to $\pm 10\%$.

Time-resolved detection of excitation and emission spectra were recorded on a TECAN Spark microplate reader working with a high energy Xenon flash lamp. Measurements were done with a time delay of 50 μ s and an integration time of 2 ms.

6.4. Titration of the nanoparticles

In a typical titration experiment, 20 μ L of a solution of NPs at 5×10^{-10} M in 0.05 M HEPES buffer at pH 7.0 were added in 16 wells of a 96-well non-binding Greiner microplate. An increasing volume of a solution of ligand at 4×10^{-5} M in the same buffer was added to these wells. The total volume in each well is completed to 200 μ L with HEPES buffer. The microplate was agitated in a microplate shaker at room temperature for 10 min. The microplate was then readout on the microplate reader.

The excitation spectra were recorded at an emission of 545 nm for Tb or 691 nm for Eu, while the emission spectra were recorded at the maximal excitation. The excitation and emission bandwidth (20-5 nm), the gain (100), as well as the z-position (17500 μm) were kept constant in order to compare the different datasets. All spectra were recorded by time-resolved detection with a time delay of 50 μs and an integration time of 2 ms.

7. References

- (1) Fan, X.; Pi, D.; Wang, F.; Qiu, J.; Wang, M. Hydrothermal Synthesis and Luminescence Behavior of Lanthanide-Doped GdF₃/Sub 3/ Nanoparticles. *IEEE Trans. Nanotechnol.* **2006**, *5* (2), 123–128. <https://doi.org/10.1109/TNANO.2006.869670>.
- (2) Yi, Z.; Luo, Z.; Qin, X.; Chen, Q.; Liu, X. Lanthanide-Activated Nanoparticles: A Toolbox for Bioimaging, Therapeutics, and Neuromodulation. *Acc. Chem. Res.* **2020**, *53* (11), 2692–2704. <https://doi.org/10.1021/acs.accounts.0c00513>.
- (3) Liu, Y.; Tu, D.; Zhu, H.; Chen, X. Lanthanide-Doped Luminescent Nanoprobes: Controlled Synthesis, Optical Spectroscopy, and Bioapplications. *Chem. Soc. Rev.* **2013**, *42* (16), 6924–6958. <https://doi.org/10.1039/C3CS60060B>.
- (4) Zheng, W.; Huang, P.; Tu, D.; Ma, E.; Zhu, H.; Chen, X. Lanthanide-Doped Upconversion Nano-Bioprobes: Electronic Structures, Optical Properties, and Biodetection. *Chem. Soc. Rev.* **2015**, *44* (6), 1379–1415. <https://doi.org/10.1039/C4CS00178H>.
- (5) Ghosh, P.; Patra, A. Understanding the Influence of Nanoenvironment on Luminescence of Rare-Earth Ions. *Pramana* **2005**, *65* (5), 901–907. <https://doi.org/10.1007/BF02704090>.
- (6) Wen, H.; Wang, F. 4 - Lanthanide-Doped Nanoparticles: Synthesis, Property, and Application. In *Nanocrystalline Materials (Second Edition)*; Tjong, S.-C., Ed.; Elsevier: Oxford, 2014; pp 121–160. <https://doi.org/10.1016/B978-0-12-407796-6.00004-X>.
- (7) Naccache, R.; Yu, Q.; Capobianco, J. A. The Fluoride Host: Nucleation, Growth, and Upconversion of Lanthanide-Doped Nanoparticles. *Adv. Opt. Mater.* **2015**, *3* (4), 482–509. <https://doi.org/10.1002/adom.201400628>.
- (8) Jacobsohn, L. G.; Kucera, C. J.; James, T. L.; Sprinkle, K. B.; DiMaio, J. R.; Kokuoz, B.; Yazgan-Kukouz, B.; DeVol, T. A.; Ballato, J. Preparation and Characterization of Rare Earth Doped Fluoride Nanoparticles. *Materials* **2010**, *3* (3), 2053–2068. <https://doi.org/10.3390/ma3032053>.
- (9) Wang, F.; Zhang, Y.; Fan, X.; Wang, M. Facile Synthesis of Water-Soluble LaF₃ : Ln³⁺ Nanocrystals. *J. Mater. Chem.* **2006**, *16* (11), 1031–1034. <https://doi.org/10.1039/B518262J>.
- (10) Tu, D.; Zheng, W.; Huang, P.; Chen, X. Europium-Activated Luminescent Nanoprobes: From Fundamentals to Bioapplications. *Coord. Chem. Rev.* **2019**, *378*, 104–120. <https://doi.org/10.1016/j.ccr.2017.10.027>.
- (11) Mohammadian, E.; Rahimpour, E.; Alizadeh-Sani, M.; Foroumadi, A.; Jouyban, A. An Overview on Terbium Sensitized Based-Optical Sensors/Nanosensors for Determination of Pharmaceuticals. *Appl. Spectrosc. Rev.* **2022**, *57* (1), 39–76. <https://doi.org/10.1080/05704928.2020.1843174>.
- (12) Leonard, J. P.; Gunnlaugsson, T. Luminescent Eu(III) and Tb(III) Complexes: Developing Lanthanide Luminescent-Based Devices. *J. Fluoresc.* **2005**, *15* (4), 585–595. <https://doi.org/10.1007/s10895-005-2831-9>.
- (13) Latva, M.; Takalo, H.; Mikkala, V.-M.; Matachescu, C.; Rodríguez-Ubis, J. C.; Kankare, J. Correlation between the Lowest Triplet State Energy Level of the Ligand and Lanthanide(III) Luminescence Quantum Yield. *J. Lumin.* **1997**, *75* (2), 149–169. [https://doi.org/10.1016/S0022-2313\(97\)00113-0](https://doi.org/10.1016/S0022-2313(97)00113-0).
- (14) Liang, X.; Wang, X.; Zhuang, J.; Peng, Q.; Li, Y. Synthesis of NaYF₄ Nanocrystals with Predictable Phase and Shape. *Adv. Funct. Mater.* **2007**, *17* (15), 2757–2765. <https://doi.org/10.1002/adfm.200600807>.

- (15) An, R.; Liang, Y.; Deng, R.; Lei, P.; Zhang, H. Hollow Nanoparticles Synthesized via Ostwald Ripening and Their Upconversion Luminescence-Mediated Boltzmann Thermometry over a Wide Temperature Range. *Light Sci. Appl.* **2022**, *11* (1), 217. <https://doi.org/10.1038/s41377-022-00867-9>.
- (16) Salzmann, B. B. V.; van der Sluijs, M. M.; Soligno, G.; Vanmaekelbergh, D. Oriented Attachment: From Natural Crystal Growth to a Materials Engineering Tool. *Acc. Chem. Res.* **2021**, *54* (4), 787–797. <https://doi.org/10.1021/acs.accounts.0c00739>.
- (17) Goetz, J.; Nonat, A.; Diallo, A.; Sy, M.; Sera, I.; Lecointre, A.; Lefevre, C.; Chan, C. F.; Wong, K.-L.; Charbonnière, L. J. Ultrabright Lanthanide Nanoparticles. *ChemPlusChem* **2016**, *81* (6), 526–534. <https://doi.org/10.1002/cplu.201600007>.
- (18) Bogachev, N. A.; Betina, A. A.; Bulatova, T. S.; Nosov, V. G.; Kolesnik, S. S.; Tumkin, I. I.; Ryazantsev, M. N.; Skripkin, M. Y.; Mereshchenko, A. S. Lanthanide-Ion-Doping Effect on the Morphology and the Structure of NaYF₄:Ln³⁺ Nanoparticles. *Nanomaterials* **2022**, *12* (17), 2972. <https://doi.org/10.3390/nano12172972>.
- (19) Maximov, B.; Schulz, H. Space Group, Crystal Structure and Twinning of Lanthanum Trifluoride. *Acta Crystallogr. B* **1985**, *41* (2), 88–91. <https://doi.org/10.1107/S0108768185001677>.
- (20) Bhattacharjee, S. DLS and Zeta Potential – What They Are and What They Are Not? *J Control Release* **2016**, *235*, 337–351. <https://doi.org/10.1016/j.jconrel.2016.06.017>.
- (21) Kielar, F.; Montgomery, C. P.; New, E. J.; Parker, D.; Poole, R. A.; Richardson, S. L.; Stenson, P. A. A Mechanistic Study of the Dynamic Quenching of the Excited State of Europium(III) and Terbium(III) Macrocyclic Complexes by Charge- or Electron Transfer. *Org. Biomol. Chem.* **2007**, *5* (18), 2975–2982. <https://doi.org/10.1039/B709062E>.
- (22) Benisvy, L.; Gamez, P.; Fu, W. T.; Kooijman, H.; Spek, A. L.; Meijerink, A.; Reedijk, J. Efficient Near-UV Photosensitization of the Tb(III) Green Luminescence by Use of 2-Hydroxyisophthalate Ligands. *Dalton Trans.* **2008**, No. 24, 3147–3149. <https://doi.org/10.1039/B805507F>.
- (23) Law, G.-L.; Pham, T. A.; Xu, J.; Raymond, K. N. A Single Sensitizer for the Excitation of Visible and NIR Lanthanide Emitters in Water with High Quantum Yields. *Angew. Chem. Int. Ed.* **2012**, *51* (10), 2371–2374. <https://doi.org/10.1002/anie.201106748>.
- (24) Samuel, A. P. S.; Moore, E. G.; Melchior, M.; Xu, J.; Raymond, K. N. Water-Soluble 2-Hydroxyisophthalamides for Sensitization of Lanthanide Luminescence. *Inorg. Chem.* **2008**, *47* (17), 7535–7544. <https://doi.org/10.1021/ic800328g>.
- (25) Miyata, K.; Konno, Y.; Nakanishi, T.; Kobayashi, A.; Kato, M.; Fushimi, K.; Hasegawa, Y. Chameleon Luminophore for Sensing Temperatures: Control of Metal-to-Metal and Energy Back Transfer in Lanthanide Coordination Polymers. *Angew. Chem. Int. Ed.* **2013**, *52* (25), 6413–6416. <https://doi.org/10.1002/anie.201301448>.
- (26) Pavlovich, V. S. Solvatochromism and Nonradiative Decay of Intramolecular Charge-Transfer Excited States: Bands-of-Energy Model, Thermodynamics, and Self-Organization. *ChemPhysChem* **2012**, *13* (18), 4081–4093. <https://doi.org/10.1002/cphc.201200426>.
- (27) Goetz, J. Biocompatible Luminescent Probes for Imaging and Inhibition of Cancer, Strasbourg University, 2018.
- (28) Gill, R.; Zayats, M.; Willner, I. Semiconductor Quantum Dots for Bioanalysis. *Angew. Chem. Int. Ed.* **2008**, *47* (40), 7602–7625. <https://doi.org/10.1002/anie.200800169>.
- (29) Wu, C.; Chiu, D. T. Highly Fluorescent Semiconducting Polymer Dots for Biology and Medicine. *Angew. Chem. Int. Ed.* **2013**, *52* (11), 3086–3109. <https://doi.org/10.1002/anie.201205133>.
- (30) Nonat, A.; Regueiro-Figueroa, M.; Esteban-Gómez, D.; de Blas, A.; Rodríguez-Blas, T.; Platas-Iglesias, C.; Charbonnière, L. J. Definition of an Intramolecular Eu-to-Eu Energy

- Transfer within a Discrete [Eu₂L] Complex in Solution. *Chem. Eur. J.* **2012**, *18* (26), 8163–8173. <https://doi.org/10.1002/chem.201200087>.
- (31) Mikhalyova, E. A.; Yakovenko, A. V.; Zeller, M.; Kiskin, M. A.; Kolomzarov, Y. V.; Eremenko, I. L.; Addison, A. W.; Pavlishchuk, V. V. Manifestation of π - π Stacking Interactions in Luminescence Properties and Energy Transfer in Aromatically-Derived Tb, Eu and Gd Tris(Pyrazolyl)Borate Complexes. *Inorg. Chem.* **2015**, *54* (7), 3125–3133. <https://doi.org/10.1021/ic502120g>.
- (32) Peterson, K. L.; Margherio, M. J.; Doan, P.; Wilke, K. T.; Pierre, V. C. Basis for Sensitive and Selective Time-Delayed Luminescence Detection of Hydroxyl Radical by Lanthanide Complexes. *Inorg. Chem.* **2013**, *52* (16), 9390–9398. <https://doi.org/10.1021/ic4009569>.
- (33) Xu, J.; Corneillie, T. M.; Moore, E. G.; Law, G.-L.; Butlin, N. G.; Raymond, K. N. Octadentate Cages of Tb(III) 2-Hydroxyisophthalamides: A New Standard for Luminescent Lanthanide Labels. *J. Am. Chem. Soc.* **2011**, *133* (49), 19900–19910. <https://doi.org/10.1021/ja2079898>.
- (34) Cross, A. M.; May, P. S.; Veggel, F. C. J. M. van; Berry, M. T. Dipicolinate Sensitization of Europium Luminescence in Dispersible 5%Eu:LaF₃ Nanoparticles. *J. Phys. Chem. C* **2010**, *114* (35), 14740–14747. <https://doi.org/10.1021/jp103366j>.
- (35) Charbonnière, L. J.; Rehspringer, J.-L.; Ziessel, R.; Zimmermann, Y. Highly Luminescent Water-Soluble Lanthanide Nanoparticles through Surface Coating Sensitization. *New J. Chem.* **2008**, *32* (6), 1055–1059. <https://doi.org/10.1039/b719700d>.
- (36) Beeby, A.; Clarkson, I. M.; Dickins, R. S.; Faulkner, S.; Parker, D.; Royle, L.; Sousa, A. S. de; Williams, J. A. G.; Woods, M. Non-Radiative Deactivation of the Excited States of Europium, Terbium and Ytterbium Complexes by Proximate Energy-Matched OH, NH and CH Oscillators: An Improved Luminescence Method for Establishing Solution Hydration States. *J. Chem. Soc. Perkin Trans. 2* **1999**, *0* (3), 493–504. <https://doi.org/10.1039/A808692C>.
- (37) Bünzli, J.-C. G. Lanthanide Luminescence for Biomedical Analyses and Imaging. *Chem. Rev.* **2010**, *110* (5), 2729–2755. <https://doi.org/10.1021/cr900362e>.
- (38) Bel'tyukova, S. V.; Egorova, A. V.; Teslyuk, O. I. Europium(III) and Terbium(III) Chelates of Quinolonecarboxylic Acid Derivatives as Labels for Immunofluorimetric Assay. *J. Anal. Chem.* **2000**, *55* (7), 682–685. <https://doi.org/10.1007/BF02828007>.
- (39) Trester-Zedlitz, M.; Kamada, K.; Burley, S. K.; Fenyö, D.; Chait, B. T.; Muir, T. W. A Modular Cross-Linking Approach for Exploring Protein Interactions. *J. Am. Chem. Soc.* **2003**, *125* (9), 2416–2425. <https://doi.org/10.1021/ja026917a>.
- (40) Fulmer, G. R.; Miller, A. J. M.; Sherden, N. H.; Gottlieb, H. E.; Nudelman, A.; Stoltz, B. M.; Bercaw, J. E.; Goldberg, K. I. NMR Chemical Shifts of Trace Impurities: Common Laboratory Solvents, Organics, and Gases in Deuterated Solvents Relevant to the Organometallic Chemist. *Organometallics* **2010**, *29* (9), 2176–2179. <https://doi.org/10.1021/om100106e>.

Chapter III

Enzymatic reaction: Hydroxylation of
isophthalates by HRP

1. Introduction

In Chapter II, Ln-NPs were developed, and their dye-sensitization was successfully demonstrated, yielding ultrabright luminescence. The next step was to find an enzymatic reaction, where the resulting product can act as the sensitizer of these NPs. Four conditions are required for an efficient system.

- Appropriate enzyme selection: the selected enzyme must be convenient with antibody (or streptavidin) conjugation for the further ELISA application of the system.
- Efficient enzymatic conversion: the enzyme must provide high reaction yield of the desired product with minimal side products, and a high kinetic rate.
- Optimal reaction blank: the substrate of the enzymatic reaction must not be able to sensitize the NPs, so in absence of enzyme, no signal amplification must be detected.
- Efficient photosensitization: the formed product must acquire the ability to coordinate to the surface of the NPs and efficiently photosensitize the Ln ions.

2. Preliminary approach

In regard of the system requirements, the first intention was to emulate the strategies used in enzyme-amplified lanthanide luminescence (EALL). The methods developed for the determination of alkaline phosphatase enzyme (AP) using phosphorylated pre-antenna as a substrate showed interesting performance and great potential.¹ This approach is based on the liberation of the phenol group as shown in Figure 65, creating appropriate function for chelating lanthanide ions, while the aromatic moiety is supposed to efficiently sensitize them.

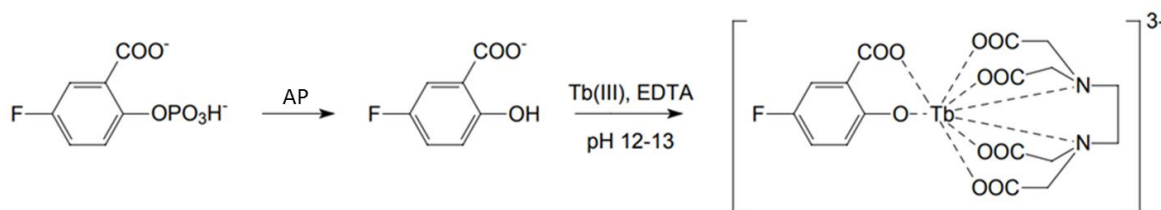


Figure 65: Example of EALL. Enzymatic formation of salicylic acid followed by Tb³⁺ photosensitization.¹

Therefore, the idea was to find Tb or Eu sensitizers containing phenol groups, which when phosphorylated, can be applied as substrates in such system.

For that, several ligands were tested for the sensitization of Tb or Eu NPs. The candidates are presented in Figure 66, and their absorption and emission properties are summarized in Table 8. These ligands were selected based on their interesting coordinating structure, optical properties, and the reported ability of some of them to sensitize lanthanide ions.^{2,3}

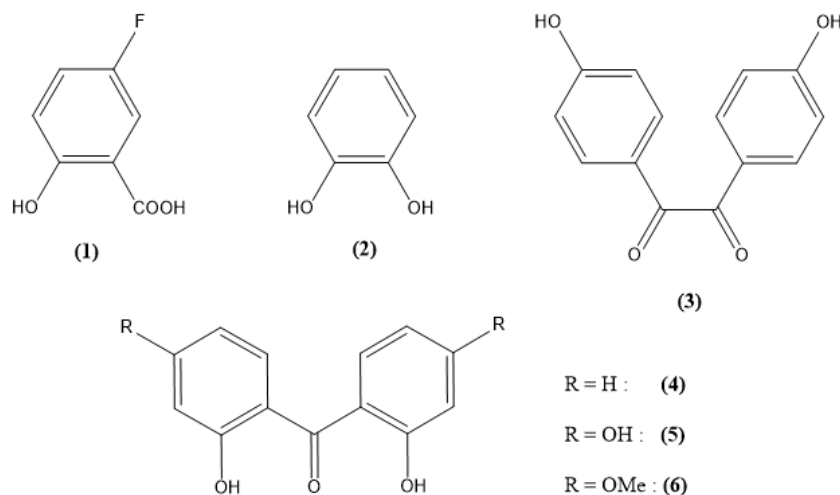


Figure 66: Ligands tested for the sensitization of Tb and Eu.

Table 8: Spectroscopic properties of tested ligands.

	Ligand	λ Absorption (nm)	ϵ ($M^{-1}.cm^{-1}$)	λ Excitation (nm)	λ Emission (nm)
(1)	5-Fluorosalicilate	308	4200	308	420
(2)	Catechol	278	2700	278	310
(3)	4,4'-Dihydroxybenzil	306	27800	290	380
(4)	2,2'-Dihydroxy benzophenone	260 335	12300 5400	296	408
(5)	2,2',4,4'-Tetrahydroxy benzophenone	285 340	10800 16100	296	380
(6)	2,2'-Dihydroxy-4,4'-dimethoxybenzophenone	285 335	13500 11500	296	366

After the study of the optical properties of these ligands, they were tested for the sensitization of Tb or Eu NPs at neutral and basic pH. Unfortunately, except of the 5-fluorosaliclyate, all other ligands did not show any sensitization ability of the NPs. That can be related either to the poor coordination of such ligands to the NPs surface due to the relatively high pKa of the phenol groups, or to an energy mismatch of the ligand triplet state with the Ln emissive state.

For the salicylate derivative, the low pKa carboxylate group can improve the coordination capacity of this ligand as represented by the sensitization of Tb-NPs. A spectroscopic titration of $\text{La}_{0.9}\text{Tb}_{0.1}\text{F}_3$ NPs was performed by the 5-fluorosaliclyate in 0.05 M HEPES at pH 7.0. Emission spectra are recorded with excitation at 340 nm, the maximum ligand excitation, and shown in Figure 67a. The evolution of the integration of Tb emission band peaking at 545 nm is plotted as a function of the added ligand equivalents per NP in Figure 67b.

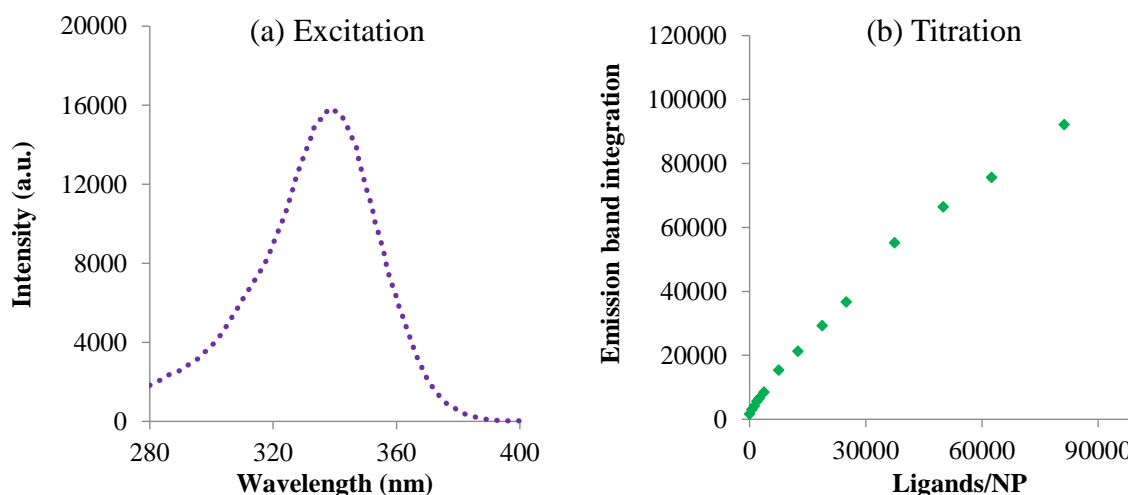


Figure 67: (a) Excitation spectrum of $\text{La}_{0.9}\text{Tb}_{0.1}\text{F}_3$ NPs ($\lambda_{em} = 545$ nm) upon 5-fluorosaliclyate addition.

(b) Evolution of the Tb emission at 545 nm ($\lambda_{exc} = 340$ nm) as a function of the ligand equivalents per NP.

The titration of $\text{La}_{0.9}\text{Tb}_{0.1}\text{F}_3$ NPs showed an increase of Tb emission band proving the sensitization by the 5-fluorosaliclyate. Surprisingly, the intensity kept increasing with ligand addition up to 100 000 ligands/NP without reaching a maximum which indicates that NPs did not reach the surface saturation even at very high ligands concentration.

5-fluorosaliclyate seems to have weaker coordination at the surface of NPs in comparison with the typical 2-hydroxyisophthalate sensitizer studied in Chapter II. The latter having two carboxylate groups exhibits better coordination than this monoacid, despite the electron-withdrawing fluoro group aiming to decrease the pKa of the phenol.

Consequently, the 5-fluorosalicylate allowed only 50 times amplification of Tb emission at 100000 ligands/NP, while the 2-hydroxyisophthalate provided an amplification of 500 times upon NPs saturation at 4500 ligands/NP. The inability to provide a high response at low concentrations makes the 5-fluorosalicylate also out of the competition.

3. Hydroxylation of isophthalate by HRP

The first attempts searching for efficient photosensitizers of the NPs failed to find better than the 2-hydroxyisophthalate ligand. Therefore, the approach adopted to develop the enzymatic system consisted in starting with this well-known efficient sensitizer and trying to produce it *via* proper enzymatic reaction.

Horseshoe peroxidase (HRP) is a haem-containing enzyme (Figure 68), extensively used in immunochemistry and biocatalytic applications.⁴

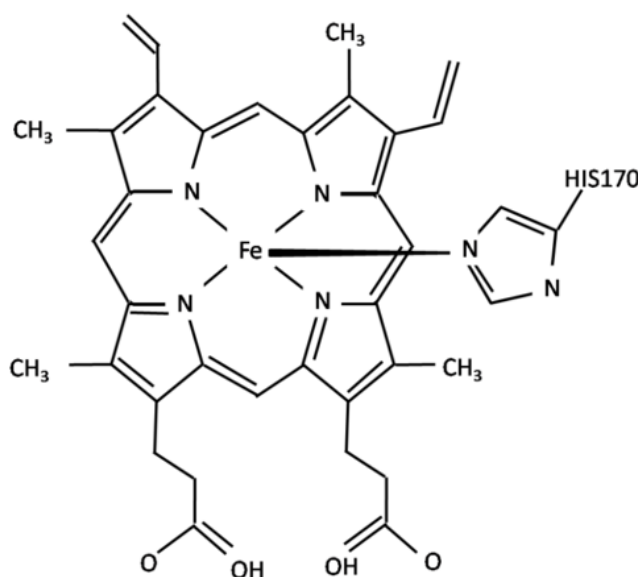
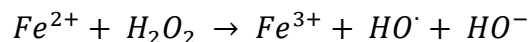


Figure 68: Structure of ferriprotoporphylin IX (or iron haem) active site of HRP enzyme.

The full catalytic activity of HRP is described in Figure 69. This enzyme mainly catalyzes the oxidation of diverse hydrogen donor substrates by hydrogen peroxide (H_2O_2) in a peroxidative reaction cycle. When the hydrogen donor is a substrate like Nicotinamide Adenine Dinucleotide (NADH), the oxidation product NAD^+ can mediate the reduction of O_2 in an oxidative cycle, forming the superoxide ($\text{O}_2^{\cdot-}$).⁵

This superoxide was later shown to be involved in the conversion of the ferric form of the enzyme haem (Fe^{3+}) into the labile perferryl form ($\text{Fe}^{2+}\text{-O}_2$) designated as Compound III and generally considered as enzymatically inactive.⁶ This latter containing Fe^{2+} , one can imagine that it can act as a Fenton reagent in a manner similar to Fe^{2+} -chelates, which results in the production of hydroxyl radicals (HO^\bullet) from H_2O_2 as follows.⁷



This novel function of peroxidase has been then widely studied for its mechanism, the involved chemical species and the factors influencing its happening.⁶

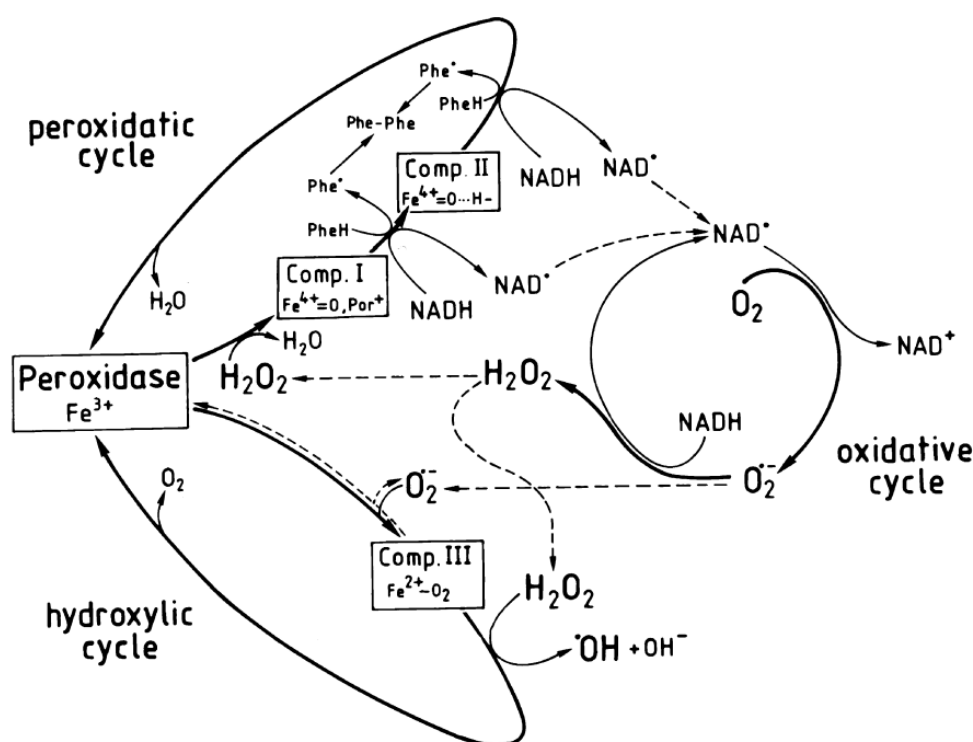


Figure 69: Reaction scheme describing the catalytic activity of peroxidase enzyme.⁶

HO^\bullet radicals are highly reactive oxidants that nonspecifically attack most of the organic molecules. Aromatic compounds, which possess an ability to undergo HO^\bullet addition reaction yielding in highly fluorescent hydroxylated products have been used as chemical detectors of HO^\bullet . These include phenol, benzoic acid, hydroxybenzoic acids, nitrophenols, coumarin and others.⁸ Peterson *et al.* raised the level by reporting an effective strategy to monitor HO^\bullet formation by H_2O_2 photolysis using a Tb-complex and a pre-antenna.⁹ The hydroxylated antenna formed by HO^\bullet attack to the pre-antenna, would coordinate and sensitize Tb ions. Interestingly, six antennas were investigated including 2-hydroxyisophthalate.

These works were inspiring to combine the enzymatic production of HO[•] radicals with their detection by hydroxylation of a pre-antenna followed by Tb sensitization. As HRP fulfills the enzyme selection criteria, and 2-hydroxyisophthalate is proven as an efficient antenna for the synthesized La_{0.9}Tb_{0.1}F₃ NPs, the aim is to study the efficiency of this enzymatic reaction to form the desired product as shown in Figure 70. In addition, different pre-antennas were investigated, and the performances of the developed system was fully evaluated.

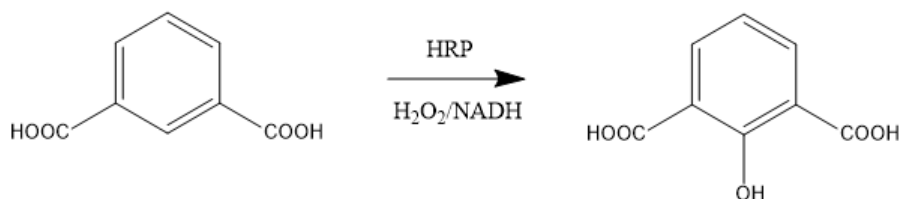


Figure 70: Hydroxylation of isophthalate catalyzed by HRP in the presence of H₂O₂ and NADH.

3.1. Antenna vs pre-antenna

This targeted detection method relies on a substantial difference in the sensitizing ability between the antenna and its corresponding non-hydroxylated analog. Therefore, it was essential to verify that no Tb sensitization occurs by the isophthalate (IP). A spectroscopic titration of La_{0.9}Tb_{0.1}F₃ NPs is performed by the IP and compared to that with 2-hydroxyisophthalate (2-HIP) in 0.05 M HEPES at pH 7.0. Emission spectra are recorded with excitation at 325 nm and the evolution of the integration of Tb emission band peaking at 545 nm is plotted as a function of the added ligand equivalents per NP in Figure 71.

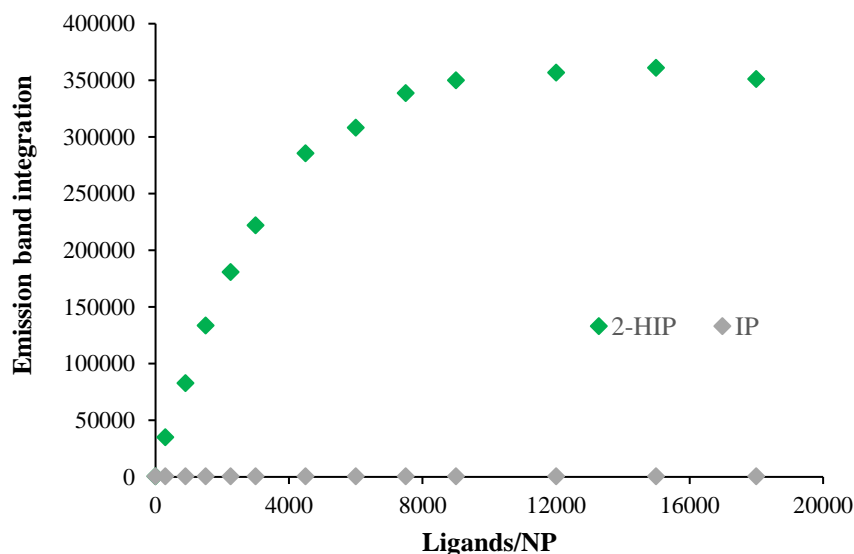


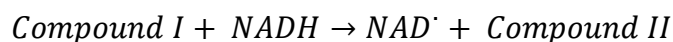
Figure 71: Spectroscopic titration of La_{0.9}Tb_{0.1}F₃ with IP and 2-HIP ($\lambda_{exc} = 325$ nm, $\lambda_{em} = 545$ nm).

The addition of IP to the $\text{La}_{0.9}\text{Tb}_{0.1}\text{F}_3$ NPs shows no increase in Tb emission bands, compared to the 500 times amplification induced by 2-HIP sensitization. Thus, a detected Tb signal increase is specific to the hydroxylation of IP. This result validates IP/2-HIP pair as appropriate pre-antenna/antenna for the enzymatic reaction monitoring.

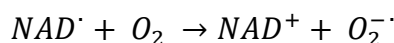
3.2. Enzymatic reaction

The HO^\bullet -producing activity of HRP was demonstrated by the hydroxylation of IP. 500 μM of IP, 1 mM of H_2O_2 and 200 μM of NADH were incubated in microplate wells at room temperature under aerobic conditions, in 10 mM sodium citrate buffer pH 6.0, an optimal pH for this system.⁸ The reaction was initiated by the addition of 0.2 μM HRP enzyme. The final volume of the reaction mixture was fixed to 200 μL in all the assays.

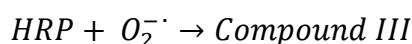
In the presence of H_2O_2 , HRP catalyzes single electron oxidation of NADH through the peroxidative cycle involving Compounds I and II as follows.



Under aerobic conditions, the oxidization product NAD^\bullet reacts with O_2 to form a superoxide radical through the oxidative cycle as follows.



The reductant $\text{O}_2^{\bullet-}$ is able to convert the haem group of HRP from the ferric form into the perferryl form as a Compound III.



The interconversion of ferriperoxidase into Compound III was photometrically confirmed after 1 min of incubation by slight red shift in the maximal absorbance as shown in Figure 72.¹⁰

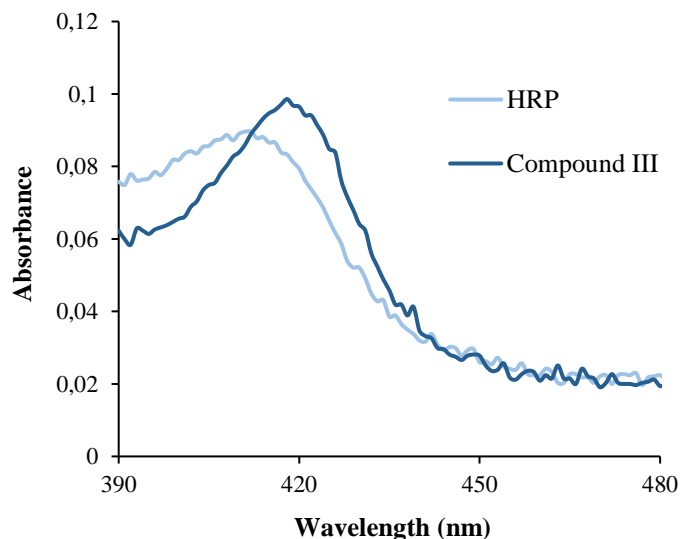
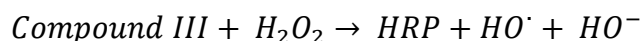


Figure 72: Absorbance spectra signaling the conversion of HRP into compound III after 1 min of incubation.

Compound III acts as a Fenton reagent to mediate the generation of HO^\bullet radicals from H_2O_2 .



These radicals are meant to exhibit the hydroxylation of IP. After a 1h of incubation, the fluorescence spectra of the reaction mixture in the presence and the absence of HRP were recorded with an excitation at 306 nm and compared to that of 2-HIP (Figure 73).

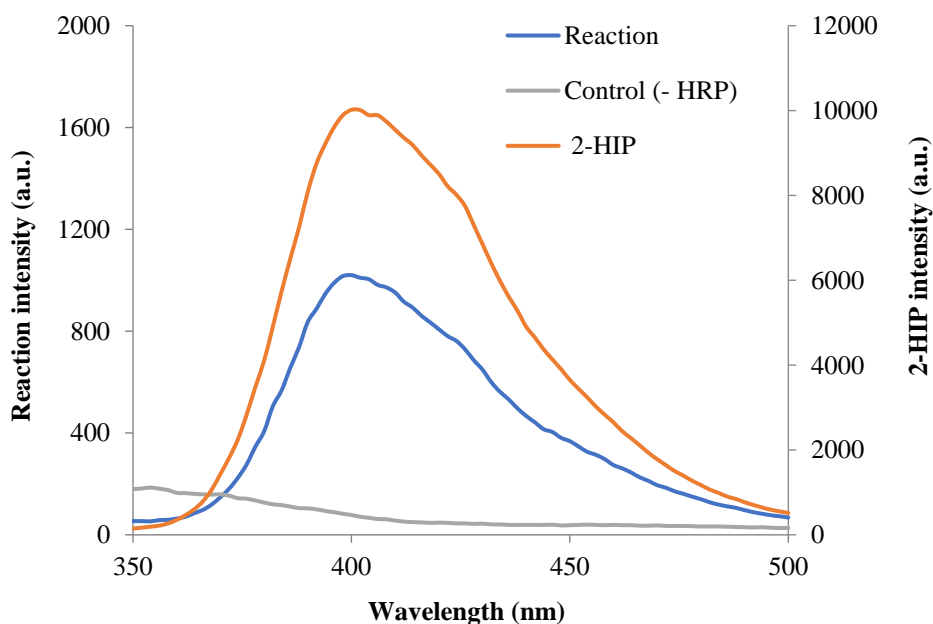


Figure 73: Fluorescence spectra of the reaction mixture ($\lambda_{\text{exc}} = 306 \text{ nm}$) in the presence and the absence of HRP.

In the absence of HRP, no emission was detected after the same duration due to the non-fluorescence of IP in these conditions. In the presence of the enzyme, the emission signal of the reaction mixture allows the identification of 2-HIP as a hydroxylation product of the reaction. However, the intensity of the formed 2-HIP corresponded to 10% yield of IP hydroxylation.

After identifying the desired product, it was important to evaluate the reaction kinetics. The formation of 2-HIP is monitored for 1h of reaction by measuring the emission intensity at 402 nm after an excitation at 306 nm as shown in Figure 74.

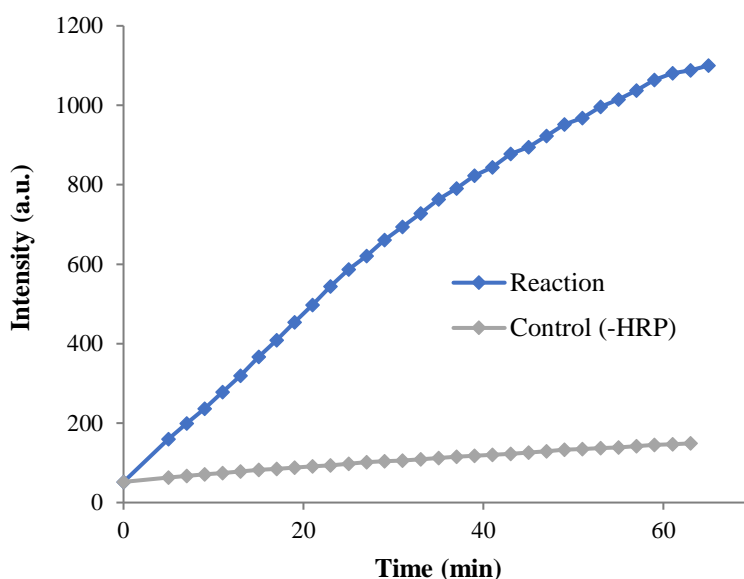


Figure 74: Reaction kinetics ($\lambda_{exc} = 306 \text{ nm}$, $\lambda_{em} = 402 \text{ nm}$) of the enzymatic IP hydroxylation.

The assay produced constant reaction kinetics for about 30 min then started to slow down. The formation of 2-HIP was dependent on the presence of native HRP. However, a low rate of hydroxylation was still observed if HRP was not added. That can be referred to a UV photolysis of H_2O_2 , forming HO^\bullet radicals at low concentrations.¹¹

The yield and the kinetics of 2-HIP formation were not impressive, and that can be due to the formation of side products. The hydroxylation by HO^\bullet attack is nonspecific, but the charge or the lack of charge on the aromatic ring affects the position at which the substitution occurs. The presence of two carboxylate groups on the IP aromatic ring allows various orientations of the hydroxylation and even multiple hydroxylations on the same ring. Buhler and Mason reported 6 different products for an HRP-catalysed benzoic acid hydroxylation.⁸ That makes the IP susceptible to hydroxylation in all available *o*-, *p*-, and *m*- positions.

3.3. Tb sensitization following the reaction

Before any further optimization, it was important to check the photosensitization of Tb-NPs by the enzymatically formed 2-HIP. After 1 hour of reaction, 2×10^{-8} M of $\text{La}_{0.9}\text{Tb}_{0.1}\text{F}_3$ NPs (20 μL) were added to the reaction mixture in presence and in absence of HRP. This concentration corresponds to 2500 antennas/NPs assuming a 10% yield of 2-HIP formation. The TR-emission spectrum after an excitation at 325 nm was then recorded (Figure 75).

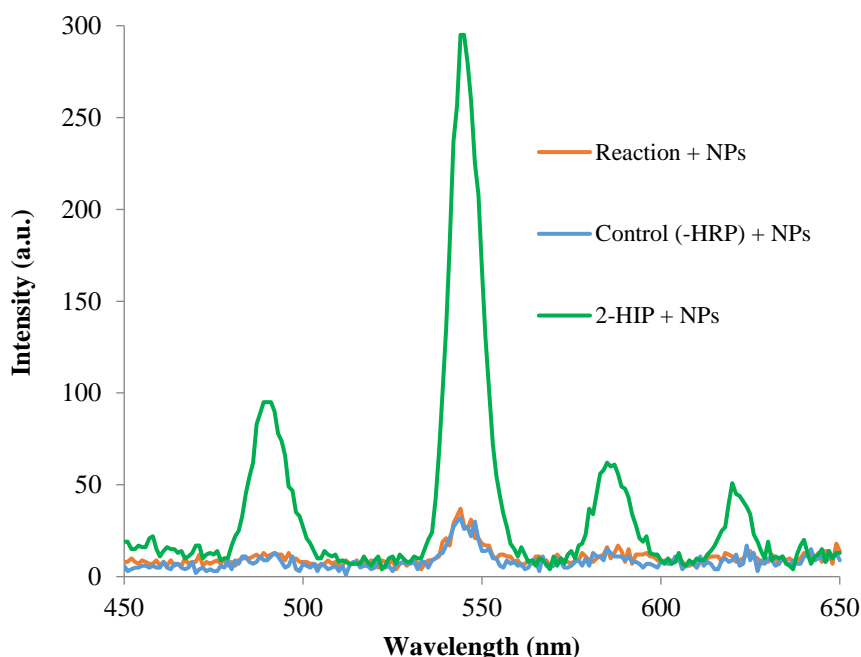


Figure 75: TR-emission spectra of $\text{La}_{0.9}\text{Tb}_{0.1}\text{F}_3$ NPs ($\lambda_{exc} = 325$ nm) after their addition to the reaction mixture.

Surprisingly, the enzymatic formation of 2-HIP did not lead to any increase in Tb emission intensity compared to that obtained when no reaction occurred. Moreover, even the synthetic 2-HIP did not show the usual efficient sensitization in these buffer conditions. These results called for further investigations of the effect of the medium on the Tb-NPs sensitization.

3.3.1. Effect of citrate on Tb sensitization

Often used for the preparation of water-soluble Ln-NPs, citrate is a very strong chelating agent due to the presence of three negatively charged carboxylate groups (Figure 76). Thus, it may be a serious competing anion for ligands to the NPs surface coordination.¹²

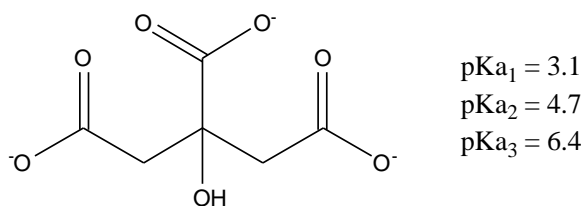
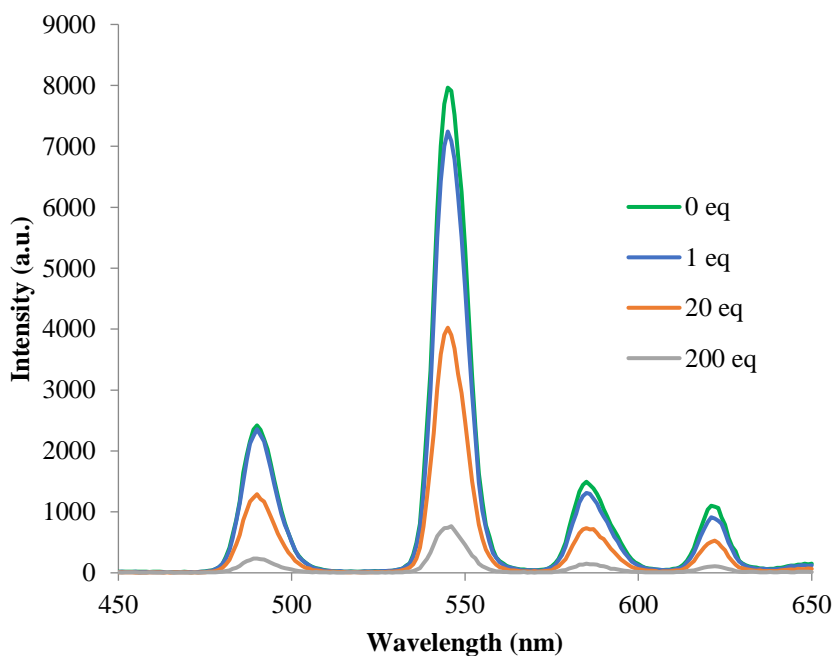


Figure 76: Citrate anion.

To investigate any competing effect of citrate on the 2-HIP sensitization of $\text{La}_{0.9}\text{Tb}_{0.1}\text{F}_3$ NPs, different equivalents of citrate anions per ligand were added to 2×10^{-8} M of 2-HIP capped NPs (2500 ligands/NP) at pH 6.0. The TR-emission spectra after an excitation at 325 nm were recorded and presented in Figure 77.

Figure 77: TR-emission spectra ($\lambda_{\text{exc}} = 325$ nm) of 2-HIP-sensitized $\text{La}_{0.9}\text{Tb}_{0.1}\text{F}_3$ NPs with increasing equivalents of citrate ions.

At a 1:1 ratio of citrate ions to 2-HIP, the intensity of Tb emission decreases by only 9% while at 20 equivalents of citrate this intensity decreases by 50%. At 200 equivalents of citrate, which correspond to the 10 mM citrate buffer used in the enzymatic reaction, the Tb emission is 90% suppressed. That can explain the weak sensitization observed in the reaction conditions.

Consequently, the buffer must be replaced by a buffer compatible with NPs sensitization, while maintaining a proper functioning of the enzymatic reaction. A large variety of compounds was demonstrated to interfere with the hydroxylation reaction as a target of HO^\bullet attack including buffers like HEPES, MOPS and Tris.¹³

On another hand, citrate and phosphate buffers were demonstrated to suppress NPs sensitization. 2-(*N*-morpholino)ethane sulfonic acid (MES) is used as a buffering agent in biology and biochemistry. It is chemically and enzymatically stable with minimal absorption in the UV-vis spectral range, and is also useful as a non-coordinating buffer.¹⁴ MES buffer was then adopted for the next experiments.

3.3.2. Effect of H₂O₂ on Tb sensitization

a) Quenching of Tb luminescence by H₂O₂

To evaluate the effect of the unreacted H₂O₂ on the 2-HIP sensitization of La_{0.9}Tb_{0.1}F₃ NPs, different equivalents of H₂O₂ per ligand were added to 2×10⁻⁸ M of 2-HIP capped NPs (2500 ligand/NP) at pH 6.0. The TR-emission spectra after an excitation at 325 nm were recorded and presented in Figure 78.

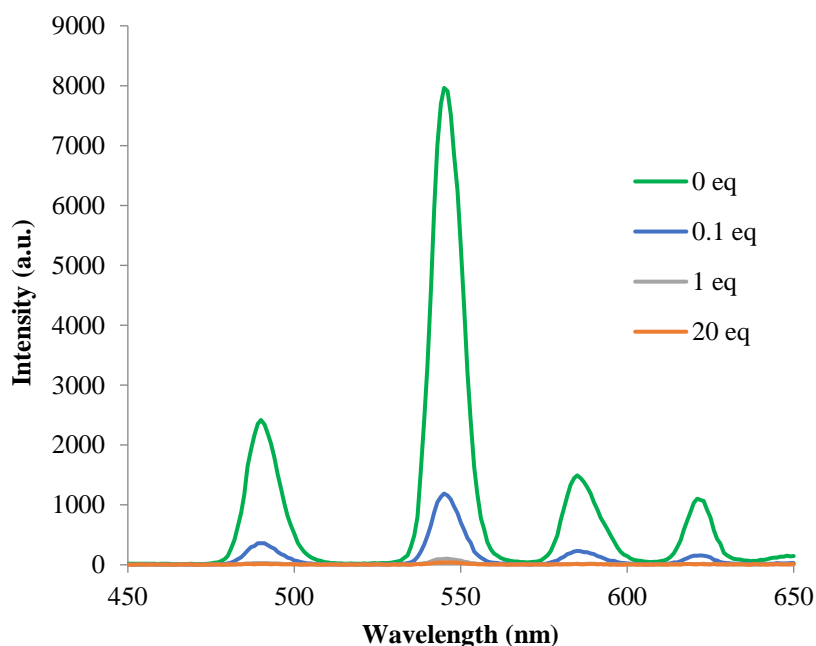
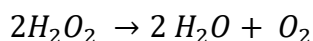


Figure 78: TR-emission spectra ($\lambda_{exc} = 325 \text{ nm}$) of 2-HIP-sensitized La_{0.9}Tb_{0.1}F₃ NPs with increasing equivalents of H₂O₂.

At 0.1 equivalent of H₂O₂ per ligand, 85% of Tb luminescence is already quenched, while at 1 equivalent the intensity decreases by 90%. At 20 equivalents of H₂O₂, which correspond to the initial H₂O₂ concentration used in the enzymatic reaction, the Tb emission is totally quenched. With a pKa of around 11.6, H₂O₂ has no preference to coordinate to the NPs and its quenching effect through vibrational energy transfer to O-H oscillators should not exceed that of H₂O.¹⁵

Although Tb(III) has a highly positive reduction potential ($E_0 = + 3.1 \text{ V}$), but it can be oxidized to its tetravalent state via ozonolysis or electrolysis.¹⁶ An oxidation of Tb(III) by H_2O_2 , a powerful oxidizing agent, is not excluded. Tb(IV) does not give any emission and its presence in any host acts as a quenching center.¹⁷ Thus, this significant quenching of Tb luminescence could be due to an oxidation by the excess of H_2O_2 . This phenomenon must be further studied to demonstrate or deny this hypothesis. Anyway, this excess of H_2O_2 must be eliminated before the signal readout in order to obtain an optimal functioning of the system.

H_2O_2 is the simplest of peroxides, which slowly decomposes to oxygen and water with a release of heat when exposed to light, and rapidly in the presence of organic or reactive compounds.¹⁸ To accelerate the decomposition of H_2O_2 , an antioxidant is usually used.



Back to the developed assay, different compounds such as ascorbic acid and sodium iodide (NaI) were shown to be inefficient in these conditions. Ascorbic acid has been also found to interfere with the luminescence of NPs, while NaI appeared to be ineffective in recovering the luminescence of sensitized NPs. After several attempts using organic and inorganic compounds, Catalase enzyme was tested to remove the excess of H_2O_2 .

b) Recovery of Tb luminescence by catalase

Catalase (CAT) is a common enzyme found in nearly all living organisms exposed to oxygen.¹⁹ It is an antioxidant enzyme which catalyzes the decomposition of H_2O_2 into water and oxygen without requiring any activators as described in Figure 79.

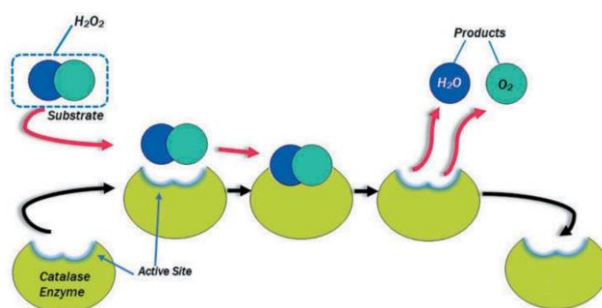


Figure 79: An overview of the CAT-catalyzed decomposition of H_2O_2 .²⁰

CAT has one of the highest turnover numbers of all enzymes. The CAT activity is defined by units per mass, where 1 unit allows the decomposition of $1 \mu\text{mol}$ of H_2O_2 per min at pH 7.0 at 25°C . Commercial bovine liver CAT activity is constant over the pH range of 4.0-8.5.²¹

CAT was evaluated to recover Tb luminescence by decomposing H_2O_2 quencher. To a 2×10^{-8} M of 2-HIP capped $\text{La}_{0.9}\text{Tb}_{0.1}\text{F}_3$ NPs (2500 ligands/NP) at pH 6.0, 20 equivalents of H_2O_2 per ligand were added. Then, 0.05 mg/mL of CAT (1 unit) were introduced to the mixture. The mixture before and after CAT addition was pretested by colorimetric peroxide test strips for a semi-quantitative detection of residual peroxide as shown in Figure 80. The results show that after 1 min of CAT addition, no H_2O_2 are left in solution.

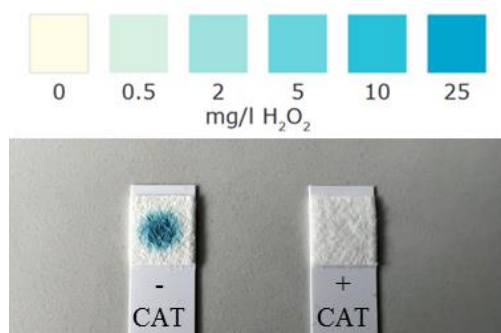


Figure 80: Peroxide test strips before and after CAT addition.

In addition, the TR-emission spectrum was recorded before and after CAT addition. The latter is also compared to the emission spectrum in absence of H_2O_2 quencher (Figure 81). CAT was shown to immediately recover almost 100% of the sensitized luminescence of Tb-NPs.

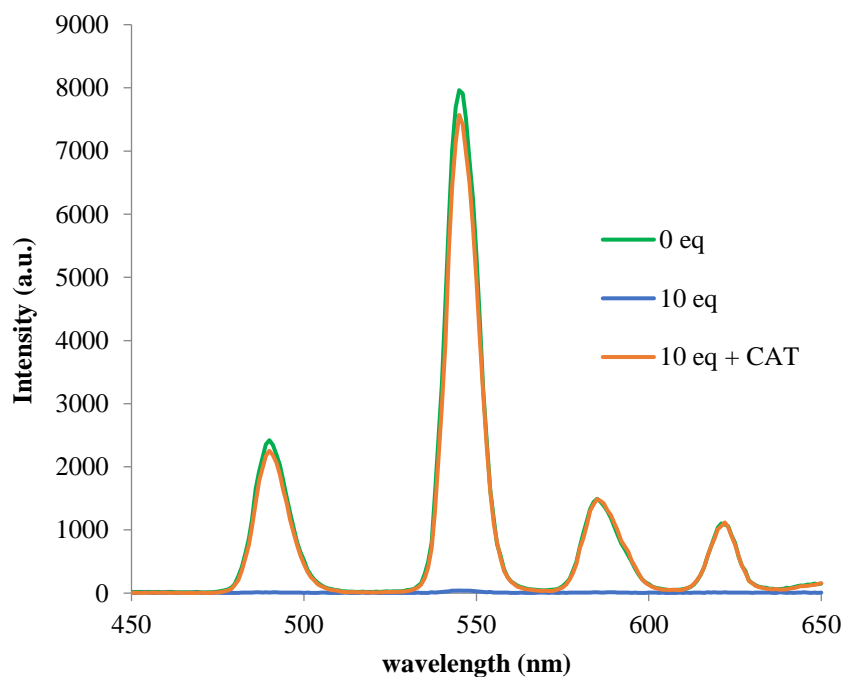


Figure 81: TR-emission spectra ($\lambda_{exc} = 325$ nm) of 2-HIP-sensitized $\text{La}_{0.9}\text{Tb}_{0.1}\text{F}_3$ NPs before and after CAT addition.

3.3.3. Final enzymatic assay

The enzymatic reaction was performed in the same conditions mentioned in part 2.2, while replacing citrate with MES buffer. The enzymatic hydroxylation of IP was verified by monitoring the increase in the emission intensity of 2-HIP at 402 nm (inset Figure 82). After 1 hour of reaction, 5 μ L of a 2 mg/mL solution of CAT were added, and the elimination of H_2O_2 was verified by the peroxide test strips. Finally, $La_{0.9}Tb_{0.1}F_3$ NPs were added as described in part 2.3 and the TR-emission spectrum after the excitation of the antenna was recorded and presented in Figure 82.

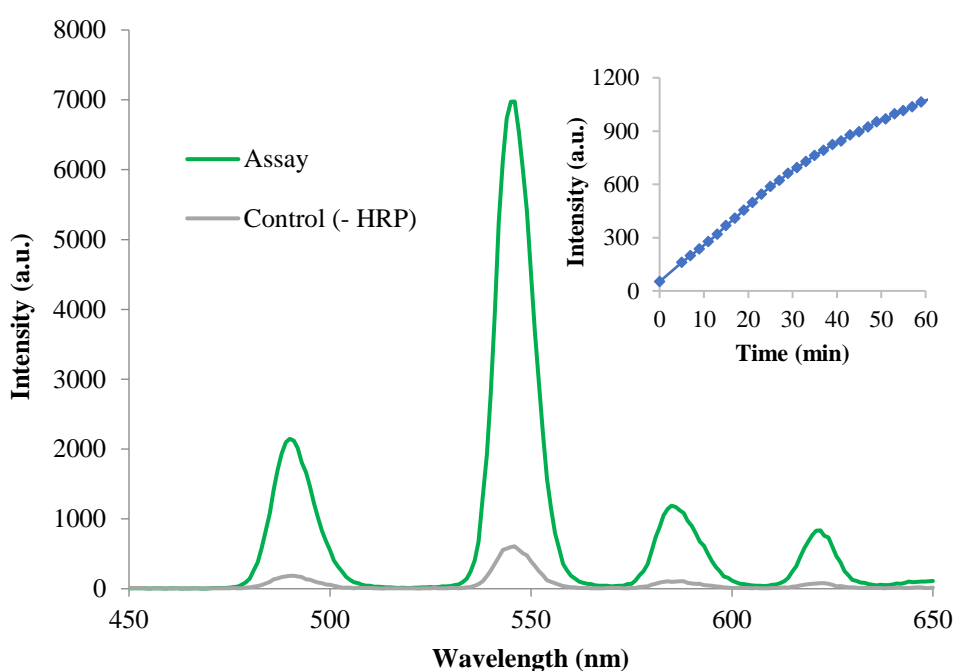


Figure 82: TR-emission spectra ($\lambda_{exc} = 325$ nm) of $La_{0.9}Tb_{0.1}F_3$ NPs after their addition to the reaction mixture. Inset : Reaction kinetics ($\lambda_{exc} = 306$ nm, $\lambda_{em} = 402$ nm) of the enzymatic IP hydroxylation.

The emission spectra showed an increase of Tb emission bands following the enzymatic reaction. This turn-on ability can be expressed by the ratio of Tb emission after the HRP-catalyzed formation of the hydroxylated antenna to that obtained in absence of the enzyme. The latter is relatively important due to low hydroxylation observed in the absence of HRP. At 0.2 μ M of HRP enzyme, an amplification factor of 10 is obtained. Compared to the enzyme concentrations used in ELISA (pM), this detection needs further optimization.

Considering the estimated 10% yield of hydroxylation, the non-specific HO^\bullet attack must have involved several inactive side products which limited the formation of the 2-HIP antenna and consequently the sensitization of Tb-NPs. It is in this regard that the system can be improved.

4. Effect of the pre-antenna

The attempt to improve the efficiency of the system consisted in the modification of the pre-antenna, trying to promote the final sensitization signal. To do so, two different IP-based candidates were selected for application in the enzymatic reaction. These are the trimesic acid and the 5-cyano isophthalic acid presented in Figure 83.

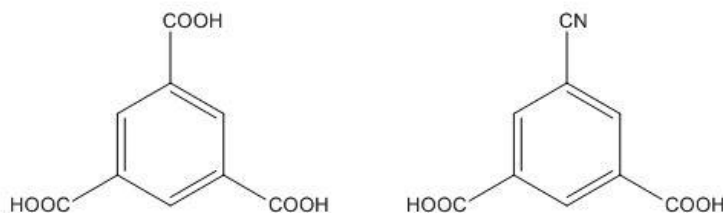


Figure 83: Trimesic acid (left) and 5-cyano isophthalic acid (right).

These two pre-antennas were selected for different reasons. The trimesate antenna has an additional benefit of three equivalent primary reaction sites for HO[•] attack.⁹ The reaction at either site results in the same product, which must increase the yield of antenna formation. On the other hand, the 5-cyano isophthalate has the benefit of the cyano group in *p*-position. This electron withdrawing group is intended to increase the energy transfer of the hydroxylated antenna to the NPs by lowering the triplet state level.²² It also helps to decrease the pKa of the enzymatically-added hydroxyl group, which allows better coordination to the surface of the NPs. Thus, these investigated pre-antennas were selected to optimize the HO[•] response and maximize the relative sensitized luminescence intensity in comparison with IP.

4.1. Study of the sensitization

To study the pre-antenna/antenna pairs, it was essential to determine and compare the ability of each antenna to sensitize Tb-NPs under identical conditions. The standard hydroxylated analogs were synthesized in the laboratory by Dr Joan Goetz according to the procedure described in the literature.²³ Then, spectroscopic titrations of La_{0.9}Tb_{0.1}F₃ NPs were performed with each antenna in 0.01 M MES at pH 6.0. First, an excitation spectrum after the addition of the different antennas was measured for an emission at 545 nm (Figure 84).

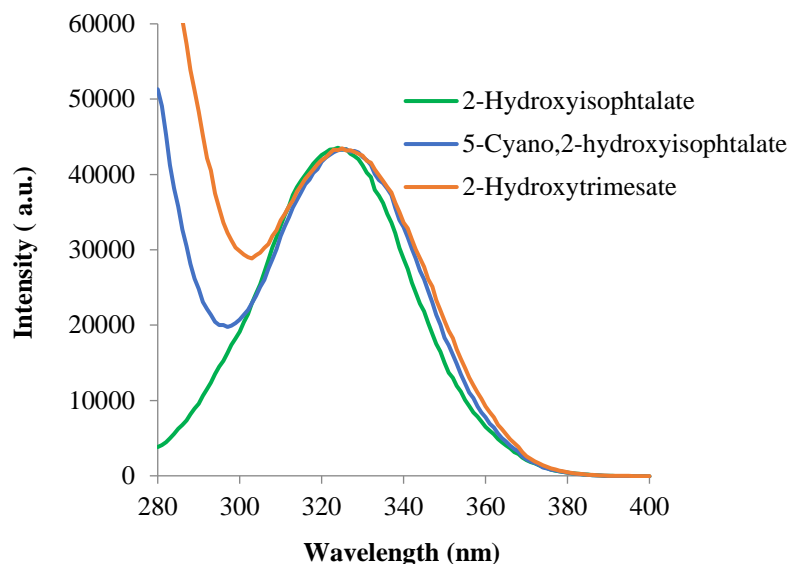


Figure 84: TR-excitation spectra ($\lambda_{em} = 545$ nm) of $Tb_{0.85}La_{0.14}Eu_{0.01}F_3$ NPs upon addition of the different antennas.

The excitation spectra upon the addition of hydroxytrimesate or 5-cyano-2-hydroxyisophthalate show a very slight red shift of the maximal excitation in comparison with that obtained with 2-hydroxyisophthalate. Keeping all experimental conditions constant, the titration of $La_{0.9}Tb_{0.1}F_3$ NPs by these three antennas can be directly compared. Figure 85 shows the evolution of Tb emission band peaking at 545 nm as a function of the added equivalents per NP of each antenna.

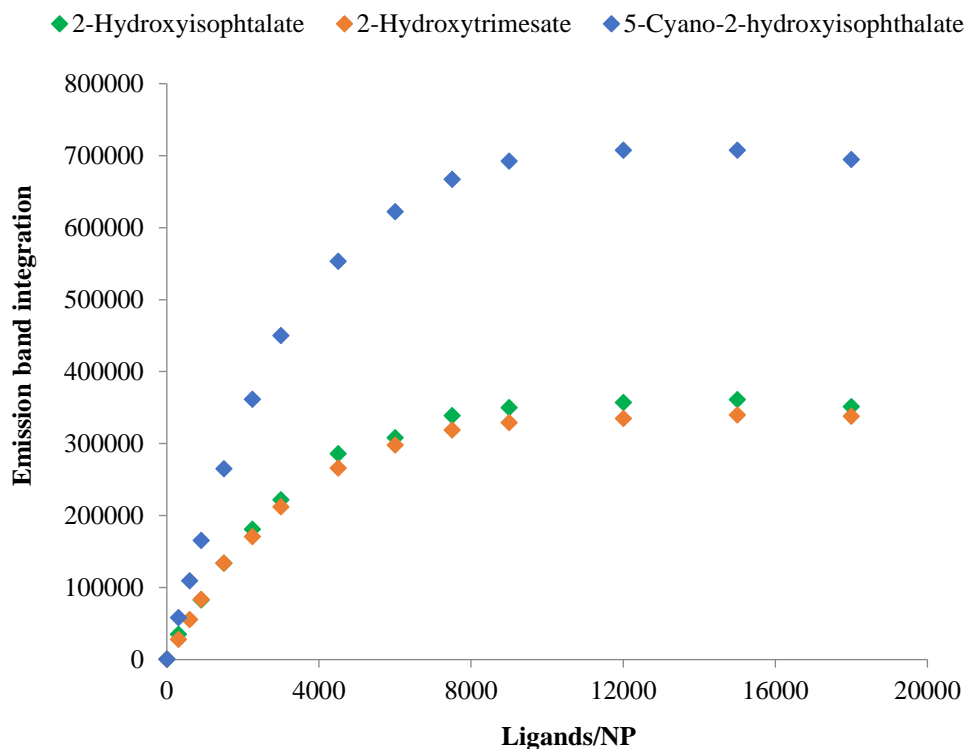


Figure 85: Spectroscopic titration of $La_{0.9}Tb_{0.1}F_3$ NPs with the different antennas ($\lambda_{exc} = 325$ nm, $\lambda_{em} = 545$ nm).

These titration curves show the same general aspect for all three antennas, with an augmentation of the Tb emission band with increasing ligand concentrations, and then a constant region signaling the full capping of the NPs. Moreover, this saturation of NPs surface indicates the same equivalent ligand number (N_{eq}) at around 4500 ligands/NP for all three antennas. That is due to the same basic isophthalate unit, preserving the same size and the same bidentate coordination to the NPs surface.

In terms of the sensitization efficiency, the hydroxytrimesate exhibits similar performance in comparison to the 2-hydroxyisophthalate. On the other hand, as expected, the 5-cyano-2-hydroxyisophthalate shows better sensitization efficiency than the other two antennas with more than two times improvement.

4.2. Enzymatic assay

The enzymatic reaction was performed with the three pre-antennas following the final conditions. The hydroxylation of each pre-antenna was verified by monitoring the increase in the emission intensity of its hydroxylated form. Due to different brightnesses, the hydroxylation kinetics of the three compounds cannot be directly compared. However, the formation yield of each antenna was estimated based on the fluorescence of the synthesized standard compound.

After 1 hour of reaction, the formation yield of 5-cyano-2-hydroxyisophthalate was estimated at only 15%, but a little higher than that obtained with 2-hydroxyisophthalate at 10%. The cyano group in the pre-antenna occupies one primary reaction site for HO \cdot attack which slightly increases the probability of hydroxylation between the two carboxylates. As for the hydroxytrimesate, a formation yield of 50% was estimated. As expected, the tricarboxylate pre-antenna provided three equivalent reaction sites for HO \cdot attack, which resulted in higher formation yield of the desired antenna.

Table 9: Estimated formation yield of each antenna based on the fluorescence response of the synthetic compound.

Pre-antenna	Isophthalate	5-Cyanoisophthalate	Trimesate
Yield of antenna formation	10 %	15 %	50 %

The reaction was stopped after 1h by adding CAT, and the elimination of H₂O₂ was verified by the peroxide test strips. Finally, La_{0.9}Tb_{0.1}F₃ NPs were added, and the TR-emission spectra after the excitation of each antenna was recorded (Figure 86).

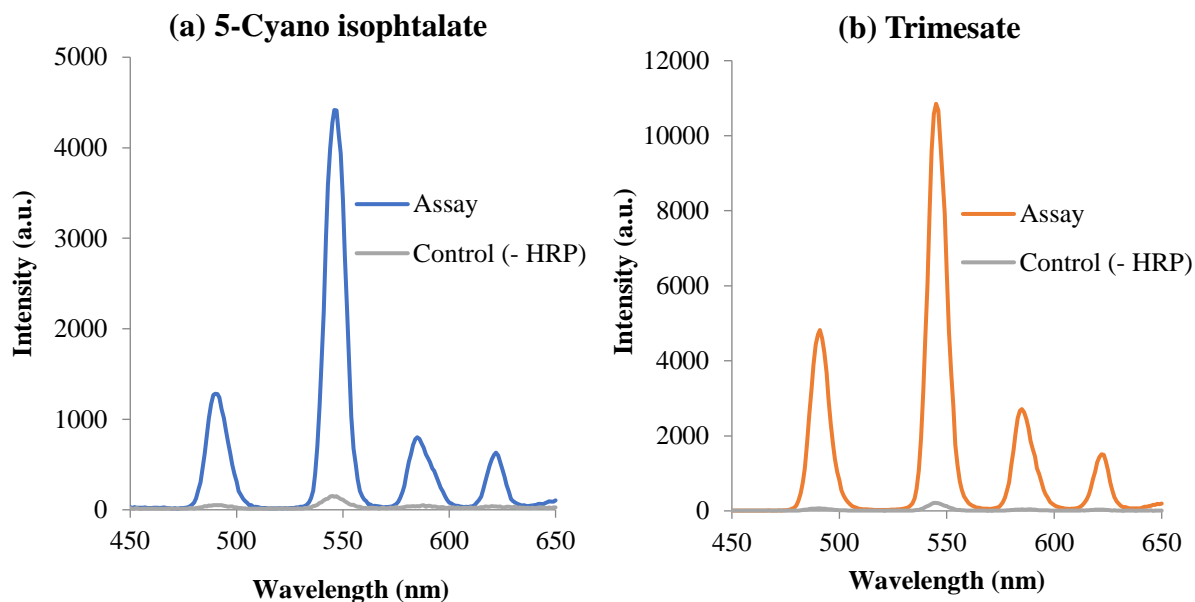


Figure 86: TR-emission spectra ($\lambda_{exc} = 328 \text{ nm}$) of La_{0.9}Tb_{0.1}F₃ NPs after their addition to the reaction with (a) 5-cyano isophthalate or (b) trimesate.

For each pre-antenna/antenna pair, the turn-on ability was determined as previously defined. Note that the comparison between the pairs is possible because all experimental and spectroscopic parameters were kept constants for all pre-antenna/antenna pairs, and the same excitation wavelength was used for the pre-antenna and antenna in each pair.

The 5-cyano isophthalate provided 30-fold amplification of the Tb emission after the enzymatic hydroxylation compared to the 10-fold amplification obtained with the IP/2-HIP pair. In turn, the trimesate shows the best assay response with a 50-fold amplification of Tb emission through its hydroxylated analog.

The signal amplification at such enzyme concentration is still feeble for an application in ELISA. In regard of the hydroxylation process, no further optimization can be done as the trimesate showed both decent reactivity towards the formation of the desired antenna, and good sensitization efficiency of Tb-NPs. In addition, the increase of initial concentration of the pre-antenna did not help to improve the kinetics nor the yield of the hydroxylation. It means that these latter are limited by the enzymatic HO[•] radicals generation process. Therefore, further attempts were done trying to improve this step.

5. Reaction kinetics study

5.1. Effect of pH

HRP enzyme is most stable in the pH range of 5.0 to 9.0, while the general optimal activity of the enzyme is in the pH range of 6.0 to 6.5.²⁴ However, this optimal pH can vary depending on the type and the form of HRP, as well as the substrate and the mechanism of the catalyzed transformation.

In order to investigate the effect of pH on the HRP-catalyzed production of HO[•] radicals, the reaction was performed at different pH in the range of 5.0 to 7.0. The HO[•] formation is monitored following the hydroxylation of the trimesate, by measuring the fluorescence of the hydroxylated compound for 1h of reaction ($\lambda_{exc} = 310$ nm, $\lambda_{em} = 405$ nm). The kinetic curves at different pH are shown in Figure 87.

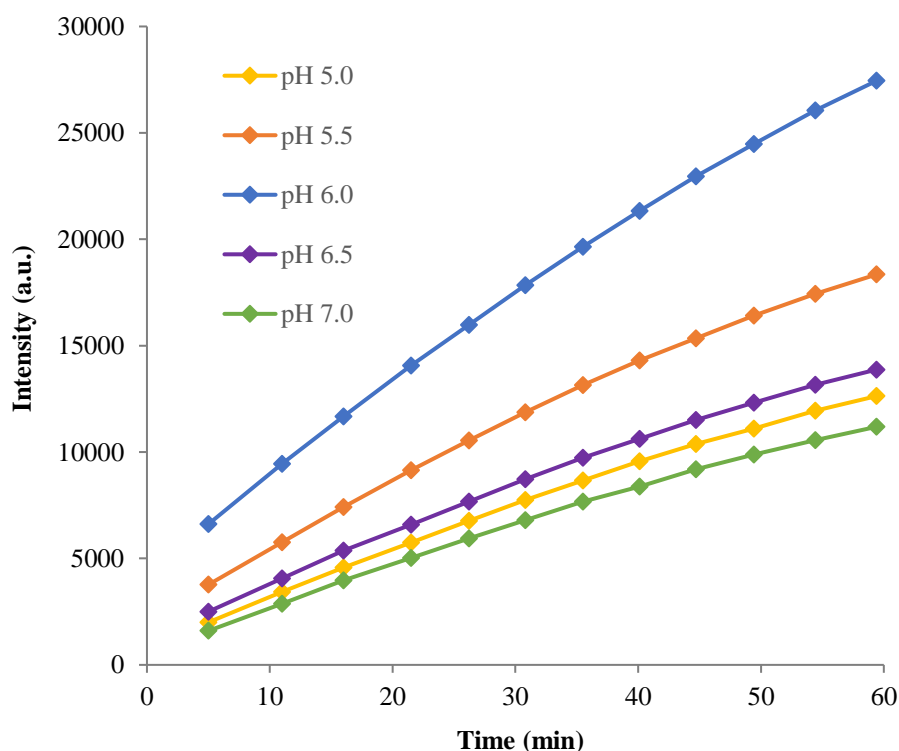


Figure 87: Reaction kinetics ($\lambda_{exc} = 310$ nm, $\lambda_{em} = 405$ nm) of trimesate hydroxylation by HRP at different pH.

The results show that the best reaction kinetics occurs at pH 6.0, in agreement with the literature observations.⁶ At higher or lower pH, the hydroxylation of trimesate significantly decreased.

As described in part 2.2, the HO \cdot formation catalyzed by HRP involves multiple steps and enzymatic cycles all the way to the formation of the compound III responsible of HO \cdot formation. The optimal pH for each step could vary depending on the reaction mechanism and the enzyme form involved, notably that of the enzyme haem.²⁵ Therefore pH 6.0 is identified as the apparent optimal pH of the entire transformation, including the hydroxylation of the aromatic compound used for detection.

5.2. Effect of the temperature

Trying to enhance the kinetics of the reaction, this was studied at higher temperature (32°C) and compared to that previously performed at room temperature. The kinetics of trimesate hydroxylation at different temperatures are presented in Figure 88, showing that the rate of trimesate hydroxylation was slightly higher at increased temperature.

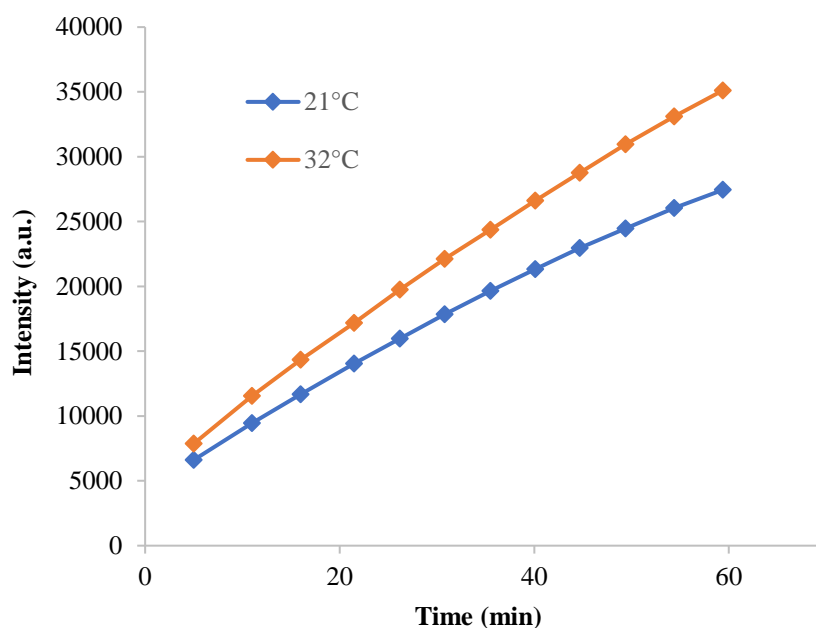


Figure 88: Reaction kinetics ($\lambda_{exc} = 310 \text{ nm}$, $\lambda_{em} = 405 \text{ nm}$) of trimesate hydroxylation by HRP at different temperature.

The sensitization of Tb-NPs by the formed hydroxytrimesate after 1h at 32°C was finally evaluated. H $_2$ O $_2$ was eliminated by CAT followed by the addition of La $_{0.9}$ Tb $_{0.1}$ F $_3$ NPs. The TR-emission spectrum after the antenna excitation was recorded. The resulting TR-emission spectra are shown in Figure 89. The trimesate provided 65-fold amplification of Tb emission after 1h of enzymatic hydroxylation at 32°C.

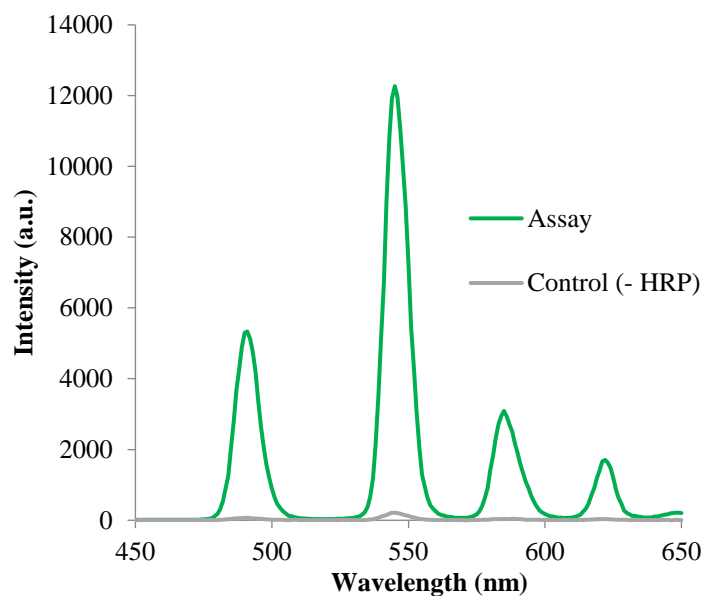
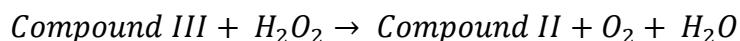


Figure 89: TR-emission spectra ($\lambda_{exc} = 328 \text{ nm}$) of $\text{La}_{0.9}\text{Tb}_{0.1}\text{F}_3$ NPs after their addition to the reaction performed at 32°C .

The attempts to optimize the HO^\bullet formation did not bring significant improvements, and the final amplification factor of 65 seems to be the best this reaction can provide at this level of enzyme concentration. A reaction temperature higher than 32°C leads to the decomposition of H_2O_2 and results in lower reaction rate,²⁵ while extending the reaction for more than 1 hour is not ideal for a further application in ELISA.

The main limitation of this enzymatic HO^\bullet formation consisted in the multistep mechanism involving different species. In this complex system, competitive reactions could alter the process of HO^\bullet formation. Miura reported that beside initiating the formation of HO^\bullet radicals, compound III can also be re-oxidized to compound II by H_2O_2 as follows.²⁶



This competitive pathway can be a reason of a low efficiency of HO^\bullet formation. In addition, it is a way of H_2O_2 consumption which decreases its availability for HO^\bullet production, and that justifies the high initial concentration of H_2O_2 needed for this reaction to occur. Indeed, further increase of the initial H_2O_2 concentration is able to enhance this reaction. Unfortunately, an additional increase of H_2O_2 is found to initiate the hydroxylation of the pre-antenna even in absence of the enzyme, thus significantly increasing the blank of the method. That could be related to the UV photolysis of H_2O_2 at high concentrations, forming HO^\bullet radicals.¹¹

6. Conclusion

In this chapter, the aim was to develop an enzymatic reaction, where the resulting product can act as an efficient sensitizer of the Ln-NPs developed in chapter II. In this regard, several ligands were tested for the sensitization of these NPs, but none brought better performance than the typical 2-hydroxyisophthalate. Therefore, the approach described in this chapter consisted in developing an enzymatic way to form this antenna.

The enzymatic reaction involving the hydroxylation of isophthalate through the generation of HO[•] radicals by HRP was fully studied. The best conditions of buffer, pH, and temperature were applied for an optimal reaction. In addition, the sensitization of the Tb-NPs by the formed product was evaluated. Notably, H₂O₂ was found to significantly quench the Ln luminescence. Thus, a critical step for the elimination of excess H₂O₂ by CAT was added to the system.

For an optimal exploitation of HO[•] formation, different IP derivatives pre-antennas were investigated. The trimesate provided an improved formation yield of the desired antenna. At 0.2 μM of HRP and under optimized conditions, this method provided 65 times amplification of Tb emission upon the hydroxylation of trimesate. Compared to the working concentration range in ELISA (pM), this signal is feeble for an application in such immunoassay.

Although some examples in the literature, HRP may be used to some extent in catalyzing hydroxylation reactions, but it is clearly not the preferential to catalyze this kind of reaction. The multistep mechanism is susceptible to competitive reactions altering the species involved in the formations of HO[•] radicals, resulting in a slow kinetics and low yield of the reaction.

One proceeding was proved to effectively boost the formation of HO[•] radicals, consisting in an exaggerated increase of H₂O₂ concentration. Unfortunately, this increase causes the hydroxylation of the pre-antenna in absence of the enzyme, potentially due to H₂O₂ photolysis. Thus, the reaction must be performed in the dark. Moreover, a high H₂O₂ concentration means more quenching, and the elimination of this excess by CAT must be investigated.

ELISA is mainly characterized by its simplicity and practicality. As for the complexity of this developed system and the relatively weak response, this approach was put on standby, and a totally different approach was adopted. The latter consisted in starting by a simple and efficient well known enzymatic reaction, then set it for an effective sensitization of the NPs. This approach will be described and evaluated in Chapter IV.

7. Experimental part

7.1. Reagents

Isophthalic acid 99%, 5-cyanoisophthalic acid 95% and trimesic acid 95% pre-antennas were purchased from Sigma. The corresponding antennas were synthesized according to the procedure described in the literature. The synthesis of 2-hydroxyisophthalic acid is detailed in Chapter II, while the other 2 antennas were synthesized in the laboratory by Dr Joan Goetz.²³

Horseradish peroxidase powder (type VI, 250 Units/mg) and Bovine liver Catalase powder (2000-5000 Units/mg) were purchased at high quality level from Sigma. Hydrogen peroxide 30%, NADH powder (grade II) and all buffers are also purchased from Sigma.

MQuant® semi quantitative colorimetric peroxide test strips, 0.5-100 mg/L (H₂O₂) were purchased from Sigma at quality level 100.

La_{0.9}Tb_{0.1}F₃ NPs were synthesized according to the procedure described in Chapter II. Freshly diluted solutions were prepared in the desired buffer from the stock solution. Other products were purchased from Acros, Alfa Aesar, fluorochem.

7.2. Spectroscopic measurements

UV/vis absorption spectra were recorded on a Analytik Jena Specord spectrometer. Steady-state excitation and emission spectra of the tested ligands were recorded on an Edinburgh Instrument FLP920 spectrometer working with a continuous 450W Xe Lamp and a red sensitive photomultiplier in Peltier housing. All spectra were corrected for the instrumental functions.

For the enzymatic assay, the fluorescence measurement of the ligands and time-resolved photoluminescence of Tb-NPs were recorded on a TECAN Spark microplate reader working with a high energy Xenon flash lamp. TR measurements were done with a time delay of 50 μs and an integration time of 2 ms.

7.3. Enzymatic assays

All enzymatic assays were performed in 96-well non-binding Greiner microplate. 500 μM of the pre-antenna (isophthalate, trimesate or 5-cyanoisophthalate), 1 mM of H_2O_2 and 200 μM of NADH were incubated in microplate wells under aerobic conditions in 10 mM of buffer at pH 6.0. Tested buffers include citrate, phosphate, HEPES, Tris and MES prepared in Milli-Q water and adjusted to pH 6.0 (except where stated otherwise) by 1 M HCl or NaOH addition. The reaction was normally initiated by the addition of 0.2 μM of HRP enzyme. The final volume in the wells was fixed at 200 μL in all assays. The microplate was agitated in a microplate shaker (400 rpm) at room temperature (except where stated otherwise) for 1 hour.

For kinetics studies, the microplate was instead agitated in the TECAN incubator and the increase in fluorescence (excitation 306 nm, emission 402 nm), mainly resulting from the formation of 2-hydroxylated antenna, was recorded every 2 or 5 min for 1 hour of reaction.

When noted, 0.05 mg/mL of CAT were introduced to the mixture, and the elimination of H_2O_2 was verified by colorimetric peroxide test strips before the addition of the NPs. Finally, 2×10^{-8} M of $\text{La}_{0.9}\text{Tb}_{0.1}\text{F}_3$ NPs were added to the reaction mixture, and the microplate was agitated for 5 mins before the spectroscopic measurements on the microplate reader. All experiments were repeated at least three times with no significant variation.

The excitation spectra were recorded at an emission of 545 nm of Tb, while the emission spectra were recorded at the maximal excitation. The excitation and emission bandwidths, the gain, as well as the z-position were kept constant in order to compare the different datasets. All Tb photoluminescence spectra were recorded by time-resolved detection with a time delay of 50 μs and an integration time of 2 ms.

8. References

- (1) Evangelista, R. A.; Pollak, A.; Gudgin Templeton, E. F. Enzyme-Amplified Lanthanide Luminescence for Enzyme Detection in Bioanalytical Assays. *Anal. Biochem.* **1991**, *197* (1), 213–224. [https://doi.org/10.1016/0003-2697\(91\)90381-3](https://doi.org/10.1016/0003-2697(91)90381-3).
- (2) Li, S.; Li, X.; Jiang, Y.; Hou, Z.; Cheng, Z.; Ma, P.; Li, C.; Lin, J. Highly Luminescent Lanthanide Fluoride Nanoparticles Functionalized by Aromatic Carboxylate Acids. *RSC Adv.* **2014**, *4* (98), 55100–55107. <https://doi.org/10.1039/C4RA09266J>.
- (3) Beeby, A.; Bushby, L. M.; Maffeo, D.; Williams, J. A. G. The Efficient Intramolecular Sensitisation of Terbium(III) and Europium(III) by Benzophenone-Containing Ligands. *J. Chem. Soc. Perkin Trans. 2* **2000**, No. 7, 1281–1283. <https://doi.org/10.1039/B003057K>.
- (4) Torres, E.; Ayala, M. *Biocatalysis Based on Heme Peroxidases: Peroxidases as Potential Industrial Biocatalysts*; Springer Science & Business Media, 2010.
- (5) Veitch, N. C. Horseradish Peroxidase: A Modern View of a Classic Enzyme. *Phytochemistry* **2004**, *65* (3), 249–259. <https://doi.org/10.1016/j.phytochem.2003.10.022>.
- (6) Chen, S. X.; Schopfer, P. Hydroxyl-Radical Production in Physiological Reactions. A Novel Function of Peroxidase. *Eur. J. Biochem.* **1999**, *260* (3), 726–735. <https://doi.org/10.1046/j.1432-1327.1999.00199.x>.
- (7) Koppenol, W. H. The Centennial of the Fenton Reaction. *Free Radic. Biol. Med.* **1993**, *15* (6), 645–651. [https://doi.org/10.1016/0891-5849\(93\)90168-T](https://doi.org/10.1016/0891-5849(93)90168-T).
- (8) Buhler, D. R.; Mason, H. S. Hydroxylation Catalyzed by Peroxidase. *Arch. Biochem. Biophys.* **1961**, *92* (3), 424–437. [https://doi.org/10.1016/0003-9861\(61\)90381-2](https://doi.org/10.1016/0003-9861(61)90381-2).
- (9) Peterson, K. L.; Margherio, M. J.; Doan, P.; Wilke, K. T.; Pierre, V. C. Basis for Sensitive and Selective Time-Delayed Luminescence Detection of Hydroxyl Radical by Lanthanide Complexes. *Inorg. Chem.* **2013**, *52* (16), 9390–9398. <https://doi.org/10.1021/ic4009569>.
- (10) Yokota, K.; Yamazaki, I. Analysis and Computer Simulation of Aerobic Oxidation of Reduced Nicotinamide Adenine Dinucleotide Catalyzed by Horseradish Peroxidase. *Biochemistry* **1977**, *16* (9), 1913–1920. <https://doi.org/10.1021/bi00628a024>.
- (11) Lojo-López, M.; Andrades, J. A.; Egea-Corbacho, A.; Coello, M. D.; Quiroga, J. M. Degradation of Simazine by Photolysis of Hydrogen Peroxide Fenton and Photo-Fenton under Darkness, Sunlight and UV Light. *J. Water Process Eng.* **2021**, *42*, 102115. <https://doi.org/10.1016/j.jwpe.2021.102115>.
- (12) Sudarsan, V.; Veggel, F. C. J. M. van; Herring, R. A.; Raudsepp, M. Surface Eu³⁺ Ions Are Different than “Bulk” Eu³⁺ Ions in Crystalline Doped LaF₃ Nanoparticles. *J. Mater. Chem.* **2005**, *15* (13), 1332–1342. <https://doi.org/10.1039/B413436B>.
- (13) Manevich, Y.; Held, K. D.; Biaglow, J. E. Coumarin-3-Carboxylic Acid as a Detector for Hydroxyl Radicals Generated Chemically and by Gamma Radiation. *Radiat. Res.* **1997**, *148* (6), 580–591. <https://doi.org/10.2307/3579734>.
- (14) Good, N. E.; Winget, G. D.; Winter, W.; Connolly, T. N.; Izawa, S.; Singh, R. M. M. Hydrogen Ion Buffers for Biological Research*. *Biochemistry* **1966**, *5* (2), 467–477. <https://doi.org/10.1021/bi00866a011>.
- (15) *CRC Handbook of Chemistry and Physics*, 95th ed.; Haynes, W. M., Ed.; CRC Press: Boca Raton, 2014. <https://doi.org/10.1201/b17118>.
- (16) Arman, M. O.; Geboes, B.; Van Hecke, K.; Binnemans, K.; Cardinaels, T. Electrochemical Oxidation of Terbium(III) in Aqueous Media: Influence of Supporting Electrolyte on Oxidation Potential and Stability. *J. Appl. Electrochem.* **2022**, *52* (3), 583–593. <https://doi.org/10.1007/s10800-021-01651-0>.

- (17) Verma, R. K.; Kumar, K.; Rai, S. B. Inter-Conversion of Tb³⁺ and Tb⁴⁺ States and Its Fluorescence Properties in MO–Al₂O₃: Tb (M = Mg, Ca, Sr, Ba) Phosphor Materials. *Solid State Sci.* **2010**, *12* (7), 1146–1151. <https://doi.org/10.1016/j.solidstatesciences.2010.04.004>.
- (18) Pędziwiatr, P. Decomposition of Hydrogen Peroxide - Kinetics and Review of Chosen Catalysts. *Acta Innov.* **2018**, No. 26, 45–52.
- (19) Chelikani, P.; Fita, I.; Loewen, P. C. Diversity of Structures and Properties among Catalases. *Cell. Mol. Life Sci.* **2004**, *61* (2), 192–208. <https://doi.org/10.1007/s00018-003-3206-5>.
- (20) Latourelle, S. M.; Elwess, N. L.; Ryan, A. B. Tried and True but Something New: Analyzing the Enzymatic Activity of Catalase. *J. Biol. Educ.* **2020**, *54* (5), 540–547. <https://doi.org/10.1080/00219266.2019.1620314>.
- (21) Chance, B. Effect of PH upon the Reaction Kinetics of the Enzyme-Substrate Compounds of Catalase. *J. Biol. Chem.* **1952**, *194* (2), 471–481.
- (22) Goetz, J.; Nonat, A.; Diallo, A.; Sy, M.; Sera, I.; Lecointre, A.; Lefevre, C.; Chan, C. F.; Wong, K.-L.; Charbonnière, L. J. Ultrabright Lanthanide Nanoparticles. *ChemPlusChem* **2016**, *81* (6), 526–534. <https://doi.org/10.1002/cplu.201600007>.
- (23) Ghosh, P.; Federwisch, G.; Kogej, M.; Schalley, C. A.; Haase, D.; Saak, W.; Lützen, A.; Gschwind, R. M. Controlling the Rate of Shuttling Motions in [2]Rotaxanes by Electrostatic Interactions: A Cation as Solvent-Tunable Brake. *Org. Biomol. Chem.* **2005**, *3* (15), 2691–2700. <https://doi.org/10.1039/B506756A>.
- (24) Schomburg, D.; Salzmann, M. Enzyme Handbook. In *Enzyme Handbook*; Schomburg, D., Salzmann, M., Eds.; Springer: Berlin, Heidelberg, 1991; pp 1–1175. https://doi.org/10.1007/978-3-642-76729-6_1.
- (25) Wang, S. A Comparative Study of Fenton and Fenton-like Reaction Kinetics in Decolourisation of Wastewater. *Dyes Pigm.* **2008**, *76* (3), 714–720. <https://doi.org/10.1016/j.dyepig.2007.01.012>.
- (26) Miura, T. A Mechanistic Study of the Formation of Hydroxyl Radicals Induced by Horseradish Peroxidase with NADH. *J. Biochem.* **2012**, *152* (2), 199–206. <https://doi.org/10.1093/jb/mvs068>.

Chapter IV

Enzymatic reaction: Dimerization
of phenols by HRP

1. Introduction

In Chapter III, an enzymatic reaction for the formation of a Tb-NPs sensitizer was developed and studied. This approach suffered from low conversion yield with slow reaction kinetics. In this chapter, a different approach was adopted. It consists in starting from a well-known efficient enzymatic reaction, then optimizing the settings in order to form an efficient antenna. In addition to a high conversion rate, the reaction must also be selected based on its ability to form a fluorophore with potential coordination and Ln sensitization.

As described in Chapter III, HRP enzyme has versatile catalytic activity involving different successive enzymatic forms and reactive cycles.¹ However, the peroxidative cycle remains the fundamental catalytic activity of this enzyme, in which it catalyzes the oxidation of diverse hydrogen donor substrates in presence of H_2O_2 . This enzymatic reaction is characterized by mild operation conditions and effectiveness over a wide range of pH, temperatures and substrate concentrations, which is highly needed in this research.²

Phenols are hydrogen donor compounds thanks to the polar hydrogen atom bonded to the strongly electronegative oxygen. Therefore, phenols were widely studied for their oxidation by HRP enzyme as described in Figure 90.³

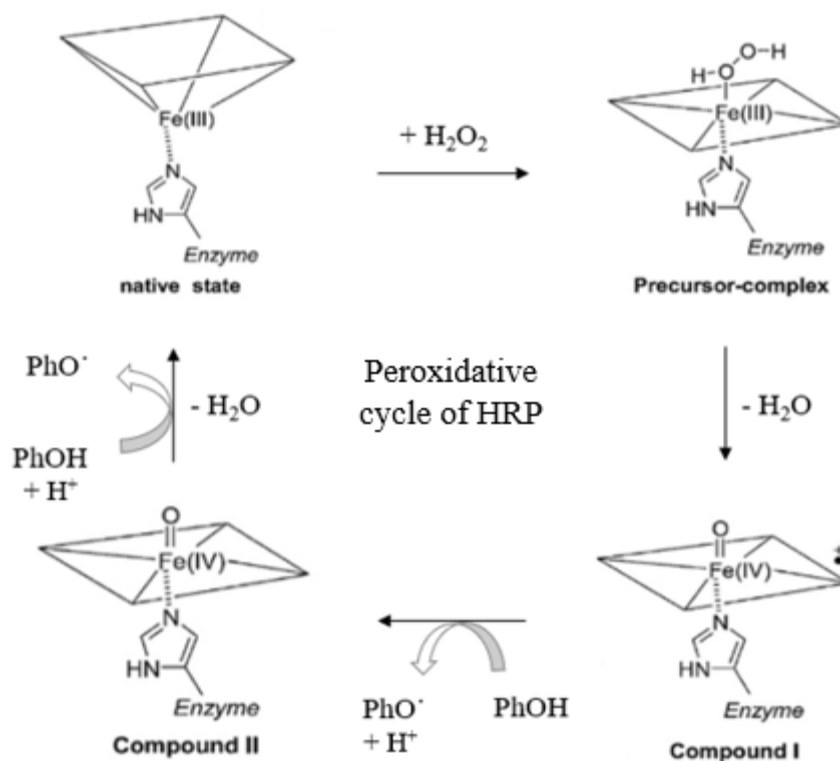
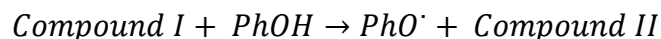


Figure 90: Oxidation of phenols through peroxidative cycle of HRP enzyme.⁴

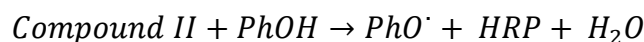
In this peroxidative cycle, the native HRP binds H_2O_2 to form an extremely short-lived complex (Fe(III)-HO-OH) that is heterolytically cleaved between the oxygen atoms resulting in a water molecule expulsion and the formation of an oxo-ferryl (Fe(IV)=O) named compound I.



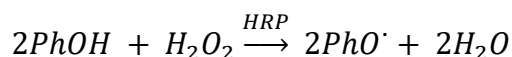
Compound I can mediate the dehydrogenation of a first phenolic molecule to give a phenoxy radical and Compound II.



The latter is also an oxo-ferryl which can react with a second substrate forming a second phenoxy radical while regenerating the native HRP by liberating a second water molecule.



In summary, within a typical cycle, two substrate molecules are oxidized by one-electron abstraction while one molecule of H_2O_2 is consumed, and two H_2O molecules are produced.



The formed phenoxy radicals and their resonant forms are very reactive and can undergo further nonenzymic reactions generating various dimeric, trimeric or oligomeric structures.⁵ Danner *et al.* reported that the only product of phenol oxidation by HRP was *o,o'*-biphenol.⁶ Later, Yu *et al.* identified different products of this oxidation using TLC and column chromatography.⁷ Figure 91 shows the products of phenol oxidation in mild conditions.

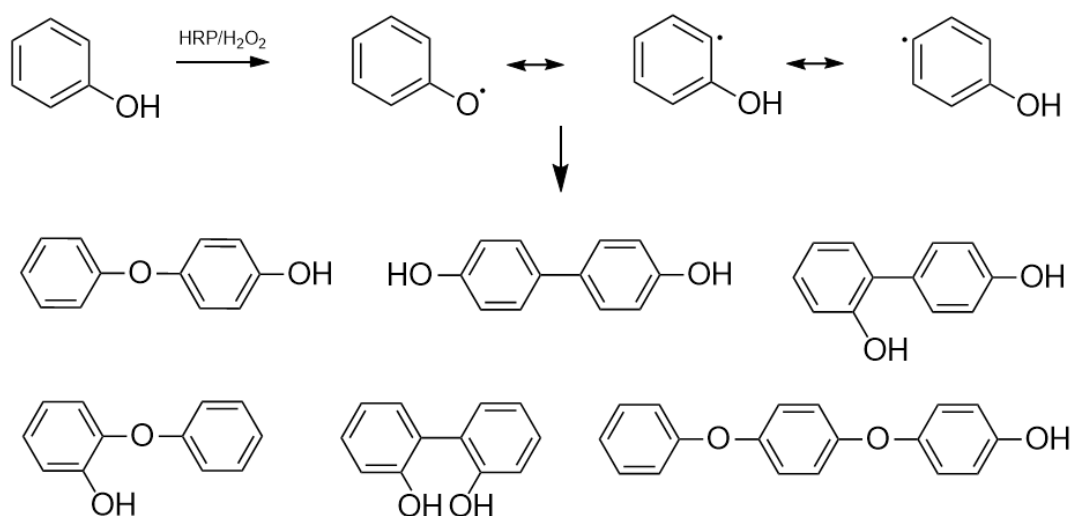


Figure 91: Radicals formed in the HRP-oxidation of phenols and their main coupling products.

This reaction was then widely studied and used in phenol derivatives removal,⁸ as well as in enzymatic polymer synthesis offering interesting advantages over conventional methods.⁹ The broad substrate specificity of this reaction allows to modify the substrate to orientate the formed product towards the desired application. Back to the scope of this work, the *o,o'*-biphenol attracted the attention for its promising structure for Ln coordination. Therefore, the modification should promote the formation of the *o,o'*-biphenol and the suppression of other dimers, while the formed dimer should be a fluorophore with the ability to sensitize Ln-NPs.

This reaction was actually applied in enzyme-amplified lanthanide luminescence (EALL), using *para*-substituted phenol substrates to sensitize Tb complexes.¹⁰ This method provided promising results but suffered from the high EDTA concentrations required to avoid the precipitation of Ln hydroxide at alkaline pH, which limited the sensitivity of the method.

Using the synthesized stable Ln-NPs, with further optimization of the phenol substrate, the reaction conditions, and the sensitization process seems promising to overcome this limitation and improve the performance of this assay. In this chapter, an enzymatic assay using HRP was developed, in which the dimerization product of a phenol compound can coordinate to Ln-NPs and sensitize Ln ions. This method was then implanted in ELISA set up in commercially available kit, and its detection performance was evaluated in terms of sensitivity.

2. Oxidation of phenols by HRP

2.1. Sensitization of Tb-NPs by the oxidation product

The first step in this work was to verify the feasibility of this method by investigating the sensitization of Ln-NPs following the oxidation of a phenol substrate by HRP. Zheng et al. were the first to demonstrate that the dimerization product of *p*-hydroxybenzoic acid (HBA) can form a ternary complex with Tb(III)EDTA and sensitize Tb ions.¹¹

To verify the ability of the formed dimer to sensitize Tb-NPs, the oxidation of HBA was executed under relatively high enzyme concentrations for a high substrate conversion. 1 mM of substrate was incubated in microplate wells with 0.5 mM of H₂O₂ in 10 mM Tris buffer pH 7.0 at room temperature. The reaction was initiated by the addition of 10⁻⁹ M of HRP enzyme, and the microplate was agitated for 1 h. The final volume of the reaction mixture was fixed to 200 μ L in all the assays. The reaction was then stopped by adding 5 μ L of a 2 mg/mL solution of catalase enzyme (CAT), to eliminate the excess of H₂O₂ from the reaction mixture.

Finally, 2×10^{-8} M of $\text{La}_{0.9}\text{Tb}_{0.1}\text{F}_3$ NPs (20 μL) were added and the mixture was agitated for additional 5 min. The process of the assay is illustrated in Figure 92.

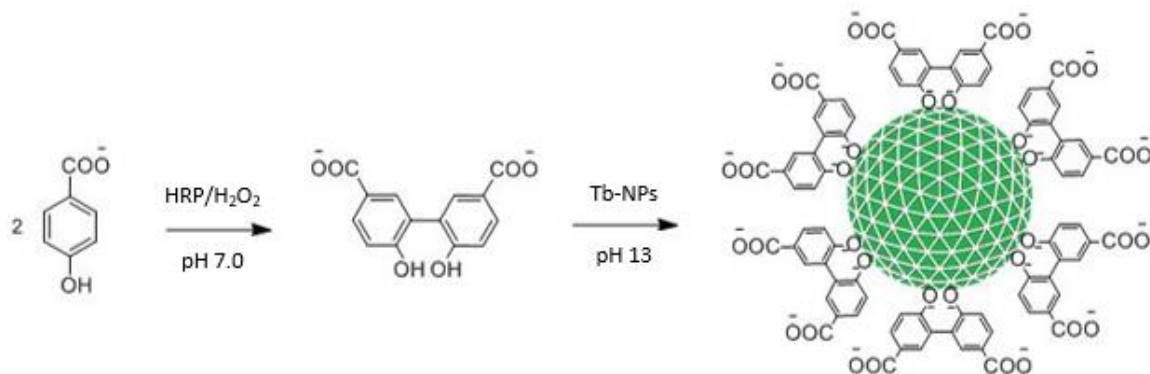


Figure 92: Reaction sequence of the enzymatic reaction followed by Tb-NPs sensitization.

After the addition of the NPs, the pH of the mixture was gradually increased by successive additions of 1 M NaOH solution, and the TR-excitation and emission spectra of Tb were measured (Figure 93). The evolution of Tb emission intensity with the addition of NaOH is shown in the inset of Figure 93. NaOH volumes are given because the measurement of the pH in the wells was not practical when followed by further NaOH additions. At pH 7.0, very weak emission of Tb was observed signaling that no sensitization occurred at neutral pH, while the addition of NaOH mediated the sensitization of Tb by the formed dimer. This indicates that an efficient coordination cannot occur through the already deprotonated carboxyl groups.

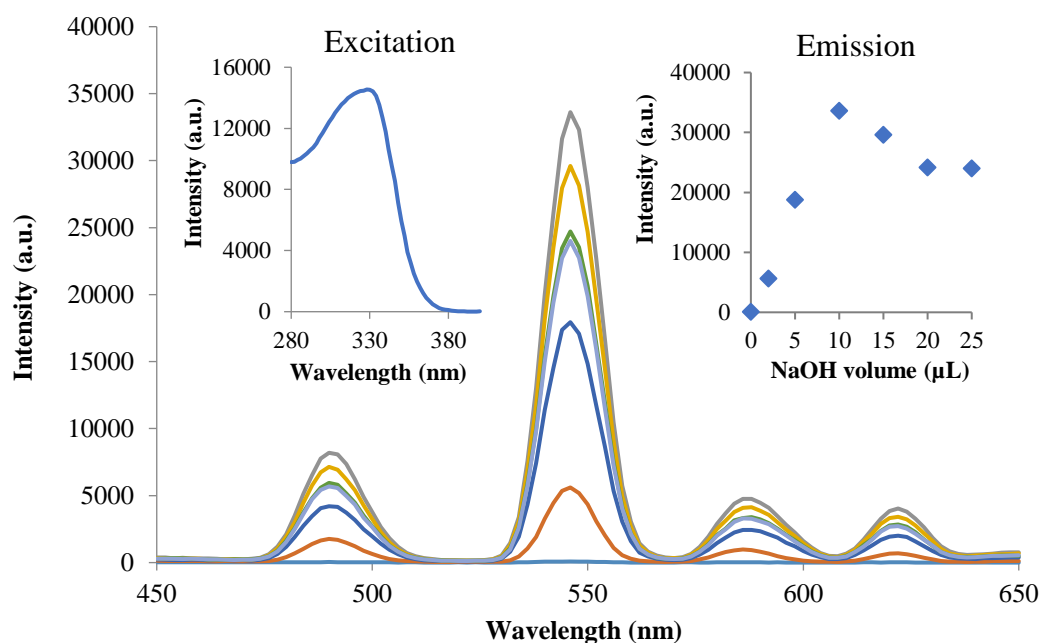


Figure 93: TR-emission spectra of $\text{La}_{0.9}\text{Tb}_{0.1}\text{F}_3$ NPs ($\lambda_{exc} = 320$ nm) after their addition to the reaction mixture. Left inset : Excitation spectra ($\lambda_{em} = 545$ nm) at pH 13.0. Right inset : Evolution of Tb emission intensity with the addition of NaOH.

In an unsubstituted *o,o'*-biphenol, the first pKa is at 7.6 while the second pKa is around 13.¹² Compared to the pKa of a phenol at 10, this splitting can be attributed to a stabilizing intramolecular hydrogen bond between -O⁻ and -OH in the monoprotonated *o,o'*-biphenol. Increasing the pH results in the deprotonation of both phenols, which helps the coordination of the dimer at the surface of NPs and allows the sensitization to occur.

With an excitation at 320 nm, maximum excitation for an emission at 545 nm (inset Figure 93), the intensity of Tb emission increased with NaOH addition to reach a maximum at around pH 13, then slightly decreased and remained stable. This decrease can be explained by the competition of HO⁻ ions abundantly present at high pH with the dimer molecules for the coordination on the surface of NPs.

In the absence of HRP, no increase of Tb emission was observed even after increasing the pH as shown in Figure 94. That demonstrates that the dimerization is only mediated by the enzymatic activity of HRP, and that the phenol substrate is unable to sensitize Tb-NPs in these conditions. The enzymatic dimerization of HBA provided 100-fold amplification of Tb emission after a 1 h reaction under unoptimized conditions but with relatively high enzyme concentration. These results demonstrated that this enzymatic reaction is able to transform an inactive substrate into an efficient sensitizer of the NPs, meeting the fundamental requirement of the system and opening the door for potential optimizations.

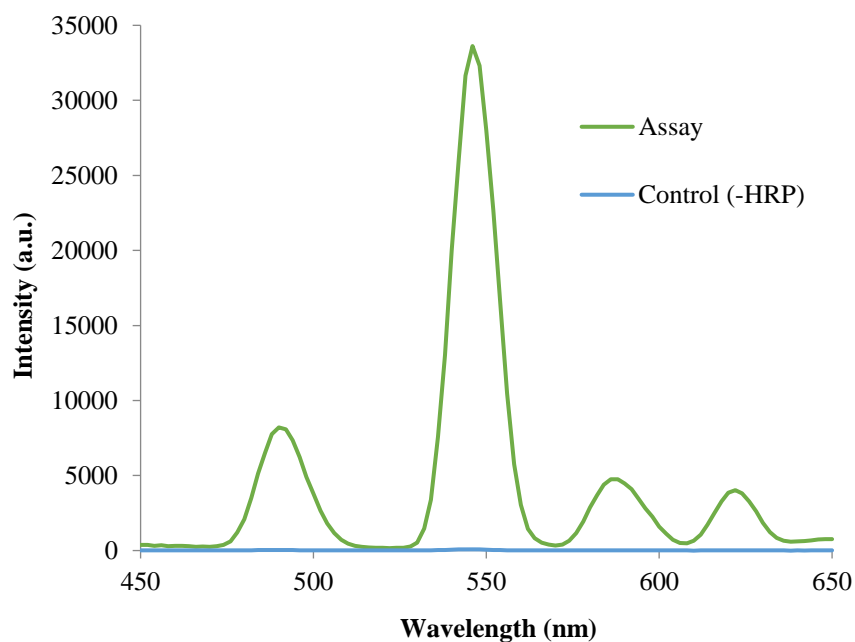


Figure 94: TR-emission spectra ($\lambda_{exc} = 320$ nm) of $La_{0.9}Tb_{0.1}F_3$ NPs after their addition to the reaction mixture in the presence or the absence of HRP, followed by increasing the pH to 13.

2.2. Effect of the substrate

As for this enzymatic reaction, the substrate selection is an important parameter influencing the performance of the assay. One strict obligation is required in the substrate to be eligible for this kind of application. A substitution in *para* position of the phenol is mandatory to avoid the formation of inactive products and to direct the reaction towards the formation of the *o,o*-dimer, the best candidate for Ln coordination.

Actually, the *p*-substituent plays a crucial role in determining the major properties of the dimerization product. It influences the solubility of the formed dimer in water depending on the polarity of the substituent, and directly affects the pKa of the phenol group, slightly higher with electron-donating substituents and significantly lower with electron-withdrawing substituents.¹² More importantly, it determines the fluorescence capacity of the oxidation product as well as its ability to sensitize specific Ln ions.¹³

To investigate the influence of this *p*-substituent on the performance of the assay, 12 substrates were subject to the oxidation by HRP followed by testing a potential sensitization of Tb-NPs. Substrates were *p*-substituted phenols with different functional groups as shown in Figure 95. This list of *p*-substituents is intended to cover different steric and electronic properties to evaluate the behavior of the substrate in different environments.

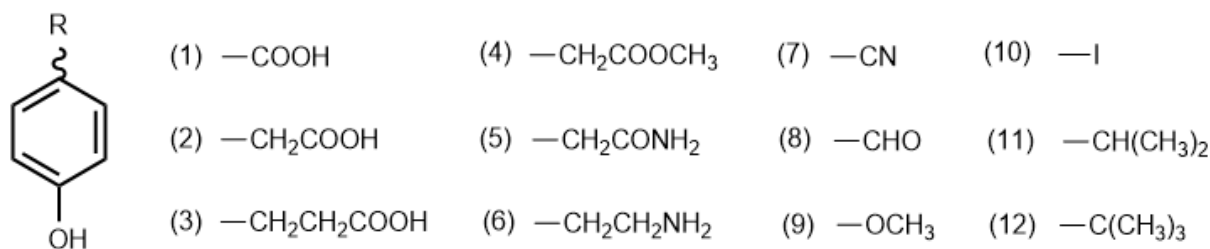


Figure 95: Substrates with different *p*-substituents tested in the assay.

For each substrate, 1 mM were incubated in microplate wells with 0.5 mM of H₂O₂ at pH 7.0, and the reaction was initiated by the addition of 10⁻⁹ M of HRP enzyme. After 1 h of reaction, CAT was added to the mixture, followed by the introduction of 2×10⁻⁸ M La_{0.9}Tb_{0.1}F₃ NPs, and the pH was increased to 13. Finally, the TR-emission spectra were measured with respect to the maximum excitation determined for an emission at 545 nm in each well. Figure 96a shows the TR-emission spectra of Tb with the substrates presenting the most interesting results, and 96b shows the turn-on amplification factor obtained with all tested substrates.

The substrates with substituents containing a carboxylic acid group (1, 2 and 3) were reported in the literature for an enzyme amplified lanthanide luminescence. However, a disagreement was noticed in terms of the functioning of these different substrates. After Zheng *et al.* reported that the oxidation of HBA (1) can be used to sensitize Tb-complexes, they claimed that substrates like *p*-hydroxyphenylacetic acid (2) and *p*-hydroxyphenylpropionic acid (3) did not induce any sensitization of Tb emission.¹¹ They concluded that the complexing site with Tb³⁺ was the carboxyl group, not the phenol group in the oxidation product, and one or two methylene groups between the phenol and carboxyl groups inhibit the dimer to form a fluorescent complex with Tb³⁺ because of ring instability. Three years later, Meyer and Karst contradicted that conclusion and demonstrated that HPPA can be efficiently used to sensitize Tb luminescence after HRP-catalyzed dimerization.¹⁴

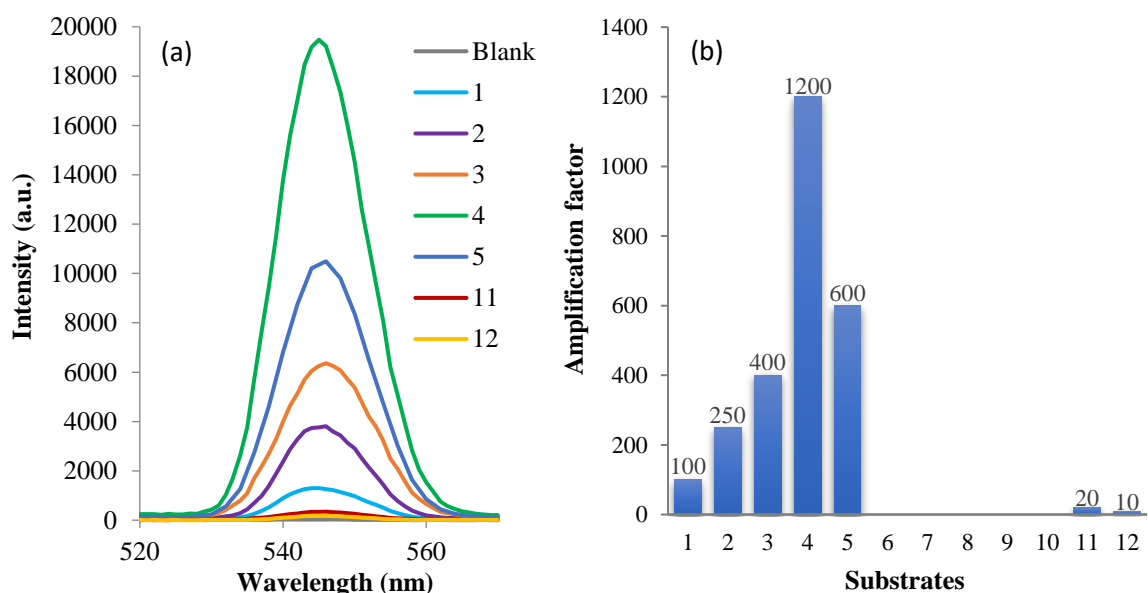


Figure 96: (a) TR-emission spectra of $La_{0.9}Tb_{0.1}F_3$ NPs ($\lambda_{exc} = 320$ nm) after HRP catalyzed oxidation of different substrates. (a) amplification factor obtained with all tested substrates.

Herein, these three substrates were found to sensitize Tb-NPs with different efficiencies. While HBA (1) oxidation resulted in 100-fold amplification of Tb emission, HPAA (2) provided an amplification of 250-fold. Interestingly, HPPA (3) showed even more efficient performance with 400-fold amplification of Tb emission upon HRP-oxidation. These results tend to prove that the coordination of the corresponding dimers on the surface of the NPs did occur through the phenolic groups. This result came in accordance with the proposition of Guilbault *et al.*, stating that a methylene group in *para* position yields to a better fluorescent dimer product.¹⁵

As a carboxyl group is not needed for the coordination to happen, the methyl 4-hydroxyphenyl acetate (4) was tested as a protected version with a methyl ester group. The oxidation of this substrate provided a drastic enhancement of Tb emission with a factor of 1200. It was hypothesized that the protection of 2 negatively charged carboxyl groups prevents the attraction to the NPs from this side and favors the coordination of the dimer through the phenolic groups. This also protects the reactive carboxyl group from any side reaction, such as its oxidation to a carboxylic radical followed by addition to the *meso*-position as proposed by Huang *et al.*¹⁶

An analogous substrate (5) with an amide group was proposed to provide better stability than the ester group at high pH. Unfortunately the oxidation of this substrate did not offer the same Tb emission amplification and settled for a factor of 600. As the fluorescent aromatic moiety of this substrate was not modified compared to substrate (4), a significant variation of the antenna triplet state is not expected. Therefore, this 2 times reduction in the sensitization efficiency is not completely related to the spectroscopic properties of these antennas but may be due to the formation yield of each one of them following the enzymatic oxidation. The NH group of the amide acts as a hydrogen donor and can be more or less reactive to HRP oxidation conducting to side products altering the formation yield of the sensitizer. This hypothesis was strengthened by the results obtained with substrate (6), containing an amine group. Despite that the obtained dimer has approximately the same spectroscopic properties as the carboxylic acid analogous,¹³ no sensitization of Tb emission was observed at all.

On another hand, different substrates were selected to investigate any effect of electron-withdrawing (7,8) or donating (9,10) substituents on the performance of the assay. The lack of a turn-on ability following the enzymatic activity can be due to an inhibition of the reaction, as the elimination of the methylene group in the side chain was demonstrated to decrease the rate of oxidation.¹³ Otherwise, electron-donating and withdrawing substituents by mesomeric effect can modify the π -electrons delocalization of the aromatic moiety which significantly alters the triplet state of the formed dimer. This can either increase the energy gap with the Tb emissive state, inhibiting the transfer, or reduce this gap resulting in back transfer to the ligand.

Finally, substrates 11 and 12 with only carbon chain substituents were also evaluated. The *p*-isopropylphenol showed only 20-fold enhancement of Tb emission upon HRP oxidation, while *p*-tert-butylphenol, showed even weaker efficiency with a factor of 10. These substrates already suffer from low solubility in water, and the dimerization of such substrate leads to the formation of a dimer with even lower solubility that risks to precipitate.⁷

Among all these substrates, the methyl 4-hydroxyphenyl acetate (MHPA) highlighted the best performance in this enzymatic assay, showing very promising turn-on ability. Regarding the selection of the substrate, further studies can be done involving additional substituents in *ortho* or *meta* positions. The enzymatic dimerization of phenol derivatives is known to be chemoselective when several reactive groups are present on the phenol derivative.¹⁷ Xu *et al.* suggested that the reaction rate was higher when *para* and *meta* substituted phenols were used as substrates.¹⁸ However, some substituents can cause side reactions that result in nonfluorescent products or fluorescent products at higher wavelength, which become incompatible with Tb sensitization.¹³

3. Oxidation of the MHPA by HRP

3.1. Spectral properties of the dimer

After the selection of the substrate, it was important to study the oxidation process. In a first step, the formed dimer was studied for its spectral properties. Figure 97 shows the excitation and emission spectra of the reaction mixture after 1 h in presence of HRP enzyme.

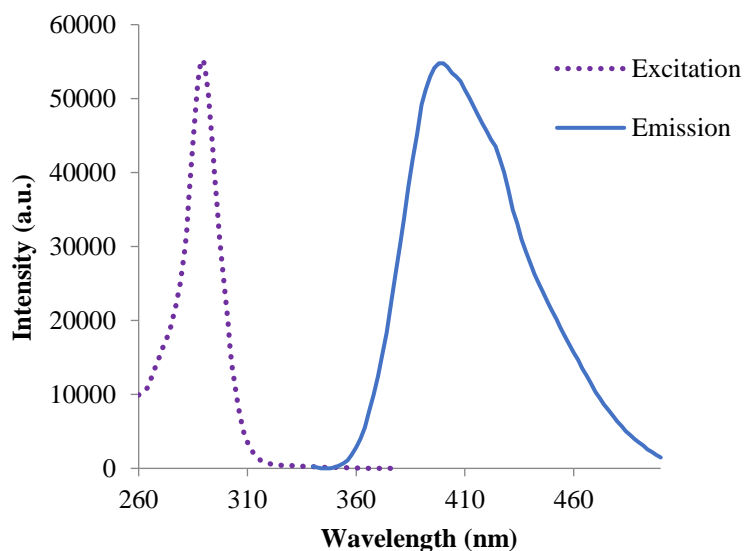


Figure 97: Excitation ($\lambda_{em} = 402$ nm) and emission spectra ($\lambda_{exc} = 289$ nm) of the MHPA oxidation product.

The oxidation product has shown the maximum excitation and emission at 290 and 402 nm, respectively. The resultant Stokes shift is large enough that the respective excitation and emission bands do not overlap. This will prevent energy loss by self-absorption and subsequently allows optimal transfer to Tb^{3+} ions when capping the NPs.

3.2. Reaction kinetics

The spectral properties determined allows monitoring the dimer formation during the reaction. To study the kinetics of this oxidation, the reaction was performed under milder enzyme concentration at 10^{-10} M. Figure 98 shows the emission intensity at 402 nm after an excitation at 290 nm as a function of the reaction time. This reaction kinetics show a dimer formation slowing down in the time.

One of the major issues that disrupt the process of the reaction is the enzyme inactivation. This inactivation results from the return of a free radical to the active site, blocking that site and preventing further catalysis as suggested by Klivanov *et al.*¹⁹ Alternatively, Nakamoto and Machida proposed that the inactivation was a result of end-product adsorption on the enzyme, blocking substrate access to the active site.²⁰ Recently, Feng *et al.* have shown that this phenomenon is not an inactivation, but rather an immobilization of the enzyme in a form with lower specific activity which can be the reason of the decrease of the reaction rate over time.²¹

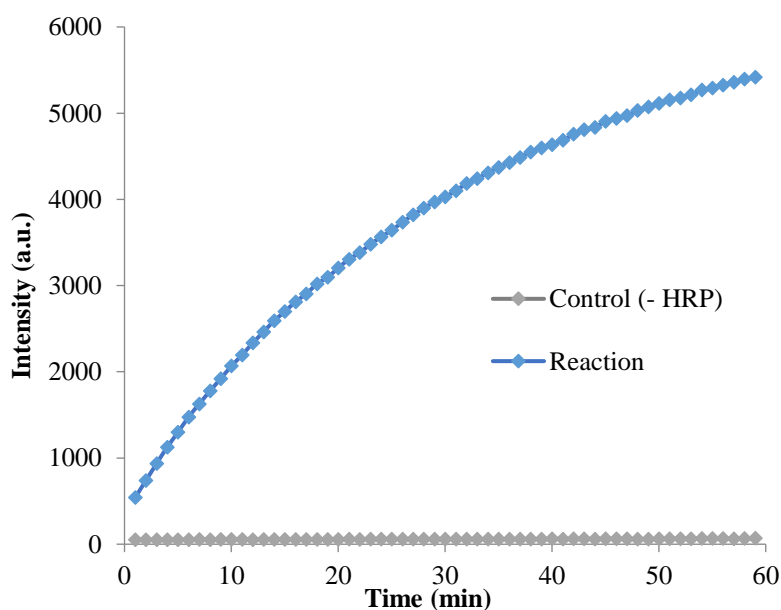


Figure 98: Reaction kinetics ($\lambda_{exc} = 289$ nm, $\lambda_{em} = 402$ nm) of MHPA oxidation by HRP at pH 7.0..

The formation of the dimer was strictly dependent on the presence of HRP enzyme in the reaction mixture as no increase of intensity was observed if HRP was not added. At this average enzyme concentration, and under unoptimized reaction conditions, a decent rate of dimerization is still observed. This result is promising in terms of sensitivity of this approach, opening up for further optimizations.

3.3. Optimization of reaction conditions

3.3.1. Effect of pH

In the last decades, the HRP catalyzed oxidation of phenols was widely studied, where several works agreed that an optimal reaction occurs over the pH range of 6.5–8.5.²² However, the HRP iron haem involved in this reaction is very sensitive to the pH of the media. A variation of the pH can change both the activity and the selectivity of this active site of HRP enzyme.

The effect of pH on MHPA oxidation was investigated in the range of 3.5–8.5 using 2 different types of buffer solutions. The pH range from 3.5 to 6.5 was obtained using a buffer solution of succinic acid 10 mM, while pH 7.0 to 8.5 was obtained using a 10 mM TRIS buffer solution. The reactions were conducted with 10^{-10} M HRP under identical conditions, with the only variation being in the pH of the media. After 1 h of reaction, all wells were brought at pH 7.0 followed by measuring the emission intensity at 402 nm after an excitation at 290 nm. The results of this study are shown in Figure 99.

Surprisingly, the highest formation of the dimer occurred at pH 4.6. At higher and lower pH, a significant decrease of dimer formation was observed. As no variables are interfering with the enzymatic reaction, this result can be only related to the functioning nature of HRP enzyme.

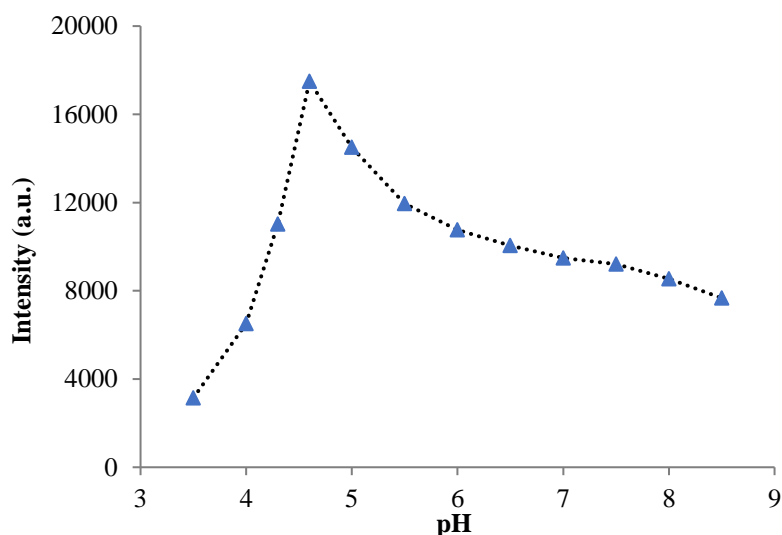


Figure 99: Effect of the pH on the formation of the MHPA dimer ($\lambda_{exc} = 289$ nm, $\lambda_{em} = 402$ nm).

Actually, different commercial preparations of the peroxidase from horseradish plant can confer different properties of this enzyme.²³ Floyd *et al.* reported differences in the amount and the nature of the products in the enzymatic reaction performed by type II or type VI HRP.²⁴

One notable difference between HRP types involves the isoelectric point (pI) as the Sigma preparations II, VI, VI-A and XII seemed to contain isoenzymes with a pI of 3.5-4.2, while type I contained predominantly isoenzymes with a pI of 5.²⁵ HRP from different suppliers can also contain more basic isoenzymes. Isoenzymes are multiple forms of the enzyme that differ in the amino acid sequence. These differences can be the source of modification of the optimal pH for a given reaction. In addition, an oxidation of several substrates by HRP was reported at acidic pH including guaiacol, 3,3',5,5'-Tetramethylbenzidine (TMB) and others.²⁶

3.3.2. Effect of H₂O₂ concentration

The ratio of H₂O₂ to HRP has been found to be a crucial parameter for the phenol oxidation efficiency. While a lack of H₂O₂ during the reaction limits the reaction rate, an excess H₂O₂ behaves as a typical suicide substrate of HRP enzyme.²⁷ In the presence of excess H₂O₂, other cycles of HRP can be triggered, where HRP is converted to Compound III as described in Chapter III, which slows down the peroxidase cycle responsible of phenol oxidation.²⁸

This phenomenon was investigated by monitoring the reaction kinetics at H₂O₂ concentrations in the range of 0.1-2 mM, while maintaining MHPA and HRP concentrations at 1 mM and 10⁻¹⁰ M respectively, in 10 mM succinic acid buffer at pH 4.6. Figure 100 shows the emission intensity at 402 nm after an excitation at 290 nm as a function of the reaction time.

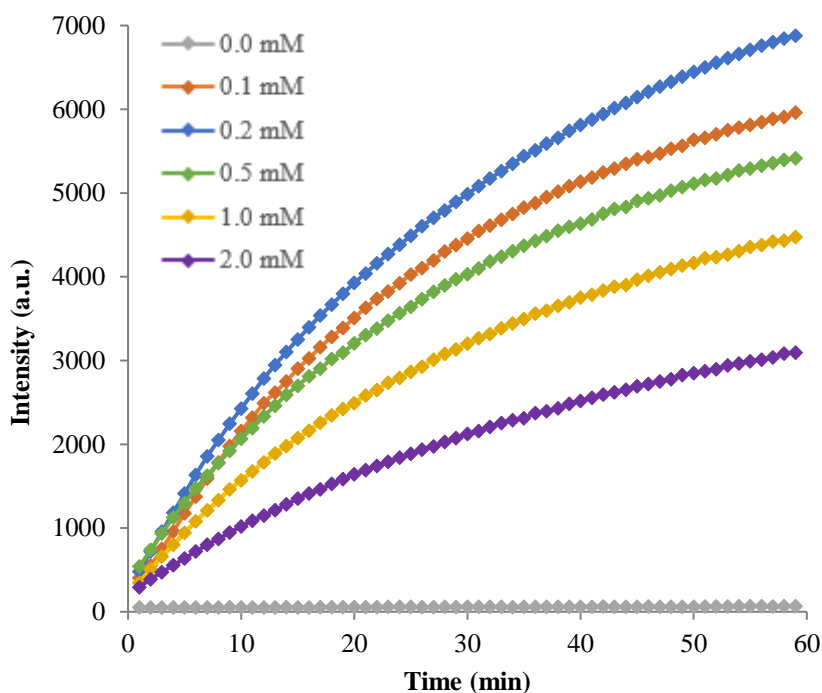


Figure 100: Reaction kinetics ($\lambda_{exc} = 289 \text{ nm}$, $\lambda_{em} = 402 \text{ nm}$) of MHPA oxidation by HRP at different H₂O₂ concentrations at pH 4.6.

In the range of 0.1-0.2 mM, the rate of the reaction increased with H₂O₂ concentration. At concentrations ≥ 0.5 mM, the reaction started to slow down, highlighting the effect of excess H₂O₂ on the deactivation of the HRP enzyme.

This study dealt with the effect of the initial H₂O₂ concentration on the rate of the reaction. However, Wu *et al.* reported that the instantaneous relative amounts of H₂O₂ and HRP during the reaction is crucial to the enzymatic reaction.²⁹ A batch and semi-batch additions of a fixed total amount of H₂O₂ can result in different instantaneous H₂O₂ concentrations in the media and can therefore affect the efficiency of the oxidation. This effect was explored by comparing the efficiency of dimer formation after different addition modes of 0.2 mM H₂O₂ (Table 10).

Table 10 : Different H₂O₂ addition modes for the oxidation of MHPA by HRP.

Time of addition (min)		0	20	30	40
[H ₂ O ₂] (mM)	Exp 1	0.2			
	Exp 2	0.1		0.1	
	Exp 3	0.067	0.067		0.066

Figure 101 shows the emission spectra of the formed dimer with excitation at 290 nm, after 1 h of reaction by three different H₂O₂ addition modes. The semi-batch addition mode of H₂O₂ was demonstrated to slightly improve the efficiency of the dimerization by optimizing the instantaneous relative amounts of H₂O₂. This process can be used for applications at high enzyme concentrations, where the effect of the semi-batch addition can be significant. Herein, at low enzyme concentrations, the improvement brought seemed not worth adding an extra step to the assay, especially for practical reasons when further applied in ELISA.

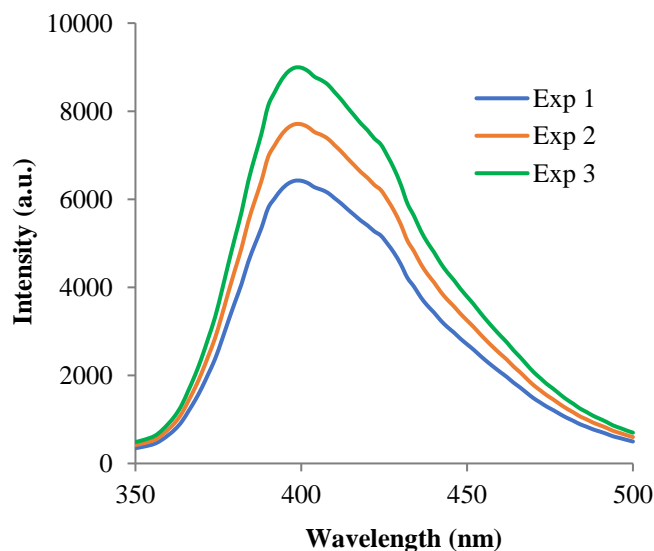


Figure 101: Fluorescence spectra ($\lambda_{exc} = 289$ nm) after MHPA oxidation with different H₂O₂ addition modes.

3.3.3. Effect of substrate concentration

The concentration of the substrate also has an effect on the efficiency of the assay. Other than the effect on the reaction rate, this concentration is important to harvest an optimal capping of the NPs by the oxidation product. An optimal substrate concentration involves the highest reaction rate, while the formed dimer should not lead to the saturation of the NPs to ensure a sensitization signal accurately proportional to the amount of formed dimer. Therefore, the substrate concentration is limited by the maximal concentration of NPs that can be introduced in the assay while maintaining their dispersibility and luminescence properties.

In order to investigate this effect, the assay was evaluated at MHPA concentrations ranging from 0.5 to 5 mM, while maintaining H_2O_2 and HRP concentrations at 0.2 mM and 10^{-10} M respectively. After 1 h of reaction at pH 4.6, the emission of the formed dimer was measured at 402 nm after an excitation at 290 nm. CAT was then added to the mixture, followed by the introduction of 2×10^{-8} M $\text{La}_{0.9}\text{Tb}_{0.1}\text{F}_3$ NPs, and the pH was increased to 13. The emission of Tb was then measured at 545 nm after an excitation at 320 nm. The variation of the fluorescence of the formed dimer as a function of MHPA concentration and the corresponding Tb photoluminescence are shown in Figure 102.

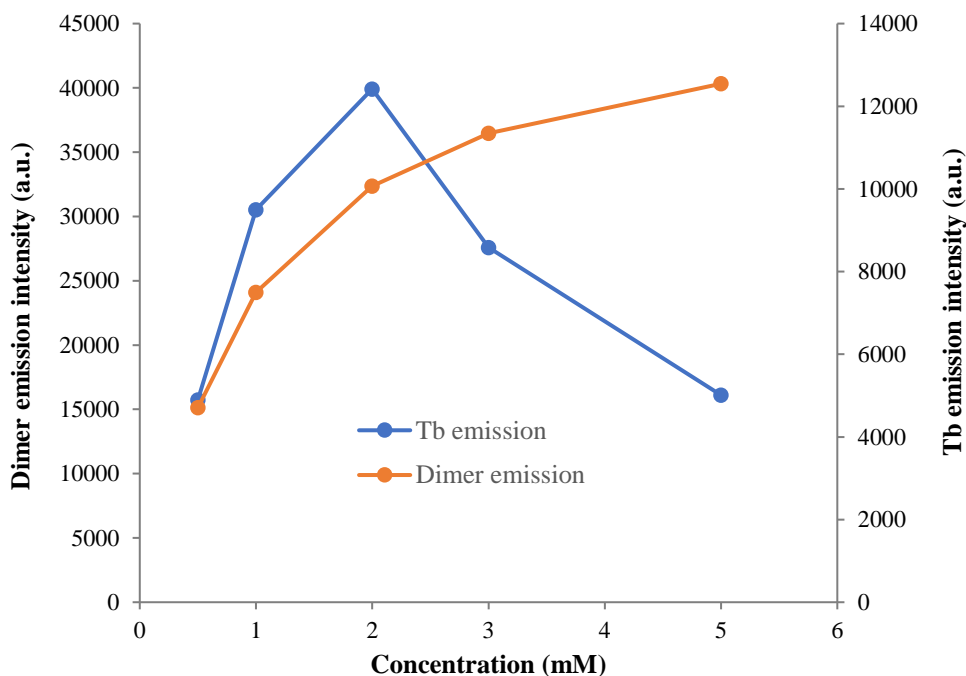


Figure 102: Variation of the fluorescence of the formed dimer ($\lambda_{exc} = 289$ nm, $\lambda_{em} = 402$ nm) and the corresponding Tb photoluminescence ($\lambda_{exc} = 320$ nm, $\lambda_{em} = 545$ nm) at different substrate concentrations.

In the range of 0.5-2 mM, the formed amount of dimer increased with the augmentation of MHPA concentration, inducing higher coverage of the NPs and stronger sensitization of Tb emission. The concentration of the substrate seemed less effective on the reaction efficiency at > 2 mM, where the increase of the dimer fluorescence is less significant. At the same time, a high decrease of Tb emission intensity was observed.

Increasing the substrate concentration and obtaining a similar conversion yield means that the excess of unreacted substrate is more important, and the substrate/dimer ratio significantly increases. With a pKa around 10, MHPA is deprotonated at the final pH of the assay and can strongly compete for the coordination on the NPs surface at a high substrate/dimer ratio.

3.3.4. Effect of the temperature

After finding the optimal pH and concentration conditions of the reaction, the effect of the temperature on the reaction kinetics was investigated. 2 mM MHPA and 0.2 mM H_2O_2 were incubated with 10^{-10} M of HRP at pH 4.6. The reaction was performed at 23 °C (room temperature) and at 37°C. The kinetics of dimer formation at different temperatures are presented in Figure 103a, showing that the reaction rate was higher at increased temperature.

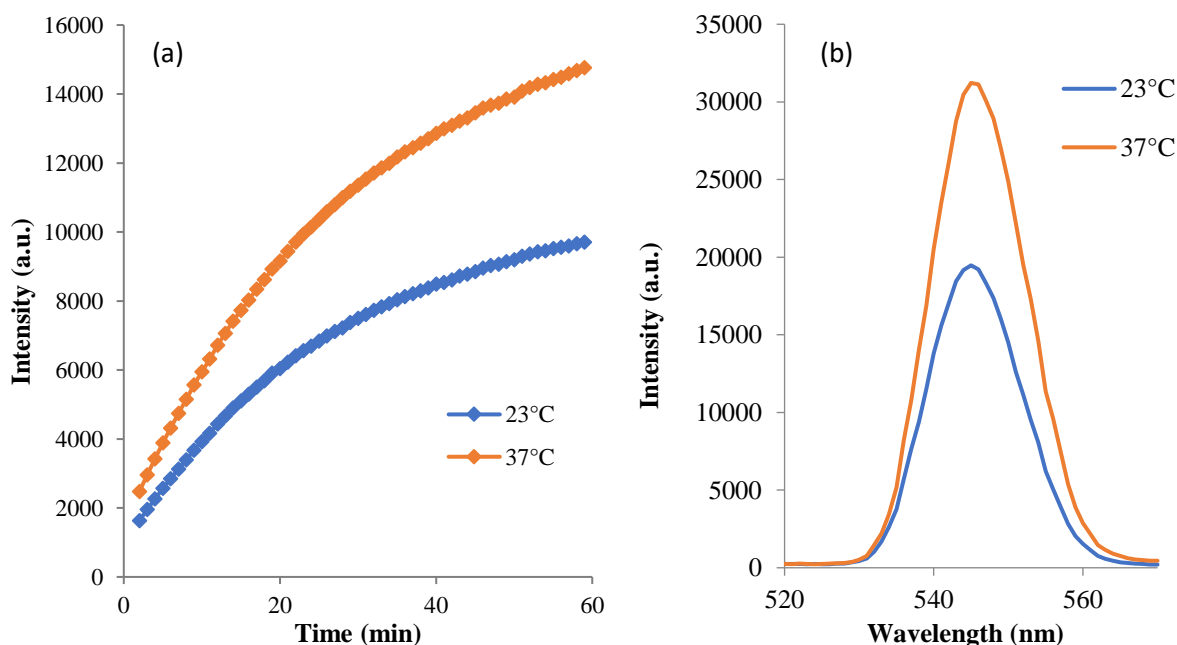


Figure 103: (a) Reaction kinetics ($\lambda_{exc} = 289$ nm, $\lambda_{em} = 402$ nm) and (b) TR-emission spectra of $\text{La}_{0.9}\text{Tb}_{0.1}\text{F}_3$ NPs ($\lambda_{exc} = 320$ nm) for MHPA oxidation at different temperature.

After 1 h, CAT was added to the mixture, followed by the introduction of 2×10^{-8} M $\text{La}_{0.9}\text{Tb}_{0.1}\text{F}_3$ NPs, and the pH was increased to 13. The TR-emission spectra were then measured for an excitation at 320 nm (Figure 103b). A higher reaction rate provided better yield of dimer formation after 1 h of reaction, resulting in stronger sensitization of Tb-NPs.

Increasing the temperature of the reaction was demonstrated to enhance the final signal of the assay. However, this process suffered from a practical drawback. When incubated, the microplate is covered by a plate sealer, which is exposed to water vapor due to the heating at 37°C . When the sealer is removed for the addition of CAT, NPs and NaOH, the vapor condensed on the sealer is lost. That presents a risk of cross contamination, as well as a poor reproducibility of the assay. Thus, as long as the assay is manually performed, room temperature has been considered the better option for accurate results.

3.4. Monitoring of the reaction by HPLC-UV

The work described above focused on the analytical performance of the assay by optimizing the efficiency of the enzymatic reaction and the final sensitization signal. Before the final evaluation of the sensitivity of this assay, it was important to investigate the reaction on a deeper level to better understand the system and to inspect any further optimization.

3.4.1. Synthesis of the MHPA-dimer

In order to have a reference for the MHPA-dimer, the main potential product of the enzymatic reaction, it was useful to synthesize and purify this compound. An enzymatic synthesis on a large scale seemed to be ineffective as at harsh conditions of HRP and H_2O_2 concentrations, the formed dimer is unstable and can undergo further transformations. Figure 104 shows the kinetics of dimer formation at 2 mM MHPA, 1 mM H_2O_2 and 10^{-8} M HRP.

The fluorescence intensity of the formed dimer reached a maximum after a 1 min reaction time then sharply dropped 60% over the next 10 min. Two potential pathways were suggested for this dimer transformation. The first involves a further polymerization of the formed dimer by acting as a substrate of the same enzymatic reaction. However, Yu *et al.* demonstrated that an *o,o*-biphenol have a very weak specific reaction rate for an oxidation by HRP due to the stabilizing effect of the intramolecular hydrogen bond.⁷ They claimed that predominant polymerization bonds in the products may be the oxygen-*para* connection whereas an *ortho-ortho* connection would hardly be found in the higher oligomers.

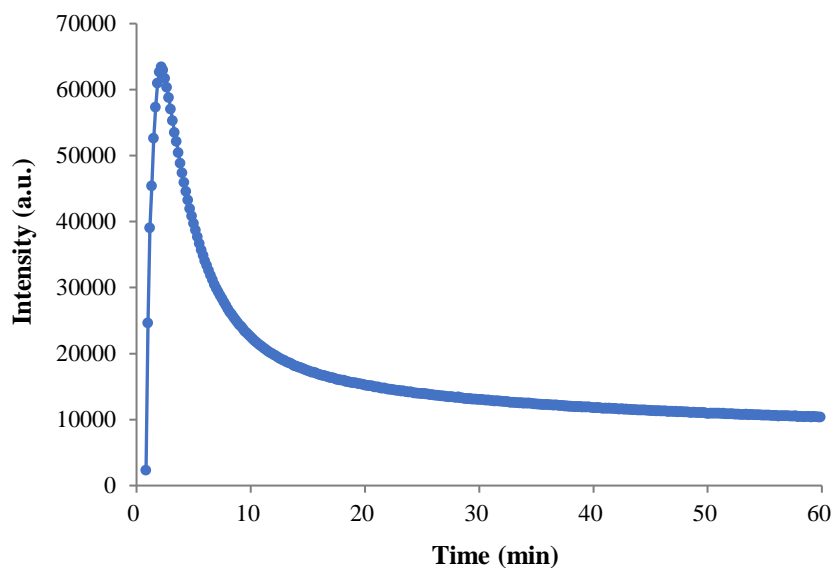


Figure 104: Reaction kinetics ($\lambda_{exc} = 289 \text{ nm}$, $\lambda_{em} = 402 \text{ nm}$) of MHPA oxidation under harsh conditions of HRP and H_2O_2 concentrations.

The second pathway involves the activation of the hydroxylic HRP cycle described in detail in Chapter III at these harsh reaction conditions. The implication of Compound III could lead to the generation of HO^\bullet able to attack the aromatic cycles of the dimer and modify its spectroscopic properties.³⁰

As this enzymatic synthesis was ineffective at larger scale, the desired dimer was organically synthesized according to the patent of Mainstein et al.³¹ The synthesis consisted in a biomimetic iron(III)-catalyzed solid-phase coupling reaction, inspired by the metalloenzymatical production of specific metabolites in plants.³² The oxidative coupling of MHPA using iron(III) as the catalyst results in the formation of a C-C bond as shown in Figure 105.

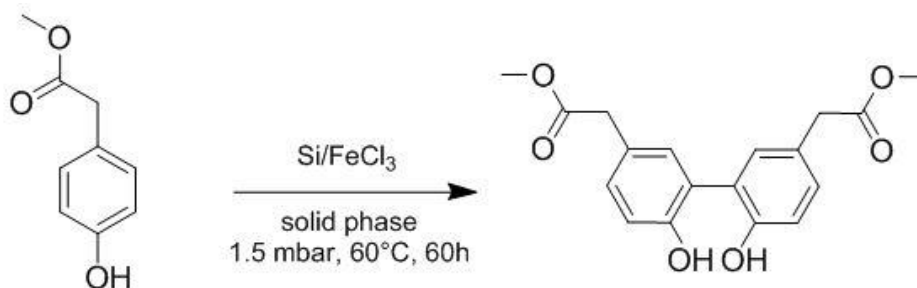


Figure 105: Iron(III)-catalyzed synthesis of dimethyl-2,2'-(6,6'-dihydroxy-[1,1'-biphenyl]-3,3'-diyl)diacetate.³²

In a first step, the silica-supported Fe(III) catalyst was prepared by wetness impregnation technique.³³ Silica gel was stirred with a solution of FeCl₃ in diethyl ether and methanol. Solvents were then removed, and the obtained yellow solid was stirred for 18 h under vacuum at 55°C. Silica support is intended to improve the performance of heterogeneous iron-containing catalysts. The dispersion of Fe within the silica might prevent its aggregating into clusters, improving the number of the active surface sites and the proximity to the reactant.³⁴

The second step consists in adding the MHPA in solution to the prepared solid catalyst. After thorough mixing, the solvent was evaporated, and the solid-phase coupling reaction was achieved under vacuum at 60°C. The mixture was then dissolved in methanol and the silica was filtrated. The product was finally purified by silica gel chromatography to obtain the final dimer with a 30% yield. The resulting dimer has been characterized by ¹H NMR. Compared to the 60% yield reported for this reaction, the loss can be related to the silica filtration step, that was repeated several times to isolate the product.

3.4.2. Identification of the reaction products

The enzymatic MHPA oxidation was studied by HPLC-UV under the conditions that yielded the higher reaction rate and the best signal amplification of Tb emission. 2 mM MHPA and 0.2 mM H₂O₂ were incubated with 10⁻¹⁰ M of HRP at pH 4.6. After 1h, a reaction mixture sample was analyzed by HPLC using a C18 reversed phase column with a diode array detector (DAD) detector. The elution conditions were determined for an optimal separation and detection ($\lambda_{\text{abs}} = 220 \text{ nm}$) of the mixture constituents using milliQ water and acetonitrile (ACN) as mobile phases. The resulting chromatogram was compared to those of the reaction mixture in absence of HRP, and the synthesized dimer as shown in Figure 106.

Compounds eluted at 2.7 min include H₂O₂ and succinic acid buffer (reaction buffer). The MHPA eluted at 4.3 min indicates the consumption of 35% of the initial concentration after a 1 h reaction. A first major product of the enzymatic reaction is eluted at 5.3 min, perfectly matching with the retention time of the synthesized *o,o*-dimer, and with its absorbance spectra (inset of Figure 106). A second minor product is eluted later at 5.9 min indicating a compound with weaker polarity. Interestingly, the addition of H₂O₂ to the reaction mixture increases the intensity of this product and decreases that of the *o,o*-dimer in a similar behavior observed in the fluorescence study.

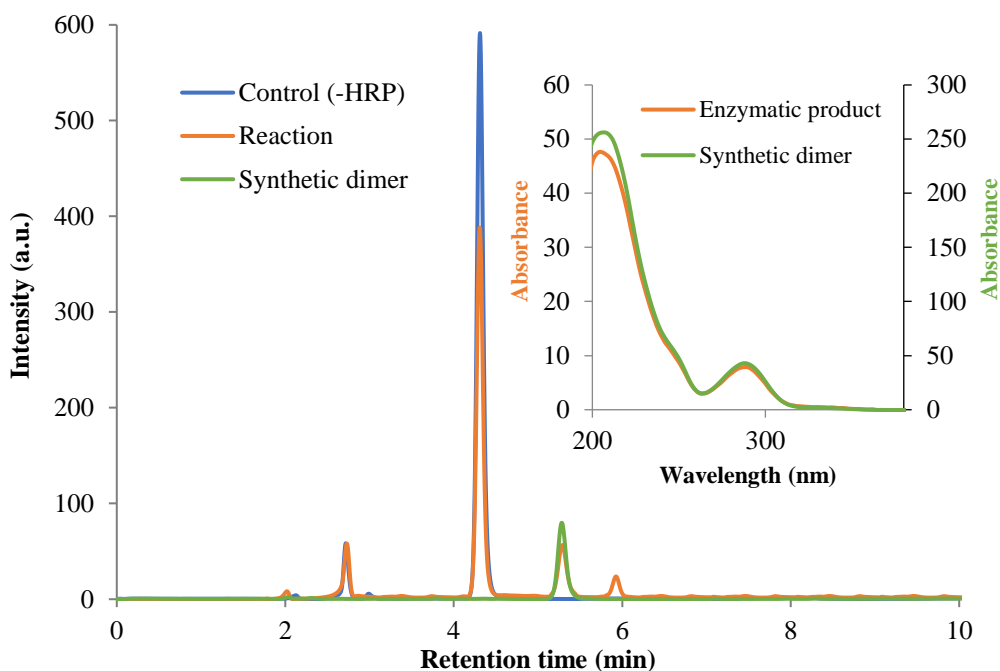


Figure 106: HPLC chromatograms of the reaction mixture in presence and absence of HRP, and the synthetic dimer ($\lambda_{abs} = 220$ nm). Inset : UV spectra of the synthetic dimer and the enzymatic product at RT=5.3 min.

Further attempts were made to identify the second product by mass spectrometry (MS). Unfortunately, MALDI-MS analysis resulted in lot of fragmentation, while ESI-MS was unable to ionize this compound. Therefore, this product remained unidentified, but the polarity information suggests that it may be a trimer resulting of a further oxidation of the *o,o*-dimer.

A major limitation of this reaction consists in the weak conversion yield of MHPA in these conditions. However, these conditions are required to maintain an optimal environment for a maximal formation of the desired compound. This excess of MHPA can compete with the formed dimer for the coordination on the surface of NPs in the next step of the assay representing one of the main limitations of this method.

3.5. Calibration of the assay

After understanding the enzymatic system and optimizing the conditions for an efficient formation of the antenna and maximal sensitization of Tb-NPs, it was essential to evaluate the final performance of the assay. The dependance of the final response on the enzyme concentration was investigated by establishing the corresponding calibration curve. The developed method was tested on a large range of HRP concentrations between 0.2 and 100 pM under optimized conditions.

2 mM MHPA were incubated in microplate wells with 0.2 mM H₂O₂ in 10 mM succinic acid buffer at pH 4.6. Different concentrations of HRP were introduced to initiate the reaction, and for each concentration, 3 replicates were executed. After 1 h, CAT was added to the mixture, followed by the introduction of 2×10^{-8} M La_{0.9}Tb_{0.1}F₃ NPs, and the pH was increased to 13. Finally, the TR-emission of Tb was measured at 545 nm in each well for an excitation at 320 nm, and the resulting calibration curve is shown in Figure 107.

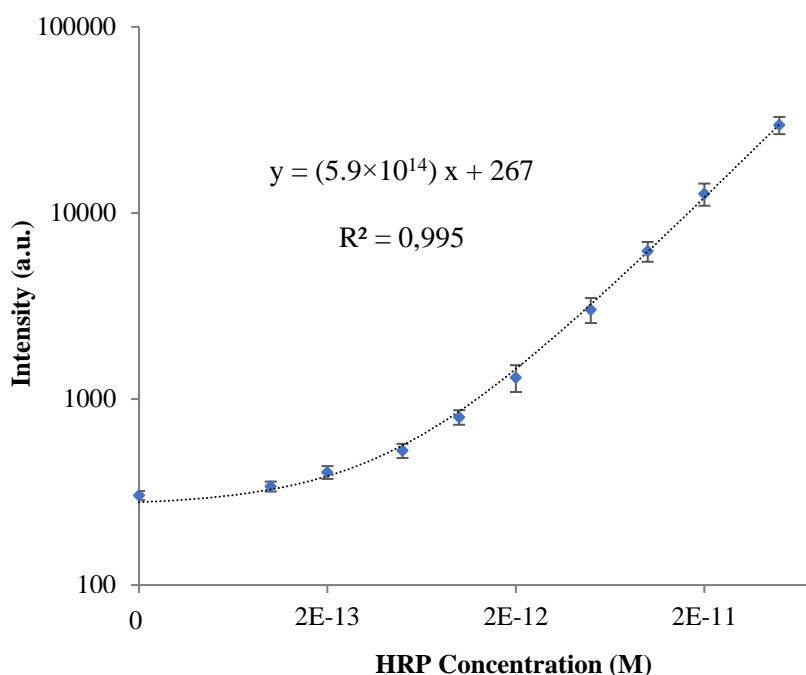


Figure 107: Calibration curve of the photoluminescence response of the assay as a function of HRP concentration ($\lambda_{exc} = 320$ nm, $\lambda_{em} = 545$ nm).

The relative response of the assay as a function of the enzyme concentration fitted well in a linear equation. The 3 replicates show decent standard deviations which indicates a good precision of the method. In addition, the working concentration range seems to be very important as the calibration curve covered 3 orders of magnitude and the higher limit of the method was not yet reached.

In this work, the main interest concerns the lower limits of detection LOD and quantification LOQ of the method. In general, the LOD is considered as the lowest concentration of an analyte (HRP) in a sample that can be reliably distinguished from “analytical noise”, the signal produced in the absence of analyte, but not necessarily quantified. The LOQ, which defines the sensitivity of the method is the lowest concentration of an analyte in a sample that can be determined with acceptable precision and accuracy under the stated conditions of test.³⁵

A traditional and typical approach to estimate LOD consists of measuring replicates of blank sample, determining the mean value (B) and the standard deviation (SD), and calculating LOD as the mean plus 2 SD. Variations of this approach use the mean plus 3, 4, or even 10 SD to provide a more conservative LOD.³⁶

Herein, LOD and LOQ were estimated using the following equations.

$$LOD = B + 3.3 SD$$

$$LOQ = B + 10 SD$$

The coefficients 3.3 and 10 are called expansion factors and are obtained assuming a 95% confidence level.³⁷ It is necessary to note that this model does not take into account the uncertainty of position of calibration line.

Using the calibration curve and the estimations above, a LOD of 10^{-13} M and a LOQ of 3×10^{-13} M were determined. In comparison with similar assays using Ln complexes, this method provides better performance in terms of sensitivity than that reported by Zheng *et al.* at 8×10^{-10} M using HBA substrate,¹¹ and Meyer *et al.* at 2×10^{-12} M using HPPA.³⁸ These results were promising for further application of the developed method in an ELISA.

4. Reaction with HRP conjugate

4.1. Oxidation of MHPA by Streptavidin-HRP

After demonstrating the effectiveness of this method using HRP in solution, it was important to investigate the reactivity of this enzyme when acting as a label. In most ELISA, HRP is not directly bound to the Ab, but conjugated to streptavidin protein (SA), ready to bind to a biotinylated Ab. This particular process provides consistent measurement of biotinylated detection Abs in sandwich ELISA applications. Therefore, a first step consisted in evaluating the enzymatic activity of SA-HRP conjugate in solution for the developed assay.

The full assay was performed following the same conditions optimized above, while replacing HRP by the SA-HRP conjugate at 10^{-10} M of enzyme. The resulting TR-emission spectra of Tb with an excitation at 320 nm are presented in Figure 108. Surprisingly, the oxidation of MHPA by SA-HRP resulted in weaker sensitization of Tb-NPs compared to the reaction with HRP at the same enzyme concentration. Actually, the conjugation of HRP to SA should not functionally alter the active site of the enzyme.³⁹

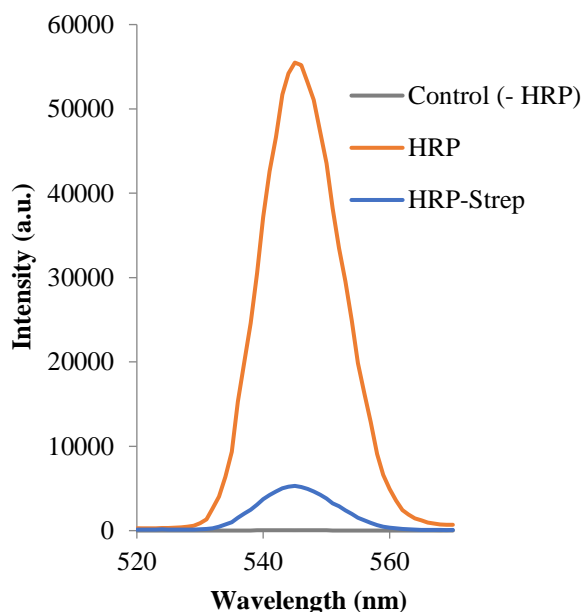


Figure 108: TR-emission spectra of $La_{0.9}Tb_{0.1}F_3$ NPs ($\lambda_{exc} = 320$ nm) after MHPA oxidation SA-HRP at pH 4.6.

4.2. Effect of the pH

The parameter that could have altered the activity of the enzyme was the pH of the reaction as it was seen that a different type of HRP can present different optimal pH values. Therefore, the oxidation of MHPA by SA-HRP was investigated in the range of 4.5-8.5 using 10 mM succinic acid buffer while keeping all other parameters as optimized. After 1 h of reaction, all wells were adjusted to pH 7.0 followed by measuring the emission intensity at 402 nm after an excitation at 290 nm. The results of this study are shown in Figure 109.

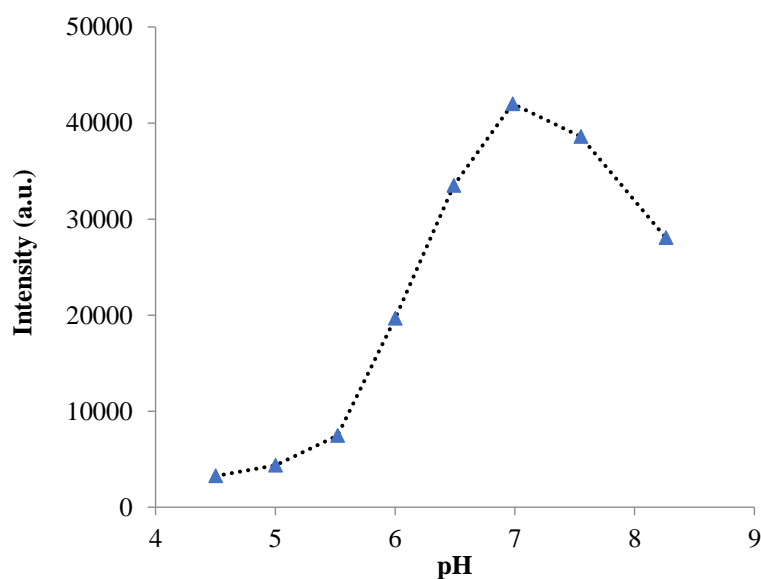


Figure 109: Effect of the pH on the formation of the dimer by SA-HRP oxidation ($\lambda_{exc} = 289$ nm, $\lambda_{em} = 402$ nm).

The results of this study completely justify the weak sensitization signal resulting from the reaction by SA-HRP. In contrast to the results observed with HRP, the optimal formation of the MHPA dimer with SA-HRP occurred at pH 7.0, while at pH 4.6, very weak formation of the dimer was observed. This can be related to the type of HRP enzyme as explained in 3.3.1.

4.3. Effect of the buffer

At pH 7.0, succinic acid is slightly out of its working buffer range. Therefore, the assay using SA-HRP was performed using different buffer solutions and the final sensitization signal was compared to that obtained using HRP. After 1h of reaction at pH 7.0 in different buffers, CAT and Tb-NPs were added followed by the pH increase. The resulting TR-emission spectra with an excitation at 320 nm are presented in Figure 110. The final sensitization signal following the oxidation of MHPA by SA-HRP at pH 7.0 is significantly higher than that obtained with a reaction at pH 4.6. Succinate buffer presented the best compatibility with NPs sensitization and showed better signal amplification than that performed in Tris or HEPES.

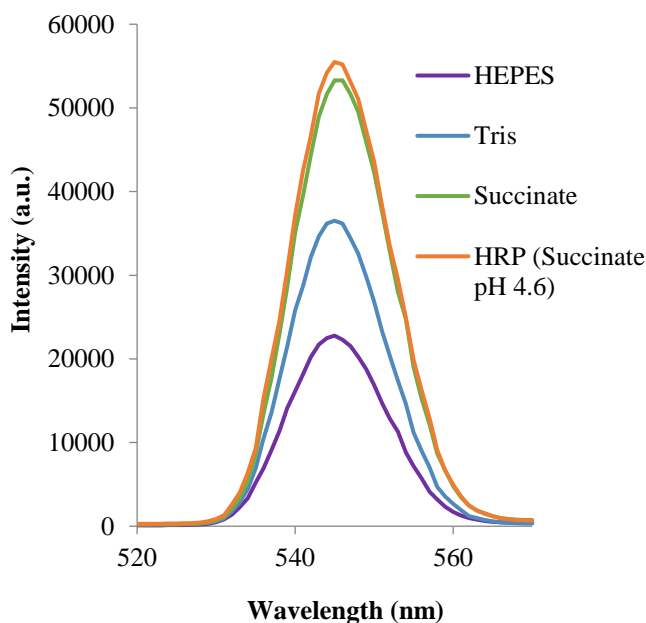


Figure 110: TR-emission spectra of $La_{0.9}Tb_{0.1}F_3$ NPs ($\lambda_{exc} = 320$ nm) after MHPA oxidation by SA-HRP in different buffers at pH 7.0.

Interestingly, the assay performed in succinate at pH 7.0 regained the same efficiency of signal amplification optimized with unconjugated HRP. Although succinate is slightly out of its working buffer range, no pH variation was noticed during 1 h of MHPA oxidation which allows to take advantage of the better assay performance provided by this buffer.

5. Application to ELISA

5.1. Proof of concept

After proving that HRP enzyme maintains its effectiveness when conjugated to SA regarding the oxidation of MHPA, the final step consisted in the application of the developed method in a typical ELISA. For that, a commercial ELISA kit was used for the quantification of human insulin in serum, plasma, or other biological media.

This assay is a sandwich ELISA, based sequentially on the capture of human insulin Ags from samples to the wells of a microtiter plate coated by monoclonal mouse anti-human insulin Abs and the binding of a second biotinylated monoclonal mouse anti-human Ab to the captured insulin. After washing away unbound materials from samples, SA-HRP is bound to the immobilized biotinylated Abs. Free enzyme conjugates are washed away, and the quantification of immobilized immunocomplex is achieved by monitoring HRP activity.

The commercial method of monitoring HRP activity consisted in the oxidation of 3,3',5,5'-tetramethylbenzidine substrate (TMB) resulting an increase in the absorption at 450 nm of the acidified product. It is at this step that the ELISA was modified as described in Figure 111 by replacing the commercial method by the method developed in this work, based on the oxidation of MHPA followed by the sensitization of Tb-NPs in alkaline conditions.

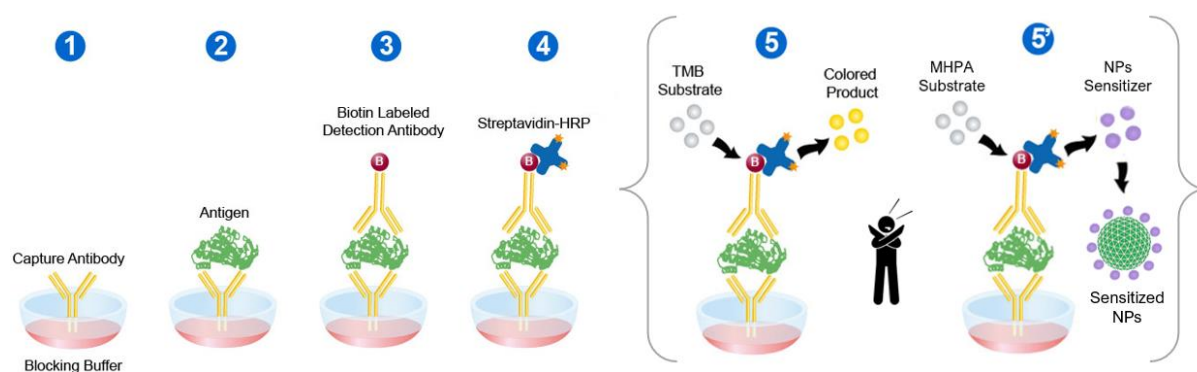


Figure 111: Procedure of sandwich ELISA for the quantification of human insulin.⁴⁰

The ELISA was performed with insulin standard at 20 $\mu\text{U}/\text{mL}$ to evaluate the response of the developed method in comparison to the commercial one. One international unit of insulin is defined as the amount of insulin required to lower the fasting blood sugar of a rabbit by 2.5 mmol/L, equivalent to 34.7 μg of pure crystalline insulin.

After the immobilization of the enzyme labeled immunocomplex, the substrate solution was added in respect of the previously optimized conditions with 2 mM MHPA and 0.2 mM H₂O₂ in 10 mM succinate at pH 7.0. After 1 h of reaction, 0.05 mg/mL CAT and 2×10⁻⁸ M La_{0.9}Tb_{0.1}F₃ NPs were added to the reaction mixture followed by the pH increase. The microplate was agitated for 5 min and the Tb emission spectra were recorded with an excitation at 320 nm. TR-emission spectra of La_{0.9}Tb_{0.1}F₃ NPs are presented in Figure 112a while the absorption spectra resulting of the commercial detection method are shown in Figure 112b.

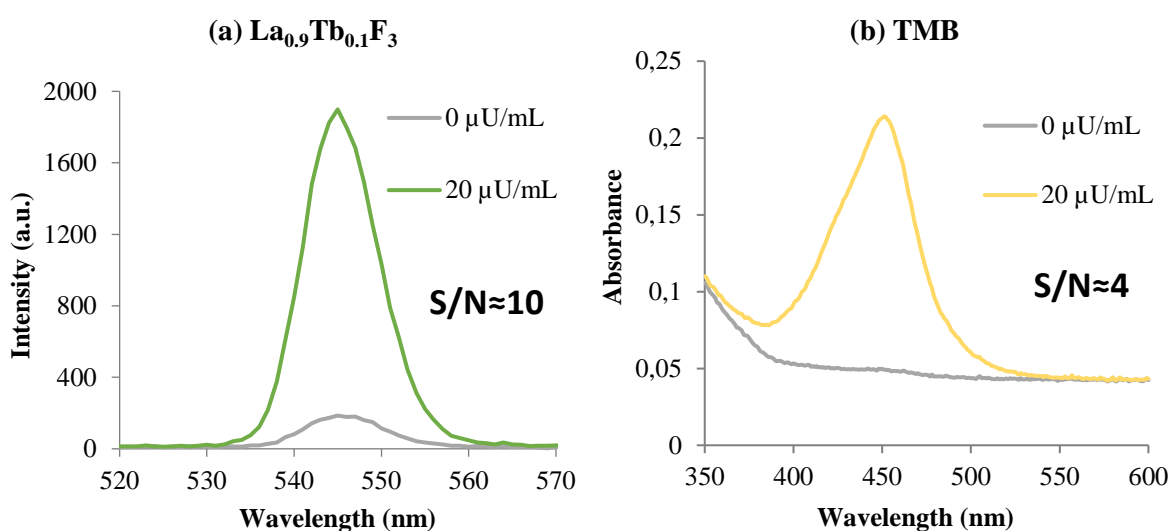


Figure 112: (a) TR-emission spectra of La_{0.9}Tb_{0.1}F₃ NPs ($\lambda_{exc} = 320$ nm) and (b) absorption spectra following an ELISA with 0 or 20 μ U/mL of insulin.

The response of the assay using time resolved detection of Tb-NPs photoluminescence provided a signal to noise ratio S/N of 10, 2.5 times higher than that of the commercial colorimetric detection method with a S/N of 4. These results were promising in terms of the sensitivity of the assay response in the developed method.

5.2. Effect of the NPs type

Despite a good S/N, an important noise representing the Tb emission intensity in absence of insulin was notably observed. Trying to optimize that issue, different types of Ln-NPs were investigated. Tb/Eu codoped NPs (Tb_{0.85}La_{0.14}Eu_{0.01}F₃) were the first candidate for their interesting luminescence properties demonstrated in Chapter II.

The assay was performed in the same conditions and the same insulin concentration. TR-emission spectra of Tb_{0.85}La_{0.14}Eu_{0.01}F₃ NPs are presented in Figure 113a.

Interestingly, these NPs exhibited similar signal intensity of Tb emission with a reduced noise. Consequently, the response of the assay using these NPs provided an enhanced S/N of 20. At first, it was hypothesized that the reduced noise was related to the different crystalline structure of these 2 types of NPs, as demonstrated in Chapter II. This results in a different environment of Tb ions in each crystal and can alter their emission.

As this interesting turn-on ability involved just the Tb emission, the role of Eu ions in $\text{La}_{0.14}\text{Tb}_{0.85}\text{Eu}_{0.01}\text{F}_3$ NPs was investigated by a systematic comparison with $\text{La}_{0.15}\text{Tb}_{0.85}\text{F}_3$ NPs. TR-emission spectra of $\text{La}_{0.15}\text{Tb}_{0.85}\text{F}_3$ NPs are presented in Figure 113b.

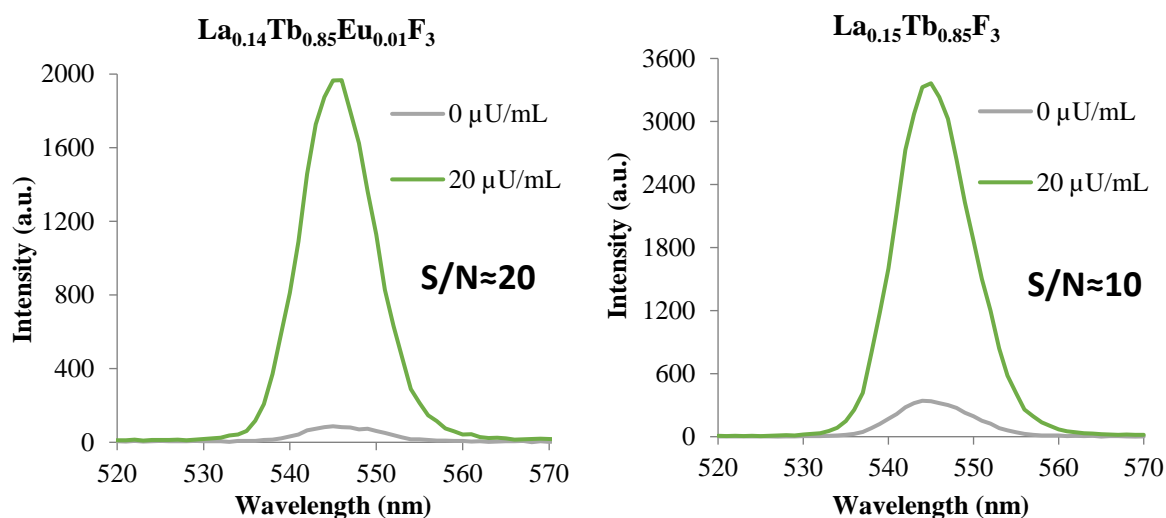


Figure 113: (a) TR-emission spectra of $\text{La}_{0.14}\text{Tb}_{0.85}\text{Eu}_{0.01}\text{F}_3$ NPs and (b) $\text{La}_{0.15}\text{Tb}_{0.85}\text{F}_3$ following an ELISA with 0 or 20 $\mu\text{U/mL}$ of insulin ($\lambda_{exc} = 320 \text{ nm}$).

These 2 types of NPs have both orthorhombic crystalline structures as demonstrated in Chapter II. However, $\text{La}_{0.15}\text{Tb}_{0.85}\text{F}_3$ NPs settled for a S/N of 10, similar to that obtained with $\text{La}_{0.9}\text{Tb}_{0.1}\text{F}_3$ NPs with both higher signal and noise intensities of Tb emission due to the higher Tb doping level. Therefore, the results obtained with $\text{La}_{0.14}\text{Tb}_{0.85}\text{Eu}_{0.01}\text{F}_3$ NPs cannot be explained by the different crystalline structure, but rather related to the presence of Eu ions. The previously demonstrated energy transfer from Tb to Eu could be the reason for the reduced Tb emission noise, while at increased presence of the antenna, the Tb emission signal starts increasing as seen in the titration of these NPs in Chapter II.

Table 11: Summary of the S/N response of different NPs in ELISA with a 20 $\mu\text{L/mL}$ insulin.

NPs	$\text{La}_{0.9}\text{Tb}_{0.1}\text{F}_3$	$\text{La}_{0.15}\text{Tb}_{0.85}\text{F}_3$	$\text{La}_{0.14}\text{Tb}_{0.85}\text{Eu}_{0.01}\text{F}_3$
S/N	10	10	20

5.3. Calibration of the final assay

In a final step, the final performance of the developed ELISA was evaluated by establishing the corresponding calibration curve. The assay was performed on a 1-100 $\mu\text{U/mL}$ range of insulin concentration under the same optimized conditions mentioned above. $\text{La}_{0.14}\text{Tb}_{0.85}\text{Eu}_{0.01}\text{F}_3$ NPs were used in this study for providing the best S/N in the assay. The resulting calibration curve describing the intensity of TR-emission of Tb at 545 nm after an excitation at 320 nm is shown in Figure 114.

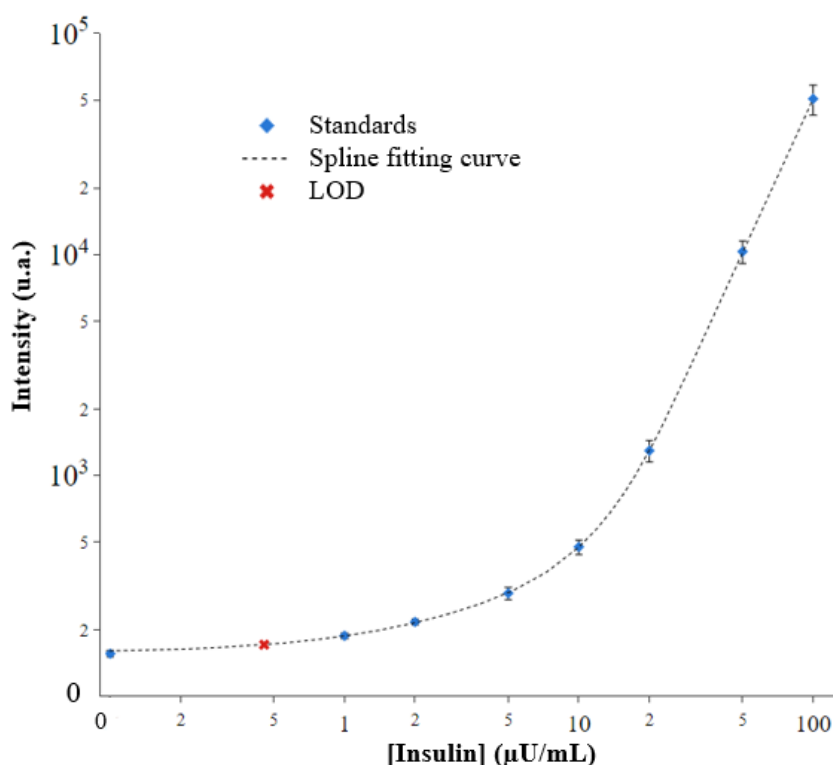


Figure 114: Calibration curve of the photoluminescence response of the assay as a function of insulin concentration ($\lambda_{exc} = 320 \text{ nm}$, $\lambda_{em} = 545 \text{ nm}$).

The relative response of the assay as a function of the enzyme concentration was fitted in a Spline curve using Assayfit Pro, an ELISA results data analysis software.⁴¹ Spline is a function defined piecewise by polynomials, allowing the fitting of complex smooth shapes. The 3 replicates show weak standard deviations which indicates a good precision of the method. In this range of insulin concentration, the calibration presented a low response curve shape.⁴²

Most importantly, the limits of detection and quantification were estimated as detailed in part 3.5 of this chapter. Using the calibration curve and assuming a 95% confidence level, a LOD of 0.5 $\mu\text{U/mL}$ and a LOQ of 1.5 $\mu\text{U/mL}$ were determined.

Meanwhile, the LOD of the assay using the commercial colorimetric detection was evaluated and determined at 1 $\mu\text{U/mL}$, matching with the LOD provided by the supplier. These results confirmed that with the developed method based on a time resolved detection of Ln-NPs photoluminescence, the sensitivity of an ELISA for the quantification of human insulin was improved by a factor of 2.

The signal of Tb emission was found to be stable for more than 30 min, whereas the absorbance of TMB must be read within 5 min. Otherwise, the results are susceptible to be completely mistaken. In addition, TMB is sensitive to light. Therefore, an overexposure can lead to a high background in the samples and significant noise in the blank of the assay, resulting in a poor S/N and bad quality of the obtained results.

6. Conclusion

In this chapter, the aim was to use an efficient enzymatic reaction, and set it up to form product that can act as an efficient sensitizer of the Ln-NPs developed in chapter II. In this regard, the oxidation of *p*-substituted phenols by HRP leading to their dimerization was fully studied. Different substrates were investigated in order to maximize the sensitization ability of the formed dimer. After identifying the MHPA as the substrate with the best turn-on ability, the best conditions of pH, concentrations and temperature were applied for an optimal reaction.

Under optimized conditions, the oxidation of MHPA formed mainly the *o,o*-dimer responsible of the sensitization of Tb-NPs, while a minor side product was observed but could not be identified. This product is most likely coming from further transformation of the dimer. Although the latter has a very weak specific reaction rate for a further oxidation by HRP, the formation of a trimer is not excluded. Another potential pathway involves the hydroxylation of the dimer by HO[•] radicals formation by HRP as described in Chapter III.

One aspect that characterizes this reaction in comparison to that developed in Chapter III is that the substrate is the pre-antenna itself and the formation of the antenna involved one typical peroxidative cycle of HRP. Consequently, this reaction proved a decent efficiency at relatively low enzyme concentration. Under optimized conditions, this method provided a LOD of 10⁻¹³ M for the detection of HRP enzyme in solution, 20 times better than those reported in similar assays.³⁸ Moreover, the application of this method in an ELISA for the quantification of human insulin improved the sensitivity of the assay compared to the commercial detection method.

The main limitation of this method consisted in the strong competition of the substrate to coordinate to the NPs surface due to the low conversion rate at low enzyme concentrations. Actually, a moderately increased temperature and sequential addition of small amounts of H₂O₂ were demonstrated to enhanced formation yield of the desired product.^{29,43} These procedures were practically unfeasible, but with an automatized assay and using injectors for the different addition steps, these are serious options to improve the response of the assay.

Another way to enhance the reaction yield consists in the addition of a compound that effectively stimulates the oxidation of the phenol by HRP enzyme. *O*-dianisidine was reported as a strong stimulator which improve the kinetics of this type of reaction.⁴⁴ Studies of the influence of such compound on the enzymatic reaction as well as the sensitization of NPs can be useful for further improvements of this system.

7. Experimental part

7.1. Reagents

Methyl 4-hydroxyphenylacetate 97% was purchased from fluorochem. The other used phenols were purchased from Sigma, fluorochem or TCI chemicals. Horseradish peroxidase powder (type VI, 250 Units/mg), Bovine liver Catalase powder (2000-5000 Units/mg), and SA-HRP conjugate (1 mg in 0.05 M HEPES pH 6.8) were purchased at high quality level from Sigma. Hydrogen peroxide 30%, succinic acid 99%, Tris 99.8% and HEPES 99.5% were also purchased from Sigma. ACN (HPLC gradient) was purchased from Fisher scientific. MQuant® semi quantitative colorimetric peroxide test strips, 0.5-100 mg/L (H₂O₂) were purchased from Sigma at quality level 100. Human insulin ELISA kit (EZHI-14K) was purchased from Merck Millipore. Ln-NPs were synthesized according to the procedure described in Chapter II. Freshly diluted solutions were prepared in the desired buffer from the stock solution.

Silica gel 60 (0.063-0.2 mm) was purchased from Machery-Nagel, and FeCl₃.6H₂O was purchased from Sigma. Other solvents and products were purchased from Sigma, Acros, Alfa Aesar, fluorochem.

7.2. Spectroscopic measurements

Steady-state fluorescence measurements of the ligands, time-resolved photoluminescence measurements of Tb-NPs, and absorbance measurements of TMB were all recorded on a TECAN Spark microplate reader working with a high energy Xenon flash lamp. TR measurements were done with a time delay of 50 μ s and an integration time of 2 ms.

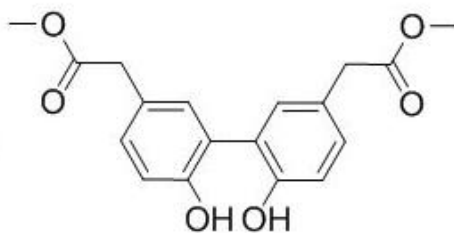
7.3. Enzymatic assays

All enzymatic assays were performed in 96-well non-binding Greiner microplate. 2 mM of the *p*-substituted phenol and 0.2 mM of H₂O₂ were incubated in microplate wells in 10 mM succinate buffer at pH 4.6 (HRP) or pH 7.0 (SA-HRP). The reaction was normally initiated by the addition of HRP enzyme. The final volume in the wells was fixed at 200 μ L in all assays. The microplate was agitated in a microplate shaker (400 rpm) at room temperature for 1 h. Concentrations, pH and temperature conditions can vary in the optimization procedure of each parameter. For kinetics studies, the microplate was instead agitated in the TECAN incubator and the increase in fluorescence ($\lambda_{exc} = 289$ nm, $\lambda_{em} = 402$ nm), was recorded for 1 h of reaction.

0.05 mg/mL of CAT were introduced to the mixture, and the elimination of H₂O₂ was verified by colorimetric peroxide test strips before the addition of the NPs. Finally, 2×10⁻⁸ M of Ln-NPs were added to the reaction mixture, and the microplate was agitated for 5 min before the spectroscopic measurements on the microplate reader. All experiments were repeated at least three times with no significant variation.

The excitation spectra were recorded at an emission of 545 nm of Tb, while the emission spectra were recorded at the maximal excitation. The excitation and emission bandwidths, the gain, as well as the z-position were kept constant in order to compare the different datasets. All Tb photoluminescence spectra were recorded by time-resolved detection with a time delay of 50 μs and an integration time of 2 ms.

7.4. Synthesis of the MHPA-dimer



Chemical Formula: C₁₈H₁₈O₆

Molecular Weight: MW = 330.33 g.mol⁻¹

Silica gel (3.62 g) was added to a solution of iron(III)chloride hexahydrate (1.76 g, 6.51 mmol) in diethyl ether (95 mL) and methanol (5 mL). The mixture was stirred vigorously. The solvents were removed under reduced pressure and a yellow residue remained. This residue was heated for 18h at 55°C under vacuum. Hydroxyphenyl acetic acid methyl ester (0.068 g, 0.41 mmol) was dissolved in dichloromethane (15 mL) and the yellow residue was added to this solution. After vigorous stirring the solvent was removed under reduced pressure to generate a black residue. This residue was heated at 60 °C under vacuum for 60 hours. The black residue was dissolved in methanol (25 mL) and filtered over Celite®. The solvent was removed under reduced pressure and the remaining residue was purified by column chromatography (petroleum ether/ethyl acetate 2:1). Yield: 30% as an amorphous solid. ¹H-NMR (400 MHz, CDCl₃): δ 7.25 (s, 2H), 7.08 (dd, ³J = 8.3, ⁴J = 2.1 Hz, 2H), 6.96 (d, J = 8.3 Hz, 2H), 3.69 (s, 6H), 3.53 (s, 4H).

7.5. Monitoring of the reaction by HPLC-UV

HPLC from Agilent technologies Series 1100 system equipped with a quaternary pump, autosampler, oven, and DAD.

Samples of the reaction mixture in presence and in absence of HRP as well as the reference compounds were separated on a C18-AQ Interchim puriFlash column (5 μ m, 4.6 \times 250 mm) with an injection volume of 10 μ L. MilliQ water and ACN were used as mobile phases with a flow rate of 1 mL/min, and following the gradient described in Table 12.

Table 12: Chromatographic conditions adopted for gradient HPLC separation of reaction components.

Time (min)	ACN	H ₂ O
00	50%	50%
08	100%	0%
10	50%	50%
15	50%	50%

7.6. ELISA procedure

All reagents were pre-warmed to room temperature immediately before setting up the assay, and the required number of strips was removed from the microtiter assay plate while unused strips were resealed in a foil pouch and stored at 2-8°C.

The washing buffer was 10-fold diluted with milliQ water. Each well was filled with 300 μ L of diluted wash buffer and incubated at room temperature for 5 min. Washing Buffer was removed from all wells by inverting the plate and tapping it smartly onto absorbent towels several times.

Then, 20 μ L assay buffer were added to the wells. In the blank well, another 20 μ L assay buffer were added. 20 μ L Human Insulin Standards of ascending concentration were added to the appropriate wells. 20 μ L biotinylated detection antibody were then added to all wells. For the best result, all additions should be completed within 30 min. The plate was covered with plate sealer and incubated at room temperature for 1 hour on an orbital microtiter plate shaker set to rotate at moderate speed (400 rpm).

The plate sealer was removed, and the solutions were decanted from the plate. All wells were washed 3 times with diluted washing buffer, 300 μ L per well per wash.

100 μ L enzyme conjugate solution were added to each well. The plate was covered with sealer and incubated with moderate shaking at room temperature for 30 min on the microtiter plate shaker.

All wells were washed again 5 times with diluted washing buffer, 300 μ L per well per wash. After this step, either the assay was conducted as mentioned in 7.2 for the developed detection method or it was completed following the commercial detection method.

100 μ L of TMB substrate solution were added to each well, and the plate was agitated for 15 min. Blue color should be formed in wells of insulin standards with intensity proportional to increasing concentrations of insulin. 100 μ L stop solution were added and the blue color should turn to yellow after acidification. Absorbance was read at 450 nm in all wells by the plate reader within 5 min.

8. References

- (1) Chen, S.; Schopfer, P. Hydroxyl-Radical Production in Physiological Reactions. *Eur. J. Biochem.* **1999**, *260* (3), 726–735. <https://doi.org/10.1046/j.1432-1327.1999.00199.x>.
- (2) Klibanov, A. M.; Alberti, B. N.; Morris, E. D.; Felshin, L. M. Enzymatic Removal of Toxic Phenols and Anilines from Waste Waters. *J Appl Biochem U. S.* **1980**, *2*:5.
- (3) Kobayashi, S.; Higashimura, H. Oxidative Polymerization of Phenols Revisited. *Prog. Polym. Sci.* **2003**, *28* (6), 1015–1048. [https://doi.org/10.1016/S0079-6700\(03\)00014-5](https://doi.org/10.1016/S0079-6700(03)00014-5).
- (4) Magario, I.; García Einschlag, F. S.; Rueda, E. H.; Zygadlo, J.; Ferreira, M. L. Mechanisms of Radical Generation in the Removal of Phenol Derivatives and Pigments Using Different Fe-Based Catalytic Systems. *J. Mol. Catal. Chem.* **2012**, *352*, 1–20. <https://doi.org/10.1016/j.molcata.2011.10.006>.
- (5) Shuttleworth, K. L.; Bollag, J.-M. Soluble and Immobilized Laccase as Catalysts for the Transformation of Substituted Phenols. *Enzyme Microb. Technol.* **1986**, *8* (3), 171–177. [https://doi.org/10.1016/0141-0229\(86\)90108-0](https://doi.org/10.1016/0141-0229(86)90108-0).
- (6) Danner, D. J.; Brignac, P. J.; Arceneaux, D.; Patel, V. The Oxidation of Phenol and Its Reaction Product by Horseradish Peroxidase and Hydrogen Peroxide. *Arch. Biochem. Biophys.* **1973**, *156* (2), 759–763. [https://doi.org/10.1016/0003-9861\(73\)90329-9](https://doi.org/10.1016/0003-9861(73)90329-9).
- (7) Yu, Jian.; Taylor, K. E.; Zou, Huixian.; Biswas, Nihar.; Bewtra, J. K. Phenol Conversion and Dimeric Intermediates in Horseradish Peroxidase-Catalyzed Phenol Removal from Water. *Environ. Sci. Technol.* **1994**, *28* (12), 2154–2160. <https://doi.org/10.1021/es00061a025>.
- (8) Alshabib, M.; Onaizi, S. A. A Review on Phenolic Wastewater Remediation Using Homogeneous and Heterogeneous Enzymatic Processes: Current Status and Potential Challenges. *Sep. Purif. Technol.* **2019**, *219*, 186–207. <https://doi.org/10.1016/j.seppur.2019.03.028>.
- (9) Zhang, L.; Zhao, W.; Ma, Z.; Nie, G.; Cui, Y. Enzymatic Polymerization of Phenol Catalyzed by Horseradish Peroxidase in Aqueous Micelle System. *Eur. Polym. J.* **2012**, *48* (3), 580–585. <https://doi.org/10.1016/j.eurpolymj.2011.12.011>.
- (10) Steinkamp, T.; Karst, U. Detection Strategies for Bioassays Based on Luminescent Lanthanide Complexes and Signal Amplification. *Anal. Bioanal. Chem.* **2004**, *380* (1), 24–30. <https://doi.org/10.1007/s00216-004-2682-2>.
- (11) Zheng, X.-Y.; Lu, J.-Z.; Zhu, Q.-Z.; Xu, J.-G.; Li, Q.-G. Study of a Lanthanide Fluorescence System With a Coupled Reaction Based on Hemin Catalysis. *Analyst* **1997**, *122* (5), 455–458. <https://doi.org/10.1039/A606560K>.
- (12) Jonsson, M.; Lind, J.; Merényi, G. Redox and Acidity Properties of 2,2'- and 4,4'-Biphenol and the Corresponding Phenoxyl Radicals. *J. Phys. Chem. A* **2002**, *106* (18), 4758–4762. <https://doi.org/10.1021/jp0129232>.
- (13) Guilbault, G. G.; Kramer, D. N.; Hackley, E. B. New Substrate for Fluorometric Determination of Oxidative Enzymes. *Anal. Chem.* **1967**, *39* (2), 271–271. <https://doi.org/10.1021/ac60246a029>.
- (14) Meyer, J.; Karst, U. Enzyme-Linked Immunosorbent Assays Based on Peroxidase Labels and Enzyme-Amplified Lanthanide Luminescence Detection. *Analyst* **2001**, *126* (2), 175–178. <https://doi.org/10.1039/b008293g>.
- (15) Guilbault, G. G.; Brignac, P. J.; Zimmer, Mary. Homovanillic Acid as a Fluorometric Substrate for Oxidative Enzymes. Analytical Applications of the Peroxidase, Glucose Oxidase, and Xanthine Oxidase Systems. *Anal. Chem.* **1968**, *40* (1), 190–196. <https://doi.org/10.1021/ac60257a002>.

- (16) Huang, L.; Colas, C.; Ortiz de Montellano, P. R. Oxidation of Carboxylic Acids by Horseradish Peroxidase Results in Prosthetic Heme Modification and Inactivation. *J. Am. Chem. Soc.* **2004**, *126* (40), 12865–12873. <https://doi.org/10.1021/ja046455w>.
- (17) Tonami, H.; Uyama, H.; Kobayashi, S.; Fujita, T.; Taguchi, Y.; Osada, K. Chemoselective Oxidative Polymerization of M-Ethynylphenol by Peroxidase Catalyst to a New Reactive Polyphenol. *Biomacromolecules* **2000**, *1* (2), 149–151. <https://doi.org/10.1021/bm000005o>.
- (18) Xu, Y.-P.; Huang, G.-L.; Yu, Y.-T. Kinetics of Phenolic Polymerization Catalyzed by Peroxidase in Organic Media. *Biotechnol. Bioeng.* **1995**, *47* (1), 117–119. <https://doi.org/10.1002/bit.260470114>.
- (19) Klibanov, A. M.; Tu, T.-M.; Scott, K. P. Peroxidase-Catalyzed Removal of Phenols from Coal-Conversion Waste Waters. *Science* **1983**, *221* (4607), 259–261. <https://doi.org/10.1126/science.221.4607.259>.
- (20) Nakamoto, S.; Machida, N. Phenol Removal from Aqueous Solutions by Peroxidase-Catalyzed Reaction Using Additives. *Water Res.* **1992**, *26* (1), 49–54. [https://doi.org/10.1016/0043-1354\(92\)90110-P](https://doi.org/10.1016/0043-1354(92)90110-P).
- (21) Feng, W.; Taylor, K. E.; Biswas, N.; Bewtra, J. K. Soybean Peroxidase Trapped in Product Precipitate during Phenol Polymerization Retains Activity and May Be Recycled. *J. Chem. Technol. Biotechnol.* **2013**, *88* (8), 1429–1435. <https://doi.org/10.1002/jctb.4075>.
- (22) Lopes, G. R.; Pinto, D. C. G. A.; Silva, A. M. S. Horseradish Peroxidase (HRP) as a Tool in Green Chemistry. *RSC Adv.* **2014**, *4* (70), 37244–37265. <https://doi.org/10.1039/C4RA06094F>.
- (23) Krainer, F.; Naeaetsaari, L.; Glieder, A.; Kulterer, M.; Reichel, V. Horseradish Peroxidase Isoenzymes. US20140363837A1, December 11, 2014.
- (24) Floyd, R. A.; Soong, L. M.; Culver, P. L. Horseradish Peroxidase/Hydrogen Peroxide-Catalyzed Oxidation of the Carcinogen N-Hydroxy-N-Acetyl-2-Aminofluorene as Effected by Cyanide and Ascorbate1. *Cancer Res.* **1976**, *36* (4), 1510–1519.
- (25) *Proteins & Enzymes*. <https://www.sigmaaldrich.com/FR/en/products/protein-biology/proteins-and-enzymes> (accessed 2022-10-12).
- (26) Veitch, N. C. Horseradish Peroxidase: A Modern View of a Classic Enzyme. *Phytochemistry* **2004**, *65* (3), 249–259. <https://doi.org/10.1016/j.phytochem.2003.10.022>.
- (27) Hiner, A. N. P.; Hernández-Ruíz, J.; Arnao, M. B.; García-Cánovas, F.; Acosta, M. A Comparative Study of the Purity, Enzyme Activity, and Inactivation by Hydrogen Peroxide of Commercially Available Horseradish Peroxidase Isoenzymes A and C. *Biotechnol. Bioeng.* **1996**, *50* (6), 655–662. [https://doi.org/10.1002/\(SICI\)1097-0290\(19960620\)50:6<655::AID-BIT6>3.0.CO;2-J](https://doi.org/10.1002/(SICI)1097-0290(19960620)50:6<655::AID-BIT6>3.0.CO;2-J).
- (28) Hoshino, N.; Nakajima, R.; Yamazaki, I. The Effect of Polymerization of Horseradish Peroxidase on the Peroxidase Activity in the Presence of Excess H₂O₂: A Background for a Homogeneous Enzyme Immunoassay. *J. Biochem.* **1987**, *102* (4), 785–791. <https://doi.org/10.1093/oxfordjournals.jbchem.a122116>.
- (29) Wu, J.; Bewtra, J. K.; Biswas, N.; Taylor, K. E. Effect of H₂O₂ Addition Mode on Enzymatic Removal of Phenol from Wastewater in the Presence of Polyethylene Glycol. *Can. J. Chem. Eng.* **1994**, *72* (5), 881–886. <https://doi.org/10.1002/cjce.5450720515>.
- (30) Buhler, D. R.; Mason, H. S. Hydroxylation Catalyzed by Peroxidase. *Arch. Biochem. Biophys.* **1961**, *92* (3), 424–437. [https://doi.org/10.1016/0003-9861\(61\)90381-2](https://doi.org/10.1016/0003-9861(61)90381-2).
- (31) Manstein, D.; PRELLER, M.; Furch, M.; Kalesse, M.; DÍAZ, N. Biphenyl Compounds for Use in Treating Malaria and Other Parasitic Disorders. EP2753599A1, July 16, 2014.

- (32) Quideau, S.; Deffieux, D.; Douat-Casassus, C.; Pouységu, L. Plant Polyphenols: Chemical Properties, Biological Activities, and Synthesis. *Angew. Chem. Int. Ed.* **2011**, *50* (3), 586–621. <https://doi.org/10.1002/anie.201000044>.
- (33) Sietsma, J. R. A.; Jos van Dillen, A.; de Jongh, P. E.; de Jong, K. P. Application of Ordered Mesoporous Materials as Model Supports to Study Catalyst Preparation by Impregnation and Drying. In *Studies in Surface Science and Catalysis*; Gaigneaux, E. M., Devillers, M., De Vos, D. E., Hermans, S., Jacobs, P. A., Martens, J. A., Ruiz, P., Eds.; Scientific Bases for the Preparation of Heterogeneous Catalysts; Elsevier, 2006; Vol. 162, pp 95–102. [https://doi.org/10.1016/S0167-2991\(06\)80895-5](https://doi.org/10.1016/S0167-2991(06)80895-5).
- (34) Pham, A. L.-T.; Lee, C.; Doyle, F. M.; Sedlak, D. L. A Silica-Supported Iron Oxide Catalyst Capable of Activating Hydrogen Peroxide at Neutral PH Values. *Environ. Sci. Technol.* **2009**, *43* (23), 8930–8935. <https://doi.org/10.1021/es902296k>.
- (35) Bernal, E.; Bernal, E. *Limit of Detection and Limit of Quantification Determination in Gas Chromatography*; IntechOpen, 2014. <https://doi.org/10.5772/57341>.
- (36) Armbruster, D. A.; Pry, T. Limit of Blank, Limit of Detection and Limit of Quantitation. *Clin. Biochem. Rev.* **2008**, *29* (Suppl 1), S49–S52.
- (37) Brunetti B, D. E. About Estimating the Limit of Detection by the Signal to Noise Approach. *Pharm. Anal. Acta* **2015**, *06* (04). <https://doi.org/10.4172/2153-2435.1000355>.
- (38) Meyer, J.; Karst, U. Peroxidase Enhanced Lanthanide Luminescence—a New Technique for the Evaluation of Bioassays. *Analyst* **2000**, *125* (9), 1537–1538. <https://doi.org/10.1039/B004973P>.
- (39) Winston, S. E.; Fuller, S. A.; Evelegh, M. J.; Hurrell, J. G. R. Conjugation of Enzymes to Antibodies. *Curr. Protoc. Mol. Biol.* **2000**, *50* (1), 11.1.1-11.1.7. <https://doi.org/10.1002/0471142727.mb1101s50>.
- (40) *Sandwich ELISA Protocol*. Leinco Technologies. <https://www.leinco.com/sandwich-elisa-protocol/> (accessed 2022-10-20).
- (41) Curve Fitting for Laboratory Assays - AssayFit Pro.
- (42) Davis, D.; Zhang, A.; Etienne, C.; Huang, I.; Malit, M. *Principles of curve fitting for multiplex sandwich immunoassays*. Bio-Rad Laboratories, Inc. Alfred Nobel Drive, Hercules, CA. (accessed 2022-10-30).
- (43) Akita, M.; Tsutsumi, D.; Kobayashi, M.; Kise, H. Structural Change and Catalytic Activity of Horseradish Peroxidase in Oxidative Polymerization of Phenol. *Biosci. Biotechnol. Biochem.* **2001**, *65* (7), 1581–1588. <https://doi.org/10.1271/bbb.65.1581>.
- (44) Iwai, H.; Ishihara, F.; Akihama, S. A Fluorometric Rate Assay of Peroxidase Using the Homovanillic Acid-o-Dianisidine-Hydrogen Peroxide System. *Chem. Pharm. Bull.* **1983**, *31* (10), 3579–3582. <https://doi.org/10.1248/cpb.31.3579>.

Chapter V

Conclusion and perspectives

In this thesis, the goal was to develop a new ultrasensitive ELISA method based on luminescent Ln-NPs. The aim of the project was to exploit the exceptional properties of Ln to overcome the limitations of commercial ELISA detection methods typically based on organic chromophores or fluorophores. This idea was suggested 20 years ago using Ln-complexes but then abandoned for these last 2 decades due to their limitation in terms of stability and brightness. Herein, Ln-NPs were proposed as alternative for application in ELISA type IAs.

The project was introduced by describing and connecting the different concepts that constitute the context of this research. A brief literature review summarized the evolution of ELISA and highlighted the main limitations of typical detection method in terms of sensitivity. Subsequently, Ln-NPs were proposed as a serious candidate to overcome these limitations thanks to their exceptional spectroscopic properties.

The first study focused on the synthesis and the characterization of Ln-NPs. The targeted NPs were then investigated for their luminescence ability through sensitization by different antennas. $\text{La}_{0.9}\text{Tb}_{0.1}\text{F}_3$ and $\text{Tb}_{0.85}\text{La}_{0.14}\text{Eu}_{0.01}\text{F}_3$ NPs were selected for their stability, remarkable brightness, and extremely long luminescence lifetimes.

The next studies consisted in developing different enzymatic reactions for potential application of the developed NPs in ELISA. By a judicious choice of the substrate, the enzyme and the enzymatic mechanism, the aim was to transform a substrate which cannot photosensitize Ln-NPs into an active form that can be properly coordinated to the surface of NPs and efficiently sensitize Ln^{3+} ions as illustrated in Figure 115.

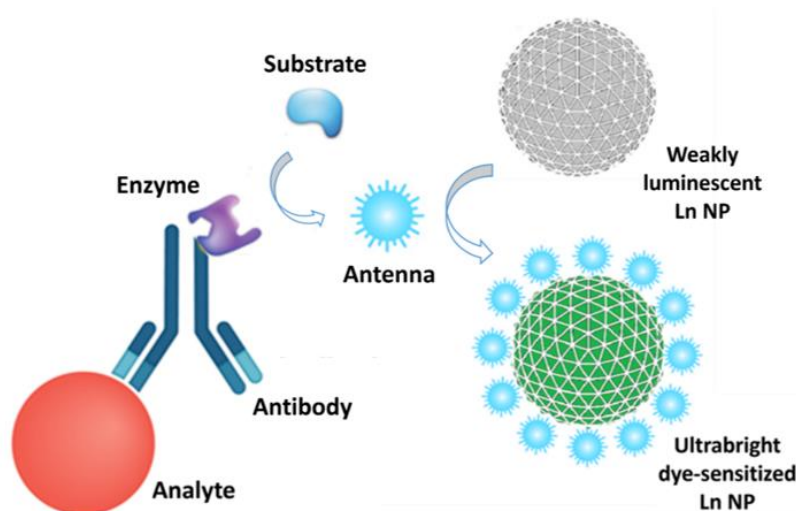


Figure 115: Principle of the developed ELISA method involving the sensitization of Ln NPs.

In order to simplify the system, the development of the enzymatic system was performed with free enzyme in solution. The first approach adopted in this regard consisted in starting from a well-known efficient sensitizer of Ln-NPs and trying to produce it *via* proper enzymatic reaction. 2-hydroxyisophthalate units were demonstrated to exhibit strong photosensitization of Tb-NPs with important signal amplification. Therefore, several attempts were evoked trying to enzymatically form this antenna.

The oxidation of NADH by HRP enzyme in presence of H₂O₂ was demonstrated to mediate the generation of HO• radicals. The latter were exploited to hydroxylate an inactive isophthalate pre-antenna, to form the desired sensitizer. The best conditions of buffer, pH, and temperature were applied for an optimal formation of HO• radicals. Moreover, different isophthalate derivatives pre-antennas were investigated to optimize the hydroxylation process. The hydroxylation of trimesate, illustrated in Figure 116, provided the best formation yield of the desired antenna. Consequently, it provided a 65-fold amplification of Tb emission upon the sensitization of Tb-NPs. At 0.2 μM of HRP and compared to the working concentration range in ELISA (pM), this signal is feeble for an application in such immunoassay.

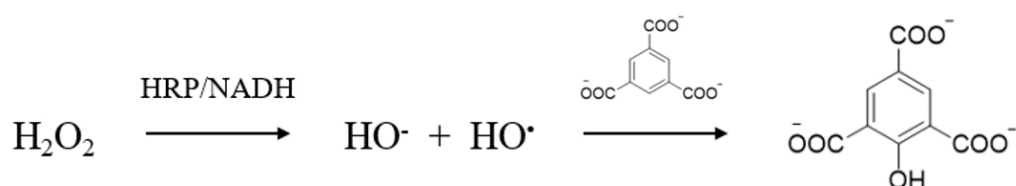


Figure 116: Hydroxylation of trimesate by enzymatic generation of HO• radicals from H₂O₂.

The main limitation of this system was the multistep mechanism involving three different enzymatic cycles of HRP, susceptible to competitive reactions altering the species involved in the formations of HO• radicals and resulting in slow kinetics and low yields of the reaction.

In order to boost the formation of HO• radicals, an exaggerated increase of H₂O₂ concentration is required. However, this increase causes the hydroxylation of the pre-antenna in absence of the enzyme, potentially due to H₂O₂ photolysis. Thus, further studies would have to be conducted in order to control the reaction at high H₂O₂ concentrations, as well as dealing with its prompt quenching effect on the sensitization of NPs. Thus, a different strategy was then adopted and fully studied.

This strategy consisted in starting from a well-known efficient enzymatic reaction, then optimizing the settings in order to form an efficient antenna. This approach was based on the fundamental peroxidative cycle of HRP enzyme in which it catalyzes the oxidation of two phenol molecules in the presence of H_2O_2 to form phenoxy radicals. These very reactive compounds can undergo further nonenzymatic reactions generating various dimeric structures, interesting candidates for NPs sensitization. In contrast to the previous approach, the substrate is the pre-antenna itself and the transformation involves one simple catalytic cycle of HRP enzyme which reduces side reactions and enhance the formation yield of the desired antenna.

In this work, the substrate was structurally selected to orientate the formation of an *o,o'*-biphenol able to coordinate to the NPs surface and sensitize Tb ions. Among the tested substrates, the MHPA highlighted the best performance in this enzymatic assay as shown in Figure 117, highlighting very promising turn-on ability. The best conditions of buffer, pH, and concentrations were applied for an optimal antenna formation and a maximal NP sensitization.

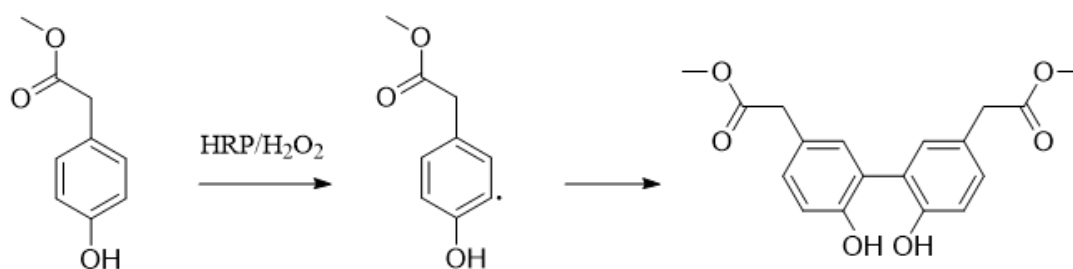


Figure 117: Oxidation of MHPA by HRP followed by its dimerization.

This method provided a LOD of 10^{-13} M for the detection of HRP enzyme in solution, 20 times better than those reported in similar assays. Finally, the main goal of the thesis was accomplished by the application of this method in an ELISA for the quantification of human insulin. It was demonstrated that the TR-detection of Ln-NPs luminescence sensitized by an enzymatically generated antenna improved the sensitivity of the assay compared to the commercial detection method.

Despite the good response obtained with this assay, it still suffers from some drawbacks. The main limitation consisted in the strong competition of the substrate to coordinate to the NPs surface due to the low conversion rate and slower kinetics, which requires to increase the time of reaction to 1 h, relatively long time compared to the reactions used in conventional ELISA.

This low conversion rate is due to the moderate H_2O_2 concentration required for an optimal formation of the desired compound and to avoid the side reactions or the inactivation of HRP. This can be compensated by a sequential addition of small amounts of H_2O_2 to enhance the conversion yield to the desired product. In addition, a moderately increased temperature was proven to improve the kinetics of the reaction with free HRP in solution. Particularly, in an ELISA where the enzyme is fixed on the Ab in the bottom of the well, the rate of the reaction is limited by the substrate diffusion to the enzyme active sites. Therefore, an increase of the temperature could have even more effect on the reaction kinetics by improving the diffusion rate.

These optimizations were practically unfeasible, but with an automatized assay and using injectors for the different addition steps, these are serious options to improve the response of the assay. Automated analyzer-based ELISA are widely used, allowing to exploit every process that can significantly enhance the sensitivity of these assays.

On another hand, this enzymatic reaction still has plenty of potential to improve its efficiency in different ways. The first involves further optimization of the substrate. The dimerization of phenol derivatives by HRP is known to be chemoselective when several reactive groups are present on the phenol. The reaction rate was reported to be higher when *para* and *meta* substituted phenols were used. Therefore, further studies could be done on the effect of such substituents on the reaction rate and the efficiency of NPs sensitization by the formed dimer.

Another way to promote this reaction consists in the addition of a compound that stimulates the enzymatic oxidation of the phenol. *O*-dianisidine was reported as a strong stimulator which improves the rate of this type of reaction. The influence of such compounds on the enzymatic reaction as well as the sensitization of NPs could be studied to evaluate any potential improvements of this system.

Finally, among the different strategies developed during the last decades to produce ultrasensitive immunoassays, only a few have made their way successfully into the healthcare and bioanalytical settings. The method developed in this project does need further work to seriously compete with these assays, but with the provided results, it is not far from being there.

Résumé en Français

Introduction :

La détection et la quantification des biomarqueurs à très faible concentrations dans des matrices complexes, est un outil de diagnostic crucial pour les cliniciens. Des kits de diagnostic actuels sont basés sur des réactions immunologiques très spécifiques entre le biomarqueur à quantifier et les anticorps qui le reconnaissent spécifiquement.¹ Les dosages d'immunoabsorption par enzyme liée ou « Enzyme linked immunosorbent assay ELISA » sont largement utilisés. Ils sont basés sur le processus d'amplification du signal de détection via la formation d'un fluorophore/chromophore catalysée par une enzyme liée à l'anticorps de détection.² Cependant, certains biomarqueurs restent trop dilués pour être détectés.³

D'autre part, la fonctionnalisation de nanoparticules (NPs) à base de lanthanides initialement peu luminescentes, par des ligands photosensibilisateurs adéquats conduit à des NPs ultra luminescentes caractérisées par une signature spectrale propre au lanthanide, avec des durées de vie d'état excité très longues.⁴ Ceci permet une détection de luminescence ultrasensible en temps résolue, en se débarrassant de la fluorescence résiduelle de la matrice.⁵

Le principe du projet est d'appliquer les NPs à base de lanthanides dans la détection des tests ELISA. Cela est réalisé par le développement d'une réaction enzymatique qui transforme un substrat non photosensibilisateur en un ligand capable d'être fortement coordonné à la surface des NPs et de les photosensibiliser. La réaction enzymatique et la méthode de détection seront ensuite implémentées dans un système ELISA, comme montré dans le Schéma 1.

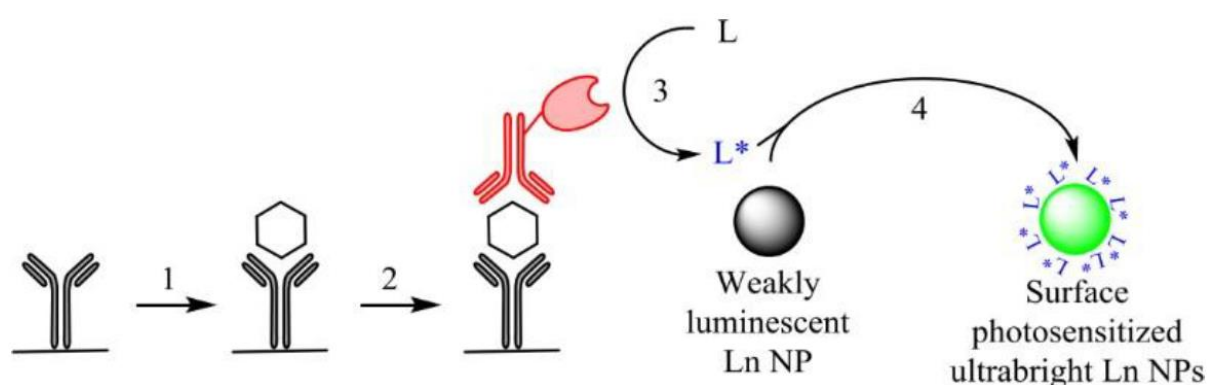


Schéma 1 : Principe de l'ELISA avec le système de détection à développer.

(1) Fixation de l'analyte. (2) Ajout de l'anticorps conjugué à l'enzyme. (3) Ajout du substrat et formation de l'antenne. (4) Photosensibilisation des NPs.

Résultats et discussions

1. Synthèse et caractérisation des NPs :

Les NPs $\text{La}_{0,9}\text{Tb}_{0,1}\text{F}_3$ et $\text{Tb}_{0,84}\text{La}_{0,15}\text{Eu}_{0,01}\text{F}_3$ ont été sélectionnées pour leurs caractéristiques de luminescence, de stabilité et de structure les plus intéressantes.⁶ La synthèse de ces NPs par chauffage au four à microondes (Figure 1), a été adaptée et améliorée au laboratoire. Elle permet d'obtenir des NPs dispersibles dans l'eau avec une bonne reproductibilité.

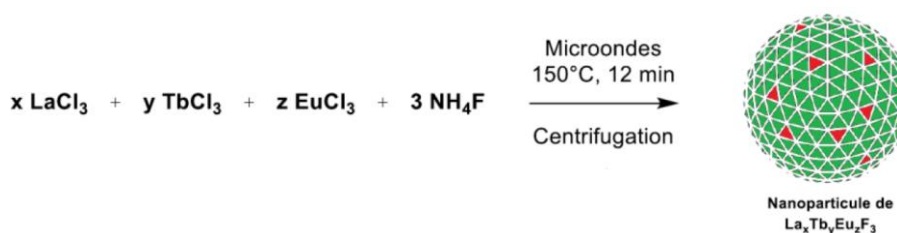


Figure 1 : Synthèse des NPs $\text{La}_x\text{Tb}_y\text{Eu}_z\text{F}_3$ (Tb en vert et Eu en rouge).

Les mesures de microscopie électronique en transmission (MET) montrent des NPs arrondies ou allongées avec un diamètre de 20 ± 6 nm pour les NPs $\text{La}_{0,9}\text{Tb}_{0,1}\text{F}_3$ (Figure 2.a) et de 35 ± 7 nm pour les NPs $\text{Tb}_{0,84}\text{La}_{0,15}\text{Eu}_{0,01}\text{F}_3$. Les mesures par diffusion dynamique de la lumière (DLS) indiquent un diamètre hydrodynamique de 49 ± 14 nm pour les NPs $\text{La}_{0,9}\text{Tb}_{0,1}\text{F}_3$ et de 62 ± 18 nm pour les NPs $\text{Tb}_{0,84}\text{La}_{0,15}\text{Eu}_{0,01}\text{F}_3$ à un pH de 5,0. La différence entre le diamètre réel et hydrodynamique indique une légère agrégation dans ces conditions.

Les propriétés de luminescence ont été évaluées par titrage avec différents ligands sensibilisateurs, montrant des augmentations très importantes dans les intensités d'émission. La Figure 2.b montre l'augmentation de l'émission de Tb après l'ajout de quantités croissantes du ligand 2-hydroxyisophtalate à pH7,0.

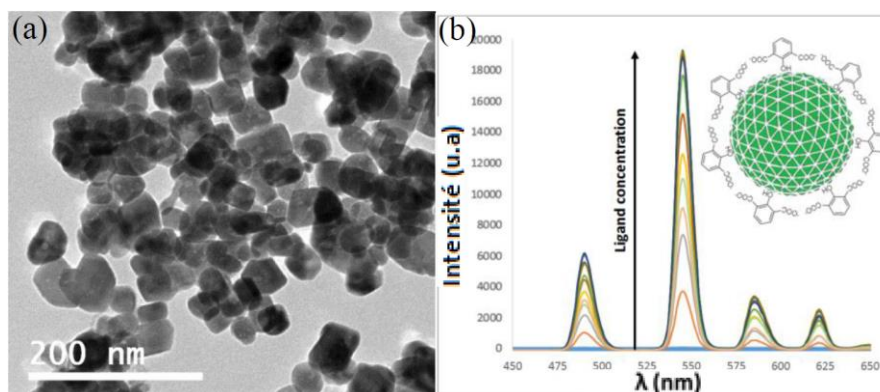


Figure 2 : (a) Image MET des NPs $\text{La}_{0,9}\text{Tb}_{0,1}\text{F}_3$. (b) Titrage spectrofluorimétrique en temps résolu des NPs $\text{La}_{0,9}\text{Tb}_{0,1}\text{F}_3$ par le 2-hydroxyisophtalate. ($\lambda_{exc} = 320$ nm).

2. Réaction enzymatique :

a) Oxydation des phénols par la Peroxydase de Raifort (HRP) :

L'oxydation des phénols par la HRP en présence de H_2O_2 conduit à leur dimérisation.⁷ En protégeant la position *para* du phénol, la dimérisation en position *ortho* (*o*) sera favorisée (schéma 2). Ce *o,o*-dimère semble un bon candidat pour la photosensibilisation des NPs.

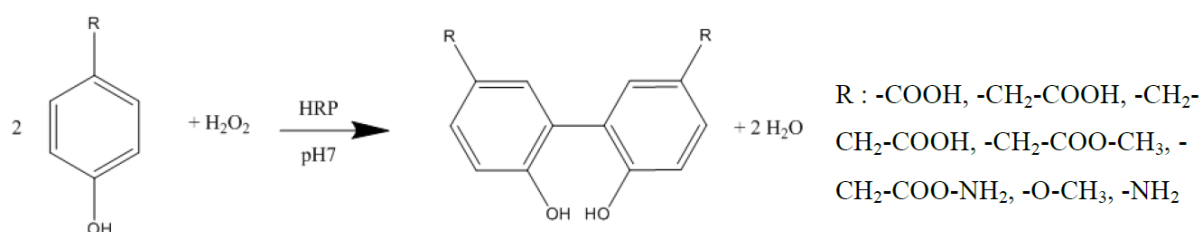


Schéma 2 : Réaction d'oxydation des phénols para-substitués par H_2O_2 en présence de la HRP.

Afin d'évaluer la capacité du substrat et du dimère formé à photosensibiliser les NPs $La_{0,9}Tb_{0,1}F_3$, différents substituants en position *para* ont été testés.⁸ La réaction est d'abord effectuée avec la HRP en solution à pH 7,0 dans des puits d'une microplaque, à température ambiante. Après agitation de la plaque pendant 1h, la réaction est arrêtée par l'ajout de 50 nM de catalase, une enzyme qui élimine l'excès de H_2O_2 , suivie par l'introduction des NPs de Tb. Ensuite, le pH est augmenté vers 12 afin de déprotoner les groupements phénols et de favoriser la coordination des ligands à la surface des NPs.

Le substrat avec l'ester éthylique comme substituant, a montré le signal de photosensibilisation le plus important. Les spectres d'excitation et d'émission du Tb avec ce substrat sont montrés dans la Figure 3.

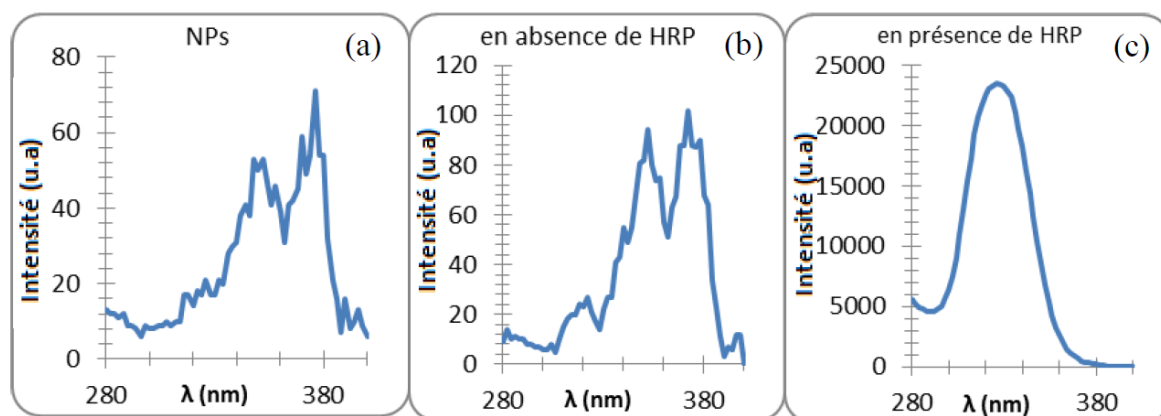


Figure 3 : Spectres d'excitation des NPs de Tb seules (a), avec le substrat (b) et après réaction (c).

($\lambda_{em} = 545 \text{ nm}$).

Les NPs nues montrent les faibles pics caractéristiques de l'excitation des ions Tb^{3+} (Figure 3.a). De même, en présence du substrat non transformé, aucun changement n'a été distingué (3.b), ce qui montre que le substrat ne photosensibilise pas ces NPs de Tb. En présence de HRP, le spectre d'excitation montre une bande intense avec un maximum à 330 nm, qui correspond à l'excitation due à la coordination du dimère formé (3.c).

Les spectres d'émission de Tb en excitant à 330 nm montre une amplification du signal jusqu'à 1200 fois pour les NPs photosensibilisées par le dimère formé en comparaison avec les NPs en présence du substrat seul (Figure 4). Cette réaction correspond au principe de notre objectif pour son application dans les tests ELISA souhaités.

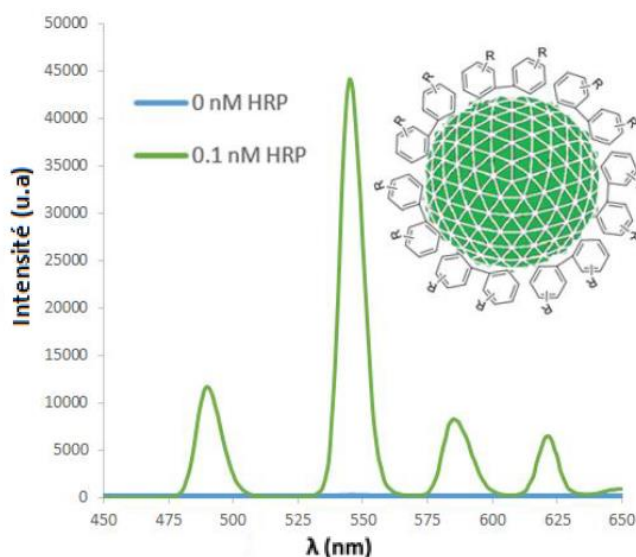


Figure 4 : Spectres d'émission des NPs de Tb avant et après réaction. ($\lambda_{exc} = 320$ nm).

b) Détermination de la limite de détection en HRP

A 0.1 nM en HRP (concentration relativement faible), la réaction semblait efficace, résultant en un rapport signal/bruit de 1200. Ceci est prometteur quant à la limite de détection (LOD) de la méthode. Pour déterminer la LOD, le protocole est effectué à des concentrations croissantes de HRP en solution.

La courbe de calibration est montrée dans la Figure 5. La courbe de calibration permet d'estimer une LOD à 100 fM alors que les LOD rapportées dans la littérature sont de l'ordre du pM.⁹

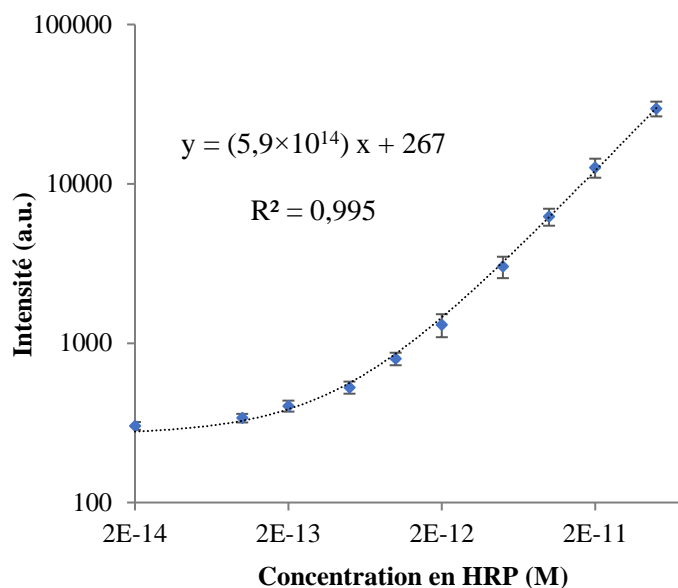


Figure 5 : Courbe de calibration de l'émission du Tb en fonction de la concentration en HRP.
 ($\lambda_{exc} = 320 \text{ nm}$, $\lambda_{em} = 545 \text{ nm}$)

3. Implémentation dans un test ELISA

La dernière étape est d'implémenter le protocole développé dans un test ELISA complet. Ceci est réalisé en utilisant un kit ELISA pour la détection et la quantification de l'insuline humaine. Après optimisation de la méthode, des essais ont été faits tout en comparant la détection colorimétrique du kit commercial avec notre méthode de détection développée.

a) Comparaison de la méthode de détection développée avec celle du kit

La méthode du kit commerciale implique le TMB comme substrat de la réaction enzymatique, suivi d'une détection colorimétrique.

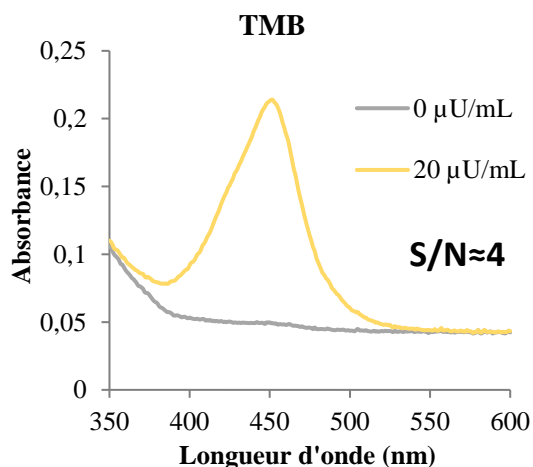


Figure 6 : Spectres d'absorbance en utilisant la méthode commerciale par détection colorimétrique.

Les méthodes sont comparées à l'aide du rapport signal sur bruit S/N pour la même concentration d'insuline. A une concentration de 20 $\mu\text{U/mL}$, la réponse par détection colorimétrique donne un $S/N=4$ (Figure 6).

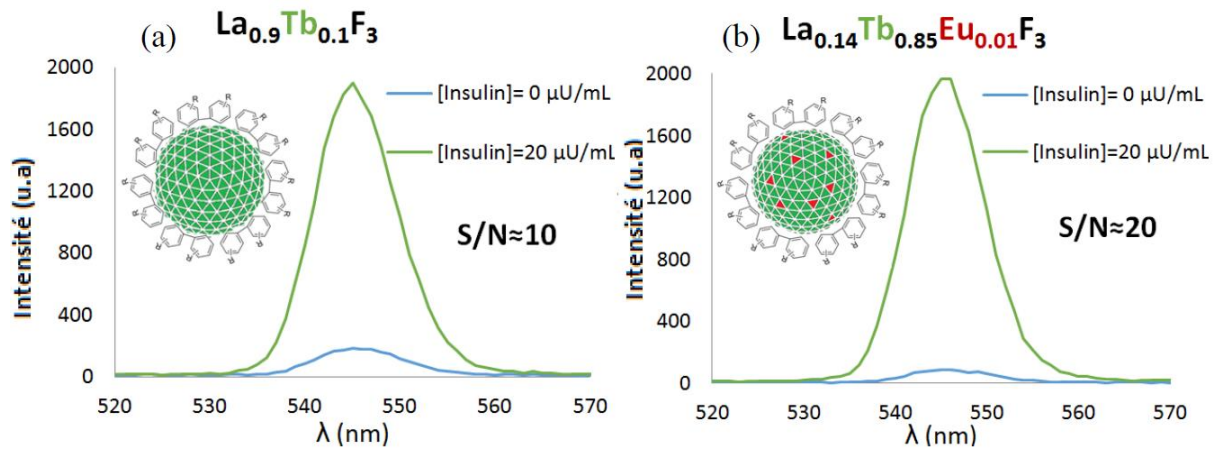


Figure 7 : Spectres d'émission de la méthode de détection développée basée sur les NPs $\text{La}_{0,9}\text{Tb}_{0,1}\text{F}_3$ (a) et $\text{Tb}_{0,84}\text{La}_{0,15}\text{Eu}_{0,01}\text{F}_3$ (b). ($\lambda_{exc} = 320 \text{ nm}$).

La réponse par émission des NPs de Tb présente un S/N de 10 (Figure 7.a). Cependant, les NPs de Tb montrent un bruit assez élevé. Ceci a été résolu en les remplaçant par les nanoparticules co-dopées en Tb et en Eu $\text{Tb}_{0,84}\text{La}_{0,15}\text{Eu}_{0,01}\text{F}_3$. Ces NPs présentent un blanc avec 2 fois moins de bruit tout en gardant la même émission du signal offrant ainsi un $S/N = 20$ (Figure 7.b).

b) Détermination de la limite de détection par la méthode développée

Le protocole de l'essai en « sandwich ELISA » est conservé et appliqué sur une gamme de concentration d'insuline entre 1 et 100 $\mu\text{U/mL}$. Après la fixation de l'antigène, l'anticorps de détection et l'enzyme, la méthode de détection développée est appliquée comme énoncé dans l'objectif principal du projet.

La courbe de calibration qui montre l'évolution du signal d'émission des NPs en fonction de la concentration d'insuline est montrée dans la Figure 8.

La courbe de calibration est fittée dans une équation Spline à l'aide du logiciel Assayfit, spécifique pour le traitement des données ELISA.

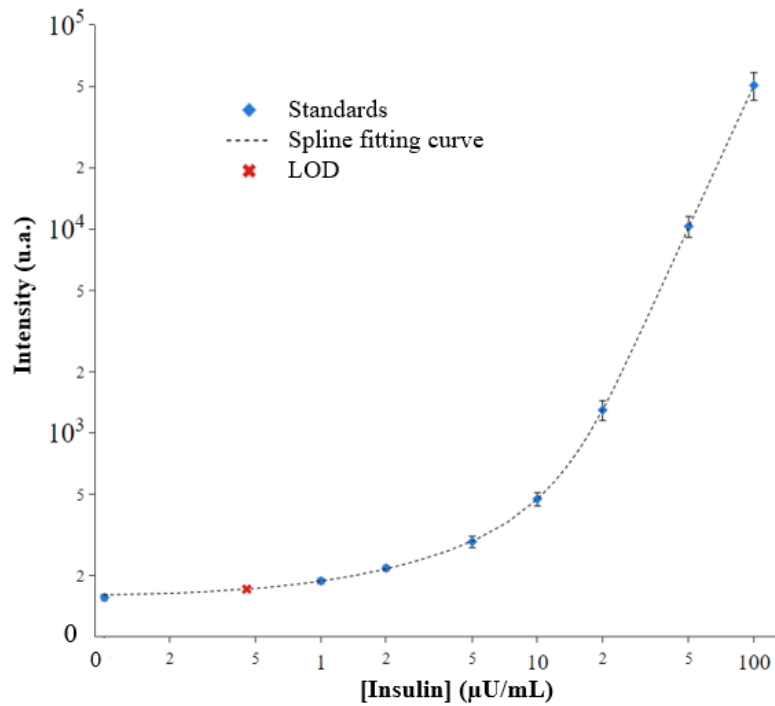


Figure 8 : Courbe de calibration de l'émission du Tb en fonction de la concentration en Insuline.
 ($\lambda_{exc} = 320 \text{ nm}$, $\lambda_{em} = 545 \text{ nm}$).

Une limite de détection est estimée par le signal minimal détecté, correspondant à :

$$\text{LOD} = m_{\text{blanc}} + 3 S_{\text{blanc}},$$

Où m_{blanc} et S_{blanc} sont respectivement la moyenne et l'écart-type sur les n mesures de blancs. Une LOD de $0.5 \mu\text{U/mL}$ a été estimée, 2 fois plus sensible que la détection colorimétrique du kit, indiquée à $1 \mu\text{U/mL}$.

Conclusion générale

✓ Le dosage d'immunoabsorption par enzyme liée « ELISA » est une technique d'analyse couramment utilisée dans de nombreuses applications, diagnostiques cliniques, pharmaceutiques, analyses des aliments, analyses environnementales, travaux de recherche ou industriels... et qui couvre une très large gamme d'analytes quantifiables.

Ces tests sont très spécifiques et relativement sensibles, mais pas suffisamment pour la détection en dessous du pM. Les recherches sont toujours continues pour la diminution des limites de détection de telle méthode.

✓ Les NPs à base de lanthanides présentent une luminescence importante avec un temps de vie extrêmement long. Grâce à une détection en temps résolue, le signal de luminescence peut être exclu de tout bruit de fond. Ces propriétés font des NPs de lanthanides un potentiel alternatif aux chromophores et fluorophores utilisés en ELISA.

✓ Par un choix judicieux de l'enzyme et du substrat, on a pu transformer un composé optiquement inactif, en un ligand qui peut se coordiner à la surface des NPs et les photosensibiliser. L'efficacité de la réaction et de la photosensibilisation des NPs ont permis de détecter des quantités minimales d'enzyme.

✓ L'application de cette méthode dans un test ELISA complet a montré des résultats très prometteurs avec une détection plus sensible qu'une détection colorimétrique classique pour un antigène donné (insuline).

✓ La méthode développée est complètement effectuée manuellement. Etant donné l'évolution très rapide des méthodes ELISA, surtout dans l'automatisation des systèmes, la performance de cette méthode est toujours susceptible d'améliorations additionnelles. En plus, un signal de luminescence peut être optimisé et amélioré grâce à des équipements plus puissants, alors que ce n'est pas exactement le cas pour un signal d'absorbance.

Références

- (1) Ito, E.; Iha, K.; Yoshimura, T.; Nakaishi, K.; Watabe, S. Chapter Four - Early Diagnosis with Ultrasensitive ELISA. *Adv Clin Chem*, **2021**; (101), 121–133. <https://doi.org/10.1016/bs.acc.2020.06.002>.
- (2) Shah, K.; Maghsoudlou, P. Enzyme-Linked Immunosorbent Assay (ELISA): The Basics. *Br J Hosp Med* **2016**, 77 (7), 98–101. <https://doi.org/10.12968/hmed.2016.77.7.C98>.
- (3) Thompson, I. M.; Ankerst, D. P. Prostate-Specific Antigen in the Early Detection of Prostate Cancer. *CMAJ*, **2007**, 176 (13), 1853–1858. <https://doi.org/10.1503/cmaj.060955>.
- (4) Bao, G.; Wen, S.; Lin, G.; Yuan, J.; Lin, J.; Wong, K.-L.; Bünzli, J.-C. G.; Jin, D. Learning from Lanthanide Complexes: The Development of Dye-Lanthanide Nanoparticles and Their Biomedical Applications. *Coord. Chem. Rev.* **2021**, (429), 213642. <https://doi.org/10.1016/j.ccr.2020.213642>.
- (5) Sy, M.; Nonat, A.; Hildebrandt, N.; Charbonnière, L. J. Lanthanide-Based Luminescence Biolabelling. *Chem. Commun.* **2016**, 52 (29), 5080–5095. <https://doi.org/10.1039/C6CC00922K>.
- (6) Goetz, J.; Nonat, A.; Diallo, A.; Sy, M.; Sera, I.; Lecointre, A.; Lefevre, C.; Chan, C. F.; Wong, K.-L.; Charbonnière, L. J. Ultrabright Lanthanide Nanoparticles. *ChemPlusChem* **2016**, 81 (6), 526–534. <https://doi.org/10.1002/cplu.201600007>.
- (7) Yu, Jian.; Taylor, K. E.; Zou, Huixian.; Biswas, Nihar.; Bewtra, J. K. Phenol Conversion and Dimeric Intermediates in Horseradish Peroxidase-Catalyzed Phenol Removal from Water. *Environ. Sci. Technol.* **1994**, 28 (12), 2154–2160. <https://doi.org/10.1021/es00061a025>.
- (8) Guilbault, G. G.; Brignac, P. J.; Juneau, Mark. Substrates for the Fluorometric Determination of Oxidative Enzymes. *Anal. Chem.* **1968**, 40 (8), 1256–1263. <https://doi.org/10.1021/ac60264a027>.
- (9) Meyer, J.; Karst, U. Enzyme-Linked Immunosorbent Assays Based on Peroxidase Labels and Enzyme-Amplified Lanthanide Luminescence Detection. *Analyst* **2001**, 126 (2), 175–178. <https://doi.org/10.1039/b008293g>.

Conferences and publications

Conferences

- International Symposium on Advances in Pharmaceutical Analysis

27-30 June 2022, online

Ultrasensitive Enzyme-linked immunosorbent Assay “ELISA” based on luminescent lanthanide nanoparticles - Oral presentation

Ali A. Kassir, Clémence Cheignon, Loïc J. Charbonnière*

- International conference on Methods and Applications in Fluorescence

11- 14 Sept 2022, Gothenburg, Sweden

Luminescent lanthanide nanoparticles for ultrasensitive Enzyme-linked immunosorbent Assay “ELISA” - Poster

Ali A. Kassir, Clémence Cheignon, Loïc J. Charbonnière*

Publications

- **Investigation of the supramolecular assembly of luminescent lanthanide nanoparticles surface functionalized by *p*-sulfonatocalix[4]arenes with charged aromatic compounds**

Eur. J. Inorg. Chem. 2021, (36), 3761–3770

Cheignon, C. ; Heurté, M. ; Knighton, R. C. ; Kassir, A. A. ; Lecointre, A. ; Nonat, A. ; Boos, A. ; Christine, C. ; Asfari, Z. ; Charbonnière, L. J.

- **Dye-sensitized lanthanide containing nanoparticles for luminescence based applications**

Nanoscale. 2022, (14), 13915–13949

Cheignon, C. ; Kassir, A. A. ; Soro, L. K. ; Charbonnière, L.

Résumé

Dans cette thèse, nous avons développé une nouvelle méthode ELISA basée sur des Ln-NPs luminescentes. Le principe était d'employer une réaction enzymatique pour convertir un substrat qui ne peut pas photosensibiliser les NPs en une forme active qui peut se coordonner à la surface et sensibiliser efficacement les ions Ln³⁺.

La première partie a porté sur la synthèse et la caractérisation des NPs Tb et Tb/Eu. Ensuite, deux approches ont été adoptées pour développer la réaction enzymatique. La première consistait en l'hydroxylation de dérivés isophtalates catalysée par la HRP pour former le 2-hydroxyisophtalate, une unité de sensibilisation efficace des NPs. La seconde consistait en l'ortho-dimérisation des phénols catalysée par la même enzyme, où le substrat a été optimisé pour favoriser la formation d'un sensibilisateur efficace des NPs. Ce dernier a fourni des résultats très prometteurs en termes de sensibilité de détection de HRP en solution.

Le système développé a été implémenté dans un ELISA complet pour la détection de l'insuline, où nous avons démontré une amélioration de la sensibilité par rapport à la méthode de détection colorimétrique du kit commercial.

Mots clés : Nanoparticules, lanthanides, luminescence, ELISA, réaction enzymatique, photosensibilisation.

Résumé en anglais

In this thesis, we developed a new ELISA method based on luminescent Ln-NPs to overcome the limitations of commercial detection methods based on organic chromophores or fluorophores. The principle was to employ an enzymatic reaction to convert a substrate which cannot photosensitize the NPs into an active form that can be coordinated to the surface and efficiently sensitize Ln³⁺ ions.

A first part focused on the synthesis and the characterization of Tb and Tb/Eu NPs. Then, two approaches were adopted to develop the enzymatic reaction. The first consisted in the hydroxylation of isophthalate derivatives catalyzed by HRP to form the 2-hydroxyisophthalate, an efficient sensitization unit of the NPs. The second consisted in the ortho-dimerization of phenols catalyzed by the same enzyme, while the substrate was optimized to promote the formation of an efficient NPs sensitizer. The latter provided very promising results in terms of sensitivity of HRP detection in solution.

The developed system was then implanted in a full ELISA for insulin detection, where we demonstrated a sensitivity improvement compared to the colorimetric detection method of the commercial kit.

Keywords : Nanoparticles, lanthanides, luminescence, ELISA, enzymatic reaction, photosensitization.